Utilising CYP199A4 from Rhodopseudomonas palustris HaA2 for Biocatalysis and Mechanistic Studies

Rebecca Chao

Supervisors:

Dr. Stephen G. Bell

Prof. Andrew D. Abell

Thesis submitted for the degree of Master of Philosophy

THE UNIVERSITY of ADELAIDE

July 2016

School of Physical Sciences

Contents

Abstract

The cytochrome P450 enzyme CYP199A4 from *Rhodopseudomonas palustris* strain HaA2 is highly specific for the regioselective oxidation of *para*-substituted benzoic acids. A selection of these compounds was tested with the enzyme with the aim of investigating the mechanism of different P450-catalysed reactions. These studies revealed that the binding affinity and oxidative activity of CYP199A4 is influenced by the substituent at the *para*-position, and that to the enzyme's known oxidative activities (demethylation, hydroxylation, heteroatom oxidation and desaturation) can be added alkene epoxidation, alkyne oxidation and aldehyde oxidation.

The active oxidants involved in these CYP199A4-catalysed oxidations were investigated using two active site mutants at the conserved acid-alcohol pair, $T252A_{CYP199A4}$ and $D251N_{CYP199A4}$, which should disrupt different steps of the catalytic cycle. There was a general increase in hydrogen peroxide uncoupling in the $T252A_{CYP199A4}$ mutant but significant levels of product formation were observed with each substrate. The D251N mutation reduced the activity of the enzyme dramatically in all but one case, suggesting that this mutation interferes with proton delivery as expected. The elevated rate of 4-ethynylbenzoic acid oxidation by $T252A_{CYP199A4}$ when compared to the wild-type enzyme suggested the involvement of Cpd 0 in alkyne oxidation, while a reduction in activity with 4-methoxybenzoic acid implicated Cpd I in demethylation. Additionally, the notable increase in product formation and coupling efficiency of $D251N_{CYP199A4}$ with 4-formylbenzoic acid suggested the involvement of the peroxo-anion in aldehyde oxidation.

Larger cinnamic acids and closely related substrates were also investigated with CYP199A4. The binding affinity and oxidative activity of the enzyme decreased in the order 4-methoxybenzoic acid > 4-methoxycinnamic acid > 3-(4-methoxyphenyl)propionic acid > 4-methoxyphenylacetic acid, highlighting its selectivity for a planar, benzoic acid- or cinnamic acid-like framework. The exclusive oxidation of cinnamic acids and related derivatives at the *para*-position further demonstrated the high regioselectivity of CYP199A4.

While CYP199A4 exhibited low oxidation activity towards *para*-methoxy substituted benzene derivatives, considerably higher levels of activity reminiscent of the demethylation of 4-methoxybenzoic acid were observed for the Ser244 → Asp244 (S244D) mutant of CYP199A4. The exclusive demethylation of the *para*-methoxy substituted benzenes by S244D revealed that the regioselectivity of CYP199A4 oxidation is maintained in this mutant.

The regioselectivity of the S244D mutant was further investigated using a selection of methyl- and ethyl-substituted derivatives. The methyl analogues were exclusively oxidised at the *para*-position to a single α-hydroxylation product. α-Hydroxylation and C_α-C_β desaturation products were generated in the turnovers of the ethyl derivatives. The alcohol was formed with high stereoselectivity. The electronic properties of the ethyl substrates were found to influence the ratio of hydroxylation/desaturation product, with the more electron donating substrates giving rise to a greater proportion of the latter. This suggested the involvement of a cationic intermediate in CYP199A4-catalysed desaturation.

Declaration

I certify that this work contains no material which has been accepted for the award of any other degree or diploma in my name, in any university or other tertiary institution and, to the best of my knowledge and belief, contains no material previously published or written by another person, except where due reference has been made in the text. In addition, I certify that no part of this work will, in the future, be used in a submission in my name, for any other degree or diploma in any university or other tertiary institution without the prior approval of the University of Adelaide and where applicable, any partner institution responsible for the joint-award of this degree.

I give consent to this copy of my thesis, when deposited in the University Library, being made available for loan and photocopying, subject to the provisions of the Copyright Act 1968.

I also give permission for the digital version of my thesis to be made available on the web, via the University's digital research repository, the Library Search and also through web search engines, unless permission has been granted by the University to restrict access for a period of time.

_____

Rebecca Chao
July 2016

Acknowledgements

First and foremost, I must begin by thanking Dr. Stephen G. Bell for his careful guidance and tireless efforts in drafting my thesis, without whom you would not be reading this right now. I don't think there are too many supervisors out there who could knock off five chapters in a single sitting!

I would like to say a big thank you to each member of the Bell group (and Pyke group), both past and present, for all of the help and fun times over the last two years; I wouldn't have made it this far without you guys! Thank you also to Prof. Andrew D. Abell, and a special mention goes to Stella Child and Nick Wells for agreeing to the arduous task of proof-reading my thesis.

Finally of course, thank you to all of my readers!

Abbreviations

AcCN	acetonitrile
BA	benzoic acid
BSTFA-TMCS	N,O-*bis*(Trimethylsilyl)trifluoroacetamide (BSTFA) with trimethylchlorosilane (TMCS)
CA	cinnamic acid
DCM	dichloromethane
DMSO	dimethyl sulfoxide
DTT	dithiothreitol
EMM	*E. coli* minimal media
GC-MS	gas chromatography-mass spectrometry
HCl	hydrochloric acid
HPLC	high performance liquid chromatography
IPTG	isopropyl β-D-thiogalactopyranoside
K_2CO_3	potassium carbonate
LB	Luria-Bertani medium
NADH	Reduced form of nicotinamide adenine dinucleotide
$NaHCO_3$	sodium bicarbonate
NCS	*N*-chlorosuccinimide
NMR	Nuclear magnetic resonance
SOC	Super Optimal broth with Catabolite repression
TBACl	tetrabutylammonium chloride
TEMPO	2,2,6,6-tetramethyl-1-piperidinyloxy
TFA	trifluoroacetic acid
WT	wild-type

List of Figures

List of Tables

This page is intentionally left blank

1 Introduction

1.1 Cytochrome P450s

Cytochrome P450s (P450s) are a superfamily of heme monooxygenases. P450s are ubiquitous in nature, and can be found in all three domains of life (bacteria, archaea and eukaryota). The name "P450" is derived from the distinctive red pigmentation of these enzymes and the 450 nm Soret absorption peak of their carbon monoxide-bound reduced forms. The P450 superfamily is currently comprised of over 21,000 members,[1] and each member is classified into a particular family and a subfamily therein. The family to which a P450 belongs is denoted by the number following its CYP prefix. Family members share $> 40\%$ amino acid sequence identity, and belong to the same kingdom (Animalia, Plantae, Fungi, Protista and Monera).[2] Subfamily members share $> 55\%$ amino acid sequence identity,[2] and are denoted by the same letter after their family number. As an example, CYP199A4 from the bacterium *Rhodopseudomonas palustris* strain HaA2 is a member of family 199, and the 4$^{\text{th}}$ member of subfamily A.[3]

While P450 enzymes can catalyse a wide range of reactions including alkene epoxidation, heteroatom oxidation, desaturation and deformylation, among others (Figure 1), the primary reaction which they catalyse is hydroxylation.[4–6] P450s contain an iron protoporphyrin IX centre which is covalently linked to the enzyme via a proximal cysteine ligand. The activation of molecular oxygen on the distal side of the heme results in the insertion of a single atom of molecular oxygen into an unreactive carbon-hydrogen (C–H) bond of an organic substrate.[4,7]

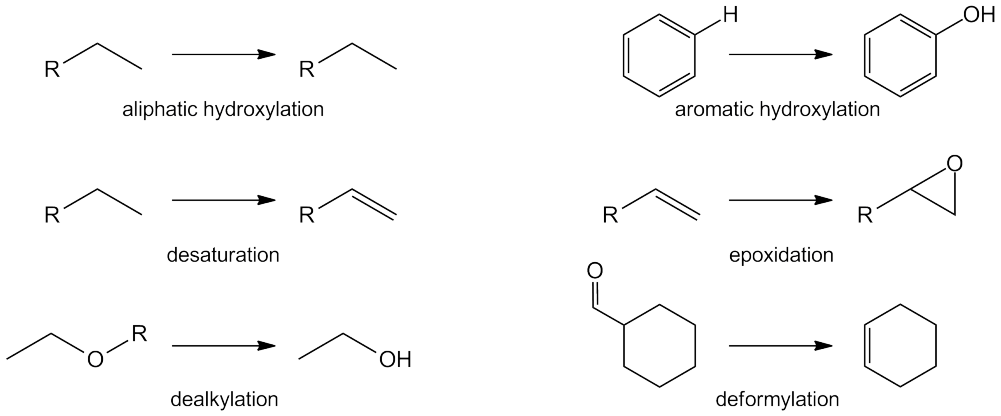

Figure 1: A selection of reactions catalysed by P450s.

Despite the vast number of these enzymes, the catalytic cycle of P450s is largely conserved for all members of the superfamily (Figure 2).[4,7] In its resting state, the ferric form of the enzyme has a water ligand bound at its 6$^{\text{th}}$ distal site (I). This water

molecule dissociates upon substrate (R–H) binding (II), causing a change from the low to high spin-state of the enzyme. Reduction by one electron to the ferrous form (III) is followed by binding of molecular oxygen to the unoccupied distal site to give the ferrous-dioxyen complex (IV). Further reduction of this species by one electron gives the ferric-peroxo anion (V). Protonation of this complex to the ferric-hydroperoxo intermediate (VI) is followed immediately by heterolytic cleavage of the O–O bond, generating a ferryl-oxo porphyrin radical cation (VII) and a molecule of water. This highly reactive species (Cpd I) introduces a single oxygen atom via radical rebound to the substrate (VIII).[8] The product (R–OH) then leaves the active site, and a water ligand can once again bind to the distal site, returning the enzyme to its resting state (I). Much of the current understanding of the catalytic cycle derives from studies on CYP101A1 ($P450_{cam}$), the camphor monooxygenase from *Pseudomonas putida*.[9] This was the first P450 to be prepared in sufficient quantities for detailed analysis and to have its three-dimensional structure solved.[10,11]

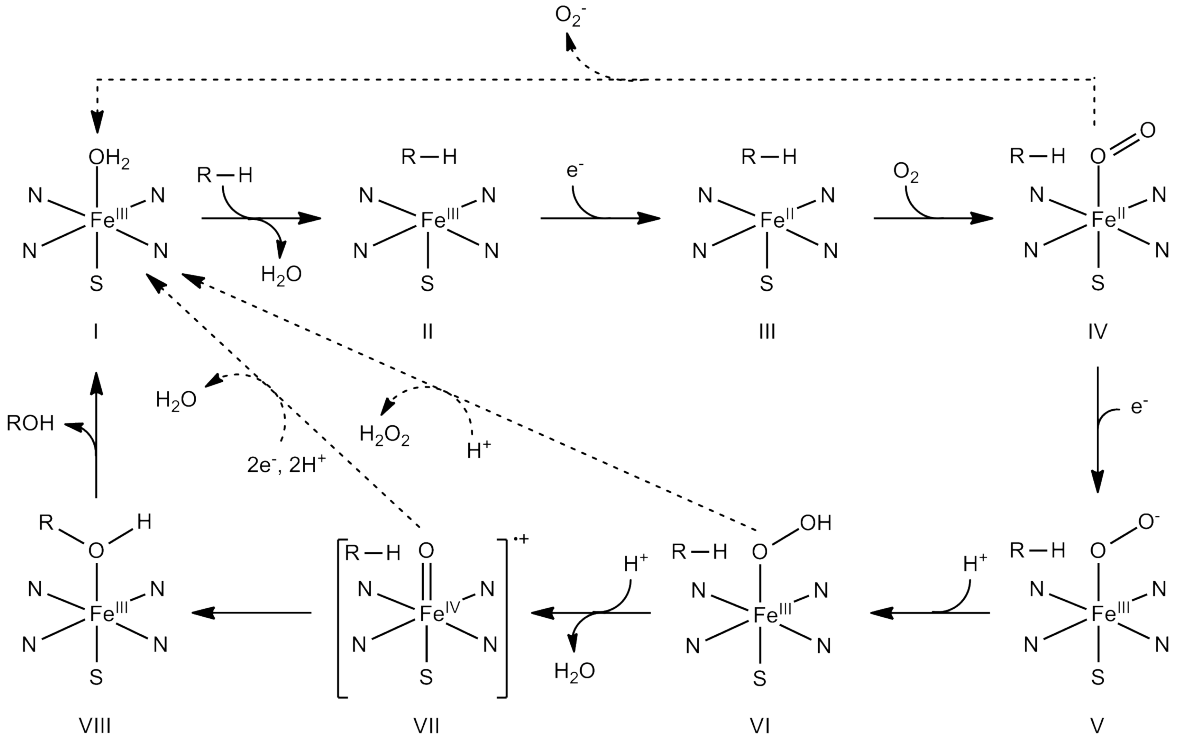

Figure 2: The catalytic cycle of P450s.

The monooxygenation reaction of P450s requires a supply of electrons for reduction of the ferric heme (II) and ferrous-dioxy complex (IV) (Figure 2). Electron transfer systems consisting of one or two electron transfer proteins, or a system fused to the P450 enzyme, are responsible for transferring these electrons, commonly sourced from NADH or NADPH, one at a time to the P450.[12] Depending on their electron transport chain, P450s are divided into one of ten different classes.[13] For example,

most mitochondrial and bacterial P450s, including $P450_{cam}$[10] and CYP199A4,[3] that belong to class I use a two-component system comprising a flavin adenine dinucleotide (FAD)-containing ferredoxin reductase and an iron-sulfur ferredoxin. The reductase transfers the electrons from NAD(P)H to the ferredoxin, which delivers them to the P450. Eukaryotic P450s, such as CYP2D6[14] and CYP2B4,[15] typically belong to class II and utilise a single, membrane-bound NADPH reductase containing FAD and flavin mononucleotide (FMN). Class III P450s, such as CYP176A1 ($P450_{cin}$),[16] are similar to those in class I, but use a flavodoxin in place of an iron-sulfur protein as their second electron transfer partner.[12,13,17] Catalytically self-sufficient P450 enzymes including CYP102A1 ($P450_{BM3}$)[18] which are fused to their eukaryotic-like diflavin reductase partner can be found in class VIII.[13]

As can be seen from Figure 2, a proton relay is also required for oxygen activation in P450s. This is regulated by a highly conserved "acid-alcohol" amino acid pair, typically an aspartate and threonine (Asp251 and Thr252 in both $P450_{cam}$ and CYP199A4).[19,20] These residues have an essential role in the transfer of protons to the peroxo and hydroperoxo intermediates from bulk solvent.[7,19,21]

The rates of electron and proton transfer throughout the catalytic cycle, among other factors, affect the rate and efficiency of substrate oxidation by P450s. If a particular electron or proton transfer step occurs too slowly, this can lead to unproductive uncoupling events at different stages of the catalytic cycle (Figure 2).[7] While every one molecule of NAD(P)H and oxygen consumed during a turnover of the catalytic cycle can in theory produce one molecule of product, this complete coupling of redox equivalents to product formation is rarely observed due to uncoupling. In the first of these possible events, superoxide is slowly released as the ferric-superoxo complex (IV) decomposes to the ferric state. This can occur when the second electron transfer step proceeds too inefficiently. The second uncoupling pathway originates from the ferric-hydroperoxide (VI). Hydrogen peroxide is released as the byproduct when the second proton transfer to the distal oxygen of this complex occurs too slowly. Peroxide uncoupling can also be accelerated by excess water in the active site, which leads to competing protonation at the proximal oxygen. The third uncoupling event, oxidase uncoupling, involves the unproductive, two-electron reduction of Cpd I to water. This can occur when no C-H bonds are in a suitable location relative to the heme centre to be oxidised. Thus, in general, the degree of uncoupling can be "limited" by an appropriate substrate fit to the active site of the P450.[9,22,23]

1.2 Reactions Catalysed by P450s

The ferryl intermediate (Cpd I, VII) is generally believed to be the oxygen-activating species in P450 catalysis, and there is strong evidence which suggests that the universal hydroxylation reaction of P450s proceeds via this electrophilic species.[24,25] However, experimental studies have suggested that the electrophilic ferric-hydroperoxide (Cpd 0, VI) and the nucleophilic ferric-peroxo anion (V) could also be responsible for some forms of monooxygenation activity.[25–29] Due to their different oxidative properties, these species may have preferences for certain reactions over others.[26,30] For example, Cpd 0 is thought to be capable of alkene (olefin) epoxidation[26,28,30] while its peroxo-anion counterpart has been implicated in aldehyde oxidation.[31] Thus, the most abundant species could dictate the outcome of substrate oxidation.

More recently, it has been proposed that rather than the involvement of multiple active oxidants, the different reactions of P450s are actually governed by the so-called "two-state-reactivity" of Cpd I. This was determined using quantum mechanical/molecular mechanical (QM/MM) and density functional theory (DFT) calculations.[32–35] Cpd I has two unpaired electrons on the iron centre in 3d π^* orbitals, and one in the porphyrin a_{2u} π^* orbital. In the high-spin quartet state ($^4A_{2u}$), these three spins are parallel while the electron in the porphyrin orbital is inverted in the low-spin doublet state ($^2A_{2u}$) (Figure 3).

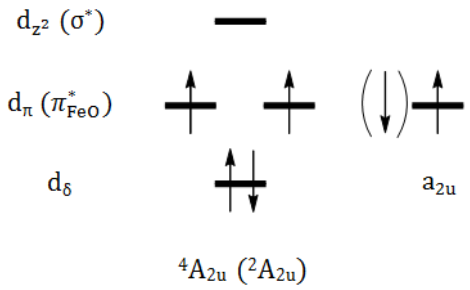

Figure 3: The electronic structure of Cpd I.

While these spin-states have virtually the same energy, the energy barriers leading from the two states for different oxidation reactions are varied. Thus, the dominant spin-state of Cpd I and the relative ease at which a reaction may proceed will decide the outcome of substrate oxidation.[36] In the contrasting "two-oxidant" model, it is the most abundant oxygenating species which determines the resulting product profile. The two-oxidant versus two-state-reactivity models will be discussed in the context of some common reactions catalysed by P450s.

1.2.1 Hydroxylation

The insertion of an oxygen atom into an unactivated C-H bond is an extremely difficult reaction to achieve using standard chemical methodologies, yet it is the most common reaction catalysed by P450s. The radical or oxygen rebound mechanism by which this reaction is believed to proceed was first proposed by Groves and McClusky in 1976 (Figure 4).[37] In the first step, the highly reactive ferryl oxygen abstracts a hydrogen atom from the alkyl substrate, giving an Fe(IV)-OH species and a substrate radical. The latter remains bound within the active site of the enzyme where it immediately recombines with a hydroxyl radical derived from the Fe(IV)-OH intermediate to give the alcohol product.

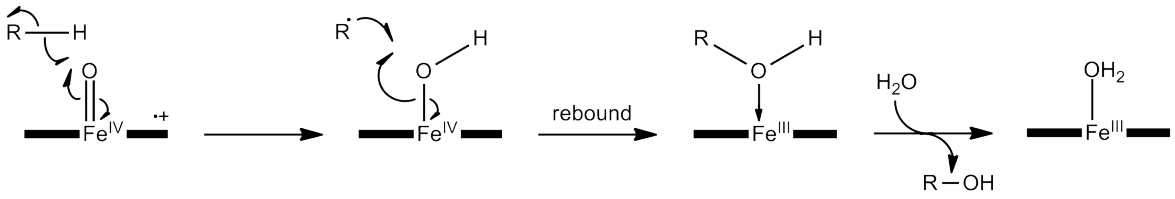

Figure 4: The radical rebound mechanism of P450s.

Radical clock substrates containing strained ring systems such as bicyclo[2,1,0]pentane were among the first to be used to measure the rate of oxygen rebound. These compounds undergo rapid ring-opening reactions at known rates via a radical intermediate. Once formed, the radical intermediate gives rise to an unrearranged and rearranged product (Figure 5). The ratio of these products together with the known rate constant of the ring-opening reaction enables the lifetime of the radical to be calculated. The oxidation of bicyclo[2,1,0]pentane by rat microsomal P450s proceeded via a radical intermediate with a lifetime of 50 ps.[38]

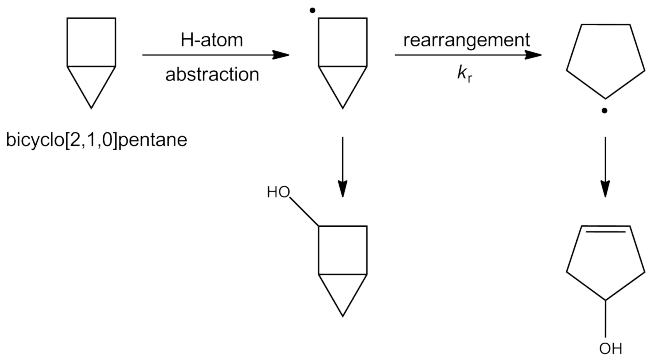

Figure 5: Bicyclo[2,1,0]pentane as a radical clock substrate for microsomal P450s.

However, when later studies using ultrafast radical clock substrates found significantly shorter lifetimes (70-200 fs) more reminiscent of the lifetimes of transition states rather than reaction intermediates, doubt was cast on the rebound mechanism.[39–42] Combined

with the observation of P450 oxidation products arising from cationic intermediates, this led to the involvement of a second oxidant, Cpd 0, being proposed.[41,43–45]

The two-state reactivity model suggests that the dominant spin-state of Cpd I is what determines whether the hydroxylation reaction proceeds via a radical or a cation intermediate. Based on DFT calculations, there is a significant energy barrier to radical rebound on the high-spin quartet pathway ($^4TS_{reb}$) while this barrier is virtually non-existent on the low-spin doublet pathway (Figure 6).[46] This suggests that hydroxylation will proceed via a radical intermediate when there is a predominance of the low-spin state of Cpd I.

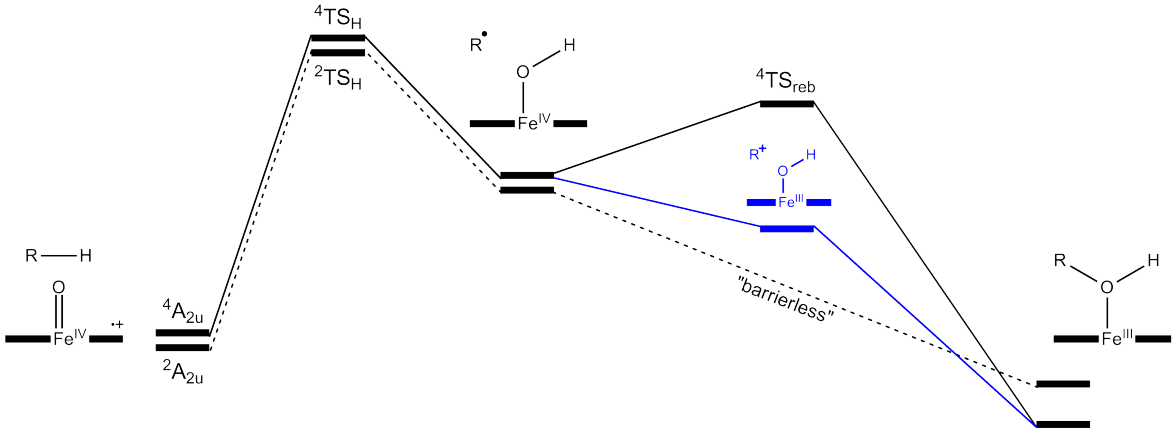

Figure 6: Energy profile for alkyl hydroxylation from the high-spin ($^4A_{2u}$, solid line) and low-spin states ($^2A_{2u}$, dotted line) of Cpd I. TS_H and TS_{reb} represent the transition states for hydrogen abstraction and radical rebound, respectively. It has been hypothesised that hydroxylation via a cation intermediate on the high-spin quartet pathway is energetically more favourable than radical rebound, as depicted.[34,46]

The "barrier-free" radical rebound on this pathway is believed to explain the short radical lifetimes found in certain radical clock experiments. Therefore, it follows that the longer radical lifetimes might be attributed to the intermediates "lingering" on the quartet pathway.[39–42] The DFT calculations also suggested that while the doublet state does not generate a cationic species, there is significant positive charge build-up on the substrate on the quartet pathway. This implies that as a large energy barrier to rebound is encountered on the quartet pathway, the reaction might continue instead via a cation intermediate (Figure 6). As the two spin-states of Cpd I are very similar in energy, multiple factors such as the substrate being oxidised and the heme environment can influence the relative abundance of the two states and the resulting radical/cation intermediates.[34,46–48]

1.2.2 Heteroatom Dealkylation

Two main mechanistic pathways have been proposed for heteroatom dealkylation by P450s. *O*-dealkylation reactions appear to proceed in the same way as hydroxylation.[5] Hydrogen abstraction followed by radical rebound at the carbon alpha to the heteroatom (HAT) yields an unstable, hydroxylated product. This product is then either cleaved between the carbon and the heteroatom or decomposes to give the dealkylated product (Figure 7a).[5]

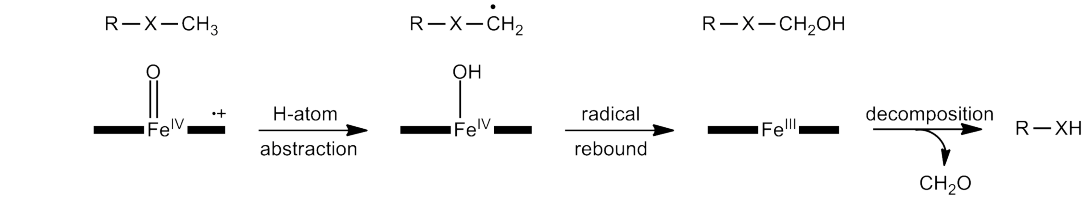

(a)

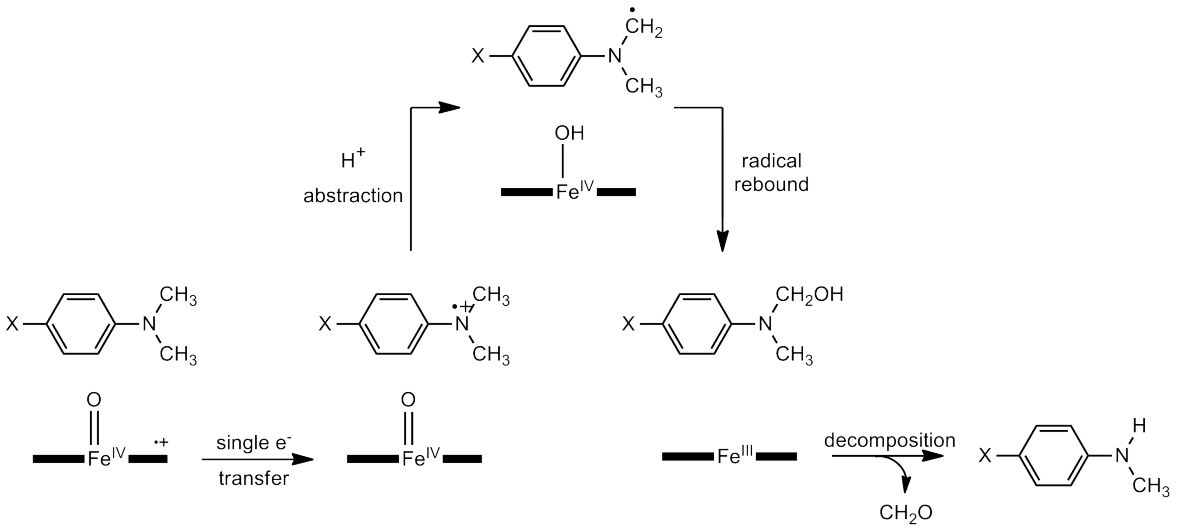

(b)

Figure 7: The mechanisms of P450-catalysed dealkylation reactions. (a) Dealkylation of a simple alkyl substrate via the HAT pathway (X = N or O). (b) Dealkylation of *para*-substituted *N,N*-dimethylalinines via the SET pathway (X = various substituents).[49,50]

It is believed that *S*- and *N*-dealkylation reactions may also involve an initial single electron transfer (SET) from the heteroatom to Cpd I to give a cation radical. Subsequent hydrogen abstraction and radical rebound give the dealkylated product (Figure 7b).[4,5,34] The SET pathway is supported by low kinetic hydrogen isotope effects (KIE ≈ 2) for *N*-demethylation of *para*-substituted *N,N*-dimethylanilines. The low KIE values are believed to arise from the ability of the Fe(IV)=O complex to readily abstract a proton from the substrate radical cation.[5,34] Further evidence in support of the SET mechanism includes the correlation of the rates of *N*-demethylation of *para*-substituted

N,N-dimethylanilines with their respective Hammett substituent parameters (σ) and redox potential values.[4,34] As the negative σ values indicated that *N*-demethylations were accelerated in the presence of electron donating substituents, this agreed with the formation of a nitrogen radical cation via a SET mechanism.[4,34]

In comparison, large intramolecular isotope effects for amide *N*-dealkylations ($\approx$ 13) and DFT studies are generally in favour of the HAT mechanism for heteroatom dealkylation.[5,6,34,49,50] DFT calculations on selected *para*-substituted *N,N*-dimethylanilines showed that the radical cation arising from the first single electron transfer on the SET pathway was significantly higher in energy than its radical counterpart on the HAT pathway (Figure 7).[49,50] The same study also found that dealkylation products can arise (via the HAT pathway) from either of the two spin-states of Cpd I depending on the nature of the substrate's substituent.[34] The doublet state is preferred when there is no substituent or a chlorine substituent (X = H or Cl in Figure 7b), but this preference decreases with increasing electron withdrawing power of the substituent (H $<$ Cl $<$ Cl $<$ NO_2), such that the two spin-states become almost degenerate.[49,50]

1.2.3 Alkene and Alkyne Oxidation

Epoxidation of alkenes (olefins) is another widespread reaction catalysed by cytochrome P450s.[4–6] As epoxidation invariably proceeds with retention of the alkene stereochemistry, it would appear that the reaction must proceed via a concerted mechanism in which the ferryl oxygen interacts with both carbons of the alkene (Figure 8).[4]

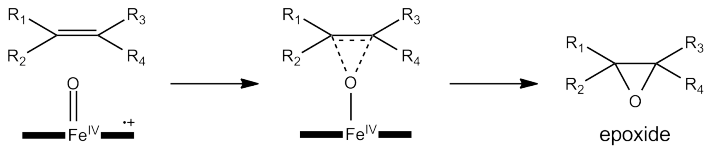

Figure 8: The concerted mechanism of alkene epoxidation by Cpd I.

However, epoxides are not the only products that can arise from P450-catalysed alkene oxidations; rearrangement products including aldehydes and ketones can also be observed, and the oxidation of terminal alkenes can result in irreversible *N*-alkylation of the porphyrin ring, rendering the enzyme inactive. As these side reactions are not observed when P450s are treated with the epoxide products, this suggests a non-concerted mechanism (Figure 9).[6,51] Thus, an intermediate other than the putative ferryl radical cation may be responsible for these reactions. Despite the mounting experimental evidence implicating the ferric-hydroperoxo intermediate,[26,31,52–57] DFT and QM/MM calculations and biomimetic studies on substrate epoxidation by synthetic iron-hydroperoxo analogues have found little evidence in support of the two-oxidant

hypothesis.[58–61] The two-state reactivity model proposes that epoxidation arises from the doublet state of Cpd I as a significant energy barrier must be overcome on the quartet state pathway, much like in hydroxylation reactions.[46,62]

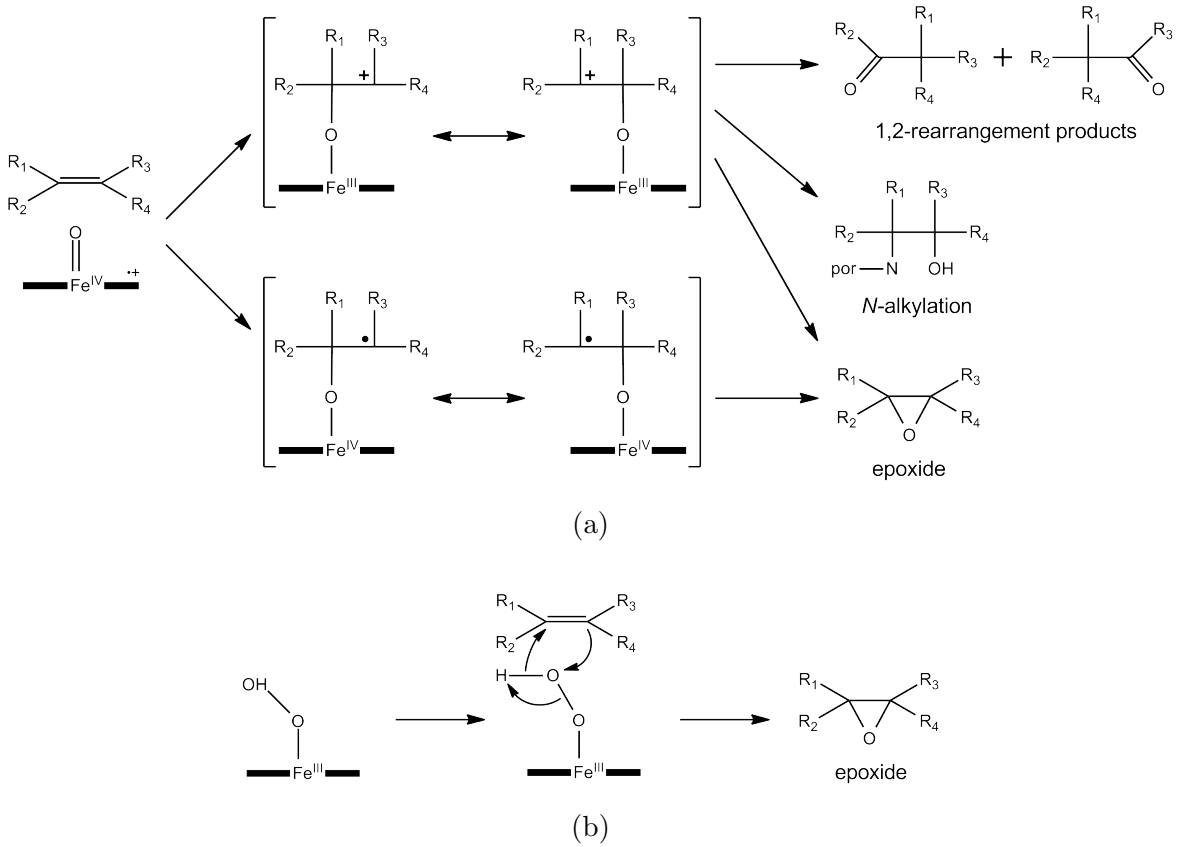

Figure 9: (a) The cationic and radical mechanisms and potential side reactions of alkene oxidation by Cpd I. (b) The mechanism of alkene epoxidation by Cpd 0.

P450s can also catalyse the oxidation of terminal alkynes (acetylenes) to ketenes, which are subsequently hydrolysed to their corresponding carboxylic acids (Figure 10).[4,63] The immediate product of alkyne oxidation should be the unsaturated epoxide (oxirene), analogous to the oxidation of alkenes, however, this is not observed as oxirenes are extremely unstable species.[64]

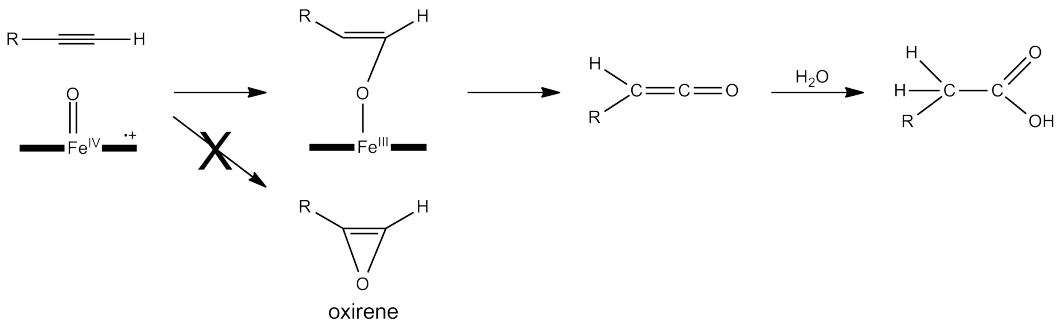

Figure 10: The mechanism of alkyne oxidation by P450s.

1.2.4 Desaturation

P450s can catalyse the desaturation (dehydrogenation) of various compounds including saturated hydrocarbons, alcohols and amines to unsaturated hydrocarbons, carbonyls and imines, respectively.[4] Although a detailed mechanism is yet to be elucidated, it has been proposed that the first steps of desaturation and hydroxylation are the same, that is, hydrogen abstraction by Cpd I to yield a carbon radical (Figure 11).[65] When this is followed by oxygen rebound, the hydroxylated product is formed. In the case of desaturation, the next step is either a) a single electron transfer from this radical species to the iron to generate a carbocation, followed immediately by proton transfer to the ferryl oxygen or b) a second hydrogen abstraction to yield the unsaturated product (Figure 11).

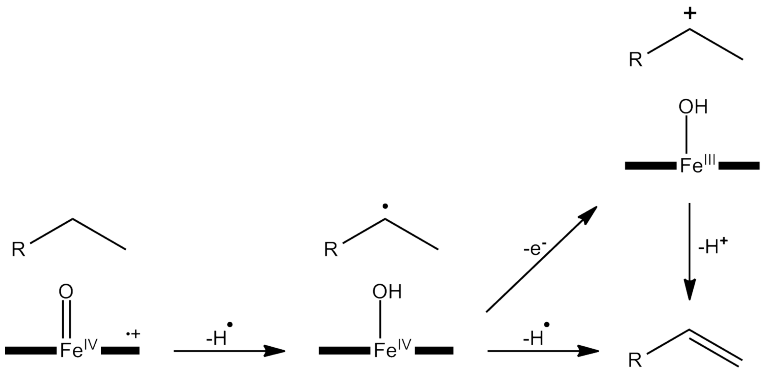

Figure 11: The mechanism of P450-catalysed desaturation reactions.

A desaturation product is generally observed in conjunction with a hydroxylation product, and DFT and QM/MM studies have been used to explore the partition between these two reactions.[66–68] The two-state reactivity model shows desaturation to arise from the doublet state of Cpd I. This state is barrierless for hydroxylation and desaturation while a significant barrier to desaturation exists on the quartet state pathway. However, the preference for hydroxylation versus desaturation is not only controlled by the energetics of the two competing pathways. Multiple factors including the type of substrate being oxidised and the nature of the enzyme active site may also influence the resulting product distribution.[66]

1.2.5 Aldehyde Oxidations

A less common reaction catalysed by P450s is the oxidation of aldehydes to (their corresponding) carboxylic acids, reactions typical of aldehyde dehydrogenases.[5] Like in P450-catalysed hydroxylations, aldehyde oxidation usually involves hydrogen atom abstraction followed by radical rebound (Figure 12a).[5,69] The weaker C–H bond of the carbonyl carbon in aldehydes lowers the barrier to abstraction compared to that of ordinary alkanes. As the subsequent oxygen rebound steps of aldehyde hydroxylation proceed barrier-free, aldehydes are more readily oxidised than their alkane counterparts.[69]

As the electrophilic aldehyde may be prone to attack by the nucleophilic ferric-peroxo anion or the distal oxygen of the ferric-hydroperoxo complex, an alternative mechanism has also been put forward (Figure 12b).[5] A recent DFT study on a series of aldehydes has shown that the energetics of aldehyde oxidation via the doublet and quartet states are comparable. The rate of oxidation was found to depend mostly on the ease of initial hydrogen abstraction by Cpd I, which was largely influenced by the structure of the substrate.[69]

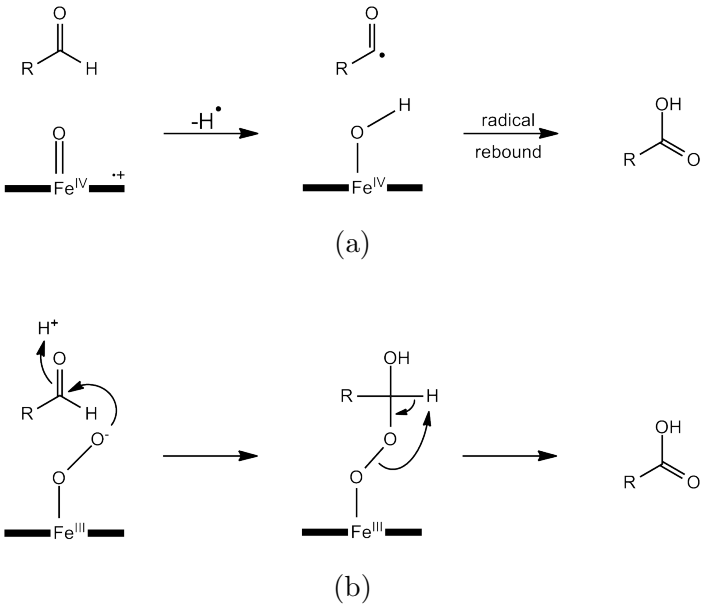

Figure 12: Mechanisms for aldehyde oxidation by (a) Cpd I and (b) the ferric-peroxo anion in P450s.

1.2.6 The Potential of P450s for Biocatalysis

The impressive array of highly selective and synthetically challenging reactions catalysed by cytochrome P450s implies an enormous potential for these enzymes in biocatalysis. The growing field of "green chemistry" and environmental concerns have sparked interest in the use of P450s in bioremediation, where certain enzymes have been shown to be capable of metabolising industrial pollutants.[70–72] Another application of cytochrome P450s is in the production of fine chemicals. For example, a whole-cell system coexpressing a mutant form of CYP199A2 and its two electron transfer partners has been reported to generate caffeic acid, an important synthetic scaffold for a variety of bioactive compounds on a gram per litre scale.[73]

At present, the use of P450s in large-scale, industrial applications is not yet extensive.[70,74,75] P450s have limited stability, where high temperatures and unfavourable solvent or storage conditions can easily render them inactive.[70,75] The need for expensive cofactors (NAD(P)H) and redox partners for catalysis is another limiting factor. With the appropriate redox partners, it is possible to regenerate the necessary reducing equivalents using whole-cell systems. However, the extent of whole-cell P450 oxidations may in turn be limited by substrate solubility, and substrate and product toxicity to the cells.[70,74,75] Methods to overcome limitations of the enzyme include directed evolution and rational protein design.[74,76,77] These methods can be used to engineer libraries of P450 enzymes with the desired substrate specificity and level of activity, and lead toward their application on a larger scale.[74,76,77]

In general, bacterial P450s have the advantage of being easily expressed in high yields and in a soluble form. The oxidative activity and efficiency of bacterial systems is often higher than that of mammalian P450s, which also tend to be membrane-bound.[74] For example, the activity of CYP199A4 for the oxyfunctionalisation of a select number of *para*-substituted benzoic acids using its physiological electron transfer partners HaPux and HaPuR exceeds 1000 min^{-1}.[3,78,79] When combined with directed evolution and rational protein design, P450 enzymes such as CYP199A4 could be utilised for biocatalysis.[4,70,74,75]

1.3 CYP199A4 from *Rhodopseudomonas palustris* HaA2

Rhodopseudomonas palustris is a purple non-sulfur phototrophic bacterium with extraordinary metabolic versatility.[80] A member of the alpha proteobacteria, this common water and soil bacterium has the ability to grow by any of the four modes of metabolism that support life: photoautotrophic, photoheterotrophic, chemoheterotrophic and chemoautotrophic.[80] *R. palustris* can grow with or without oxygen, fix nitrogen, produce hydrogen gas, convert carbon dioxide into biomass and also degrade a variety of compounds including those found in industrial wastes such as chlorinated fatty acids.[81–84] Studies have shown that members of the *Rhodopseudomonas* family have adapted to a range of ecologically distinct habitats, with different species developing uniquely modified genomes best-suited to their microenvironment.[85] The genome of *R. palustris* strain HaA2 is known to contain nine P450 genes,[80,86] and as the enzymes that they encode belong to different bacterial P450 families, this suggests that each could oxidise a unique range of substrates.

Using two electron transfer partners, a [2Fe-2S] ferredoxin (HaPux) and a flavin-dependent ferredoxin reductase (HaPuR) with NADH as the electron source, CYP199A4 from *R. palustris* HaA2 efficiently oxidises a range of *para*-substituted benzoic acids.[3,78,79,87] The enzyme has very high affinity for 4-methoxybenzoic acid (K_d = 0.28 µM), which is exclusively demethylated to 4-hydroxybenzoic acid (Figure 13).[3]

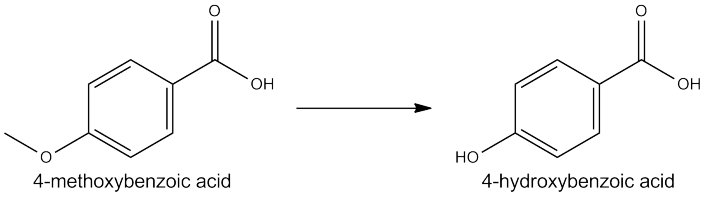

Figure 13: The demethylation of 4-methoxybenzoic acid to 4-hydroxybenzoic acid by CYP199A4.

Crystal structures of CYP199A4 in complex with a selection of benzoic acid substrates have provided a detailed understanding of the interactions that govern the selectivity and outcome of substrate oxidation (PDB: 4DO1, 4EGM, 4EGN and 4EGO).[20,79] These structures reveal that the carboxylate group forms hydrogen bonds with the side chains of active site amino acids Arg92, Ser95, Ser244 and, via a bridging water molecule, Arg243 (Figure 14). Strong van der Waals interactions between the substrate benzene ring and side chains of aliphatic amino acids including Leu98 and Ala248 also play a role in holding the substrate within the active site.[79] Higher up in the active site, Phe185 contacts the substrate benzene ring while Phe182 and Phe298 contact the methoxy group.[20] These residues are essential for substrate-recognition and binding

by CYP199A4, and together, they hold the *para*-substituent above the heme iron, consistent with exclusive attack at this position. The highly conserved acid-alcohol amino acid pair, Asp251 and Thr252 in CYP199A4, is found close to the active site of the enzyme.

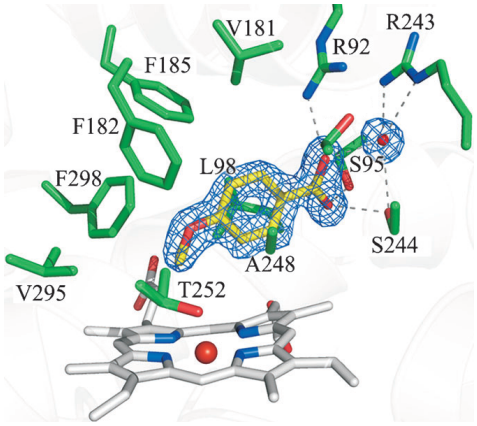

Figure 14: The active site of 4-methoxybenzoic acid-bound CYP199A4. 4-Methoxybenzoic acid is shown in yellow, the heme in grey and the active site residues in green.[20]

Recently, a study on the oxidation of a range of substituted benzoic acid derivatives by CYP199A4 highlighted the importance of the *para*-substituted framework for tight-binding to the enzyme and efficient catalytic turnover. The study reaffirmed that a methoxy group in this position is essential for optimal activity.[78] Additionally, CYP199A4 has been shown to bind closely-related benzoic acid derivatives with high affinity and display a range of activities including hydroxylation, desaturation and heteroatom oxidation.[20,79,87] For example, CYP199A4 hydroxylates and desaturates 4-ethylbenzoic acid to 4-(1-hydroxyethyl)benzoic acid ($> 50\%$) and 4-vinylbenzoic acid ($\approx 40\%$), respectively.[3] While 4-methylaminobenzoic acid is dealkylated to 4-aminobenzoic acid, the sulfur-containing analogue 4-methylthiobenzoic acid is oxidised exclusively to 4-methylsulfinyl benzoic acid (Figure 15).[88]

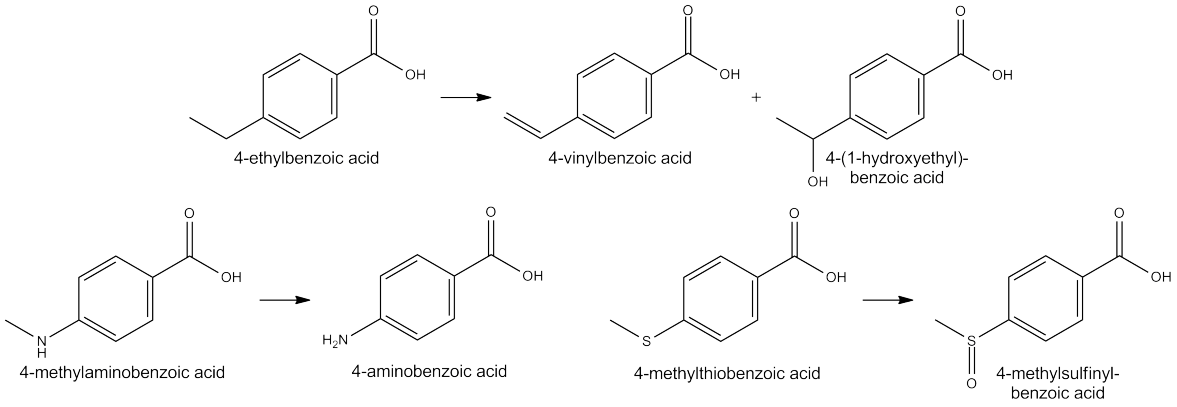

Figure 15: Different reactions catalysed by CYP199A4.

1.4 Thesis Objectives

To further explore the substrate binding properties and oxidative potential of CYP199A4, the enzyme will be tested with a series of *para*-substituted benzoic acids containing different functionalities at this position (Figure 16a). These include an ester (4-acetoxy-), alkene (4-vinyl-), alkyne (4-ethynyl-), amide (4-acetamido-), aldehyde (4-formyl-) and ketone (4-acetyl-benzoic acid) group. As the enzyme-benzoic acid interactions should help position the substituent above the heme iron, these substrates will enable new activities of CYP199A4 to be investigated.

Importantly, these reactions will also serve as a means to explore the two-oxidant theory for oxygen activation in P450s. Experiments on $P450_{cam}$ and its conserved residue mutants, $D251N_{cam}$ and $T252A_{cam}$, clearly identify the ferryl intermediate as the active oxidant in camphor hydroxylation.[89–93] This acid-alcohol pair is also conserved in CYP199A4. Thus, a threonine ($T252A_{CYP199A4}$) and an aspartate ($D251N_{CYP199A4}$) mutant of CYP199A4 will be tested with the above mentioned benzoic acid derivatives and used as mechanistic probes for oxygen activation in CYP199A4.

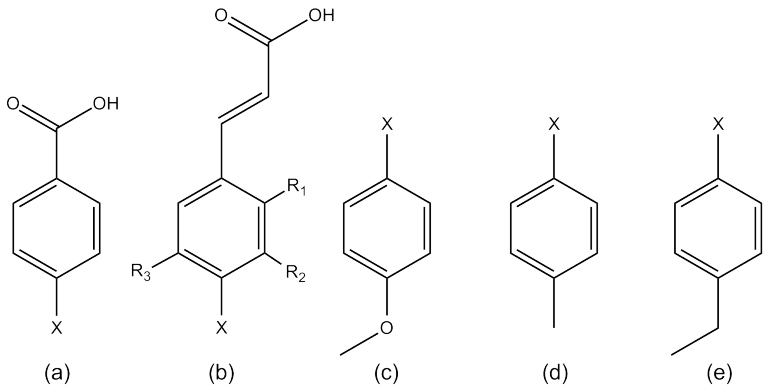

Figure 16: The different types of substrates to be tested with CYP199A4, where X = various functional groups. (a) *para*-Substituted benzoic acids (b) substituted cinnamic acids (c) *para*-methoxy substituted aromatic substrates (d) *para*-methyl substituted aromatic substrates and (e) *para*-ethyl substituted aromatic substrates.

In addition to *para*-substituted benzoic acids, CYP199A4 can also oxidise 6-indolecarboxylic acid and 2-naphthoic acid (Figure 17).[79,94,95] Despite being larger, 6-indolecarboxylic acid binds in much the same way as 4-methoxybenzoic acid within the active site (PDB: 4DO1 and 4EGO).[20] This is not the case for 2-naphthoic acid. When this substrate is bound, the water molecule which normally bridges the substrate carboxylate group and Arg243 is displaced, leaving the carboxylate to hydrogen bond directly with the side chain of Arg243 (PDB: EGP).[20] In order for the hydrogen bonding interactions with Ser95 and Ser244 to remain intact, Ser95 undergoes a large positional shift. Taken together, these observations indicate that CYP199A4 is able

to accommodate substrates larger than benzoic acids.[20] The closely related enzyme CYP199A2 from *R. palustris* strain GCA009, which shares > 85% sequence identity with CYP199A4, has been shown to efficiently oxidise both 3-hydroxy- and 4-hydroxycinnamic acid to 3,4-dihydroxycinnamic acid (Figure 17).[73,96] To further investigate the interactions required for tight-binding to CYP199A4 and the influence of the substrate on efficient turnover, a range of substituted cinnamic acids will be tested with CYP199A4 (Figure 16b).

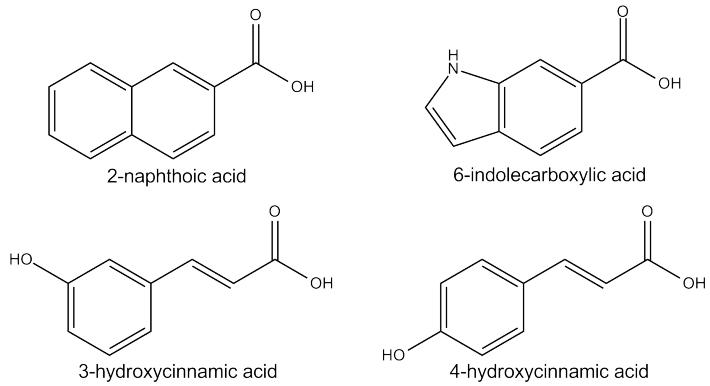

Figure 17: Substrates of CYP199A4 and CYP199A2.

Studies so far on CYP199A4 have demonstrated that the enzyme is highly specific for the binding and oxidation of aromatic carboxylic acids.[3,78,79,87] While the substrate-specificity of CYP199A4 for *para*-substituted benzoic acids can be very useful for probing different oxidative activities and the active oxidants in CYP199A4 catalysis, it does however imply a limited substrate range for the enzyme. In order to expand the substrate range of CYP199A4, active site residues of CYP199A4 will be mutated. The resulting CYP199A4 mutants will be screened for activity with substrates in which the carboxylate of 4-methoxybenzoic acid has been modified (carboxy-modified substrates) (Figure 16c). This will also enable us to investigate whether the selectivity of the enzyme for demethylation at the *para*-position is retained in the presence of additional functional groups.

Finally, the activity of CYP199A4 with alkyl *para*-substituted aromatic compounds will similarly be investigated. CYP199A4 has been shown to exclusively hydroxylate 4-methylbenzoic acid at the *para*-position.[79] The comparatively larger 4-ethylbenzoic acid undergoes competing hydroxylation and desaturation reactions to give an α-hydroxylation and a desaturation product (Figure 15). Whether these regioselective oxidations still occur with *para*-substituted methyl and ethyl analogues will be explored (Figure 16d and 16e). In addition, as the partition between hydroxylation/desaturation for larger alkyl substrates is believed to be influenced by the electronic effects of the substrate, this will also be investigated using the ethyl derivatives.

2 Experimental

2.1 General

General reagents, HPLC solvents, organic substrates and derivatisation agents were purchased from Sigma-Aldrich, VWR, Fluorochem, Acros Organics, Tokyo Chemical Industry and Matrix Scientific. Antibiotics, isopropyl β-D-thiogalactopyranoside (IPTG) and dithiothreitol (DTT) were purchased from Astral Scientific.

UV/Vis spectra and spectroscopic activity assays were recorded at 30 ± 0.5 °C on a Varian Cary 5000 or Cary 60 spectrophotometer. High performance liquid chromatography (HPLC) analysis was performed on an Agilent 1260 Infinity pump equipped with an autoinjector and Agilent Eclipse Plus C18 column (250 mm x 4.6 mm, 5 µm). For chiral HPLC analysis, a Lux 3u Cellulose-1 column (100 mm x 4.6 mm x 3 µm; Phenomenex) was used. Preparative HPLC was performed using an Agilent HP 1100 Series preparative pump equipped with a SUPELCOSIL LC-18 HPLC column (250 mm x 10 mm, 5 µm), or Gilson 322 pump with a Kinetex 5u EVO C18 100 Å column (150 mm x 21.2 mm, 5 µm; Phenomenex). Gas chromatography-mass spectrometry (GC-MS) analysis was performed on a Shimadzu GC-17A equipped with a QP5050A GC-MS detector and DB-5 MS fused silica column (30 m x 0.25 mm, 0.25 µm). The injector was held at 250 °C and the interface at 280 °C. GC analysis was performed on a Shimadzu TRACERA with a BID detector and DB-5 MS fused silica column (30 m x 0.25 mm, 0.25 µm). For chiral GC analysis, a β-DEX column was used and both the injector and detector were held at 230 °C. NMR spectra were obtained using an Agilent DD2 spectrometer operating at 500 MHz for ^{1}H or 126 MHz for ^{13}C NMR.

2.2 Enzymes and Molecular Biology

Proteins were stored in Tris (50 mM, pH 7.4) containing 50% v/v glycerol at -20 °C and desalted before use using a PD-10 column (GE Healthcare). HaPuR was provided by Dr. S. G. Bell, produced using methods previously described.[3] The DNA for the CYP199A4 mutants was provided by Dr. S. G. Bell and Prof. J. J. De Voss from the University of Queensland.[20]

The media solutions used for cell growths are listed in Table 1.

Table 1: Growth media constituents.

Medium	**Constituents (L^{-1})**
LB	tryptone (10 g), yeast extract (5 g), NaCl (10 g)
SOC	tryptone (20 g), yeast extract (5 g), $MgCl_2$ (1 g), NaCl (0.5 g), KCl (0.2 g), glucose (0.2% w/v)
2x YT	tryptone (16 g), yeast extract (10 g), NaCl (5 g)
Trace Elements	Na_2EDTA(20.1 g), $FeCl_3.6H_2O$ (16.7 g), $CaCl_2.H_2O$ (0.74 g), $CoCl_2.6H_2O$ (0.25 g), $ZnSO_4.7H_2O$ (0.18 g), $MnSO_4.4H_2O$ (0.132 g), $CuSO_4.5H_2O$ (0.10 g)
EMM	K_2HPO_4 (7 g), KH_2PO_4 (3 g), $(NH4)_2SO_4$ (1 g), Na_3Citrate (0.5 g), $MgSO_4$ (0.1 g), 20% glucose (20 mL)

2.2.1 Production and Purification of CYP199A4 Enzymes

BL21(DE3) *E. coli* competent cells were transformed with a pET28 plasmid harbouring the appropriate wild-type (WT) or mutant *CYP199A4* gene and grown on an LB plate containing 30 mg L^{-1} kanamycin.[3] A single colony was used to inoculate 500 mL of 2x YT media containing 30 mg L^{-1} kanamycin (2x YT_{kan}) to a total of 3 L $2YT_{kan}$ and grown at 37 °C and 110 rpm overnight. The incubation temperature was lowered to 18 °C for 30 min before the addition of 0.02% v/v benzyl alcohol and 2% v/v ethanol. After a further 30 min, protein expression was induced by the addition of 0.1 mM IPTG (from a 0.5 M stock in water) and the culture grown for a further 48 h to 72 h. The red cell pellet was harvested by centrifugation (5000 *g*, 10 min) and resuspended in 200 mL buffer T (50 mM Tris, pH 7.4, 1 mM DTT). The cells were lysed by sonication using an Autotune CV334 Ultrasonic Processor equipped with a standard probe (136 mm x 13 mm; Sonics and Materials, US) using 60 x 20 s pulses with 40 s intervals. The cell debris was removed by centrifugation (30 000 *g*, 30 min, 4 °C) and the protein was fractionated from the supernatant using ammonium sulfate precipitation (0-25% and 25-60% fractions). The protein pellet was redissolved in buffer T and a Sephadex G-25 Coarse grain column (250 mm x 40 mm; GE Healthcare) pre-equilibrated with the same buffer was used to desalt the protein. The protein was loaded onto a DEAE Sepharose column (XK50, 200 mm x 40 mm; GE Healthcare) and eluted using a linear salt gradient of 100 mM to 400 mM KCl in buffer T at a flow rate of 6 mL min^{-1}. The red-coloured fractions were combined and concentrated using ultrafiltration (10 kDa exclusion membrane). The protein was then desalted using a Sephadex G-25 Medium grain column (250 mm x 40 mm; GE Healthcare). The desalted protein was loaded onto a Source-Q ion-exchange column (XK26, 80 mm x 30 mm; GE Healthcare)

coupled to an AKTA pure and eluted using a linear salt gradient from 0 mM to 250 mM KCl in buffer T. Fractions with $A_{419}/A_{280} > 2$ were combined and concentrated using ultrafiltration. The protein concentration was determined using $\epsilon_{419} = 119\ \text{mM}^{-1}\ \text{cm}^{-1}$.[3]

2.2.2 Production and Purification of HaPux

BL21(DE3) competent cells transformed with pETDuet-*HaPux* and grown on an LB plate containing 100 mg L^{-1} ampicillin.[3] A single colony was used to inoculate 500 mL 2x YT containing 100 mg L^{-1} ampicillin (2x YT_{amp}) to a total of 5 L of 2x YT_{amp} and grown at 37 °C and 110 rpm overnight. The incubation temperature was lowered to 18 °C for 30 min before the addition of 0.02% v/v benzyl alcohol and 2% v/v ethanol. After a further 30 min, protein expression was induced by the addition of 0.1 mM IPTG and the culture grown for a further 48 h to 72 h. The brown cell pellet was harvested by centrifugation (5000 *g*, 10 min) and resuspended in 300 mL 10 mM, pH 7.4 Tris buffer containing 20% v/v glycerol, 2 mM DTT, 1% v/v β-mercaptoethanol, 1 mg mL^{-1} lysozyme and 2 mL Tween. After stirring for 1 h at 4 °C on ice, the cells were lysed by sonication using 60 x 20 s pulses with 40 s intervals. The cell debris was removed by centrifugation (30 000 *g*, 30 min, 4 °C). The protein was loaded onto a DEAE Sepharose column (XK50, 200 mm x 40 mm, GE Healthcare) and eluted using a linear salt gradient of 150 to 300 mM KCl in buffer T at a flow rate of 6 mL min^{-1}. The brown-coloured fractions were combined and concentrated using ultrafiltration (5 kDa exclusion membrane). The protein was then desalted using a Sephadex G-25 Medium grain column (250 mm x 40 mm; GE Healthcare) pre-equilibrated with buffer T. The desalted protein was loaded onto a Source-Q ion-exchange column (XK26, 80 mm x 30 mm; GE Healthcare) AKTA pure and eluted using a linear salt gradient from 0 to 300 mM KCl in buffer T. Fractions with $A_{325}/A_{280} > 0.65$ were combined and concentrated using ultrafiltration. The protein concentration was determined using $\epsilon_{416} = 11.2\ \text{mM}^{-1}\ \text{cm}^{-1}$.[3]

2.2.3 Construction of the *In Vivo* Systems

pET28 plasmids harbouring the genes encoding the CYP199A4 mutants were digested with *Nco* I and *Hin*d III. The mutant CYP199A4 genes were purified by agarose gel electrophoresis and ligation of the extracted DNA with pRSFDuet-*HaPux* (which was digested with *Nco* I and *Hin*d III) was performed using T4 DNA ligase.[3]

2.3 Substrate Binding Assays

The WT and mutant CYP199A4 enzymes were diluted to ≈ 1 µM using 50 mM, pH 7.4 Tris buffer and their UV/Vis spectra were recorded. Aliquots of substrate (1 µL) from a 100 mM stock solution (in ethanol or DMSO) were added to 500 µL of the protein until the shift from low-spin (LS) (420 nm) to high-spin (HS) (390 nm) had stopped. The spectra of camphor-free and camphor-bound $P450_{cam}$ from ≈ 0% to ≈ 100% HS was used to estimate the % HS of the CYP199A4 enzymes.

The WT and mutant CYP199A4 enzymes were diluted to ≈ 2 µM using 50 mM, pH 7.4 Tris buffer. An aliquot of substrate (from 0.5 µL up to 5.0 µL) from either a 1, 10 or 100 mM stock solution was added to 2.5 mL of protein. The sample was mixed and the peak-to-trough difference in absorption was recorded on a UV/Vis spectrophotometer from 300 to 600 nm. Further aliquots of substrate were added until the peak-to-trough difference in absorption did not increase any further. To determine the dissociation constant, K_d, the difference in absorption was plotted against the substrate concentration and fitted to the hyperbolic equation (1):

$$\Delta A = \frac{\Delta A_{max} \times [S]}{K_d + [S]} \tag{1}$$

where ΔA is the peak-to-trough absorption difference, ΔA_{max} is the maximum absorption difference, and [S] is the substrate concentration. For the substrates which exhibited tight-binding, the data was fitted to the tight-binding (Morrison) quadratic equation (2):

$$\Delta A = \Delta A_{max} \times \frac{[E] + [S] + K_d - \sqrt{([E] + [S] + K_d)^2 - 4[E][S]}}{2[E]} \tag{2}$$

where ΔA is the peak-to-trough absorption difference, ΔA_{max} is the maximum absorption difference, [S] is the substrate concentration and [E] is the enzyme concentration.

2.4 *In Vitro* NADH Activity Assays

NADH activity assays were performed by preparing a 1.2 mL mixture containing 0.5 µM of a CYP199A4 enzyme, 5 µM ferredoxin (HaPux), 1 µM ferredoxin reductase (HaPuR) and oxygenated 50 mM, pH 7.4 Tris buffer. The mixture was equilibrated at 30 °C for 2 min before adding ≈ 320 µM NADH (A_{340} ≈ 2.0) and monitoring the

absorbance at 340 nm using a UV/Vis spectrophotometer (Figure 18). The substrate was then added to a final concentration of 1 mM. The rate of NADH turnover was calculated using the gradient of the plot of A_{340} against time and $\epsilon_{340} = 6.22$ mM^{-1} cm^{-1}. As 4-methoxynitrobenzene absorbs strongly at 340 nm and its oxidation product 4-nitrophenol absorbs strongly at 410 nm, the absorbance at 410 nm was monitored for this particular substrate. The rate of product formation was calculated using the gradient of the plot of A_{410} against time and $\epsilon_{410} = 18.3$ mM^{-1} cm^{-1}.

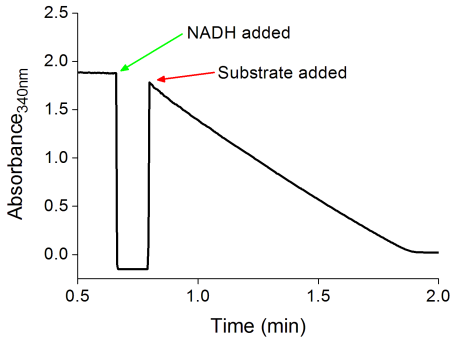

Figure 18: An example of an *in vitro* NADH turnover with 4-vinylbenzoic acid monitored at 340 nm over time.

The concentration of hydrogen peroxide generated during the NADH turnovers due to uncoupling was determined using a horseradish peroxidase (HRP)/phenol/4-aminoantipyrine (4-AP) assay.[97] To 400 µL of the turnover incubation mixture was added 200 µL of a solution of 50 mM phenol (pH 7.4, Tris buffer) and 200 µL of 5 mM 4-AP (pH 7.4, Tris buffer). The absorbance of the resulting mixture at 510 nm was set to zero, and 1 µL of a 20 mg mL^{-1} solution of HRP was added. The absorbance at 510 nm was recorded immediately. The peroxidase-mediated oxidation of phenol by hydrogen peroxide and resulting reaction with 4-AP generates a quininoneimine that absorbs strongly at 510 nm ($\epsilon = 6580$ M^{-1} cm^{-1}). The concentration of the quinoneimine, in µM, is calculated using equation (3):

$$[quinoneimine] = \frac{A_{510} \times 10^6}{6580} \tag{3}$$

As 2 molecules of hydrogen peroxide are needed to form the quinone and the incubation mixture was diluted 2-fold (400 µL to 800 µL), the concentration of peroxide formed is then calculated using equation (4):

$$[H_2O_2] = 4 \times \frac{A_{510} \times 10^6}{6580} \tag{4}$$

2.5 *In Vivo* Activity Assays

pETDuet-*HaPuR* and the pRSFDuet-*HaPux-CYP199A4* plasmid harbouring the appropriate WT or mutant *CYP199A4* gene were both transformed into competent BL21(DE3) cells and grown on LB plates containing 100 mg L^{-1} ampicillin and 30 mg L^{-1} kanamycin.[3] A single colony was used to inoculate 500 mL 2x $YT_{amp/kan}$ containing 1.5 mL trace elements solution and grown at 37 °C and 110 rpm overnight. The incubation temperature was lowered to 18 °C for 30 min before the addition of 0.02% v/v benzyl alcohol and 2% v/v ethanol. After a further 30 min, protein expression was induced by the addition of 0.1 mM IPTG and the culture grown for a further 24 h. The cells were harvested by centrifugation (5000 *g*, 10 min).

For large scale *in vivo* turnovers, the harvested cells were resuspended in 1 L of *E. coli* minimal media (EMM). This culture was split into 200 mL aliquots in 2 L baffled flasks. Substrate, 0.5 mM, was added to each flask and the whole-cell reaction mixtures were shaken at 160 rpm and 30 °C. Additional substrate (0.5 mM) was added after 0.5, 1, 2 and 3 h. After 2 h, 1% v/v glucose (20% in water) was added, and a 1 mL aliquot was removed for analysis after 4 h. Finally, after 6 h, 2 mM of substrate, 1% v/v glucose and 2.5% v/v PBS was added and the whole-cell reaction mixture left to shake for a further 16 h. The cell debris was then removed by centrifugation (5000 *g*, 10 min, 4 °C).

For small scale *in vivo* turnovers, the resuspended cells were split into 15 mL aliquots of EMM. Substrate, 2 mM, was added and the whole-cell reaction mixtures were shaken at 160 rpm and 30 °C. After 3 and 18 h, a 1 mL aliquot was removed for analysis.

2.6 Analysis of Metabolites

The turnovers were analysed via HPLC or GC-MS. For HPLC analysis, 150 µL of the reaction mixture was mixed with 50 µL of AcCN and 2 µL of internal standard (20 mM 9-hydroxyfluorene in ethanol) and used directly for analysis. Samples were eluted with a 0-50%, 20-50% or 20-95% gradient of AcCN in water with 0.1% trifluoroacetic acid (TFA).

For GC-MS analysis, 990 µL of the reaction mixture was mixed with 10 µL of internal standard. For acids and alcohols which required derivatisation, the reaction mixture was acidified with 3 µL of 3 M HCl. The mixture was extracted three times with 400 µL of ethyl acetate. The combined organic extracts were used directly for GC-MS analysis where derivatisation was not required. Where derivatisation was required, the

extracts were dried over $MgSO_4$ and concentrated under a stream of nitrogen. The sample was dissolved in 200 µL anhydrous AcCN and 30 µL of BSTFA/TMCS (99:1) was added. The mixture was left to react for 2 h at 37 °C to produce the trimethylsilyl ester of the carboxylic acid group and trimethylsilyl ether of the alcohol, if present. This reaction mixture was then used for GC-MS analysis. For the acids and compounds which required derivatisation, the oven temperature was held at 120 °C for 3 min and then increased at 10 °C min^{-1} up to 220 °C before being held for a further 7 min. For all other substrates, the oven temperature was initially held at 60 °C for 3 min and increased at 10 °C min^{-1} up to 140 °C. This temperature was held for 5 min and then increased at 25 °C min^{-1} up to 220 °C before being held for 1 min.

Products were calibrated against authentic product samples where available (Figure 19). Where these were unavailable, the coupling was estimated based on the closest available compound. For example, 4-hydroxyacetophenone was used to calibrate for the product concentrations of 4-(hydroxymethyl)acetophenone. When large scale *in vivo* turnovers were used to generate the oxidation products in a higher yield, the cell debris was removed by centrifugation. The supernatant was acidified with 32% HCl to pH ≈ 2.5 and extracted three times with ethyl acetate. The combined organic extracts were washed twice with saturated brine solution, dried over $MgSO_4$ and concentrated under reduced pressure. The crude product was dissolved in a minimum volume of 20% AcCN in water and isolated and purified by semi-preparative HPLC, eluting with a 0-50%, 20-45% or 20% isocratic gradient of AcCN in water with 0.1% TFA. The identities of the products were confirmed via GC-MS or NMR analysis.

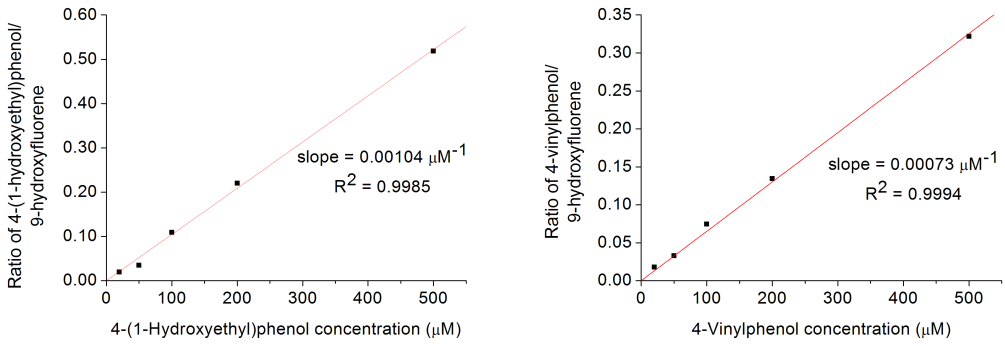

(a) (b)

Figure 19: An example of calibration curves used in determining the amount of product formed in CYP199A4 turnovers. The calibration curves for (a) 4-(1-hydroxyethyl)phenol and (b) 4-vinylphenol have been shown.

2.7 Chiral Product Synthesis

4-(1-Hydroxyethyl)acetophenone: To a stirring solution of 1,4-diacetylbenzene (100 mg, 0.6 mmol) in ethanol (4 mL) was added portionwise sodium borohydride (23 mg, 0.6 mmol) over 5 min. The reaction was monitored by GC-MS.

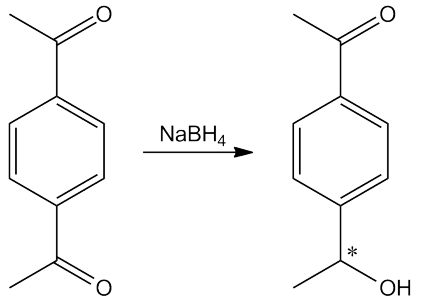

4-(1-Hydroxyethyl)benzaldehyde: To a stirring solution of 4-acetylbenzaldehyde (100 mg, 0.7 mmol) in methanol (4 mL) was added portionwise sodium borohydride (50 mg, 1.4 mmol) over 5 min. GC-MS analysis of the reaction mixture revealed that all of the 4-acetylbenzaldehyde starting material had been consumed after 30 min, and the sole product was the twice reduced diol 4-(1-hydroxyethyl)benzyl alcohol. The reaction mixture was quenched with 3 drops of water and concentrated under reduced pressure to give 4-(1-hydroxyethyl)benzyl alcohol. 4-(1-Hydroxyethyl)benzyl alcohol (1 mmol), TEMPO (11 mg, 0.1 mmol) and TBACl (19 mg, 0.1 mmol) were suspended in 1:1 DCM/aqueous solution of $NaHCO_3$ (0.5 M) and K_2CO_3 (0.05 M) and vigourously stirred at room temperature for 5 min. NCS (100 mg, 1.1 mmol) was added and the reaction monitored by GC-MS.

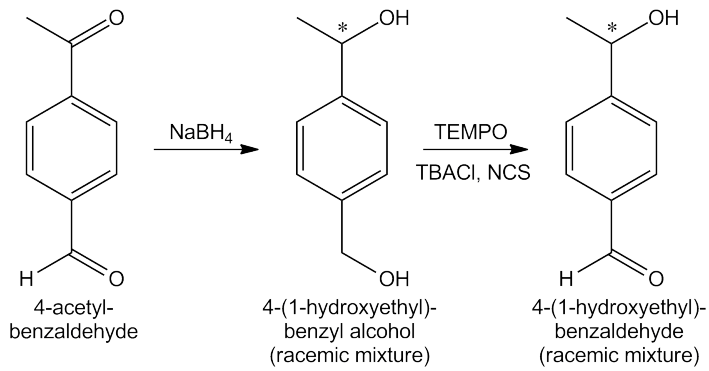

3 Reactions Catalysed by CYP199A4

3.1 Introduction

CYP199A4 preferentially binds and exclusively demethylates *para*-substituted methoxybenzoic acids at the *para*-position.[78] The enzyme has very high affinity for 4-methoxybenzoic acid (K_d = 0.28 µM, > 95% shift), which it oxidises to 4-hydroxybenzoic acid at a rate of 1219 min^{-1} with 91% coupling efficiency. CYP199A4 also exhibits high activity and affinity for closely related benzoic acid substrates.[20,79,87] As an example, replacement of the *para*-methoxy substituent with a methyl group does not significantly alter binding; the methyl derivative binds tightly to CYP199A4 (K_d = 0.66 µM, 70% spin-state shift), albeit more weakly than 4-methoxybenzoic acid. Replacement with a larger ethyl (K_d = 0.34 µM, > 95% shift) or even isopropyl group (K_d = 0.29 µM, > 95% shift) induces only very small changes in binding affinity. These alkyl derivatives are rapidly oxidised by CYP199A4 with ≈ 90% coupling efficiency, and demonstrate the enzyme's hydroxylation and desaturation activities.[79]

Substrates including 4-methylthio- and 4-methylamino-benzoic acid, in which the substituents incorporate a sulfur or nitrogen atom rather than the oxygen atom of 4-methoxybenzoic acid, have also been tested with CYP199A4 (Figure 20).[87] The binding affinity of the enzyme for 4-methylthio- and 4-methylamino-benzoic acid remained relatively high (K_d = 2.3 µM and 1.6 µM, respectively), and these substrates were turned over with high activity and efficiency (1175 min^{-1}, 83% and 669 min^{-1}, 64%, respectively). Interestingly, the sulfur-containing analogue underwent heteroatom oxidation while a dealkylation product was observed for the nitrogen-containing analogue, showing that CYP199A4 is capable of catalysing other P450 catalytic oxidations on suitably *para*-substituted benzoic acids.[87]

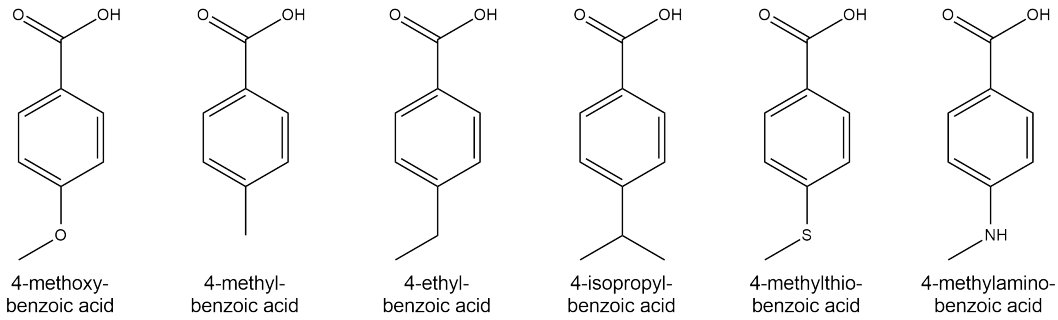

Figure 20: A selection of substrates tested with CYP199A4.

To further explore the substrate binding properties and activity of CYP199A4, the enzyme will be tested with a series of benzoic acids containing different function-

alities at the *para*-position including an ester (4-acetoxy-), alkene (4-vinyl-), alkyne (4-ethynyl-), amide (4-acetamido-), aldehyde (4-formyl-) and ketone (4-acetyl-benzoic acid, Figure 21). As these substrates involve only moderate structural changes from 4-methoxybenzoic acid, the interactions of the substrate carboxylate and benzene ring with active site amino acids should remain intact and hold the *para*-substituent above the heme iron for selective oxidation. This will enable the effect of the *para*-substituent on substrate binding to be further investigated, and for the potential oxidative activities of CYP199A4, including aldehyde oxidation with 4-formylbenzoic acid and alkene epoxidation with 4-vinylbenzoic acid, to be explored.

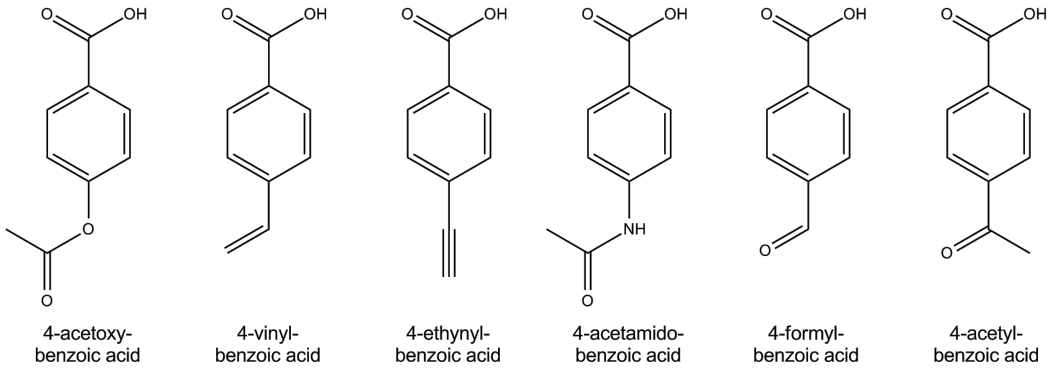

Figure 21: Benzoic acid substrates of CYP199A4.

3.2 Results

4-Vinylbenzoic acid induced a large type I spin-state shift (80%, Figure 22a) and bound tightly to CYP199A4 ($K_{\mathrm{d}} = 0.46$ µM, Figure 23a). As this substrate differs from 4-ethylbenzoic acid by only a double bond between the α- and β-carbons, it is likely that the interactions facilitating tight-binding of 4-ethylbenzoic acid to the active site of CYP199A4 remain intact when the vinyl derivative is bound.

4-Ethynylbenzoic acid, which induced a 70% spin-state shift (Figure 22b), bound over 2-fold more weakly than 4-vinylbenzoic acid ($K_{\mathrm{d}} = 1.2$ µM, Figure 23b). The large spin-state shift suggests that the alkyne functionality is positioned close enough to the heme centre to displace the distal water ligand. However, the weaker binding indicates that the interactions of the substrate binding pocket with the linear alkyne are less favourable than those with the "bent" ethyl, vinyl and methoxy substituents.

A smaller shift (25%) and comparably weaker binding to the enzyme was observed with 4-formylbenzoic acid ($K_{\mathrm{d}} = 48$ µM, Figure 22c and 23c). This substrate shares features of both 4-vinyl- and 4-methoxy-benzoic acid; it differs from 4-vinylbenzoic acid by only an oxygen atom, and the positions of the substituent's oxygen and carbon atoms have effectively been interchanged with those of the methoxy group. Thus, we expect that all three substrates should bind in similar conformations within the active site. The smaller shift and weaker binding observed with 4-formylbenzoic acid suggests that binding is suboptimal for this substrate. It is possible that the carbonyl oxygen interacts with the heme iron or interferes with removal of the water ligand.

Addition of the ketone analogue 4-acetylbenzoic acid to CYP199A4 red-shifted the low-spin Soret band at 418 nm by ≈ 1 nm (Figure 22d). In spite of this shift, a type I difference spectrum with a characteristic peak at 390 nm and trough at 420 nm was observed for 4-acetylbenzoic acid (Figure 23d). As the substrate absorbs very strongly at 250 nm and a shoulder of this band interfered with the increase in absorbance at 390 nm, only the decrease in absorbance at 420 nm was used in the determination of the dissociation constant for 4-acetylbenzoic acid. The enzyme concentration used was also increased to approximately twice the normal concentration (4.1 µM) due to the small shift induced by this substrate. 4-Acetylbenzoic acid was found to bind over 2-fold more weakly than the aldehyde 4-formylbenzoic acid ($K_{\mathrm{d}} = 140$ µM). As the aldehyde derivative did not bind very tightly, it follows that the same may be true of the ketone derivative. The oxygen of 4-acetylbenzoic acid could also interact with the heme iron, resulting in the red-shift, and interfere with displacement of the water molecule and substrate binding.

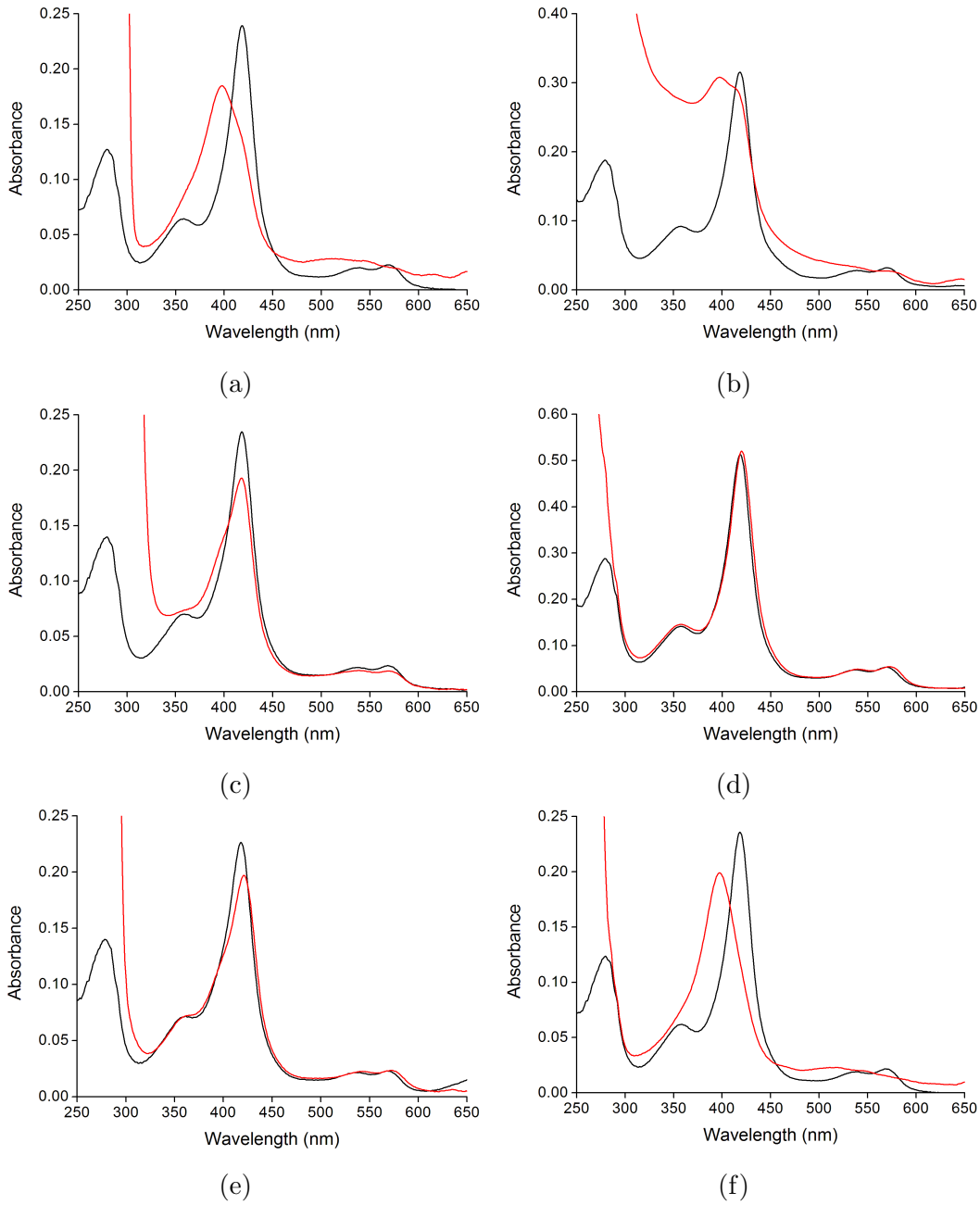

Figure 22: Spin-state shifts of CYP199A4 with (a) 4-vinylbenzoic acid (b) 4-ethynylbenzoic acid (c) 4-formylbenzoic acid (d) 4-acetylbenzoic acid (e) 4-acetamidobenzoic acid and (f) 4-acetoxybenzoic acid.

4-Acetamidobenzoic acid shifted the Soret band from 418 nm → 421 nm on binding to CYP199A4 (Figure 22e). The absolute and difference spectra, where the latter had a trough at 414 nm and peak at 432 nm, were both representative of type II binding (Figure 23e). Type II binding is generally the result of direct coordination of strong ligands such as nitrogen to the heme iron, giving a six-coordinate complex. Nitrogen-containing compounds, typically in the form of imidazoles, pyridines and amines, have been reported to red-shift the Soret band from anywhere between 2-8 nm.[98–101] The relatively weak binding observed for 4-acetamidobenzoic acid (K_d = 62 µM) suggests

that the nitrogen atom may not be positioned in the best location for binding to the heme.

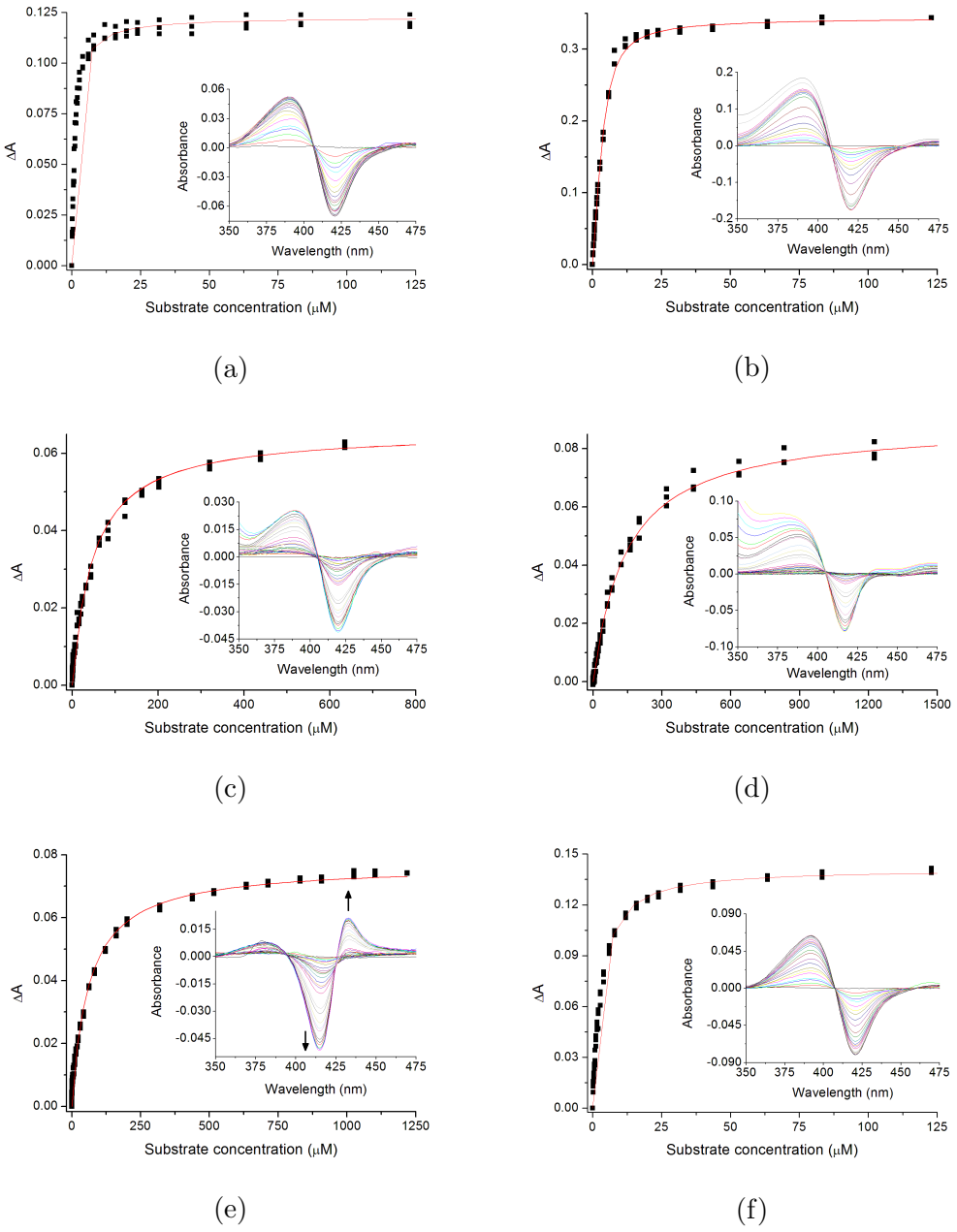

Figure 23: Dissociation constant analyses of CYP199A4 with (a) 4-vinylbenzoic acid (b) 4-ethynylbenzoic acid (c) 4-formylbenzoic acid (d) 4-acetylbenzoic acid† (e) 4-acetamidobenzoic acid and (f) 4-acetoxybenzoic acid. †The enzyme concentration was doubled (4.1 μM) due to the small shift induced by this substrate.

Interestingly, despite being larger than the ketone analogue and very similar in size to the amide analogue, 4-acetoxybenzoic acid induced a large type I spin-state shift (95%) and bound tightly to CYP199A4, with a dissociation constant of 2.5 μM (Figure 22f and 23f). The type I shift observed indicates that the substrate is unlikely to be coordinated to the heme through one of its oxygen atoms, and suggests that the terminal methyl

group of 4-acetoxybenzoic acid may be bound closest to the heme where it can induce complete dissociation of the water ligand.

The NADH oxidation and product formation rates were determined for each of the above *para*-substituted benzoic acids. These provide a measure of the catalytic activity of CYP199A4 towards each substrate. Unless otherwise stated, the product of each CYP199A4-catalysed turnover was identified by HPLC coelution of the turnover with an authentic sample of the product. Products were calibrated against these authentic product standards where available. When an authentic sample was unavailable, the coupling was estimated based on the closest available compound. For example, for 4-vinylbenzoic acid for which no authentic standard was available, the product peak was calibrated against the derivatised substrate, and this was then used to estimate the concentration of the derivatised product peak using GC-MS analysis.

The rate of NADH oxidation by CYP199A4 with 4-acetoxybenzoic acid was 385 nmol.nmol-P450^{-1}.min^{-1} (henceforth abbreviated to min^{-1}), over 3-fold slower than that observed with 4-methoxybenzoic acid (Table 2).[78] However, this compound was discovered to undergo ester hydrolysis to 4-hydroxybenzoic acid under the reaction conditions. Hydrolysis also occurred in the absence of the turnover constituents (CYP199A4, HaPux, HaPuR and NADH) in only aqueous buffer (50 mM Tris, pH 7.4). As the hydrolysis was fast, no CYP199A4 oxidation product could be confirmed for 4-acetoxybenzoic acid (Appendix A1).

Table 2: Substrate binding and *in vitro* turnover data for CYP199A4 with benzoic acid substrates. The data are given as mean ± S.D. with $n \geq 3$. Rates are given as nmol.nmol-P450^{-1}.min^{-1}. The average leak rate was 9.0 nmol.nmol-P450^{-1}.min^{-1}.

Substrate	% HS	K_d (μM)	NADH (min^{-1})	PFR (min^{-1})	Coupling (%)	H_2O_2 (%)
4-methoxyBA[78]	> 95	0.28 ± 0.01	1340 ± 28	1219 ± 120	91 ± 2	2 ± 0.2
4-vinylBA	80	0.46 ± 0.03	517 ± 3	220 ± 20	43 ± 4	2.5 ± 0.4
4-ethynylBA	70	1.2 ± 0.3	171 ± 6	110 ± 6	66 ± 1	19 ± 2
4-formylBA	25	48 ± 2	130 ± 5	10 ± 0.4	8 ± 0.3	1.5 ± 0.3
4-acetylBA	red-shift	140 ± 5	407 ± 4	260 ± 24	65 ± 6	4.7 ± 0.6
4-acetoxyBA	95	2.5 ± 0.1	385 ± 9	-[a]	-[a]	2 ± 0.2
4-acetamidoBA	type II	62 ± 2	18 ± 1	-[a]	-[a]	1.5 ± 0.1

[a]No product formation.

No product could be detected for 4-acetamidobenzoic acid (Appendix A2). Addition of this substrate to CYP199A4 resulted in an NADH oxidation rate of only 18 min^{-1}, which is not too dissimilar from the leak rate of the system in the absence of substrate.

Substrates which induce a type II binding spectrum commonly act as inhibitors by preventing reduction of the heme iron and oxygen binding, and it appears that 4-acetamidobenzoic acid may fall within this category.[98,101–103]

Of the substrates which gave rise to product, the slowest rate of NADH oxidation was observed for 4-formylbenzoic acid (129 min^{-1}). Poor coupling of redox equivalents to product formation (8%) resulted in the production of low levels of terephthalic acid at 10 min^{-1} (Figure 24). As the hydrogen peroxide levels detected in the turnover using a horseradish peroxide-based assay were very low, this suggests that the unproductive redox equivalents were predominantly lost to oxidase uncoupling.

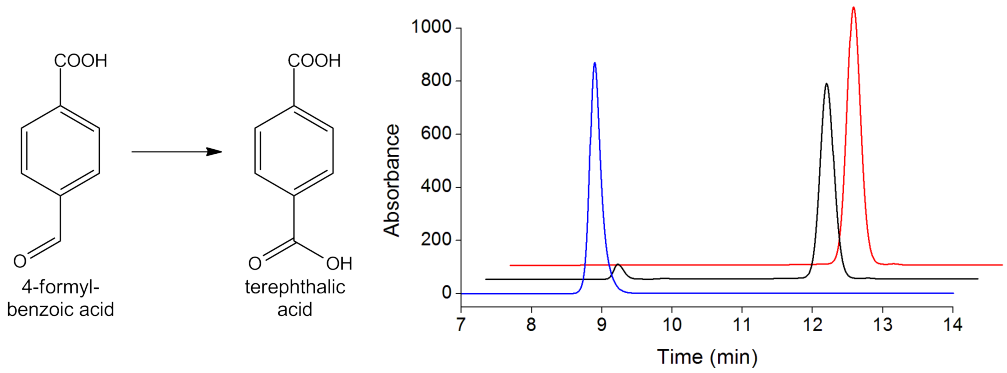

Figure 24: The oxidation of 4-formylbenzoic acid to terephthalic acid by CYP199A4. The HPLC analysis of the turnover is in black, 4-formylbenzoic acid substrate control (t_R = 11.8 mins) in red and terephthalic acid product control (t_R = 8.9 mins) in blue. For clarity the chromatograms have been offset along the x and y axes.

Additionally, it is possible that the carbonyl oxygen of the formyl derivative may be interacting with the heme iron to hinder efficient oxygen binding and substrate oxidation. In spite of the low oxidation activity of CYP199A4 for 4-formylbenzoic acid, these results reveal that aldehyde oxidation can be added to the enzyme's oxidative activities.

The NADH oxidation rate of CYP199A4 with 4-ethynylbenzoic acid was not much faster than the enzyme with 4-formylbenzoic acid (171 min^{-1}). However the coupling efficiency of the reaction was much higher (66%), generating 4-carboxyphenylacetic acid at a rate of 110 min^{-1} (Figure 25). The majority of the unproductive redox equivalents (19%) were lost to peroxide uncoupling. This level of peroxide uncoupling is more significant than in all the other turnovers ($< 5\%$). The linear nature of the alkyne substituent could potentially allow increased water access to the active site, which has been reported as a cause of increased uncoupling.[9,22,23] P450s are believed to oxidise alkynes to ketenes, which are hydrolysed to their corresponding carboxylic acids (Figure 10). The oxidation of 4-ethynylbenzoic acid to 4-carboxyphenylacetic

acid by CYP199A4 is the first observation of alkyne oxidation by this enzyme.

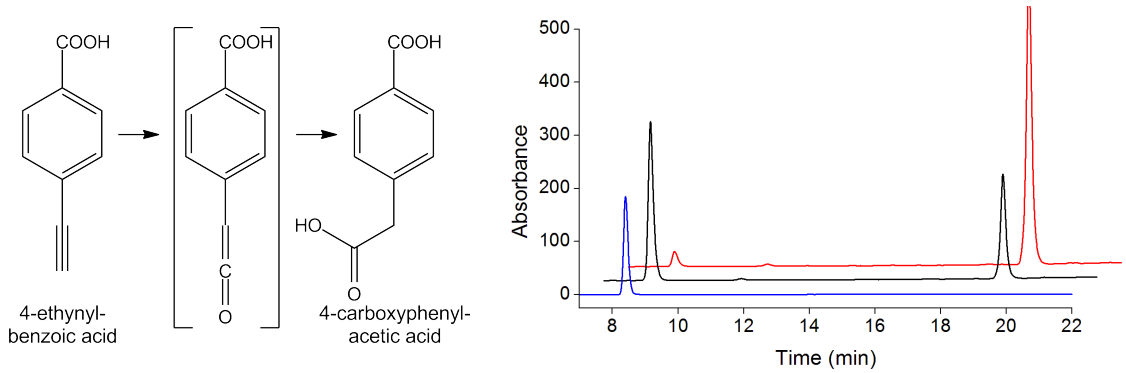

Figure 25: The oxidation of 4-ethynylbenzoic acid to 4-carboxyphenylacetic acid by CYP199A4. The HPLC analysis of the turnover is in black, 4-ethynylbenzoic acid substrate control (t_R = 19.4 mins) in red and 4-carboxyphenylacetic acid product control (t_R = 8.4 mins) in blue. For clarity the chromatograms have been offset along the x and y axes. We note that low levels of 4-carboxyphenylacetic acid are observed in the substrate control. However, turnover controls in the absence of P450 and NADH resulted in no increase in the levels of product (Appendix A3).

Of the substrates tested here, the fastest rate of NADH oxidation by CYP199A4 was observed with 4-vinylbenzoic acid (517 min^{-1}). The substrate was turned over at a rate of 220 min^{-1}. GC-MS analysis of the trimethylsilyl (TMS)-derivatised turnover showed a parent ion peak with a m/z of 236.2, in agreement with the expected product m/z of 236.3 for 4-(oxiran-2-yl)benzoic acid (Appendix A4). To confirm the identity of the product, the epoxide was chemically synthesised in higher yield using an excess of hydrogen peroxide with 4-vinylbenzoic acid in the presence of manganese(II) sulfate,[104] purified via semi-prep HPLC and characterised via NMR (Appendix A5). The 4-(oxiran-2-yl)benzoic acid product also co-eluted with the CYP199A4 turnover of 4-vinylbenzoic acid using GC-MS, where identical retention times and fragmentation patterns in the mass spectra were observed (Figure 26 and Appendix A4). The oxidation of 4-vinylbenzoic acid to 4-(oxiran-2-yl)benzoic acid demonstrates the enzyme's ability to catalyse alkene epoxidation, albeit less efficiently than the demethylation of 4-methoxy-substituted benzoic acids.[78] We note that peroxide uncoupling was much lower for 4-vinylbenzoic acid (2.5%) when compared to 4-ethynylbenzoic acid. This could again imply that the "bent" alkene is a better fit for the active site of CYP199A4 than the linear alkyne.

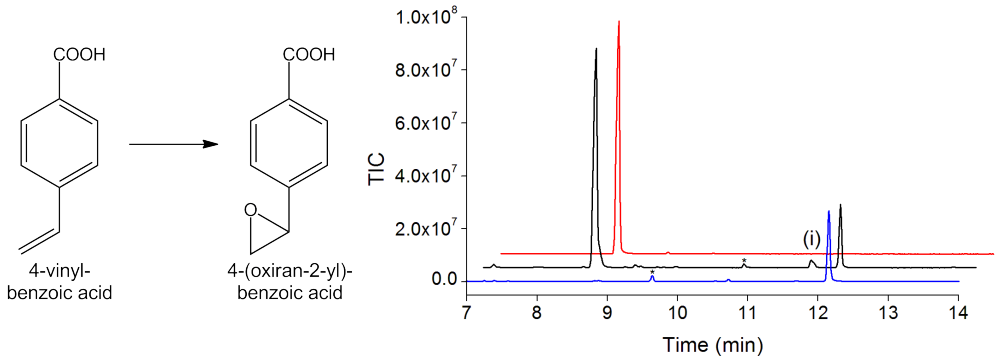

Figure 26: The oxidation of 4-vinylbenzoic acid to 4-(oxiran-2-yl)benzoic acid. The GC-MS analysis of the derivatised turnover is in black, 4-vinylbenzoic acid substrate control ($t_R = 8.6$ mins) in red and 4-(oxiran-2-yl)benzoic acid product control ($t_R = 12.2$ mins) in blue. [(i)]The m/z (236.2) and mass spectrum of this peak at 11.8 mins suggest it to be the aldehyde rearrangement product (Figure 9). For clarity the chromatograms have been offset along the x and y axes. Impurities are marked (*).

While the rate of NADH oxidation by CYP199A4 with 4-acetylbenzoic acid was slower than with the vinyl derivative (407 min^{-1} vs. 517 min^{-1}), the oxidation of 4-acetylbenzoic acid proceeded more rapidly at 260 min^{-1} because the productive enzyme turnover was more tightly coupled (65%). A single product was observed in the turnover of 4-acetylbenzoic acid (Figure 27). This was generated using a whole-cell oxidation system and isolated and purified by prep-scale HPLC. The product was identified by NMR as 4-(2-hydroxyacetyl)benzoic acid, where a characteristic 2H singlet at 4.82 ppm was observed (Appendix A6). We note here that while the addition of 4-acetylbenzoic acid to CYP199A4 resulted in a small red-shift of the Soret peak at 418 nm, a type I difference spectrum was observed (Figure 22d and 23d). This indicates that while the oxygen atom may interact with the heme iron, the substrate does not act as an inhibitor of CYP199A4 and the methyl group must be suitably positioned for oxidation.

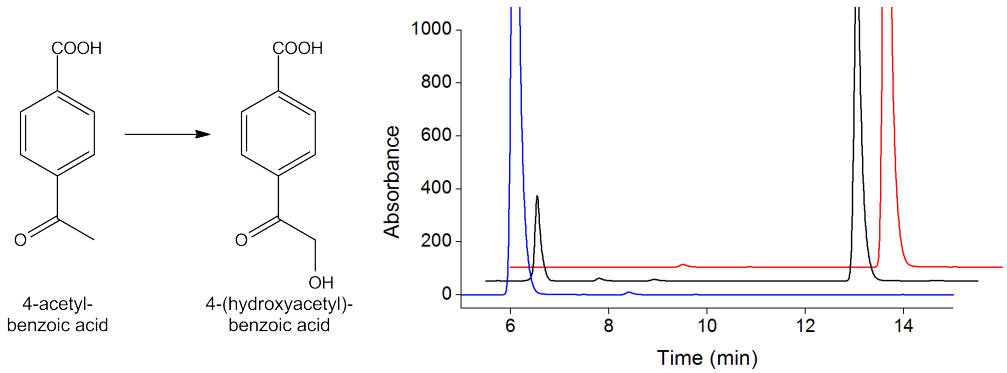

Figure 27: The oxidation of 4-acetylbenzoic acid to 4-(2-hydroxyacetyl)benzoic acid by CYP199A4. The HPLC analysis of the turnover is in black, 4-acetylbenzoic acid substrate control ($t_R = 12.8$ mins) in red and 4-(2-hydroxyacetyl)benzoic acid product control after purification by semi-prep HPLC ($t_R = 6.0$ mins) in blue. For clarity the chromatograms have been offset along the x and y axes.

3.3 Discussion

CYP199A4 binds and selectively oxidises methoxy-substituted benzoic acids and closely related substrates at the *para*-position.[20,78,79] The current work confirms that a range of *para*-substituted benzoic acids can be accommodated within the active site of CYP199A4, and the nature of the substituent clearly influences the binding affinity of the enzyme. However, the reduction in binding affinity when the *para*-substituent is modified is smaller than when the carboxy terminus is modified, for example, to an aldehyde (4-methoxybenzaldehyde) or alcohol (4-methoxybenzyl alcohol).[79,87] Larger functionalities can also be accommodated within the active site of CYP199A4, as previously suggested by the binding of 2-napthoic acid and 6-indole-carboxylic acid, albeit with reduced affinity.[79]

The results indicate that to the enzyme's known hydroxylation, demethylation, desaturation and heteroatom oxidation activities[3,78,79,87] can be added alkene epoxidation and alkyne and aldehyde oxidation. Oxidative demethylation is the most rapid reaction catalysed by CYP199A4,[3,78,79] which is followed by hydroxylation, as demonstrated by the oxidation of alkyl benzoic acids[3,79,87] and 4-acetylbenzoic acid in the current work. We note that no additional oxidation activity such as a Baeyer-Villiger rearrangement was observed in the turnover of 4-acetylbenzoic acid.[105–108] The Baeyer-Villiger oxidation involves the insertion of an oxygen atom into a C–C bond of a ketone or cyclic ketone species to give an ester or a lactone. This reaction is believed to be mediated by the nucleophilic ferric-peroxo anion in P450s, where observed.[7,109] The Baeyer-Villiger rearrangement step in the 14α-demethylation of lanosterol catalysed by members of the CYP51 family is shown in Figure 28.[110,111]

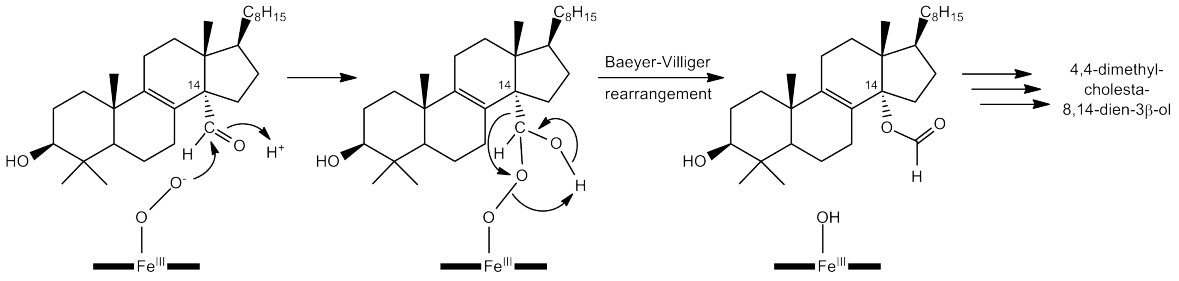

Figure 28: The Baeyer-Villiger rearrangement step in lanosterol 14α-demethylation.[110,111]

CYP199A4-catalysed alkene and alkyne oxidation occur more slowly than demethylation or hydroxylation, as exemplified by the turnovers of 4-vinyl- and 4-ethynyl-benzoic acid. Even slower still is aldehyde oxidation of 4-formylbenzoic acid. As terephthalic acid was the only product detected in the turnover of 4-formylbenzoic acid, this suggested the absence of any Dakin oxidation type chemistry. The Dakin oxidation involves

the reaction of aromatic benzaldehydes with hydrogen peroxide in the presence of a base to produce phenols (Figure 29).[112–114]

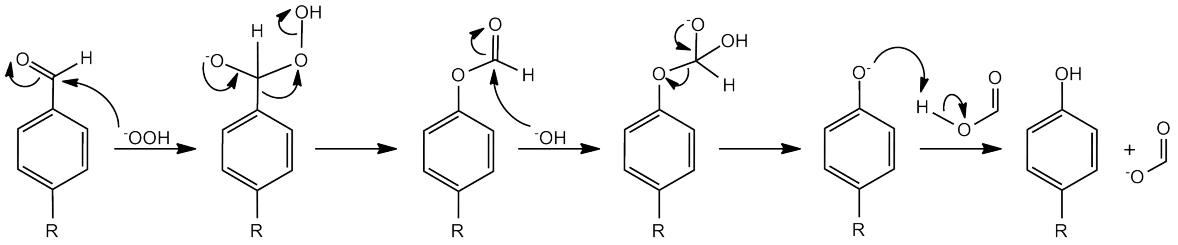

Figure 29: The mechanism of Dakin oxidation.[112,113]

With the exception of 4-ethynylbenzoic acid, the levels of hydrogen peroxide formed in these turnovers were very low in all cases, $< 5\%$ (Table 2). This suggests that the unproductive reducing equivalents have most likely been funnelled into an oxidase uncoupling event, where water is produced as the byproduct. Uncoupling due to autooxidation of the ferrous-dioxygen species is unlikely to be significant given the efficient electron transfer partners of the CYP199A4 system, and based on previous studies with other P450s.[7,115–117] Substrate binding has also been shown to significantly increase the lifetime of the ferrous-dioxygen complex and reduce the rate of autooxidation.[115,116] Additionally, as the superoxide byproduct released during autooxidation rapidly dismutates to hydrogen peroxide, the low concentrations of hydrogen peroxide detected in the CYP199A4 turnovers do not suggest significant autooxidation.[7,117] The high levels of oxidase uncoupling presumably indicates that the *para*-substituents of some of the benzoic acid derivatives tested here were not positioned close enough to the heme to be oxidised with high efficiency, or at least further away than that of 4-methoxybenzoic acid.[78]

The relative rates of substrate oxidation were also consistent with the magnitudes of the spin-state shifts observed in the enzyme. For example, 4-formylbenzoic acid which induced a small shift (25%) was oxidised slowly (10 min^{-1}) while 4-vinylbenzoic acid which induced a much larger shift (80%) was turned over much more rapidly (220 min^{-1}). As substrate binding displaces the heme-bound water ligand and triggers the first electron transfer from the redox partner to the ferric iron, the size of the spin-state shift provides an indication of the relative rates of NADH oxidation and consequently product formation.[18,118]

Overall, the results show that oxidative demethylation remains the most rapid and efficient of the reactions catalysed by CYP199A4. Importantly, they also reveal the high selectively of the enzyme for oxidation solely at the *para*-position. Therefore, the CYP199A4 system could be used to investigate the mechanisms of P450 oxidation reactions which are as yet unclear using different *para*-substituted benzoic acids.

Specifically, CYP199A4 and appropriate active site mutants of the enzyme could be used to probe the active oxidant(s) in different oxidative P450 catalytic reactions. For example, alkene and aldehyde oxidation (deformylation) have been proposed to occur via Cpd 0 and the ferric-peroxo anion, respectively. Using 4-vinyl- and 4-formyl-benzoic acid, the oxidant(s) responsible for these reactions can be investigated.

4 The Active Oxidant(s) in CYP199A4 Catalysis

4.1 Introduction

The mechanism of oxygen activation in P450s clearly implicates a proton relay or shuttle system.[91–93] As shown in Figure 30, the peroxo-anion, formed after reduction of the ferrous-dioxy complex (Figure 2), accepts a proton to give the hydroperoxy intermediate (Cpd 0). Subsequent protonation of this species triggers heterolytic O–O bond scission to give Cpd I (Figure 30).

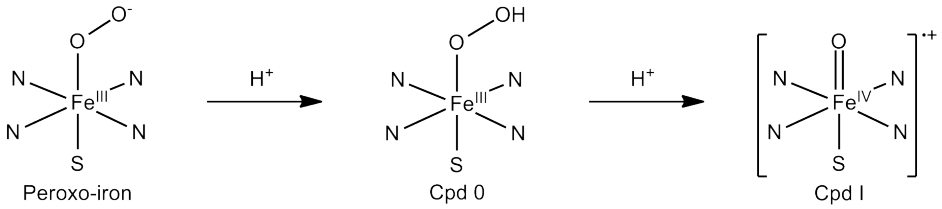

Figure 30: The reactive iron-species of P450s.

These proton transfer events are believed to involve a highly conserved "acid-alcohol" amino acid pair, typically aspartate (or glutamate) and threonine (or serine). In CYP199A4, these residues are Asp251 and Thr252 from the oxygen-binding groove of the I helix.[20] In the most-studied system, $P450_{cam}$, the conserved residues are also Asp251 and Thr252.[89,90,92,93] When oxygen binds to the ferric iron, a large conformational change is induced in the region of the I helix to which the conserved residues belong. The peptide carbonyl of Asp251 is flipped 90° relative to its previous orientation, and this is accompanied by the repositioning of Thr252 to hydrogen bond to the dioxygen molecule. These structural rearrangements open up the I helix, allowing entry of two new water molecules into the active site.[19] These "catalytic" water molecules contribute to a hydrogen bond network connecting the threonine, oxygen, and water molecules, enabling efficient proton delivery to generate Cpd I, which is widely accepted to be the active oxidant in P450 catalysis (Figure 31).[19,89,90,92,93]

4.1.1 The Conserved Alcohol Residue of P450s

Wild-type (WT) $P450_{cam}$ hydroxylates camphor at ≈ 1000 min^{-1} with almost 100% coupling efficiency.[89–92] However, when the conserved threonine is mutated ($T252A_{cam}$), while there is little change in the rate of NADH consumption, the enzyme becomes almost completely uncoupled with 95% of the reducing equivalents channelled into hydrogen peroxide formation.[89,90] It was originally suggested that Thr252 served as a

direct proton source for the hydroperoxy intermediate (Cpd 0), but this was challenged when a Thr252-OMe$_{cam}$ mutant – where the side chain OH was replaced with a methoxy group – demonstrated considerable activity.[119] Recently, it has been proposed that the conserved threonine acts as a hydrogen bond acceptor for Cpd 0, helping to stabilise this intermediate and facilitate the second proton transfer step (Figure 31).[19,120] This is consistent with the observation that P450$_{cam}$ remains highly active when Thr252 is replaced by a serine residue.[89] Thus, when threonine is mutated to an aliphatic alanine in T252A$_{cam}$, Ala252 can no longer accept a hydrogen bond from Cpd 0 to promote heterolytic O–O scission, causing this species to accumulate. Subsequent protonation on the proximal rather than distal oxygen of Cpd 0 leads to hydrogen peroxide formation rather than camphor hydroxylation.

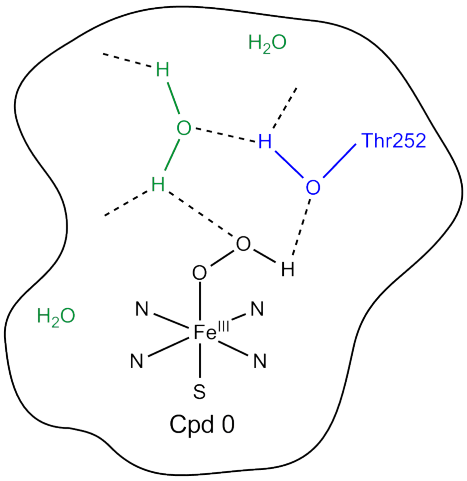

Figure 31: The interaction of the conserved threonine with Cpd 0.

While studies with P450$_{cam}$ clearly implicate Cpd I as the oxygenating species in camphor hydroxylation, experimental evidence suggests its precursors Cpd 0 and the peroxo-anion may also be involved in P450-catalysed oxidations.[26,28,30,31,44,52,56,57] This is in agreement with studies on T252A$_{cam}$ using C=C bond-containing analogues of camphor[25] and some of the early findings of Vaz and Coon on the T303A mutant of CYP2E1 with model olefin substrates (Figure 32).[26] In the presence of the native substrate, camphor, oxidation by T252A$_{cam}$ occurs at 1% of the rate of WT$_{cam}$ due to uncoupling of the reducing equivalents to peroxide. However, when the mutant was tested with 5-methylenylcamphor and 5-norbornene-2-ene, both were efficiently epoxidised at 15-20% of the rate of WT$_{cam}$ camphor hydroxylation, suggesting the involvement of another oxidant, the now more abundant Cpd 0. When Vaz and Coon tested styrene, cyclohexene, *cis*- and *trans*-butene with T303A$_{CYP2E1}$, they observed enhanced epoxidation in all cases, along with decreased allylic hydroxylation with cyclohexene and butene. However, when the same substrates were tested with the T302A mutant of CYP2B4, a significant decrease in both activities was observed, leading to

the conclusion that both Cpd 0 and Cpd I may be involved in olefin epoxidation.[26]

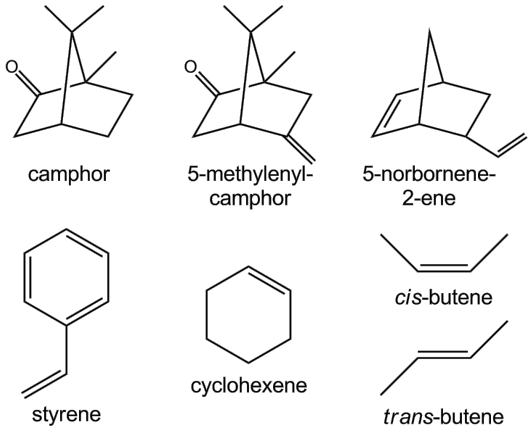

Figure 32: Alkene substrates of $T252A_{cam}$ (top) and $T303A_{CYP2E1}$ and $T302A_{CYP2B4}$ (bottom).

Studies on the T268A mutant of the fatty acid monooxygenase $P450_{BM3}$ have shown reductions in both the NADPH oxidation and product formation activities when compared to WT_{BM3}.[121,122] For example, a 3.5-fold decrease in the rate of NADPH oxidation together with poor coupling of redox equivalents to product formation was observed with lauric acid (16% vs. $\approx$ 100% for WT_{BM3}).[121] Peroxide uncoupling was determined to account for 67% of the unproductive reducing equivalents, with the remaining NADPH being funnelled into the reduction of oxygen to water rather than substrate oxidation.[121] These results suggest an important role for Thr268 in fatty acid hydroxylation, and support the involvement of Cpd I as the active oxidant. However, it was noted that $P450_{BM3}$ is less sensitive to the Thr $\rightarrow$ Ala mutation than $P450_{cam}$, where virtually no oxidation product was formed.[90,121,122] More recently, studies have demonstrated that the activity of WT_{BM3} can be maintained by the T268A mutant with certain fatty acids.[56] This suggested a possible substrate-dependence for the activity of $P450_{BM3}$, and a less critical role for the conserved threonine in this enzyme.

In a similar study to probe oxygen activation in CYP17A1, which is involved in steroidogenesis, the conserved threonine was mutated to a number of different residues.[123] These mutants were tested with three model substrates; pregnenolone was used to probe the mechanism of hydroxylation, and its oxidation product 17α-hydroxypregnenolone together with 3β-hydroxyandrost-5-ene-17β-carbaldehyde, were used to investigate acyl-carbon cleavage (Figure 33). The acyl-carbon cleavage reactions occurred at 29% and 42% of the rate of $WT_{CYP17A1}$, respectively, while hydroxylation occurred at only 6% of the rate.[123] Importantly, the ratio of aldehyde cleavage/hydroxylation activity was increased from 3.5 for $WT_{CYP17A1}$ to 25.6 for the T306A mutant, clearly suggesting that a species other than the putative ferryl radical cation may play a role in this cleavage reaction.[123]

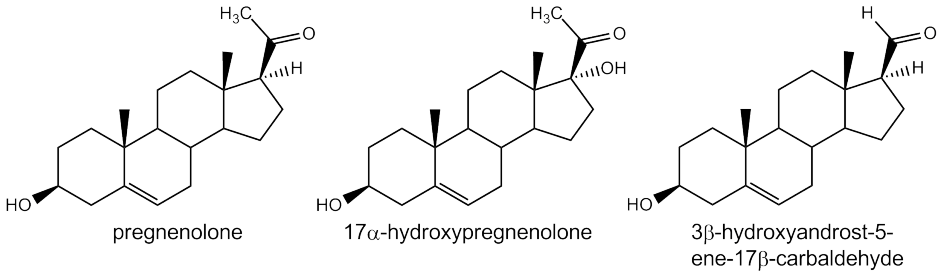

Figure 33: Substrates tested with the T306A mutant of CYP17A1.

Given their different reactivities, it is not surprising that the different oxidants may favour certain reactions over others (Chapter 1.2). Therefore, it follows that a mutation of the conserved threonine could alter the balance between the peroxo-, hydroperoxo- and ferryl-iron species and ultimately affect the outcome of substrate oxidation.

4.1.2 The Conserved Acidic Residue of P450s

Similar experiments have also been conducted for conserved aspartate or glutamate residue mutants of P450s in order to probe the mechanism of oxygen activation. Mutation of Asp251 in $P450_{cam}$ to a neutral asparagine residue ($D251N_{cam}$) resulted in drastically reduced NADH oxidation activity and camphor hydroxylation at 1% of the rate of the WT enzyme.[93] The crystal structure of WT_{cam} reveals that Asp251 interacts strongly with Lys178 and Arg186, and this is hypothesised to play an important role in the differences between the D251N mutant and WT enzyme.[19] When the peptide side chain of Asp251 flips upon oxygen binding, a strain is imposed on the I helix. The I helix moves to try and negate this strain, but movement is confined to only a small region of the helix due to the interaction of Asp251 with Lys178 and Arg186. However, in $D251N_{cam}$ such strong contacts are absent, allowing a larger degree of conformational freedom. Thus, the I-helix opens up to a lesser extent than in the WT enzyme, and there is insufficient space for new water molecules to be accommodated within the active site near Thr252 and the ferrous-dioxygen complex to establish a Thr-OH - - - O=O - - - OH_2 network.[19] Kinetic isotope and proton inventory experiments have demonstrated that this lack of ordered solvent slows delivery of the first proton to the oxygen.[93] Importantly, this implies a persistence of the ferric-peroxo anion in $D251N_{cam}$. Therefore, if a mutation at the conserved acidic residue – in which the peroxo-anion is now more abundant – were to exhibit higher oxidation activity than the corresponding WT enzyme, this could implicate the peroxo-anion in oxygen activation, demonstrating the existence of multiple active oxidants.

Other studies have found analogous reductions in the rate of NADH oxidation activity

by a conserved acidic residue mutant.[53–55,57,123–127] For example, in a recent study on the D241N mutant of CYP176A1 ($P450_{cin}$), a close analogue of $P450_{cam}$ which is unusual in that it has an asparagine residue in place of the conserved threonine,[16] the rate of cineole hydroxylation was reduced to only 2% of that of WT_{cin}, and coupling from 80% to 31%.[54] However, the binding affinity for cineole was unchanged, suggesting a largely unaltered active site.[54]

In $P450_{BM3}$, the equivalent mutation of Glu267 to glutamine ($E267Q_{BM3}$) also resulted in significant reductions in NADH oxidation and hydroxylation activity, but the extent of these changes appeared highly substrate-dependent. For example, the product formation rate was decreased to 16% of WT_{BM3} for laurate and to a mere 0.3% of WT_{BM3} for palmitate.[55] However, minimal levels of hydrogen peroxide were detected in the mutant turnovers, and only minor changes in the binding affinity were observed. An interesting observation was the altered distribution of the ω-1, ω-2 and ω-3 hydroxylation products arising from fatty acid oxidation by $E267Q_{BM3}$. In WT_{BM3}, fatty acids are predominantly hydroxylated at the ω-1 position. However, the ω-3 hydroxylation product was the major product of $E267Q_{BM3}$ oxidation. Combined with the lack of hydrogen peroxide in the mutant turnovers, these results suggested that the mutation perturbs the active site architecture of $P450_{BM3}$ such that fatty acid substrates are held further away from the heme iron, hindering efficient substrate oxidation.[55]

Given the complexity of the mechanism of oxygen activation and the vast number of P450s, it comes as no surprise that the role of the conserved residues in these enzymes, as well as the active oxidant, might vary. However, the contrasting two-state-reactivity hypothesis claims that there is predominantly only one active oxidant, Cpd I, and attributes the "appearance" of multiple oxidants in P450 reactions to the doublet and quartet spin-states of this species (Chapter 1.2).[35] Whether or not more than one oxygen-activating species exists remains an ongoing debate.

To this end, we decided to probe the mechanism of oxygen activation in CYP199A4 from the perspective of the two-oxidant model, using threonine and aspartate mutants. As the benzoic acid moiety is important for substrate binding to CYP199A4, we tested a selection of *para*-substituted benzoic acids studied in the previous chapter with $T252A_{CYP199A4}$ and $D251N_{CYP199A4}$. These substrates bind relatively tightly to $WT_{CYP199A4}$ and participate in different oxidative reactions despite minimal structural changes between them. Therefore, a comparison of the activities of the mutants with $WT_{CYP199A4}$ will enable us to gain insight into the active intermediate responsible for these reactions.

4.2 Results

4.2.1 Investigation of the Activity of T252A$_{\mathbf{CYP199A4}}$

The spin-state shifts of T252A$_{\mathrm{CYP199A4}}$ upon addition of the benzoic acid analogues were similar to those observed for WT$_{\mathrm{CYP199A4}}$ (Table 3). The shift with 4-acetoxybenzoic acid increased by 5% and those with 4-vinyl- and 4-ethynyl-benzoic acid both increased by 10%. The spin-state shifts of the remaining substrates were unchanged (Appendix B1). In general, the binding affinity was also comparable to that of the WT enzyme for most substrates (Table 3 and Appendix B3). 4-Methoxybenzoic acid bound slightly more tightly to T252A$_{\mathrm{CYP199A4}}$ (K_{d} = 0.22 µM vs. 0.28 µM). The binding affinity for 4-vinylbenzoic acid was also increased relative to the WT enzyme (K_{d} = 0.30 µM vs. 0.46 µM). A similar increase in binding was observed for 4-acetylbenzoic acid (K_{d} = 110 µM vs. 150 µM). In contrast, a small decrease in affinity was observed for 4-acetamido- (K_{d} = 76 µM vs. 62 µM), 4-formyl- (K_{d} = 54 µM vs. 48 µM) and 4-ethynyl-benzoic acid (K_{d} = 1.5 µM vs. 1.2 µM). 4-Acetoxybenzoic acid also bound slightly more weakly to T252A$_{\mathrm{CYP199A4}}$ (K_{d} = 2.8 µM vs. 2.5 µM).

Table 3: Substrate binding and *in vitro* turnover data for T252A$_{\mathrm{CYP199A4}}$. The data are given as mean ± S.D. with $n \geq 3$. Rates are given as nmol.nmol-P450^{-1}.min^{-1}. The average leak rate was 7.5 nmol.nmol-P450^{-1}.min^{-1}.

Substrate	% HS	K_{d} (µM)	NADH (min^{-1})	PFR (min^{-1})	Coupling (%)	H_2O_2 (%)
4-methoxyBA	> 95	0.22 ± 0.02	833 ± 8	570 ± 56	68 ± 5	31 ± 4
4-vinylBA	90	0.30 ± 0.02	814 ± 3	210 ± 15	26 ± 1	59 ± 3
4-ethynylBA	80	1.49 ± 0.09	306 ± 5	200 ± 15	65 ± 4	30 ± 2
4-formylBA	25	54 ± 2	56.3 ± 0.3	31 ± 2	54 ± 3	4.5 ± 0.3
4-acetylBA	red-shift	110 ± 3	447 ± 5	220 ± 12	49 ± 3	52 ± 1
4-acetoxyBA	95	2.8 ± 0.1	562 ± 3	-[a]	-[a]	49 ± 1
4-acetamidoBA	type II	76 ± 3	39 ± 1	-[a]	-[a]	2.4 ± 0.1

[a]No product formation.

The moderate changes in the spin-state shift and binding affinity suggest that mutation of the conserved threonine does not greatly perturb the active site environment of CYP199A4. Similar observations have been made for T252A$_{\mathrm{cam}}$[93] and the equivalent Thr → Ala mutants of CYP101D1[128] and CYP2D6,[52] where only minor differences in the binding affinity between the mutant and WT enzymes were observed for their native substrates.

In all cases where product was formed with the WT enzyme, the same, single product was observed in the turnovers by $T252A_{CYP199A4}$. The largest change in activity was observed for the turnover of 4-methoxybenzoic acid. The mutation reduced the rate of NADH oxidation to 833 min^{-1} and coupling to 68%, causing the rate of demethylation to be less than half that of $WT_{CYP199A4}$ at 565 min^{-1} (Table 3). The unproductive reducing equivalents ($\approx$ 31%) were channelled into the production of hydrogen peroxide. We note that these changes in coupling and product formation activity are much less severe than in $T252A_{cam}$ with camphor where, in spite of the small change in the rate of NADH oxidation, 95% of the reducing equivalents were lost to hydrogen peroxide formation.[89,90] The oxidation of 4-methoxybenzoic acid by $T252A_{CYP199A4}$ is perhaps more reminiscent of fatty acid hydroxylation by $T268A_{BM3}$, where more moderate changes in the activity are observed.[28]

The rate of NADH oxidation by $T252A_{CYP199A4}$ upon the addition of 4-acetylbenzoic acid was comparable to $WT_{CYP199A4}$ (447 min^{-1} vs. 407 min^{-1}). However, the oxidation of 4-acetylbenzoic acid to 4-(2-hydroxyacetyl)benzoic acid was slightly slower for the mutant (220 min^{-1} vs. 260 min^{-1}), due to weaker coupling of NADH equivalents to product formation (49% vs. 65%, Figure 34a). The remaining redox equivalents (52%) contributed to hydrogen peroxide production.

NADH oxidation by $T252A_{CYP199A4}$ with 4-formylbenzoic acid was less than half that of $WT_{CYP199A4}$ (56 min^{-1} vs. 130 min^{-1}). Interestingly, the formation of terephthalic acid was 3 times faster due to a 7-fold increase in the coupling efficiency from 8% to 54% (Figure 34b). Unlike for the above-mentioned substrates, the remaining NADH equivalents could not be attributed to the peroxide uncoupling pathway, as no notable increase in peroxide levels were observed (Table 3).

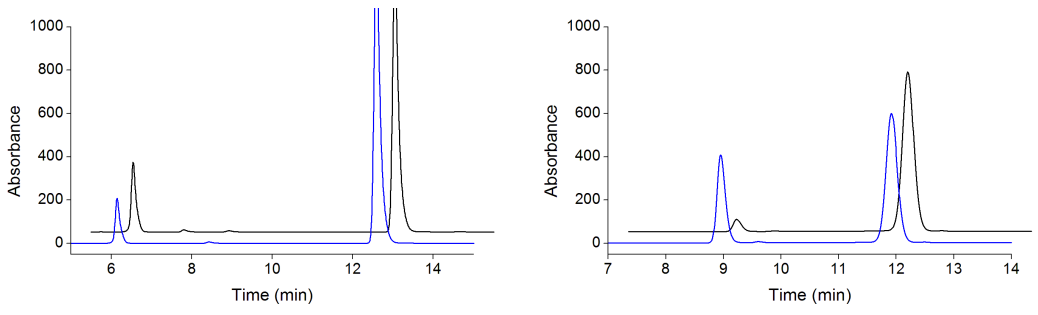

(a) (b)

Figure 34: HPLC analysis of the $WT_{CYP199A4}$ (black) and $T252A_{CYP199A4}$ (blue) turnovers of (a) 4-acetylbenzoic acid (t_R = 12.8 mins) to 4-(hydroxyacetyl)benzoic acid (t_R = 6.0 mins) and (b) 4-formylbenzoic acid (t_R = 11.9 mins) to terephthalic acid (t_R = 8.9 mins). For clarity the chromatograms have been offset along the x and y axes.

A notable increase in the rate of NADH oxidation by $T252A_{CYP199A4}$ was observed

with 4-ethynylbenzoic acid (306 min^{-1} vs. 171 min^{-1}). As the coupling efficiency was unchanged (65%), a 2-fold increase in the rate of 4-carboxyphenylacetic acid formation was observed (200 min^{-1} vs. 110 min^{-1}, Figure 35a). Most of the unproductive redox equivalents (30%) were funnelled into the production of hydrogen peroxide.

A comparable, 1.6-fold increase in the NADH oxidation rate by the threonine mutant was observed with 4-vinylbenzoic acid (814 min^{-1} vs. 514 min^{-1}). However, the rate of epoxidation to 4-(oxiran-2-yl)benzoic acid was virtually unchanged (210 min^{-1} vs. 220 min^{-1}) as a consequence of the reduced coupling efficiency of the $T252A_{CYP199A4}$ reaction (26% vs. 43%, Figure 35b). Peroxide uncoupling accounted for 59% of the unproductive NADH equivalents, with the remaining ≈ 15% presumably lost to oxidase or other uncoupling pathways.

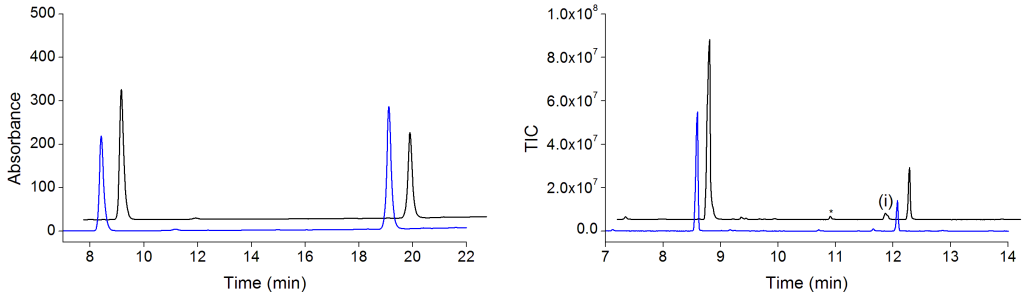

Figure 35: (a) HPLC analysis of the $WT_{CYP199A4}$ (black) and $T252A_{CYP199A4}$ (blue) turnovers of 4-ethynylbenzoic acid (t_R = 19.2 mins) to 4-carboxyphenylacetic acid (t_R = 8.4 mins). (b) GC-MS analysis of the derivatised turnovers of 4-vinylbenzoic acid (t_R = 8.4 mins) to 4-(oxiran-2-yl)benzoic acid (t_R = 12.1 mins). [(i)]This could be the aldehyde rearrangement product (Figure 9). For clarity the chromatograms have been offset along the x and y axes. Impurities are marked (*).

No oxidation product was observed for 4-acetoxy- or 4-acetamido-benzoic acid with $T252A_{CYP199A4}$. An increase in the peroxide levels were detected for the ester analogue with $T252A_{CYP199A4}$ (49% vs. 2%), while no notable change in the peroxide concentrations were observed for the amide (2.4% vs. 1.5%). The lack of peroxide formation with 4-acetamidobenzoic acid provides further evidence in support of the inhibition of the catalytic cycle by this substrate. Coordination to the heme iron most likely prevents oxygen binding to the heme, such that subsequent steps in the cycle which could lead to incorrect protonation of Cpd 0 and the release of peroxide do not occur.

Overall, it appears that mutation of the conserved threonine has less of an effect on product formation activity in CYP199A4 than in $T252A_{cam}$, where camphor hydroxylation is effectively abolished.[89,90] This large reduction in product formation implied an accumulation of the hydroperoxy intermediate, and implicated Cpd I as the active oxidant in camphor hydroxylation. It appears that Cpd I formation may be less im-

paired in the T252A mutant of CYP199A4. However, the elevated peroxide levels in the $T252A_{CYP199A4}$ turnovers do suggest some build-up or destabilisation of Cpd 0. The unproductive reducing equivalents were almost entirely lost to peroxide formation in the 4-methoxy-, 4-ethynyl- and 4-acetyl-benzoic acid turnovers (Table 3). This is in stark contrast to the $< 5\%$ of peroxide formed in the WT turnovers, where the majority of the unproductive NADH equivalents were likely lost to oxidase uncoupling. Changes in the rates of product formation and degree of peroxide uncoupling between the T252A mutant of CYP199A4 and the WT enzyme, in particular with 4-ethynyl- and 4-formyl-benzoic acid, could imply that Cpd I may not be the sole active oxidant in P450 catalysis. How this affects our understanding of the oxidant(s) will be discussed later.

4.2.2 Investigation of the Activity of $D251N_{CYP199A4}$

The addition of 4-methoxybenzoic acid to $D251N_{CYP199A4}$ resulted in the same, $> 95\%$ spin-state shift previously observed for both $WT_{CYP199A4}$[78] and $T252A_{CYP199A4}$. In comparison, much smaller shifts – up to 40% less than in the WT enzyme – were induced by the remaining substrates in $D251N_{CYP199A4}$ (Table 4). The spin-state shift of 4-formylbenzoic acid was decreased from 25% to 10%, and the shifts for 4-acetoxy- and 4-vinyl-benzoic acid were reduced from 90% and 80%, respectively, to 55%. The largest reduction in the shift was observed for 4-ethynylbenzoic acid (30% vs. 70%, Appendix B2).

Table 4: Substrate binding and *in vitro* turnover data for $D251N_{CYP199A4}$. The data are given as mean ± S.D. with $n \geq 3$. Rates are given as nmol.nmol-P450^{-1}.min^{-1}. The average leak rate was 9.0 nmol.nmol-P450^{-1}.min^{-1}.

Substrate	% HS	K_d (µM)	NADH (min^{-1})	PFR (min^{-1})	Coupling (%)
4-methoxyBA	> 95	0.17 ± 0.01	7 ± 0.8	3.5 ± 0.9	59 ± 3
4-vinylBA	55	0.06 ± 0.01	18 ± 0.6	5.0 ± 0.2	28 ± 1
4-ethynylBA	30	0.7 ± 0.1	30 ± 0.7	4.2 ± 0.2	14.5 ± 0.1
4-formylBA	10	10.8 ± 0.4	25 ± 0.8	18 ± 1	72 ± 4
4-acetylBA	type II	2.2 ± 0.2	19 ± 0.6	6.4 ± 0.5	34 ± 2
4-acetoxyBA	55	0.26 ± 0.05	14 ± 0.9	-[a]	-[a]
4-acetamidoBA	type II	3.8 ± 0.2	28 ± 1.7	-[a]	-[a]

[a]No product formation.

Interestingly, substrate binding to $D251N_{CYP199A4}$ was tighter in all cases compared to

both $WT_{CYP199A4}$ and $T252A_{CYP199A4}$ (Appendix B4). The smallest changes in affinity were observed for 4-methoxy- (K_d = 0.17 µM) and 4-ethynyl-benzoic acid (K_d = 0.69 µM). A 4- and 7-fold increase in binding was observed for 4-formyl- (K_d = 11 µM) and 4-vinyl-benzoic acid (K_d = 0.06 µM), respectively, while an even larger 10-fold change was observed for 4-acetoxybenzoic acid (K_d = 0.26 µM). 4-Acetamidobenzoic acid bound 24 times more tightly to $D251N_{CYP199A4}$ than the WT enzyme (K_d = 2.6 µM), but the most dramatic change was observed for 4-acetylbenzoic acid, where binding increased by 2 orders of magnitude or approximately 70 times (K_d = 2.2 µM vs. 140 µM) (Table 4). Although this substrate red-shifted the Soret band at 418 nm by 1 nm in all three enzymes, the difference spectrum of 4-acetylbenzoic acid with $WT_{CYP199A4}$ and $T252A_{CYP199A4}$ were representative of type I binding. However, with $D251N_{CYP199A4}$ the difference spectrum was consistent with that of a type II substrate, with a decrease in the absorption at 412 nm and an increase at 430 nm (Figure 36). This could suggest a stronger interaction of the oxygen of 4-acetylbenzoic acid with the heme iron in $D251N_{CYP199A4}$.

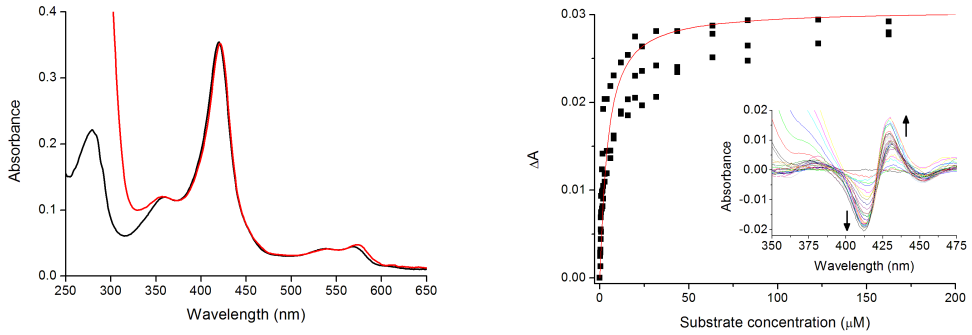

(a) (b)

Figure 36: (a) Spin-state shift and (b) dissociation constant analysis of $D251N_{CYP199A4}$ with 4-acetylbenzoic acid.

Overall, the Asp → Asn mutation resulted in a modification of the binding affinity of and the interactions with CYP199A4 for the substrates tested, suggesting a role for Asp251 in substrate recognition and binding in CYP199A4. Additionally, theses changes in the substrate binding affinity of $D251N_{CYP199A4}$ could also be indicative of a subtly altered active site environment, as has been suggested for the acidic residue mutants of $P450_{BM3}$,[55] CYP17A1[123] and CYP19A1.[126]

The products of the turnovers with $D251N_{CYP199A4}$ were also the same as those observed for $WT_{CYP199A4}$ and $T252A_{CYP199A4}$ (Figure 37). The most notable change was the considerably lower and near leak rate oxidation of NADH by $D251N_{CYP199A4}$ when compared with $WT_{CYP199A4}$ (Table 4). The NADH oxidation rate varied between 14

min^{-1} for 4-acetoxybenzoic acid and 30 min^{-1} for 4-ethynylbenzoic acid. Except in the presence of 4-formylbenzoic acid, the levels of product formation and the coupling efficiency of the aspartate mutant was also reduced in all cases. This is presumably due in part to autooxidation of the electron transfer partners, which can now compete with the slow rate of the catalytic cycle.[7,23] The coupling decreased from 65% to 34% for 4-acetylbenzoic acid and 43% to 28% for 4-vinylbenzoic acid. A larger reduction from 66% to 15% was observed for 4-ethynylbenzoic acid. In contrast, coupling was increased by 9-fold (72% vs. 8%) for 4-formylbenzoic acid (Figure 37).

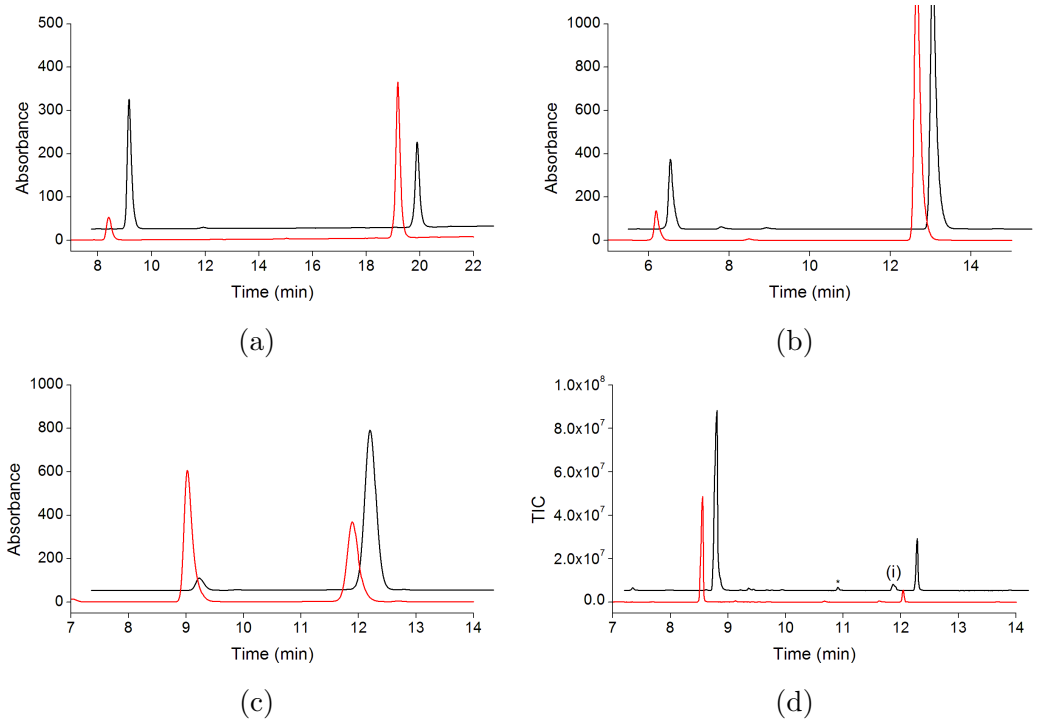

Figure 37: HPLC analysis of the $WT_{CYP199A4}$ (black) and $D251N_{CYP199A4}$ (red) turnovers of (a) 4-ethynylbenzoic acid ($t_R = 19.2$ mins) to 4-carboxyphenylacetic acid ($t_R = 8.4$ mins) (b) 4-acetylbenzoic acid ($t_R = 12.8$ mins) to 4-(hydroxyacetyl)benzoic acid ($t_R = 6.0$ mins) and (c) 4-formylbenzoic acid ($t_R = 11.9$ mins) to terephthalic acid ($t_R = 8.9$ mins). (d) GC-MS analysis of the derivatised turnovers of 4-vinylbenzoic acid ($t_R = 8.4$ mins) to 4-(oxiran-2-yl)benzoic acid ($t_R = 12.1$ mins). $^{(i)}$This could be the aldehyde rearrangement product (Figure 9). For clarity the chromatograms have been offset along the x and y axes. Impurities are marked (*).

4.3 Discussion

When Thr252 was mutated to an alanine in CYP199A4, the binding affinity of the enzyme for most of the benzoic acid substrates was largely unaffected, most likely due to a relatively unperturbed active site. This is consistent with other studies on equivalent Thr → Ala mutants of $P450_{cam}$,[93] CYP101D1[128] and CYP2D6.[52] In comparison, mutation of the conserved aspartate in CYP199A4 modified substrate binding for all of the substrates tested in the current work. The slight increase in affinity for 4-methoxybenzoic acid is comparable to the small increase reported for the binding of camphor to $D251N_{cam}$.[91] The most dramatic change was observed for 4-acetylbenzoic acid, where binding affinity increased by 70-fold. Additionally, a type II difference spectrum was observed for 4-acetylbenzoic acid with $D251N_{CYP199A4}$, in contrast to the type I difference spectra observed with $WT_{CYP199A4}$ and $T252A_{CYP199A4}$. Changes in the substrate binding affinity, both increases and decreases, have been reported for acidic residue mutants of $P450_{BM3}$,[55] CYP1A2,[57] CYP2A1,[127] CYP17A1[123] and CYP19A1.[126] It has been suggested that changes in both the binding affinity and enzymatic activity of the aspartate mutants may be a consequence of a subtly altered active site.[55,57,129]

When compared to $WT_{CYP199A4}$, the relative rates of the oxidation reactions catalysed by $T252A_{CYP199A4}$ remained unchanged. That is, the rate of $T252A_{CYP199A4}$ catalysed demethylation > hydroxylation ≥ alkene/alkyne epoxidation > aldehyde oxidation. However, notable changes in the product formation rates and the partition between the coupling and different uncoupling pathways were observed. The $T252A_{CYP199A4}$ mutant does not induce total uncoupling via the peroxide pathway for any substrate, suggesting that Cpd I can still be formed to a significant degree. These results along with those from the $P450_{BM3}$ system previously described[56,121,122] show that it cannot be assumed that Cpd I formation in P450s is completely inhibited by mutating the threonine residue of the conserved amino-acid pair.

As shown in Figure 38, peroxide uncoupling originates from Cpd 0 and oxidase uncoupling from Cpd I. If product formation arose exclusively from Cpd I, then the ratio of oxidase uncoupling/product formation is not predicted to vary between the Thr → Ala mutant and the WT enzyme, unless protonation or reduction of Cpd I to water is affected by the mutation. As shown in Table 5, there appears to be a general reduction in oxidase uncoupling in $T252A_{CYP199A4}$, in particular with 4-ethynyl- and 4-vinyl-benzoic acid, suggesting that Cpd I might not be the sole active oxidant mediating CYP199A4 catalysis.

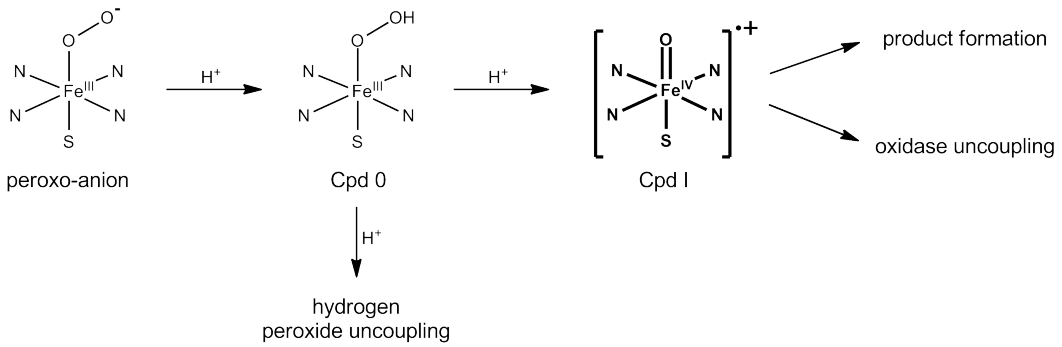

Figure 38: Product formation and uncoupling pathways in P450 catalysis.

In a recent hybrid quantum mechanical/molecular mechanical (QM/MM) and molecular dynamics (MD) study by Shaik and coworkers, an additional coupling pathway originating from Cpd 0, but involving Cpd I as the sole and final oxidant, was proposed in the epoxidation of 5-methylenylcamphor by $T252A_{cam}$. This pathway involves the less well-studied hydrogen peroxide complex, Fe(III)-O_2H_2. The Fe(III)-O_2H_2 species, generated by protonation of Cpd 0 on the proximal rather than distal oxygen, can follow one of two routes. On the established hydrogen peroxide uncoupling pathway, H_2O_2 is lost, as observed in $T252A_{cam}$ with camphor. In contrast, on the alternative coupling pathway, Fe(III)-O_2H_2 converts to the true active oxidant, Cpd I, via a tightly-controlled O-O homolysis/H-abstraction mechanism (Figure 39).

Table 5: Product formation and uncoupling in $WT_{CYP199A4}$ and $T252A_{CYP199A4}$.

Substrate	PFR (min^{-1})	Product (%)	H_2O_2 (%)	Oxidase (%)
4-methoxyBA	1219 ± 120	91 ± 2	2 ± 0.2	≈ 7
4-methoxyBA_{T252A}	570 ± 56	68 ± 5	31 ± 4	≈ 1
4-vinylBA	220 ± 20	43 ± 4	2.5 ± 0.4	≈ 55
4-vinylBA_{T252A}	210 ± 15	26 ± 1	59 ± 3	≈ 15
4-ethynylBA	110 ± 6	66 ± 1	19 ± 2	≈ 14
4-ethynylBA_{T252A}	200 ± 15	65 ± 4	30 ± 2	≈ 5
4-acetylBA	260 ± 24	65 ± 6	4.7 ± 0.6	≈ 30
4-acetylBA_{T252A}	220 ± 12	49 ± 3	52 ± 1	≈ 0

Which of the two pathways predominates was hypothesised to depend on the persistence of the Fe(III)-O_2H_2 intermediate, which can be carefully modulated by both the enzyme and the substrate being oxidised.[130] It has been hypothesised that in WT_{cam}, the stabilisation of Fe(III)-O_2H_2 through hydrogen bonding interactions with Thr252 and also Gly248 enables this intermediate to efficiently transform into the active oxidant, Cpd I.[130] As hydrogen bonding to Thr252 is no longer possible in the $T252A_{cam}$,

the substrate plays an important role in stabilising the Fe(III)-O_2H_2 intermediate. When 5-methylenylcamphor is bound by $T252A_{cam}$, the bulkier olefinic functionality is proposed to trap the peroxide moiety within the active site, thereby extending the lifetime of the Fe(III)-O_2H_2 intermediate to enable subsequent formation of Cpd I and substrate epoxidation. However, when camphor is bound, the lack of the C=C bond and larger degree of conformational freedom available leads to the loss of H_2O_2, such that efficient transformation of Fe(III)-O_2H_2 intermediate to Cpd I is no longer possible. If a similar coupling pathway exists in CYP199A4, this could have implications for our results with $T252A_{CYP199A4}$. However, we note that while 5-methylenylcamphor is larger than camphor, most of our substrates are a similar size to 4-methoxybenzoic acid.

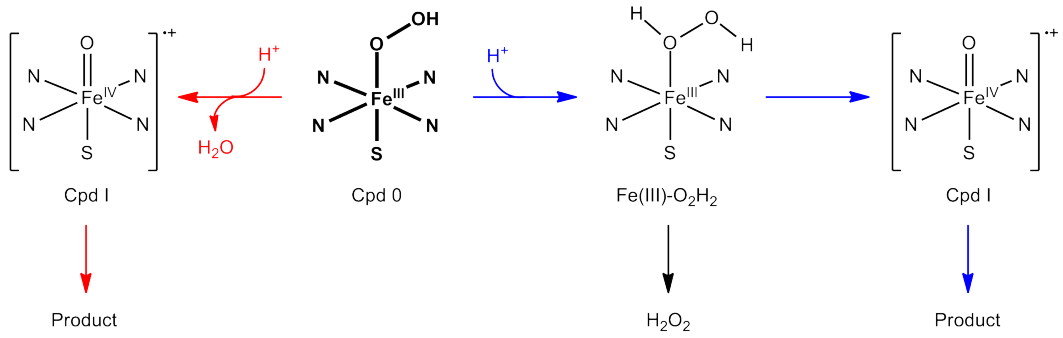

Figure 39: An additional coupling pathway leading to product formation in $T252A_{cam}$.

In the T252A turnover of 4-ethynylbenzoic acid, there is a decrease in the oxidase uncoupling/product formation ratio along with a lower increase in peroxide uncoupling compared to most other substrates tested. Most notably, the product formation rate was accelerated to almost twice that of $WT_{CYP199A4}$. From the perspective of the two-oxidant model, these results suggest the possible involvement of Cpd 0 in alkyne oxidation by CYP199A4. Based on the QM/MM and MD study, it might be possible that the linear alkyne can trap the peroxide moiety of Fe(III)-O_2H_2 in $T252A_{CYP199A4}$, leading to efficient conversion of this species to Cpd I for faster substrate oxidation. However, we note here that the relatively high degree of peroxide uncoupling of $WT_{CYP199A4}$ with 4-ethynylbenzoic acid suggests that this transformation may not be particularly efficient. In a different study, Shaik and coworkers have also proposed that the Fe(III)-O_2H_2 intermediate may be directly responsible for sulfoxidation reactions.[131]

For the alkene analogue, 4-vinylbenzoic acid, there is also a decrease in the oxidase uncoupling/product formation activities of $T252A_{CYP199A4}$, but very little change in the rate of epoxidation (Table 5). If there is in fact more than one active oxidant, this makes it less immediately clear whether Cpd I, another species or multiple oxidants are involved in CYP199A4-catalysed epoxidations.

The large decrease in the rate of 4-methoxybenzoic acid demethylation with $T252A_{CYP199A4}$, together with the observed increase in uncoupling to peroxide, suggests that Cpd I could be responsible for CYP199A4-catalysed demethylations. This would be consistent with a recent study on the T309V mutant of the human P450, CYP2D6.[52] Here, the authors found that Thr319 carefully modulates the balance between the different reactive oxygen species, and that *O*-dealkylation reactions were mediated by Cpd I.[52]

Both experimental and theoretical studies have implicated Cpd I in P450 hydroxylation reactions.[24,25,34,46] In the current work, the hydroxylation of 4-acetylbenzoic acid by $T252A_{CYP199A4}$ was only very slightly diminished when compared to $WT_{CYP199A4}$. As peroxide uncoupling appeared to account for all of the unproductive redox equivalents in the $T252A_{CYP199A4}$ reaction with 4-acetylbenzoic acid, there may be little to no oxidase uncoupling. However, the results and, in particular, the increase in peroxide formation, do not rule out the possible involvement of Cpd 0 in CYP199A4-catalysed hydroxylation. We note that no additional oxidation activity such as Baeyer-Villiger oxidation was observed with 4-acetylbenzoic acid in any of the WT, T252A or D251N turnovers.[105–108,132]

Additionally, it is possible that Thr252 in CYP199A4 is less essential for oxygen activation than the equivalent residue in $P450_{cam}$. A less-than-essential role has also been proposed for Thr319 in CYP1A2, where increased levels of methanol hydroxylation together with minimal hydrogen peroxide production were observed with $T319A_{CYP1A2}$.[124] Here, the authors suggested that CYP1A2 may use a different proton relay system, potentially one involving the hydroxyl group of the substrate as a proton donor.[124] This idea of "substrate-assisted" catalysis has similarly been proposed for other P450s including P450eryF[133] and CYP158A2.[134] Some of the benzoic acids tested in the current work might also be capable of assisting enzymatic catalysis. For example, the carbonyl oxygen of 4-acetylbenzoic acid could potentially hydrogen bond to water molecules and facilitate their recruitment to the active site for protonation of the peroxo and hydroperoxo (Cpd 0) species.

Of the substrates which gave rise to product, 4-formylbenzoic acid is the only substrate for which no notable increase in hydrogen peroxide was observed with $T252A_{CYP199A4}$. This implies that there was no accumulation of Cpd 0. The oxidation of 4-formylbenzoic acid was increased 3-fold by $T252A_{CYP199A4}$ and together, these results suggest that the elevated rate of 4-formylbenzoic acid oxidation may not have been mediated by Cpd 0. The turnover of 4-formylbenzoic acid was faster with the D251N mutant of CYP199A4, in stark contrast to the greatly reduced rates of product formation for

all of the other substrates with $D251N_{CYP199A4}$ (Table 4). The D251N mutation in CYP199A4 is predicted to slow the rate of the first proton transfer to the peroxo-anion during the catalytic cycle leading to a persistence of the ferric-peroxo anion. Combined with the results obtained for $T252A_{CYP199A4}$ with 4-formylbenzoic acid, the accelerated turnover of this substrate by $D251N_{CYP199A4}$ suggests that the peroxo-anion may be capable of, and responsible for aldehyde oxidation in CYP199A4. This would be consistent with previous studies which identified the nucleophilic peroxo-anion as the active oxidant in aldehyde deformylation (Chapter 1.2.5).[31,135–137] Additionally, we note here that no products arising from Dakin oxidation type chemistry were detected in the WT, T252A and D251N turnovers of 4-formylbenzoic acid.[112–114]

The demethylation, hydroxylation, epoxidation and alkyne oxidation activities of $D251N_{CYP199A4}$ were all greatly reduced relative to the WT enzyme (Table 4), suggesting a lack of peroxo-anion involvement in these reactions. Overall, these results demonstrate an important role for Asp251 in CYP199A4 in modulating the rate of the first proton transfer to the peroxo species and consequently substrate oxidation.

In spite of the experimental evidence which suggests the presence of multiple oxygenating species, theoretical studies are yet to implicate a species other than Cpd I as the active oxidant in P450 hydroxylation, epoxidation and sulfoxidation reactions, and Fe(III)-O_2H_2 in the latter.[58–61,131] Where Cpd 0 has been investigated theoretically, this species has been identified as a sluggish oxidant with higher energy barriers to oxygen activation than Cpd I.[58–61] As discussed, the observation of more than a single oxidant is ascribed to the doublet and quartet spin-states of Cpd I. While only inferences can be made from our experimental results, overall, they suggest that more than one active oxidant could potentially be involved in CYP199A4-catalysed reactions.

Crystallographic studies of $T252A_{CYP199A4}$ and $D251N_{CYP199A4}$, which are currently underway, will provide further insight into the role of the conserved acid-alcohol pair and the active oxidant(s) in CYP199A4 catalysis.[11,19,24] These reactive intermediates could potentially be trapped using cryoradiolytic reduction experiments, enabling further characterisation of these species and their role in substrate oxidation.[25,138,139]

Future work will involve investigating the activity of $T252A_{CYP199A4}$ and $D251N_{CYP199A4}$ with benzoic acid substrates similar to those tested in this work, in order to verify our current findings. Compounds such as those shown in Figure 40, could also be tested with CYP199A4 to probe for additional oxidative activities including lyase and deformylation activity. The responsible oxidant(s) in these reactions could then be explored using $T252A_{CYP199A4}$ and $D251N_{CYP199A4}$. All of these reactions and those from the current work could be investigated at different pH or performed in

D_2O, where the rates of the proton transfer steps will presumably be affected. These studies could help distinguish between the reactions which involve the unprotonated peroxo-anion as the active oxidant, and those requiring a protonated iron-species, Cpd 0 or Cpd I.

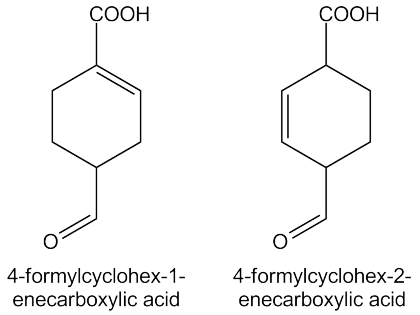

Figure 40: Potential substrates of CYP199A4.

The activities of additional threonine mutants could be studied and compared to help further understand the role of this residue in oxygen activation and substrate oxidation. For example, changes in the activity between a T252V mutant and $T252A_{CYP199A4}$ could provide information on how residue size at position 252 affects activity. To verify the role of Thr252 in stabilising Cpd 0 for protonation in CYP199A4, a T252S mutant could be constructed. Asn252 has been suggested to be able to sufficiently stabilise Cpd 0 in $P450_{cam}$.[140] A similar mutation could be introduced in CYP199A4 (T252N), and the relative activity of the mutant explored. The effect of other mutations at position 251 could also be studied. For example, mutation of the conserved aspartate to the closely related glutamate residue (D251E), and an aliphatic amino acid such as valine (D251V), could confirm the need for an acidic residue at this position.

5 The Oxidation of *para*-Substituted Cinnamic Acid Derivatives by CYP199A4

5.1 Introduction

CYP199A4 can selectively oxidise a range of *para*-substituted benzoic acids (Chapter 3).[78,79,87] In addition, the enzyme has been shown to oxidise larger substrates including 6-indolecarboxylic acid and 2-naphthoic acid (Figure 17).[79] Crystal structures of several substrate-bound CYP199A4 complexes reveal that the enzyme can accommodate two closely related substrate binding modes, which are distinguished from one another by the presence of the active site water molecule which interacts with the carboxylate group, or lack there-of (Figure 41).[79]

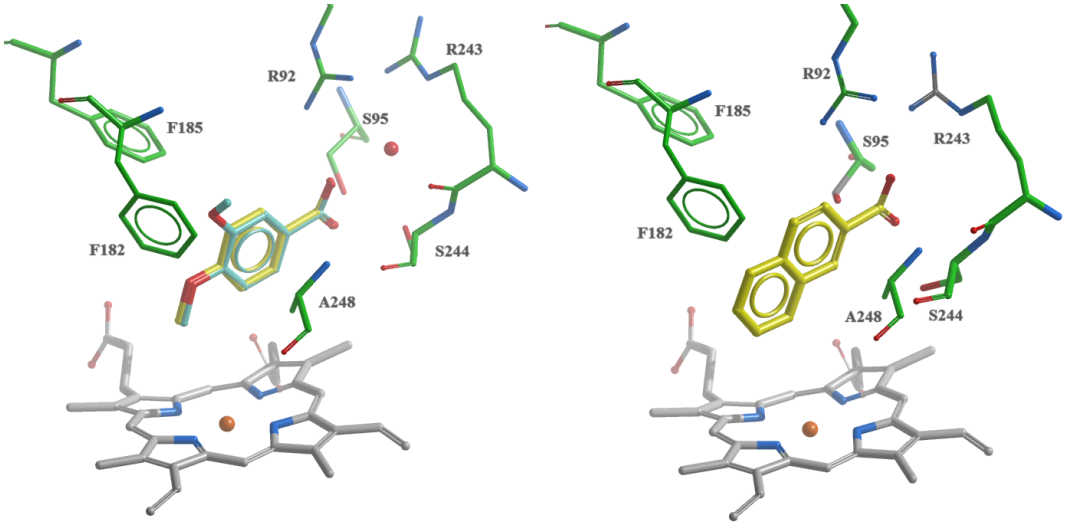

(a) (b)

Figure 41: The active site of CYP199A4 with (a) 3,4-dimethoxybenzoic acid, cyan, superimposed on 4-methoxybenzoic acid, yellow, and (b) 2-naphthoic acid, yellow. The heme and active site residues are shown in grey and green, respectively. The active site water is shown as a red sphere in (a).

The first mode of binding is observed with substrates including 4-methoxybenzoic acid and 4-ethylbenzoic acid (PDB: 4DO1 and 4EGM), where the hydrogen bond between the substrate carboxylate group and the side chain of Arg243 is bridged by the water molecule (Wat170 in 4-methoxybenzoic acid-bound CYP199A4, PDB: 4DO1).[20] This same binding configuration is also adopted by larger substrates including 3,4-dimethoxybenzoic acid and 6-indolecarboxylic acid (PDB: 4EGN and 4EGO). The benzene rings and carboxylate groups of these substrates are at virtually identical locations to those in the 4-methoxybenzoic acid and 4-ethylbenzoic acid-bound structures (Figure 41a), and the hydrogen bonding interactions between the substrate carboxy-

late group and Arg92, Ser95, Ser244 and, via the water molecule, Arg243, all remain intact.[20] However, the active site water molecule is displaced when 2-naphthoic acid (PDB: 4EGP), which is similar in size to 6-indolecarboxylic acid, is bound (Figure 41b), and the substrate carboxylate group hydrogen bonds directly with the side chain of Arg243. In order to maintain the hydrogen bonding interactions with Ser95 and Ser244, Ser95 undergoes a large positional shift.[20] Taken together, these observations indicate that substrates larger than benzoic acids can be accommodated within the active site of CYP199A4.

CYP199A2 from *R. palustris* strain GCA009, which shares > 85% sequence identity with CYP199A4, has been shown to oxidise 6-indolecarboxylic acid, 2-naphthoic acid, and 3-hydroxy- and 4-hydroxy-cinnamic acid.[3,73,94,95] Mutagenesis studies on CYP199A2 have identified a mutant capable of producing high levels of 3,4-dihydroxycinnamic acid (caffeic acid), a powerful antioxidant and important synthetic scaffold for a variety of bioactive compounds through the whole-cell oxidation of 4-hydroxycinnamic acid (*p*-coumaric acid) using an *Escherichia coli* system.[73]

Cinnamic acids are naturally found in plants and are involved in the biosynthesis of numerous secondary metabolites including flavonoids, stilbenes and tannins. These products have important physiological roles including the regulation of plant growth and disease resistance.[141] Common sources of cinnamic acids include coffee beans, tea, cocoa and berries, among others.[142] Cinnamic acids possess important biological properties including antimicrobial, antiviral, anticancer, anti-inflammatory and antioxidant activities.[141] Additionally, while these compounds can be extracted from plants, the methods employed are typically energy-intensive and non-environmentally friendly, making cinnamic acids and their derivatives attractive synthetic targets.[143] With this in mind, CYP199A4 could potentially be utilised for the biocatalytic production of cinnamic acid derivatives for pharmaceutical applications.

Here, we will investigate the activity of CYP199A4 with a range of cinnamic acid derivatives (Figure 42). This will provide further insight into the enzyme-substrate interactions required for tight-binding to CYP199A4, and substituent effects on efficient enzymatic turnover. A detailed understanding of these features will aid in the potential application of CYP199A4 as a biological catalyst on a synthetically useful scale.

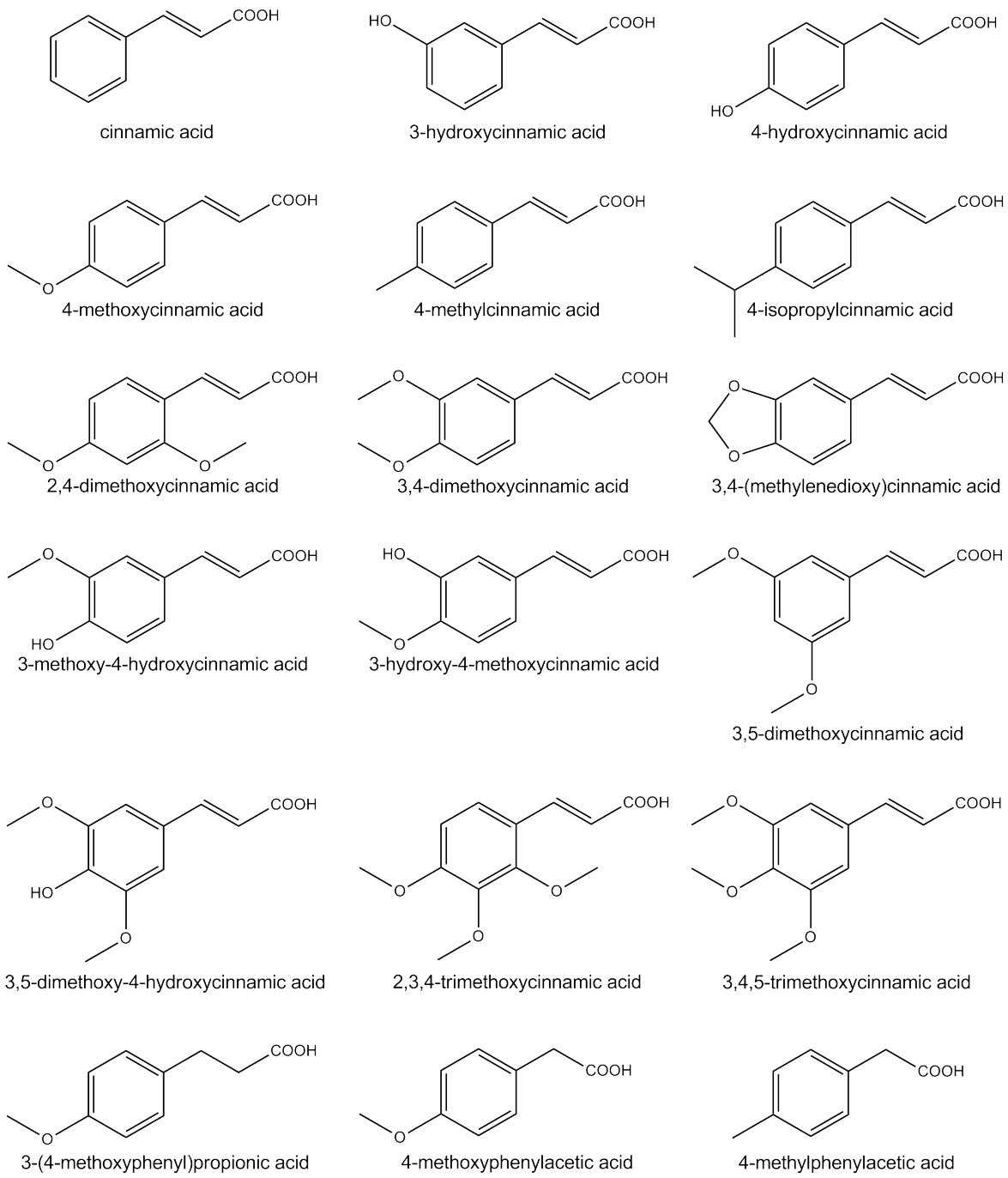

Figure 42: Cinnamic acid derivatives tested with CYP199A4.

5.2 Results

5.2.1 Substrate Binding Studies on Cinnamic Acid Derivatives

3-Hydroxy- and 4-hydroxy-cinnamic acid are reported to be efficiently oxidised to 3,4-dihydroxycinnamic acid (caffeic acid) by a whole-cell oxidation system containing CYP199A2. Little or no oxidation activity was observed for the enzyme with the parent compound, cinnamic acid.[73,96] Upon addition of these compounds to CYP199A4, cinnamic acid and 3-hydroxycinnamic acid induced a $< 5\%$ spin-state shift, while 4-hydroxycinnamic acid did not induce any change in the spin-state (0%, Appendix C1). As a consequence of their negligible shifts, accurate dissociation constants were unable to be determined for these substrates.

As 4-methoxybenzoic acid binds tightly to CYP199A4,[3] we investigated the binding of its cinnamic acid counterpart, 4-methoxycinnamic acid. The substrate induced a 70% spin-state shift and bound tightly to the enzyme, with a dissociation constant of 3.6 µM (Figure 43). This improvement in binding observed with the *para*-methoxy substituted analogue over the parent molecule, cinnamic acid, is reminiscent of the considerably tighter binding of 4-methoxybenzoic acid when compared to benzoic acid.[78]

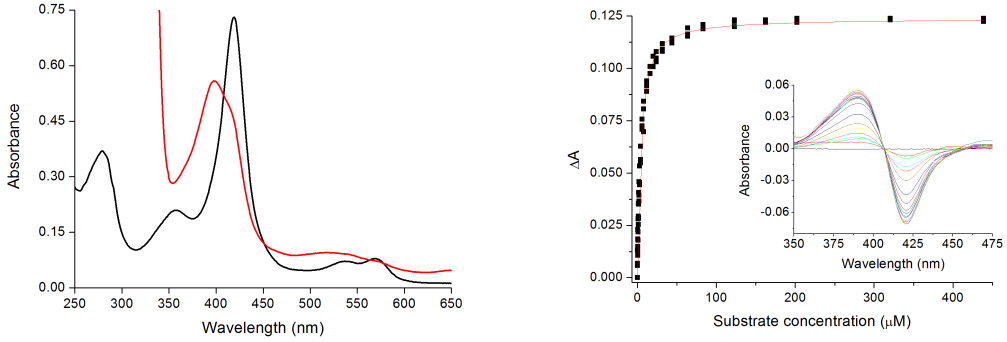

(a) (b)

Figure 43: (a) Spin-state shift and (b) dissociation constant analysis of CYP199A4 with 4-methoxycinnamic acid.

3-(4-Methoxyphenyl)propionic acid, which differs from 4-methoxycinnamic acid by only the lack of a double bond between the α- and β-carbons, was also tested with CYP199A4. This substrate induced a smaller 20% shift and bound almost 10-fold more weakly (K_d = 31 µM). The binding of the closely-related molecules 4-methoxy- and 4-methyl-phenylacetic acid was also investigated. Minimal changes were observed in the spin-state of the enzyme upon addition of 4-methoxyphenylacetic acid (5%), which bound 2500-fold more weakly than 4-methoxybenzoic acid (K_d = 690 µM). The binding

of 4-methylphenylacetic acid was even weaker (K_d = 2300 µM, Appendix C2 and C3). Taken together, these results suggest that the planar nature of the *para*-substituted cinnamic acid and benzoic acid frameworks may be important for substrate binding. Based on these initial findings and the activity of CYP199A4 with *para*-substituted benzoic acids, a selection of cinnamic acids were investigated.

2,4-Dimethoxycinnamic acid induced a small change in the spin-state of the heme iron upon addition to CYP199A4 (10%) and bound with moderate affinity to the enzyme (K_d = 86 µM, Figure 44a). Despite the larger spin-state shift (20%), the binding of 3,4-dimethoxycinnamic acid to CYP199A4 was nearly 10-fold weaker than that of 2,4-dimethoxycinnamic acid (K_d = 840 µM, Figure 44b).

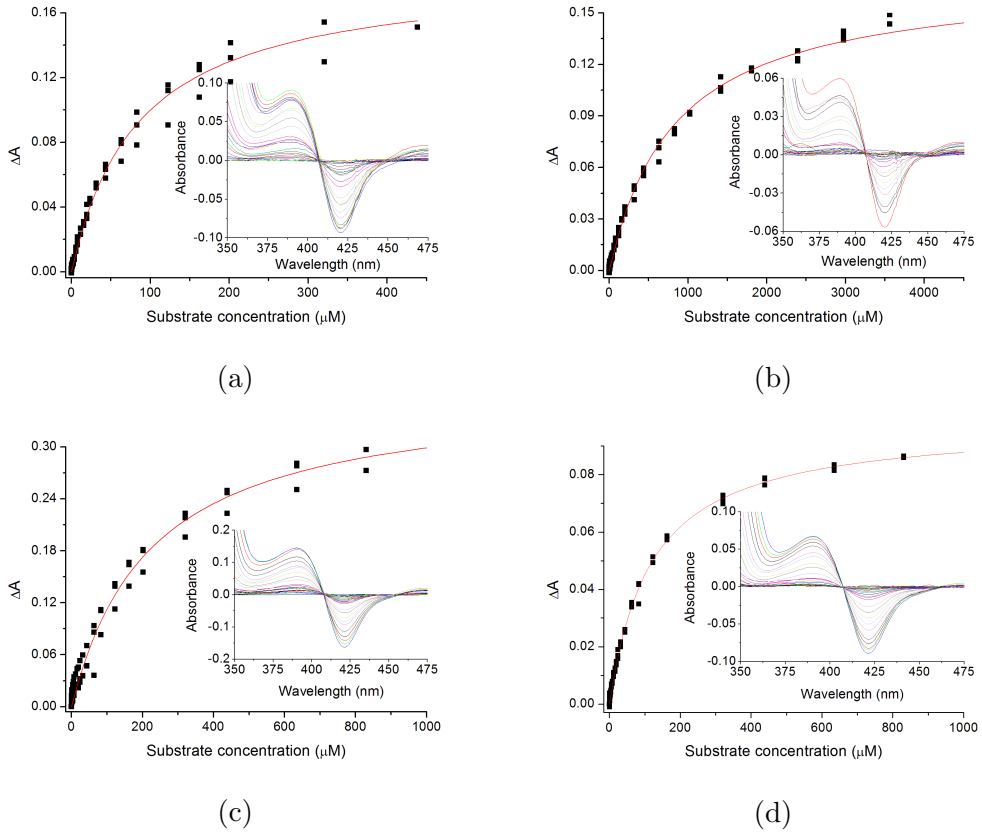

Figure 44: Dissociation constant analyses of CYP199A4 with (a) 2,4-dimethoxycinnamic acid (b) 3,4-dimethoxycinnamic acid (c) 3-hydroxy-4-methoxycinnamic acid and (d) 3,4-(methylenedioxy)cinnamic acid.

3-Hydroxy-4-methoxycinnamic acid induced a similar spin-state shift to its 3,4-dimethoxy counterpart (25%) but bound 4-fold more tightly to the enzyme (K_d = 220 µM, Figure 44c). A 30% shift was observed upon the addition of 3,4-(methylenedioxy)cinnamic acid to CYP199A4, which bound more tightly than both 3-hydroxy-4-methoxy- and 3,4-dimethoxy-cinnamic acid (K_d = 120 µM, Figure 44d and Table 6). This may be due to favourable hydrophobic interactions between the

methylenedioxy ring and active site amino acids which are not possible with the hydroxyl group in 3-hydroxy-4-methoxycinnamic acid, and the smaller size of the substituent relative to the 3,4-dimethoxy analogue. The tighter binding of 3-hydroxy-4-methoxycinnamic acid when compared to the 3,4-dimethoxy derivative also suggests that the smaller hydroxy group is better-tolerated at the 3-position.

Table 6: Substrate binding data on CYP199A4 with cinnamic acid derivatives. The data are given as mean ± S.D. with $n \geq 3$.

Substrate	% High-spin	Dissociation constant (μM)
4-methoxycinnamic acid	70	3.6 ± 0.1
cinnamic acid	5	-[a]
3-hydroxycinnamic acid	< 5	-[a]
4-hydroxycinnamic acid	0	-[a]
3,4-dimethoxycinnamic acid	20	840 ± 33
2,4-dimethoxycinnamic acid	10	86 ± 4.5
3-hydroxy-4-methoxycinnamic acid	25	220 ± 13
3-(4-methylenedioxy)cinnamic acid	30	120 ± 2.0
3,5-dimethoxycinnamic acid	< 5	-[a]
3,5-dimethoxy-4-hydroxycinnamic acid	<5	-[a]
3-methoxy-4-hydroxycinnamic acid	< 5	-[a]
4-methylcinnamic acid	70	21 ± 0.4
4-isopropylcinnamic acid	> 95	3.4 ± 0.1
2,3,4-trimethoxycinnamic acid	< 5	-[a]
3,4,5-trimethoxycinnamic acid	< 5	-[a]
3-(4-methoxyphenyl)propionic acid	20	31 ± 1
4-methoxyphenylacetic acid	5	690 ± 70
4-methylphenylacetic acid	5	2300 ± 160

[a]Not determined due to minimal spin-state shifts.

3-Methoxy-4-hydroxy-, 3,5-dimethoxy- and 3,5-dimethoxy-4-hydroxy-cinnamic acid induced meagre spin-state shifts of $< 5\%$ in CYP199A4 (Table 6). Dissociation constants were unable to be determined for these compounds which either lack a *para*-substituent or do not have a methoxy group at this position. Negligible changes in the spin-state were also observed upon the addition of 2,3,4- and 3,4,5-trimethoxycinnamic acid to CYP199A4. This is presumably because they are too large for the substrate binding pocket of the enzyme, resulting in steric clashes of the substituents at the *ortho*- and *meta*-positions with active site amino acids. It is noted that all of the above mentioned methoxy-substituted cinnamic acids induced smaller spin-state shifts ($\leq 30\%$)

than 4-methoxycinnamic acid (Table 6). The results so far demonstrate that while a *para*-methoxy group is important for tight-binding to CYP199A4, additional substituents at the *ortho*- and *meta*-positions are unfavourable for binding.

The binding of two alkyl-substituted cinnamic acids to CYP199A4, 4-methyl- and 4-isopropyl-cinnamic acid, was also investigated. 4-Methylcinnamic acid induced a similar spin-state shift to 4-methoxycinnamic acid (70%) but bound 6-fold more weakly (K_d = 21 µM, Figure 45a and 45b).

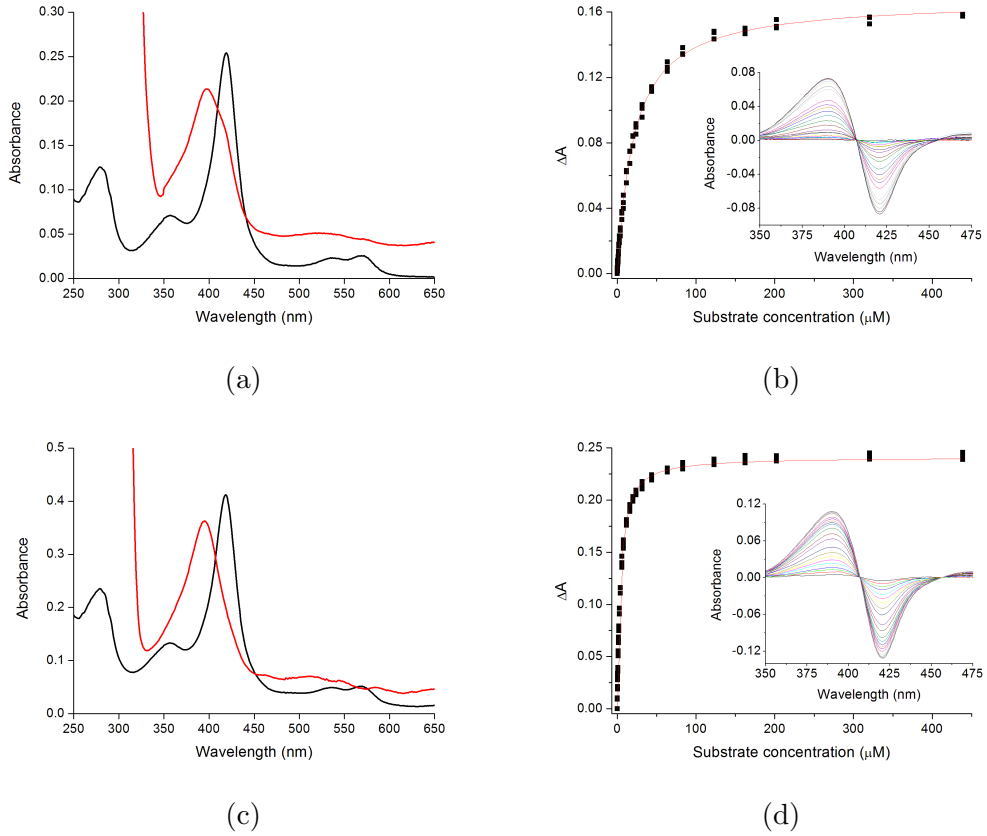

Figure 45: The respective spin-state shifts and dissociation constant analyses of CYP199A4 with 4-methylcinnamic acid (a) and (b) and 4-isopropylcinnamic acid (c) and (d).

4-Isopropylcinnamic acid induced the largest spin-state shift of all the cinnamic acids (> 95%) and bound as tightly as 4-methoxycinnamic acid to CYP199A4 (K_d = 3.4 µM, Figure 45c and 45d). It is possible that the smaller methyl substituent of 4-methylcinnamic acid forms fewer interactions with active site amino acids compared to the larger methoxy and isopropyl substituents, resulting in weaker binding. The isopropyl moiety of 4-isopropylcinnamic acid must be a very good fit for the substrate binding pocket of the enzyme. This is consistent with the tight-binding observed for 4-isopropylbenzoic acid, which also bound as tightly as 4-methoxybenzoic acid to CYP199A4 (K_d = 0.29 µM vs. 0.28 µM).[87] The results obtained for 4-methyl- and 4-isopropyl-cinnamic acid again emphasise the importance of a *para*-substituent for

tight-binding to CYP199A4.

5.2.2 Activity and Product Formation Assays with Cinnamic Acid Derivatives

The NADH oxidation and product formation rates were measured for each of the cinnamic acid derivatives (Table 7). The product of each CYP199A4-catalysed *in vitro* turnover was identified by HPLC or GC-MS coelution of the turnover with an authentic sample of the product, or NMR analysis after purification by semi-prep HPLC.

Table 7: *In vitro* turnover data for CYP199A4 with cinnamic acid derivatives. The data are given as mean ± S.D. with $n \geq 3$. Rates are given as nmol.nmol-P450^{-1}.min^{-1}. The average leak rate was 9.0 nmol.nmol-P450^{-1}.min^{-1}.

Substrate	NADH (min^{-1})	PFR (min^{-1})	Coupling (%)
4-methoxycinnamic acid	562 ± 10	180 ± 9	32 ± 1
cinnamic acid	24 ± 1	-[a]	-[a]
3-hydroxycinnamic acid	9.0 ± 0.1	-[a]	-[a]
4-hydroxycinnamic acid	16 ± 1	-[a]	-[a]
3,4-dimethoxycinnamic acid	400 ± 18	300 ± 17	75 ± 4
2,4-dimethoxycinnamic acid	441 ± 30	280 ± 25	64 ± 2
3-hydroxy-4-methoxycinnamic acid	408 ± 25	240 ± 5	59 ± 3
3-(4-methylenedioxy)cinnamic acid	51 ± 1	6.6 ± 0.2	13 ± 0.4
3,5-dimethoxycinnamic acid	22 ± 1	0.3 ± 0.02	3.3 ± 0.2
3,5-dimethoxy-4-hydroxycinnamic acid	50 ± 2	-[a]	-[a]
4-methylcinnamic acid	202 ± 7	85 ± 1	42 ± 0.8
4-isopropylcinnamic acid	190 ± 13	130 ± 10	69 ± 3
2,3,4-trimethoxycinnamic acid	39 ± 2	24 ± 1	61 ± 3
3,4,5-trimethoxycinnamic acid	12 ± 0.3	-[a]	-[a]
3-(4-methoxyphenyl)propionic acid	98 ± 5	43 ± 3	43 ± 2
4-methoxyphenylacetic acid	21 ± 2	5.0 ± 0.6	23 ± 2
4-methylphenylacetic acid	15 ± 0.3	6.2 ± 0.2	42 ± 2

[a]No product formation.

The rate of NADH oxidation by CYP199A4 with 4-methoxycinnamic acid was 560 min^{-1}, which is over 2-fold slower than that observed with 4-methoxybenzoic acid, but comparable to alkyl substituted benzoic acids such as 4-methylbenzoic acid.[79] 4-Methoxycinnamic acid was turned over to 4-hydroxycinnamic acid at a moderate rate

of 180 min^{-1} (Figure 46). However, the coupling of this demethylation reaction is notably lower than that of 4-methoxybenzoic acid (32% vs. 91%). We note that the HPLC analysis shows the presence of two peaks in the substrate and product controls of 4-methoxycinnamic acid, which also appear in the turnover. Similar observations were made for a number of the cinnamic acid substrates. Based on the analysis of the turnovers and authentic samples of the substrates and products, the two peaks were identified as the *cis* and *trans* isomers of the compound. In each case, NMR analysis shows that the authentic samples are those of the *trans* isomers (> 99%), suggesting isomerisation is occurring before or during analysis (Appendix C).[144,145]

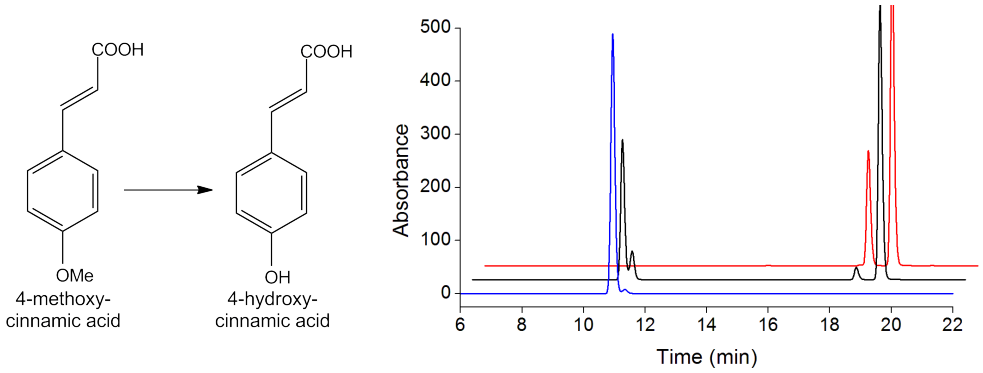

Figure 46: HPLC analysis of the CYP199A4 turnover (black) of 4-methoxycinnamic acid. The substrate control (t_R = 18.5 mins, *cis* and t_R = 19.4 mins, *trans*) is in red and 4-hydroxycinnamic acid product control (t_R = 11.0 mins) in blue. For clarity the chromatograms have been offset along the x and y axes.

Despite their smaller shifts and weaker binding to CYP199A4 relative to 4-methoxycinnamic acid, comparable rates of NADH oxidation were observed for 3,4-dimethoxy- (400 min^{-1}) and 3-hydroxy-4-methoxy-cinnamic acid (408 min^{-1}). These substrates were exclusively demethylated at the *para*-position. The coupling efficiencies of these reactions (75% and 59%, respectively) were higher than that of 4-methoxycinnamic acid and the product formation rates of 3-methoxy-4-hydroxy- (300 min^{-1}) and 3,4-dihydroxy-cinnamic acid (240 min^{-1}) were as a consequence faster (Appendix C4).

Slower NADH oxidation (98 min^{-1}) and product formation (43 min^{-1}) activity was observed for the moderately coupled (43%) demethylation of 3-(4-methoxyphenyl)propionic acid to 4-(hydroxyphenyl)propionic acid. In comparison, the activity of CYP199A4 with the phenylacetic acids was even lower (Table 7). The low levels of NADH oxidation and modest coupling resulted in the production of 4-hydroxyphenylacetic acid from 4-methoxyphenylacetic acid at a mere 5.0 min^{-1}. As the coupling of redox equivalents to product formation was higher with the methyl derivative (42% vs. 23%), a slightly faster product formation rate of 6.2 min^{-1} was

achieved for 4-(hydroxymethyl)phenylacetic acid (Appendix C5).

The oxidation of 3-(4-methylenedioxy)cinnamic acid to 3,4-dihydroxycinnamic acid by CYP199A4 occurred at a comparable rate of 6.6 min^{-1}, which is nearly 30- and 50-fold slower than the oxidation of 4-methoxy- and 3,4-dimethoxy-cinnamic acid, respectively (Figure 47). This can be partly attributed to the poor coupling of redox equivalents to product formation (13%). Importantly, this suggests that, relative to the methyl moieties of the *para*-methoxy substituents of 4-methoxy- and 3,4-dimethoxy-cinnamic acid, the more activated methylene C-H bonds of 3-(4-methylenedioxy)cinnamic acid are held less favourably in the substrate binding pocket for attack by Cpd I.

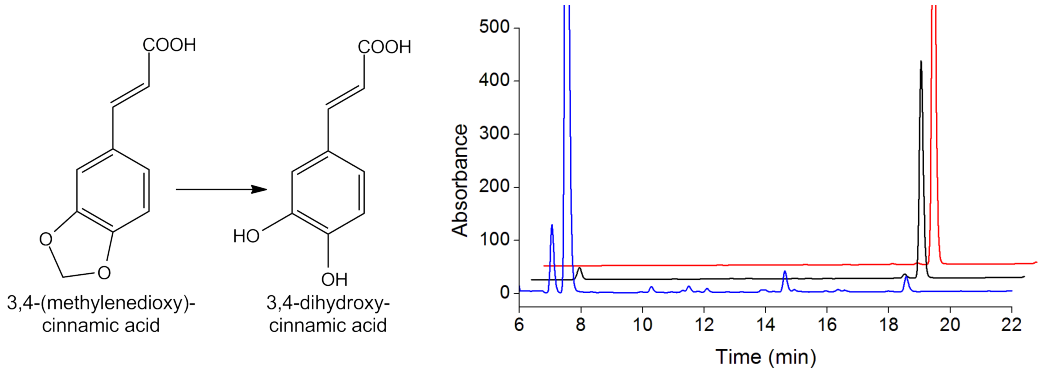

Figure 47: HPLC analysis of the CYP199A4 turnover (black) of 3,4-(methylenedioxy)cinnamic acid. The substrate control (t_R = 18.8 mins) is in red and 3,4-dihydroxycinnamic acid product control (t_R = 7.1 mins, *cis* and t_R = 7.6 mins, *trans*) in blue. For clarity the chromatograms have been offset along the x and y axes.

The rates of NADH oxidation in the presence of cinnamic acid (24 min^{-1}) and 3- and 4-hydroxycinnamic acids (9.0 min^{-1} and 17 min^{-1}, respectively) were comparable to the leak rate of CYP199A4 in the absence of substrate (Table 7). The turnover of 3-hydroxycinnamic acid resulted in the production of extremely low levels of 3,4-dihydroxycinnamic acid (Figure 48), while minute quantities of 3- and 4-hydroxycinnamic acid, which are most likely due to trace amounts of impurities in the substrate rather than enzymatic oxidation, were detected in the turnover of cinnamic acid (Appendix C4). No oxidation product was observed for 4-hydroxycinnamic acid.

Similarly, no product could be detected in the turnovers of 3-methoxy-4-hydroxy- (ferulic acid) and 3,5-dimethoxy-4-hydroxy-cinnamic acid (sinapic acid), despite the somewhat elevated rate of NADH oxidation (50 min^{-1}) with sinapic acid. It is possible that a hydroxyl group at the *para*-position could interact with the heme iron to hinder the binding of molecular oxygen, resulting in a lack of monooxygenase activity.

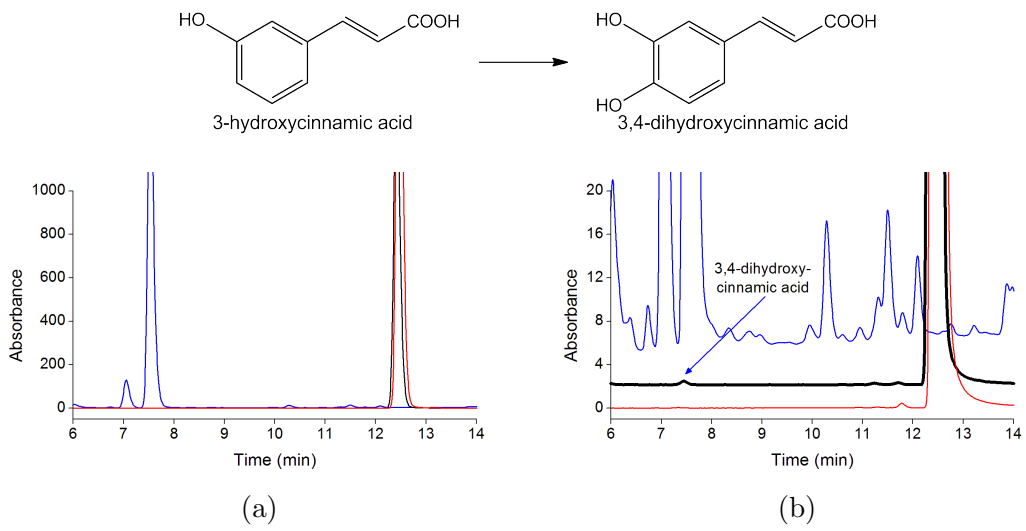

Figure 48: HPLC analysis of the CYP199A4 turnover (black) of (a) 3-hydroxycinnamic acid with (b) the product region highlighted. The substrate control (t_R = 12.5 mins) is in red and 3,4-dihydroxycinnamic acid product control (t_R = 7.1 mins, *cis* and t_R = 7.6 mins, *trans*) in blue. For clarity the chromatograms in (b) have been offset along the y axis.

A very small amount of product was observed in the turnover of 3,5-dimethoxycinnamic acid. GC-MS analysis of the TMS-derivatised turnover showed a product m/z of 338.2, consistent with the predicted m/z of 338.6 for TMS-derivatised 3-hydroxy-5-methoxycinnamic acid arising from a single demethylation (Figure 49). This is similar to the production of very small amounts of 3-hydroxy-5-methoxybenzoic acid in the turnover of 3,5-dimethoxybenzoic acid.[78] It has been proposed that when 3,5-dimethoxybenzoic acid is bound by CYP199A4, one of its methoxy groups is oriented towards the heme iron and close enough to undergo demethylation.[78] When only a single *meta*-substituent is present, it presumably points away from the heme like the 3-methoxy group in 3,4-dimethoxybenzoic acid-bound CYP199A4 (PDB code: 4EGN).[79]

The NADH oxidation and product formation activities of CYP199A4 were high with 2,4-dimethoxycinnamic acid (441 min^{-1} and 280 min^{-1}, respectively). The oxidation product of this substrate was generated in a higher yield using a whole-cell oxidation system consisting of CYP199A4 and its electron transfer partners HaPux and HaPuR,[3] and the product was isolated and purified via semi-preparative HPLC. A comparison of the product and substrate NMR spectra revealed the absence of a 3H singlet at 3.86 ppm in the product NMR, indicating the loss of a methoxy group (Appendix C9). Taking into account the exclusive oxidation of the *para*-methoxy substituent observed for CYP199A4, the product was assigned as 2-methoxy-4-hydroxycinnamic acid. This product was also co-eluted with the CYP199A4 turnover of 2,4-dimethoxycinnamic acid using HPLC, where identical retention times were observed (Appendix C4).

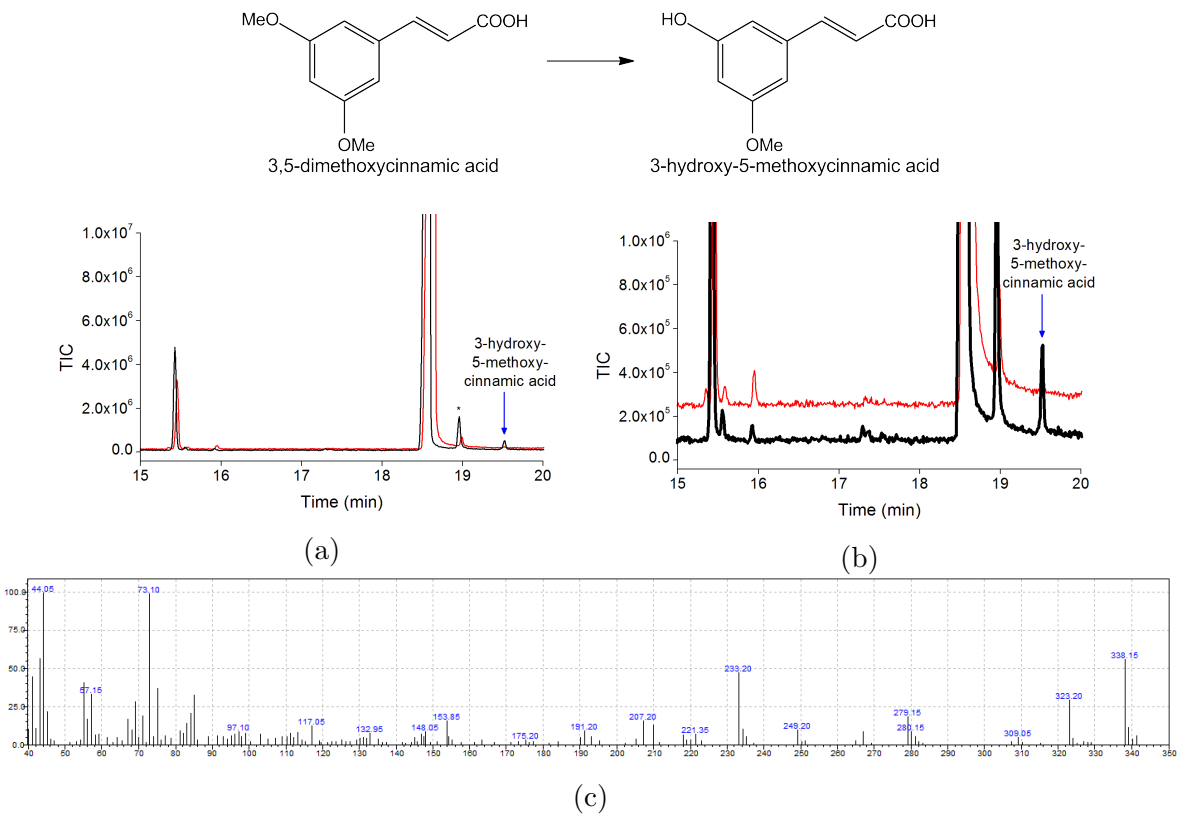

Figure 49: GC-MS analysis of the derivatised CYP199A4 turnover (black) of (a) 3,5-dimethoxycinnamic acid with (b) the product region highlighted. The substrate control (t_R = 15.4 mins, *cis* and t_R = 18.6 mins, *trans*) is in red. For clarity the chromatograms in (b) have been offset along the y axis. (c) Mass spectrum of the derivatised demethylation product.

Very low levels of NADH oxidation activity were detected for CYP199A4 with 3,4,5-trimethoxycinnamic acid, which did not yield any product. In the presence of 2,3,4-trimethoxycinnamic acid, NADH was oxidised at a rate of 39 min^{-1}, and the substrate was turned over into a single product at 24 min^{-1} (Figure 50). GC-MS analysis of the derivatised turnover identified a m/z of 368.0, which agrees with the predicted m/z of 368.6 for a product arising from a single demethylation (Appendix C15). The product was thus assigned as 2,3-dimethoxy-4-hydroxycinnamic acid.

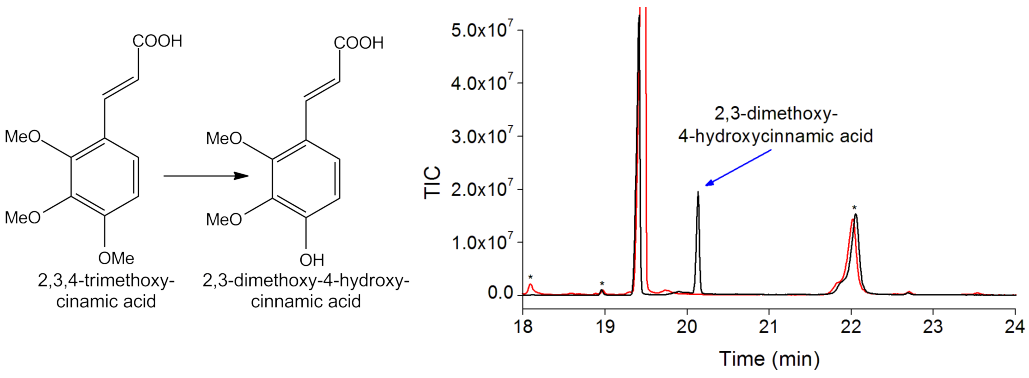

Figure 50: GC-MS analysis of the derivatised CYP199A4 turnover (black) of 2,3,4-trimethoxycinnamic acid. The substrate control (t_R = 19.4 mins) is in red. Impurities are marked (*).

Despite the similar sizes of their spin-state shifts, the NADH oxidation (202 min^{-1}) and product formation (85 min^{-1}) rates of CYP199A4 with 4-methylcinnamic acid were less than half that of the enzyme with 4-methoxycinnamic acid (Table 7). A single oxidation product was observed in the turnover of 4-methycinnamic acid (Figure 51). This was produced in a larger quantity using a whole-cell oxidation system, and was isolated and purified via semi-preparative HPLC. The product was identified by NMR as 4-(hydroxymethyl)cinnamic acid, where a characteristic 2H singlet at 4.52 ppm was observed (Appendix C10). Coelution of the isolated 4-hydroxymethylcinnamic acid with the CYP199A4 turnover of 4-methylcinnamic acid using HPLC showed identical retention times for the oxidation products (Figure 51).

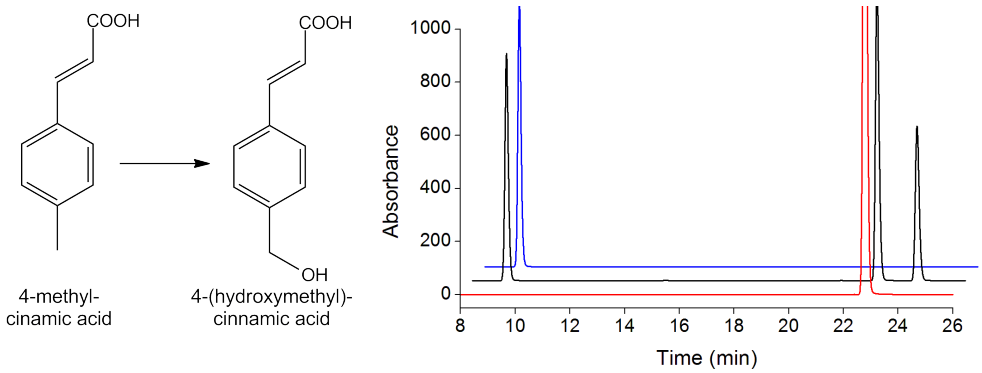

Figure 51: HPLC analysis of the CYP199A4 turnover (black) of 4-methylcinnamic acid. The substrate control (t_R = 22.6 mins) is in red and product control after purification by semi-preparative HPLC (t_R = 9.3 mins) in blue. The internal standard (t_R = 24.3 mins) is also shown. For clarity the chromatograms have been offset along the x and y axes.

While the rate of NADH oxidation with 4-isopropylcinnamic acid was slightly lower than that with the methyl derivative, the coupling was higher (69% vs. 42%), leading to a more rapid product formation rate of 131 min^{-1}. Four products were detected in the derivatised turnover of 4-isopropylcinnamic acid (Figure 52). GC-MS analysis indicated two products from hydroxylation, one from desaturation, and one from further oxidation of an alcohol or the desaturation product (Figure 52 and Appendix C15). These products were also generated in a higher yield using the whole-cell oxidation system. The major product (58%) of the *in vitro* turnover was characterised via NMR as 4-(1-hydroxyisopropyl)cinnamic acid, where a distinctive 6H singlet at 1.42 ppm was observed. The second product, a comparatively minor proportion of the total product distribution (9%), was identified as 4-(2-hydroxyisopropyl)cinnamic acid from the signals of the α- (2.82 ppm) and two β-hydrogens (3.50 ppm and 3.44 ppm, respectively) and their coupling patterns (Appendix C11 and C12). The minor product (2%) was identified as 4-(1,2-epoxyisopropyl)cinnamic acid, based on the coupling (J = 10.8 Hz) between the two epoxide hydrogens at 3.42 ppm and 3.39 ppm (Appendix C13 and C14). The epoxide product likely arises from further oxidation of the desaturation

product, 4-(prop-1-en-2yl)cinnamic acid (31%). Due to their similar retention times, the desaturation product was unable to be separated from the substrate for NMR analysis. However, this product was able to be identified via GC-MS based on the m/z of the derivatised product (260.3), and by the presence of the epoxide. We note here that in the whole-cell turnover, the concentration of 4-(1-hydroxyisopropyl)cinnamic acid > 4-(1,2-epoxyisopropyl)cinnamic acid > 4-(2-hydroxyisopropyl)cinnamic acid > 4-(prop-1-en-2yl)cinnamic acid, suggesting increased further oxidation of the desaturation product.

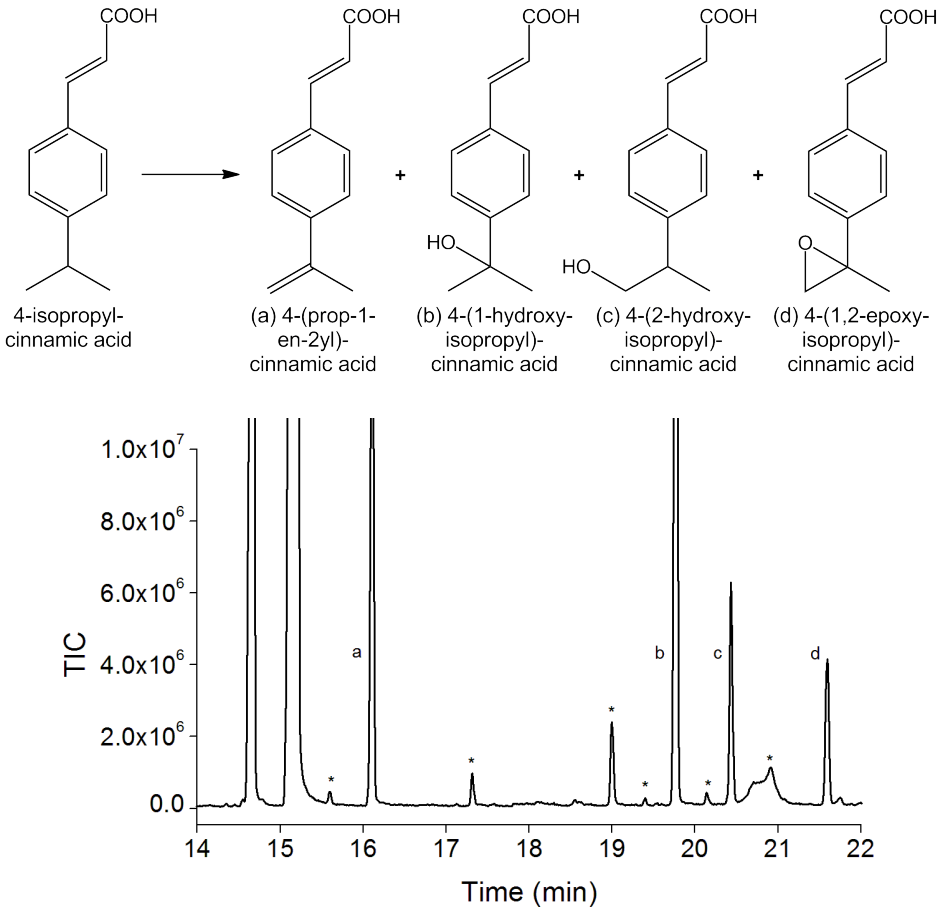

Figure 52: GC-MS analysis of the derivatised CYP199A4 turnover of 4-isopropylcinnamic acid (t_R = 15.2 mins) to (a) 4-(prop-1-en-2yl)cinnamic acid (t_R = 16.1 mins) (b) 4-(1-hydroxyisopropyl)cinnamic acid (t_R = 19.7 mins) (c) 4-(2-hydroxyisopropyl)cinnamic acid (t_R = 20.4 mins) and (d) 4-(1,2-epoxyisopropyl)cinnamic acid (t_R = 21.5 mins). The internal standard (t_R = 14.6 mins) is also shown. Impurities are marked (*).

5.2.3 Whole-cell Oxidations of Cinnamic Acid Derivatives by CYP199A4

A previous study has investigated the oxidation of cinnamic acid, 3- and 4-hydroxycinnamic acid (*m*- and *p*-coumaric acid) by wild-type ($WT_{CYP199A2}$) and mutant forms of CYP199A2 using a whole-cell system comprised of the enzyme and its electron transfer partners Pux and putidaredoxin reductase.[146] Both *m*- and *p*-coumaric acid can both be oxidised by CYP199A2 to 3,4-dihydroxycinnamic acid (caffeic acid), which has many desirable properties for human health and a number of pharmaceutical applications.[141] Using small scale (250 µL), high cell density (50 g cell wet weight L^{-1}) cultures, 1 mM of *p*-coumaric acid was converted into caffeic acid within 4 hours by $WT_{CYP199A2}$ using the *in vivo* oxidation system. When the same system was used on a larger scale (50 mL, 50 g cell wet weight L^{-1}), 2.4 mM of product was generated after 24 hours.[73] Of the CYP199A2 mutants that were constructed, the highest level of *p*-coumaric acid oxidation was observed with $F185L_{CYP199A2}$, which generated 5 mM of caffeic acid in 15 hours. Interestingly, the mutant also acquired oxidative activity for the double hydroxylation of cinnamic acid to caffeic acid, with which the $WT_{CYP199A2}$ enzyme is inactive.[73] We note that cinnamic acid, *m*- and *p*-coumaric acid are poor substrates for CYP199A4, as exemplified by the minimal changes in the spin-state and lack of oxidation activity of the enzyme with these compounds.

Based on this study, we investigated the whole-cell turnover of cinnamic acids and the closely related 3-(4-methoxyphenyl)propionic and 4-methoxyphenylacetic acids by CYP199A4 with its electron transfer partners HaPux and HaPuR using a similar *E. coli* system.[3] Substrate (2 mM) was added to medium scale, low cell density cultures (35 mL, 3 g cell wet weight L^{-1}) at 0 and 4 hours. Samples (1 mL) of the supernatant from the cell cultures were taken after 4 and 24 hours and analysed by HPLC, which revealed that the whole-cell oxidation products were the same as those of the *in vitro* turnovers in all cases.

3-(4-Methoxyphenyl)propionic acid and 3-hydroxy-4-methoxycinnamic acid were the only substrates to be completely turned over in the first 4 hours (Figure 53). HPLC analysis showed only the presence of 3,4-dihydroxycinnamic acid in the turnover of 3-hydroxy-4-methoxycinnamic acid after 24 hours, making it the sole substrate to be converted into product in its entirety. Approximately 20% of the substrate still remained in the turnover of 3-(4-methoxyphenyl)propionic acid after 24 hours.

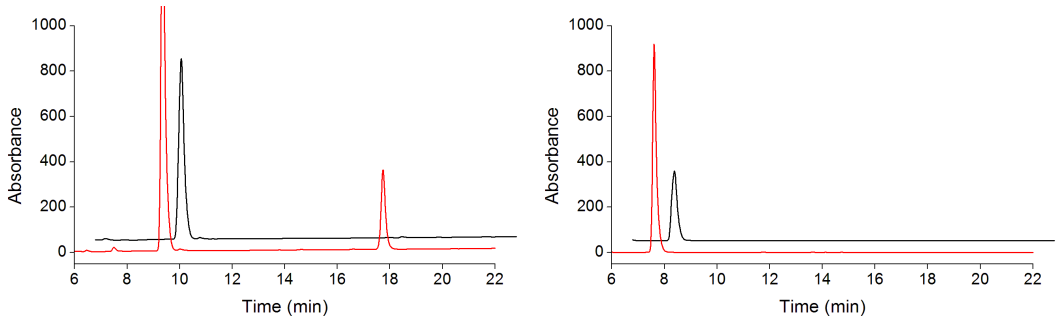

Figure 53: HPLC analysis of the *in vivo* CYP199A4 turnovers after 4 hours (black) and 24 hours (red) of (a) 3-(4-methoxyphenyl)propionic acid (t_R = 17.9 mins) to 3-(4-hydroxyphenyl)propionic acid (t_R = 9.6 mins) and (b) 3-hydroxy-4-methoxycinnamic acid (t_R = 12.8 mins) to 3,4-dihydroxycinnamic acid (t_R = 7.8 mins). For clarity the chromatograms have been offset along the x and y axes.

In the turnovers of both 4-methoxy- and 4-methyl-cinnamic acid, nearly all of the substrate ($\geq$ 95%) was converted into product after 4 and 24 hours. In the turnover of 2,4-dimethoxycinnamic acid, most of the substrate ($\approx$ 75%) had also been oxidised after 4 hours, but the substrate concentration exceeded that of the product after 24 hours (Figure 54a). 3,4-Dimethoxycinnamic acid was turned over at a slower rate compared to 2,4-dimethoxycinnamic acid in the first 4 hours, with over half of the substrate still remaining after this time. Comparable amounts of substrate and product were observed after 24 hours (Figure 54b). Similarly, in the whole-cell oxidation of 4-methoxyphenylacetic acid, approximately 50% of the substrate was depleted after 4 and 24 hours (Appendix C6).

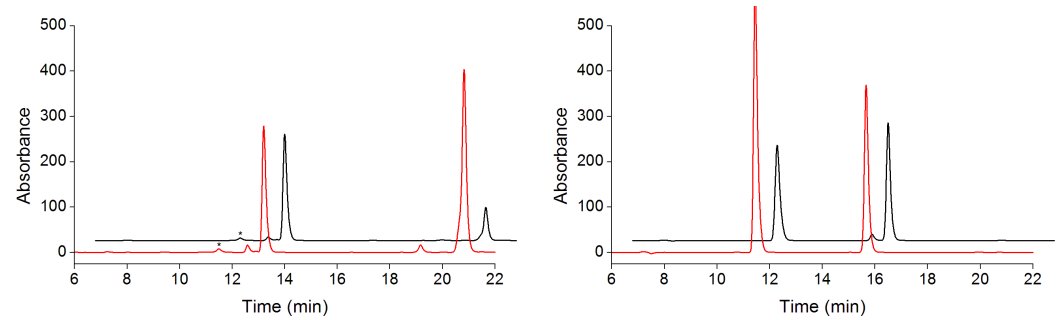

Figure 54: HPLC analysis of the *in vivo* CYP199A4 turnovers after 4 hours (black) and 24 hours (red) of (a) 2,4-dimethoxycinnamic acid (t_R = 19.2 mins, *cis* and t_R = 21.0 mins, *trans*) to 2-methoxy-4-hydroxycinnamic acid (t_R = 12.7 mins, *cis* and t_R = 13.3 mins, *trans*) and (b) 3,4-dimethoxycinnamic acid (t_R = 15.0 mins, *cis* and t_R = 15.9 mins, *trans*) to 3-methoxy-4-hydroxycinnamic acid (t_R = 11.6 mins). For clarity the chromatograms have been offset along the x and y axes. Impurities are marked (*).

While no oxidation product was detected in the *in vitro* turnover of *p*-coumaric acid, the whole-cell oxidation reaction yielded very low levels of caffeic acid (Figure 55a).

No oxidation product could be detected in the turnover of 3,5-dimethoxycinnamic acid after this time. However, a very small amount of product was observed after 24 hours (Figure 55b). The turnovers of cinnamic, *m*-coumaric and 3,5-dimethoxy-4-hydroxycinnamic acid did not yield any detectable product even after 24 hours. This was not unexpected based on the results of their *in vitro* turnovers. Overall, the amount of product formed in the whole-cell turnovers closely reflected the oxidative activity of CYP199A4 in the *in vitro* reactions.

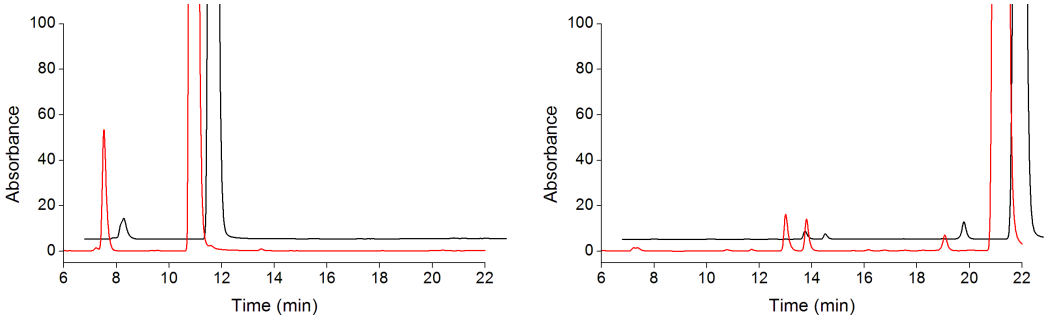

(a) (b)

Figure 55: HPLC analysis of the *in vivo* CYP199A4 turnovers after 4 hours (black) and 24 hours (red) of (a) *p*-coumaric acid (t_R = 11.0 mins) to caffeic acid and (b) 3,5-dimethoxycinnamic acid (t_R = 19.0 mins, *cis* and t_R = 21.0 mins, *trans*) to 3-methoxy-5-hydroxycinnamic acid (t_R = 13.0 mins, *cis* and t_R = 13.9 mins, *trans*). For clarity the chromatograms have been offset along the x and y axes.

5.3 Discussion

CYP199A4 can bind and selectively oxidise a range of *para*-substituted cinnamic acids. Despite the longer length of cinnamic acids when compared to benzoic acids, the trends in the substrate binding affinity for these compounds were similar to those previously observed with the enzyme and similarly-substituted benzoic acids.[20,78,79] The presence of additional substituents at the *ortho*- or *meta*-positions reduced the substrate binding affinity compared to 4-methoxycinnamic acid. However, a methoxy group at the *ortho*-position (2,4-dimethoxycinnamic acid) appeared to be better tolerated than at the *meta*-position (3,4-dimethoxycinnamic acid). Additionally, the tighter binding of 3-hydroxy-4-methoxycinnamic acid relative to the 3,4-dimethoxy derivative suggested that the smaller hydroxy group is better accommodated than the larger methoxy group at the 3-position. *para*-Alkyl substituted cinnamic acids (4-methyl- and 4-isopropylcinnamic acid) were also well-accommodated within the active site of CYP199A4, and bound equally as tightly as 4-methoxycinnamic acid in the case of the isopropyl derivative.

The products of the *in vitro* CYP199A4-catalysed turnovers were generally mirrored by the whole-cell oxidation system with a given substrate. Interestingly, low levels of caffeic acid, which were absent from the *in vitro* oxidation of *p*-coumaric acid, were detected in the whole-cell turnover of this substrate. The 4-hydroxyphenylacetate 3-hydroxylase (4HPA3H) complex native to *E. coli* has been shown to be capable of hydroxylating *p*-coumaric acid in addition to its natural substrate 4-hydroxyphenylacetic acid.[147–149] As overexpression of the 4HPA3H complex was required for any significant hydroxylation activity with *p*-coumaric acid,[147] it is possible that the caffeic acid produced in the *in vivo* turnover of *p*-coumaric acid may have been the result of 4HPA3H rather than CYP199A4 activity. Overall, the comparable product distributions of the *in vitro* and *in vivo* oxidation reactions indicate that either system may be used to accurately demonstrate the activity of CYP199A4.

In all cases, the methoxy-substituted cinnamic acids were exclusively demethylated at the *para*-position, consistent with previous results obtained for their corresponding benzoic acids.[78] The fastest rates of *in vitro* NADH and substrate oxidation were observed with cinnamic acids containing a *para*-substituted framework, though all were slower when compared to 4-methoxybenzoic acid. Replacement of the *para*-methoxy group with a methyl moiety in 4-methylcinnamic acid yielded a single product which was hydroxylated at the 4-position. Two products from hydroxylation, one from desaturation and another from further oxidation were observed for 4-isopropylcinnamic acid, while only a single hydroxylation and desaturation product have been reported

for the turnover of 4-isopropylbenzoic acid by CYP199A4.[79] In the absence of a *para*-substituent, little to no oxidative activity was observed, highlighting the regioselectivity of the enzyme for this position.

The current work shows that in spite of their larger size when compared to benzoic acids, a range of *para*-substituted cinnamic acids can be accommodated within the active site of CYP199A4. The binding affinity and oxidative activities of CYP199A4 with *para*-(methoxy) substituted benzoic acids[78] $\geq$ *para*-substituted cinnamic acids $>$ 3-(4-methoxyphenyl)propionic acid $>$ phenylacetic acids. The activity of CYP199A4 with cinnamic acid substrates closely resembles that of the enzyme with the equivalent benzoic acids, and highlights the selectivity of the enzyme for a planar, benzoic acid- or cinnamic acid-like framework.

Structural studies on the enzyme in complex with a selection of cinnamic acid substrates would provide further insight into the specificity and selectivity of the enzyme. Additionally, a crystal structure of 4-isopropylcinnamic acid-bound CYP199A4 or similar complex could provide insight into the product distribution observed, and shed further light on the mechanisms of CYP199A4-catalysed desaturation reactions.

It is reported that the F185L mutant of the closely-related CYP199A2 enzyme has achieved the highest levels of biotechnological production of caffeic acid through the oxidation of *p*-coumaric acid.[73] Active site mutants of CYP199A4 could be constructed and screened with cinnamic acid derivatives to optimise the binding and activity of the enzyme with these and related compounds. Crystal structures of cinnamic acid-bound CYP199A4 would also aid this avenue of investigation.

Cinnamic acids possess many important medicinal properties including antimicrobial, antiviral, anticancer and antioxidant activities.[141] While these compounds can be extracted from plants where they are naturally found, energy-intensive methods are required, making cinnamic acids attractive synthetic targets.[143] CYP199A4 could be utilised as a biocatalyst in the production of these physiologically important compounds. Additionally, the high regioselectivity of CYP199A4 for oxidation at the *para*-position could be useful for selective hydroxylation, protection and deprotection reactions in synthetic chemistry, especially in the presence of the reactive α,β-unsaturated carboxylic acid moiety of cinnamic acid.

6 Expanding the Substrate Range of CYP199A4

6.1 Introduction

The carboxy terminus of *para*-substituted benzoic acids is important for tight-binding to CYP199A4. Replacement of the carboxy group with an aldehyde or an alcohol has been shown to result in significantly diminished substrate binding and turnover by the enzyme.[79,87] The aldehyde derivative is reported to induce a large, 80% spin-state shift, though binding was 700-fold weaker when compared to 4-methoxybenzoic acid (K_d = 197 µM). No change in the spin-state was observed upon the addition of 4-methoxybenzyl alcohol, which presumably binds very weakly to the enzyme.[79] 4-Methoxybenzamide has also been tested with CYP199A4, but despite inducing a comparable shift to 4-methoxybenzoic acid (> 95%), the substrate bound 2000-fold more weakly (K_d = 660 µM).[87] The oxidation activity of CYP199A4 for these non-benzoic acid derivatives is also very low, occurring between 200-700 times more slowly than the demethylation of 4-methoxybenzoic acid.[79,87] These results, combined with those in Chapter 5, suggest that the substrate range of CYP199A4 may be limited to *para*-substituted benzoic and cinnamic acids and related acidic substrates.

Crystal structures of CYP199A4 in complex with *para*-substituted benzoic acids show that the active site residues Ser95, Ser244, Arg92, and, through a water molecule, Arg243, hydrogen bond to the carboxy group of the substrate (Figure 14). These interactions help hold the *para*-substituent over the heme iron, and account for the substrate specificity and product selectivity of CYP199A4 for aromatic carboxylic acid substrates.[20,79]

The roles of Arg92, Arg243 and Ser95 have also been investigated using mutagenesis studies.[20] Mutation of Arg92 → Glu (R92E) and Arg243 → Thr (R243T) resulted in a large reduction in the affinity of CYP199A4 for 4-methoxybenzoic acid and in the enzyme's NADH oxidation and product formation activities, though coupling remained high.[20] When Ser95 was mutated to valine, the addition of 4-methoxybenzoic acid resulted in no change in the spin-state and greatly diminished rates of NADH oxidation and product formation when compared to the WT enzyme.[20] Phe185, which forms part of the ceiling of the substrate binding pocket of CYP199A4, was also mutated. Mutation to isoleucine and valine (F185V and F185I) lowered the affinity for 4-methoxybenzoic acid, albeit to a lesser extent than in the R92E and R243T mutants. The activities of the F185V and F185I mutants were also much lower than $WT_{CYP199A4}$, and the reduction in activity was more severe for F185I.[20]

Here, we attempted to expand the substrate range of CYP199A4 through mutation of a range of active site and substrate access channel amino acids of the enzyme. These included the above mentioned Arg243, Ser95 and Ser244; Pro94 located at the entrance of the substrate access channel; and Phe182, Phe185 and Thr252 which help define the substrate binding pocket (Figure 56).[20,146] Together, these residues confer the substrate specificity of CYP199A4. In total, thirteen mutants were tested: P94V, S95A, S95D, S95N, F182L, F185V, R243L, R243T, S244A, S244D, S244N, T252N and T252S. These were screened for oxidation activity against a selection of substrates in which the carboxylate group of 4-methoxybenzoic acid has been modified (henceforth referred to as carboxy-modified substrates).

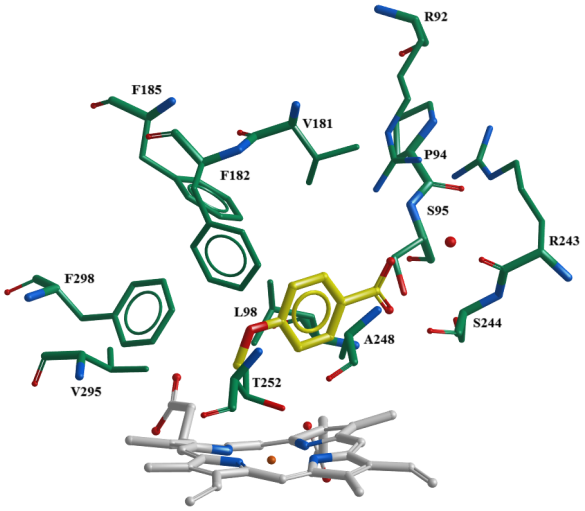

Figure 56: The active site of CYP199A4 with 4-methoxybenzoic acid. The amino acid residues which help confer the substrate specificity of the enzyme have been shown. 4-Methoxybenzoic acid is shown in yellow, the heme in grey and the amino acids in green.[20]

Activity assays with the CYP199A4 variants and a range of carboxy-modified substrates will enable us to explore the selectivity of the enzyme (or lack thereof) for demethylation at the *para*-methoxy position in the presence of additional functional groups. The affinity of the CYP199A4 mutants for these carboxy-modified substrates will also provide further insight into the enzyme-substrate interactions required for substrate binding.

6.2 Results

6.2.1 *In Vivo* Screening of CYP199A4 Mutants

The active site mutants mentioned previously and the redox partners of CYP199A4, HaPux and HaPuR,[3] were expressed in *E. coli* as whole-cell systems. Four substrates, 4-methoxybenzoic acid, 4-methoxyacetophenone, 4-methoxyphenol and 4-methoxynitrobenzene (4-nitroanisole), were added to a final concentration of 2 mM to small scale, low cell density cultures (15 mL, 3 g cell wet weight L^{-1}). These substrates were chosen based on their noticeably different functionalities *para* to the methoxy group, and provided an indication of the likely affinity and activity of the mutants towards carboxy-modified substrates. In addition, the yellow 4-nitrophenol product arising from 4-nitroanisole *O*-demethylation gives a visual indication on the progress of substrate oxidation. The whole-cell turnovers were analysed after 3 and 18 hours by HPLC and in the case of 4-nitroanisole, UV/Vis spectrometry.

The oxidation activities of most of the mutants were high for 4-methoxybenzoic acid. After 3 hours, no substrate remained in the whole-cell turnovers of 4-methoxybenzoic acid by the P94V, S95A, F185V, R243L, R243T, S244A and S244D variants. Most of the substrate had been oxidised to product in 3 hours in the S95N turnover, while approximately half still remained in the T252S oxidation reaction. The remaining substrate in these turnovers was converted into product after 18 hours (Figure 57). Small amounts of 4-hydroxybenzoic acid were observed in the S244N and T252N whole-cell oxidations after 3 hours, with a similar ratio of substrate to product being observed after an additional 15 hours. Only trace quantities of 4-hydroxybenzoic acid were generated by S95D and F182L even after 18 hours (Figure 57).

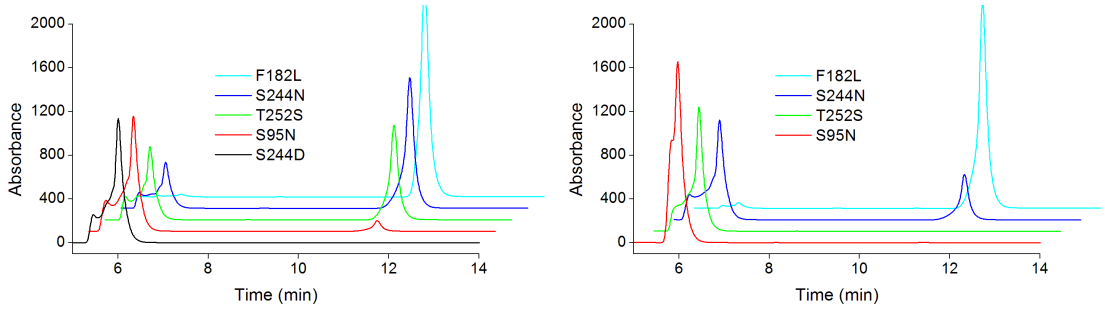

Figure 57: HPLC analysis of the whole-cell oxidation of 4-methoxybenzoic acid (t_R = 11.4 mins) to 4-hydroxybenzoic acid (t_R = 6.0 mins) by CYP199A4 variants after (a) 3 hours and (b) 18 hours. The split-peak of 4-hydroxybenzoic acid is also observed in the HPLC analysis of the authentic product sample. For clarity the chromatograms have been offset along the x and y axes.

The oxidation activities of the mutants for 4-methoxyacetophenone were considerably lower. Only in the S244D turnover was a large amount of product generated after 3 hours (Figure 58a). A small amount of 4-hydroxyacetophenone was produced by S244A after this time, and even smaller quantities were observed in the whole-cell oxidations by S95A, R243L and R243T. Very low levels of 4-hydroxyacetophenone were detected in the turnovers of P94V, S95D, S95N, F182L and S244N, with barely any product observed in the remaining whole-cell oxidations by T252S, T252N and F185V (Figure 58a). After 18 hours, only small increases in the product concentrations were observed but almost all the substrate was converted in the S244D mutant (Figure 58b).

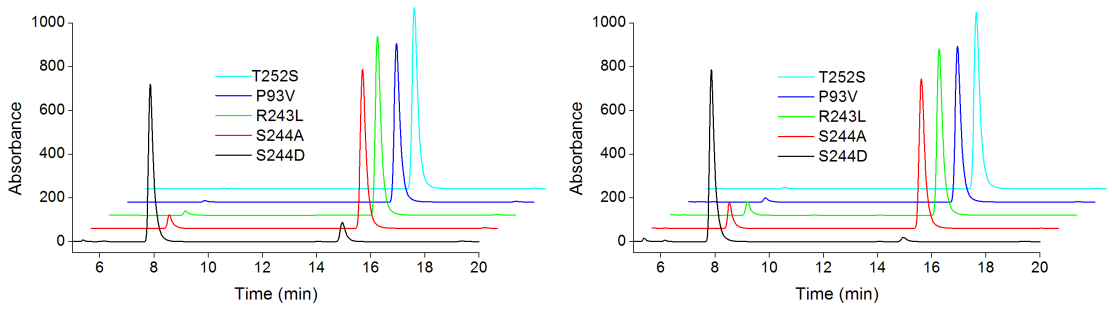

Figure 58: HPLC analysis of the whole-cell oxidation of 4-methoxyacetophenone (t_R = 15.0 mins) to 4-hydroxyacetophenone (t_R = 8.0 mins) by CYP199A4 variants after (a) 3 hours and (b) 18 hours. For clarity the chromatograms have been offset along the x and y axes.

The S244D variant also exhibited noticeably higher oxidation activity with 4-methoxyphenol compared to the other mutants, converting all of the substrate to product in the first 3 hours. Considerably lower, though comparable levels of product were formed by F182L and S95D after this time (Figure 59). Very low levels of product, if any, were detected in the remaining turnovers after 3 hours, and minimal conversion of substrate to product occurred in the whole-cell oxidations after a further 15 hours.

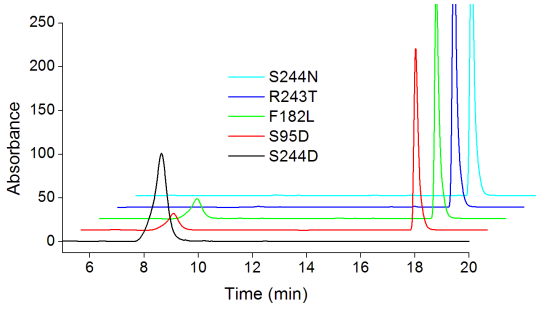

Figure 59: HPLC analysis of the whole-cell oxidation of 4-methoxyphenol (t_R = 18.2 mins) to hydroquinone (t_R = 8.5 mins) by CYP199A4 variants after 3 hours. For clarity the chromatograms have been offset along the x and y axes.

In the colourimetric assay of 4-nitroanisole turnover, noticeably more yellow 4-

nitrophenol product, greater than 3 times as much as in the other turnovers, was formed by S244D in the first 3 hours (Figure 60a). The other whole-cell reactions were visibly paler in colour compared to S244D. After 18 hours, S244A had generated comparable levels of product to S244D while the product concentrations of the remaining whole-cell oxidations were less than half that of S244D and S244A (Figure 60b).

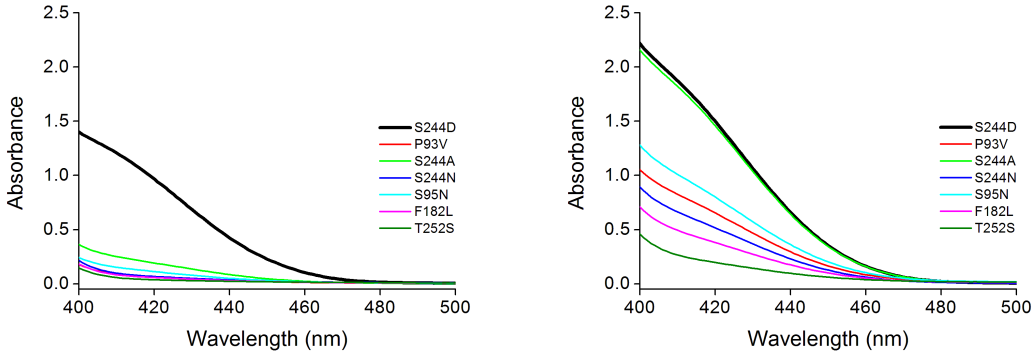

Figure 60: UV/Vis spectra of the supernatant from 4-nitroanisole oxidation by CYP199A4 variants after (a) 3 hours and (b) 18 hours.

With the caveat that some mutations may have an effect on CYP199A4 folding and therefore production levels, these results indicate that the S244D mutant of CYP199A4 exhibited the highest oxidation activity with 4-methoxyacetophenone, 4-methoxyphenol and 4-nitroanisole. A comparison of the total combined product levels of each substrate revealed that behind S244D, the activity of the other mutants for the carboxy-modified substrates was: S244A > S95N > R243L ≈ R243T > P94V ≈ S244N ≈ S95A ≈ S95D > F182L ≈ T252S ≈ F185V ≈ T252N. Therefore, S244D was selected for further study with a range of carboxy-modified substrates (Figure 61). For comparison and to ascertain the reliability of our whole-cell screening process, the S244N mutant, which demonstrated only modest oxidation activity, was also investigated.

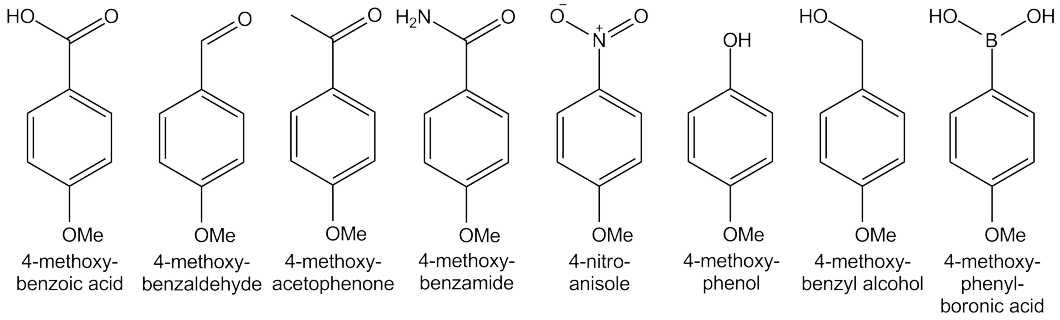

Figure 61: Carboxy-modified substrates of WT, S244D and S244N CYP199A4.

6.2.2 Activity and Product Formation Assays with the S244D and S244N Mutants of CYP199A4

The NADH oxidation and product formation rates were measured for a range of carboxy-modified substrates (Table 8). The products were identified by HPLC coelution of the turnovers with authentic product samples. In all cases, substrates were exclusively demethylated at the *para*-methoxy group.

Table 8: *In vitro* turnover data for WT, S244D and S244N CYP199A4 with carboxy-modified substrates. The data are given as mean ± S.D. with $n \geq 3$. Rates are given as nmol.nmol-P450^{-1}.min^{-1} (min^{-1}). The average leak rate was 9.0 min^{-1}, 3.0 min^{-1} and 5.0 min^{-1} for WT, S244D and S244N CYP199A4, respectively.

Substrate	NADH (min^{-1})	PFR (min^{-1})	Coupling (%)
4-methoxybenzoic acid[78]	1340 ± 28	1219 ± 120	91 ± 2
4-methoxybenzoic acid$_{S244D}$	566 ± 2	460 ± 27	82 ± 4
4-methoxybenzoic acid$_{S244N}$	25.9 ± 2.2	15 ± 1	58 ± 1
4-methoxynitrobenzene	-[a]	14 ± 2[b]	71 ± 3
4-methoxynitrobenzene$_{S244D}$	-[a]	270 ± 14[b]	81 ± 4
4-methoxynitrobenzene$_{S244N}$	-[a]	2.5 ± 0.1[b]	21 ± 1
4-methoxyacetophenone	9.1 ± 0.2	1.4 ± 0.1	15 ± 1
4-methoxyacetophenone$_{S244D}$	160 ± 7	140 ± 3	85 ± 2
4-methoxyacetophenone$_{S244N}$	11.1 ± 1.2	2.5 ± 0.4	23 ± 2
4-methoxybenzaldehyde[79]	15 ± 2.0	3.0 ± 0.1	17 ± 1
4-methoxybenzaldehyde$_{S244D}$	868 ± 32	860 ± 33	99 ± 2
4-methoxybenzaldehyde$_{S244N}$	6.31 ± 0.53	2.1 ± 0.1	34 ± 2
4-methoxybenzamide[87]	15 ± 2.1	1.8 ± 0.1	13 ± 1.6
4-methoxybenzamide$_{S244D}$	1050 ± 6	1050 ± 52	100 ± 5
4-methoxybenzamide$_{S244N}$	12.5 ± 0.2	4.8 ± 0.3	38 ± 2
4-methoxyphenylboronic acid	15 ± 1	4.0 ± 0.5	27 ± 2
4-methoxyphenylboronic acid$_{S244D}$	131 ± 8	55 ± 6	42 ± 2
4-methoxyphenylboronic acid$_{S244N}$	10.9 ± 1.0	2.8 ± 0.4	26 ± 2
4-methoxyphenol	8 ± 0.3	0.7 ± 0.1	9 ± 0.5
4-methoxyphenol$_{S244D}$	841 ± 56	600 ± 35	72 ± 4
4-methoxyphenol$_{S244N}$	20.3 ± 1.2	2.4 ± 0.4	12 ± 1
4-methoxybenzyl alcohol	19 ± 1	4.0 ± 0.6	21 ± 2
4-methoxybenzyl alcohol$_{S244D}$	295 ± 2	260 ± 25	90 ± 2
4-methoxybenzyl alcohol$_{S244N}$	10.1 ± 1.0	2.4 ± 0.3	24 ± 3

[a]Not determined due to interfering absorbance at 340 nm. [b]Determined by monitoring the 4-nitrophenol formed using the A_{410}.

In the turnover of 4-methoxybenzoic acid, S244D oxidised NADH at less than half the rate of the WT enzyme (566 min^{-1}).[78] However, the reaction remained tightly coupled (82%), resulting in the formation of 4-hydroxybenzoic acid at 463 min^{-1}. The activity of S244N with 4-methoxybenzoic acid was considerably lower (Table 8). The NADH oxidation and product formation rates were 50- and 80-fold slower than $WT_{CYP199A4}$ (26 min^{-1} and 15 min^{-1}, respectively), and the coupling efficiency of the reaction was also reduced (58%, Appendix D1).

The rates of NADH oxidation and product formation by S244D with 4-methoxybenzaldehyde were nearly 60- and 300-fold faster when compared to $WT_{CYP199A4}$.[79] The coupling of redox equivalents to product formation was also significantly improved (99% vs. 17%), generating 4-hydroxybenzaldehyde at 860 min^{-1}. In the turnover of 4-methoxybenzaldehyde by S244N, almost no change in NADH oxidation above the leak rate of the enzyme in the absence of substrate was observed. The coupling efficiency of the reaction was moderate (34%) and 4-hydroxybenzaldehyde was produced at a diminished rate of 2.1 min^{-1} (Appendix D1).

The activity of S244D was highest with 4-methoxybenzamide, where the NADH oxidation and product formation rates were improved by 70- and 600-fold, respectively (Figure 62a). The coupling of redox equivalents to product formation was complete and resulted in the production of 4-hydroxybenzamide at a rate of 1050 min^{-1} (Figure 63). The rate of NADH oxidation by S244N with 4-methoxybenzamide was comparable to that of the WT enzyme, but product formation was slightly faster (4.8 min^{-1} vs. 3.0 min^{-1}) due to the higher coupling efficiency of the reaction (38% vs. 13%).

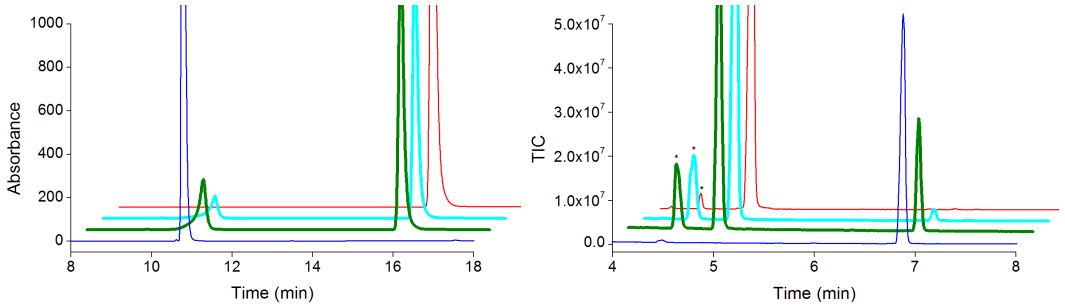

(a) (b)

Figure 62: (a) HPLC analysis of the S244D (green) and S244N CYP199A4 (cyan) turnovers of 4-methoxybenzamide. The substrate control (t_R = 15.9 mins) is shown in red and product control (t_R = 10.9 mins) in blue. (b) GC-MS analysis of the S244D (green) and S244N (cyan) turnovers of 4-methoxyphenol. The substrate control (t_R = 4.9 mins) is in red and product control (t_R = 6.9 mins) in blue. For clarity the chromatograms have been offset along the x and y axes. Impurities are marked (*).

A similar result was obtained for S244N with the ketone derivative, 4-

methoxyacetophenone. Only a very small increase was observed in the NADH oxidation rate relative to $WT_{CYP199A4}$, but the coupling efficiency was higher (23% vs. 15%), resulting in faster production of 4-hydroxyacetophenone (2.5 min^{-1} vs. 1.4 min^{-1}, Table 8). In comparison, a 100-fold increase in the rate of product formation was observed with S244D (140 min^{-1}), and the reaction was much more tightly coupled (85%, Appendix D1).

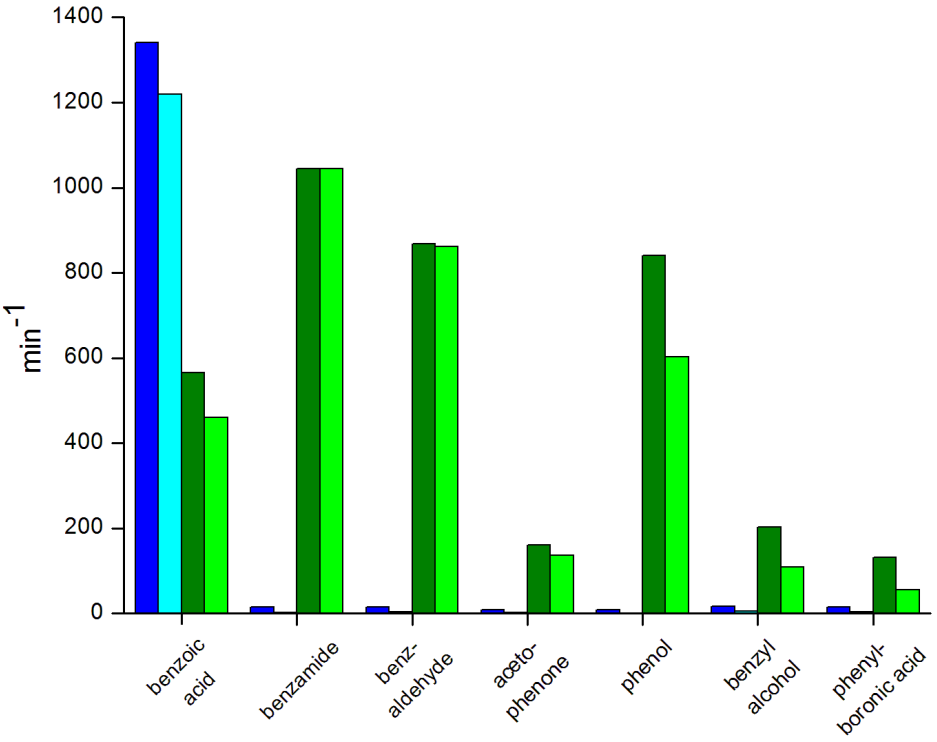

Figure 63: The respective NADH oxidation and product formation rates of WT (blue and cyan) and S244D CYP199A4 (green and lime) with selected carboxy-modified substrates. The activity of S244N has not been shown as it is comparable with WT except with 4-methoxybenzoic acid (Table 8).

The most dramatic improvement in activity was observed in the S244D turnover of 4-methoxyphenol (Figure 63), where the rates of NADH oxidation and product formation were accelerated by 100- and 900-fold (841 min^{-1} and 600 min^{-1}, respectively). The coupling efficiency was also much higher than that of the WT enzyme (72% vs. 9%, Table 8). A single product was identified as hydroquinone after derivatisation using BSTFA/TMSCl and GC-MS analysis. In comparison, only a very small amount of product was observed in the turnover of 4-methoxyphenol by S244N (Figure 62b). The turnover of the 4-methoxybenzyl alcohol substrate was also improved by S244D, albeit to a lesser extent. A 10-fold increase was observed in the rate of NADH oxidation (202 min^{-1} vs. 16 min^{-1}), along with a 20-fold increase in product formation (110 min^{-1} vs. 5.6 min^{-1}). The activity of S244N with 4-methoxybenzyl alcohol was slightly lower than the WT enzyme due to reduced levels of NADH oxidation (10 min^{-1}) and comparable coupling (24%, Appendix D1).

A decrease in the product formation rate was observed with the asparagine mutant in the presence of 4-methoxyphenylboronic acid relative to $WT_{CYP199A4}$ (2.8 min^{-1} vs. 4.0 min^{-1}) due to slower NADH oxidation (11 min^{-1} vs. 15 min^{-1}). However, the rate of NADH oxidation was noticeably faster with S244D (131 min^{-1}), which, together with an increase in the coupling efficiency (42% vs. 27%), resulted in the production of 4-hydroxyphenylboronic acid at 55 min^{-1} (Appendix D1).

The rates of NADH oxidation with 4-nitroanisole could not be determined as the substrate absorbs strongly at 340 nm. However, as the oxidation product 4-nitrophenol absorbs strongly at 410 nm, this wavelength was used to measure the product formation rate using UV/Vis spectrometry (Figure 64). The product formation rate of S244N was slower than the WT enzyme (2.5 min^{-1} vs. 14 min^{-1}) as was the coupling efficiency of the reaction (21% vs. 71%). While only a modest increase in coupling was observed with S244D (81%), the rate of product formation was approximately 20 times faster (270 min^{-1}).

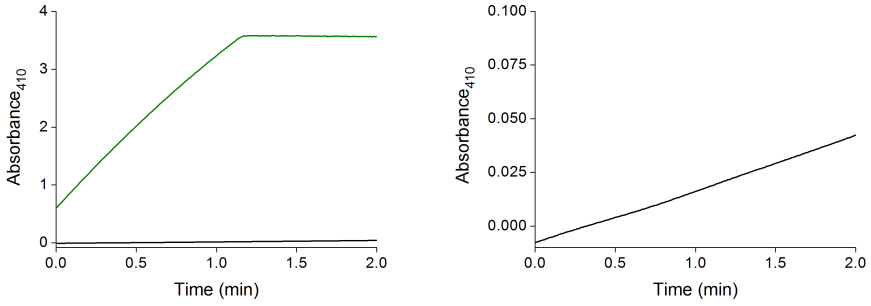

(a) (b)

Figure 64: (a) The WT (black) and S244D CYP199A4 (green) turnovers of 4-nitroanisole monitored at 410 nm with (b) a zoomed in version of the WT turnover. The S244N turnover has not been shown as it is similar to that of the WT enzyme.

Overall, the results show a significant improvement in the oxidation activity of S244D relative to $WT_{CYP199A4}$ while little to no improvement was observed for S244N (Figure 63). These observations reflect the relative activity of S244D and S244N from the initial screening studies.

6.2.3 Activity and Product Formation Assays with S244D CYP199A4

As S244D was very active with the above substrates, the enzyme was tested with additional carboxy-modified derivatives (Figure 65). The same substrates were also tested with $WT_{CYP199A4}$ to determine the relative improvements in oxidation activity (or lack thereof) with the aspartate mutant.

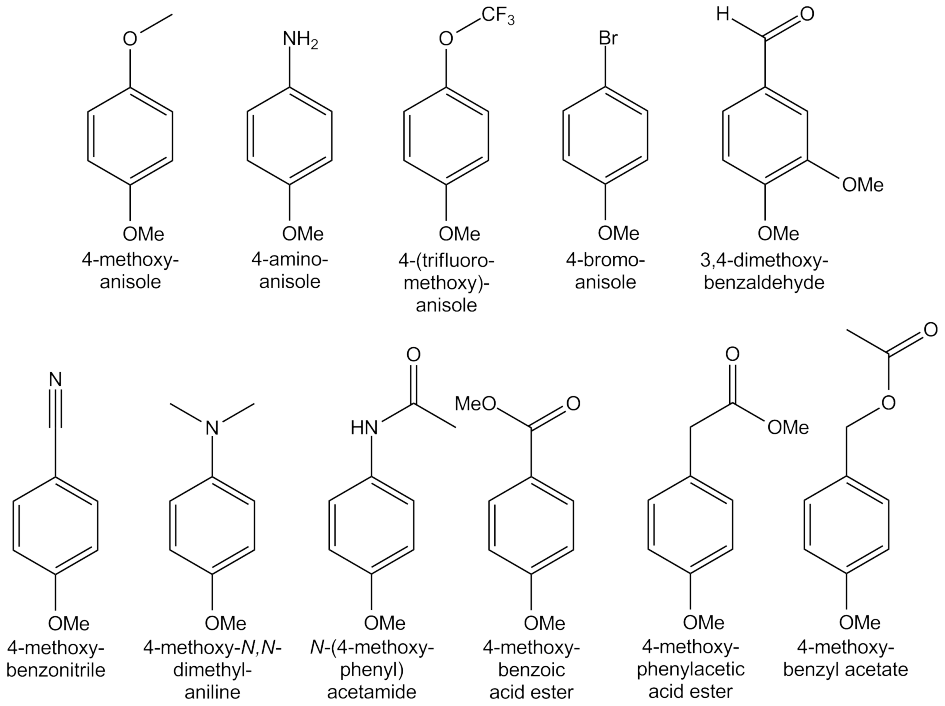

Figure 65: Carboxy-modified substrates of WT and S244D CYP199A4.

Moderate improvements were observed in the turnover of 4-methoxybenzonitrile. The NADH oxidation rate (89 min^{-1} vs. 20 min^{-1}) and coupling efficiency (37% vs. 19%) were higher with S244D, resulting in a 10-fold increase in the generation of 4-cyanophenol (33 min^{-1} vs. 3.8 min^{-1}, Figure 66).

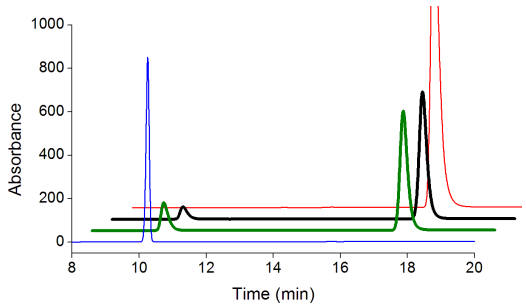

Figure 66: HPLC analysis of the WT (black) and S244D CYP199A4 (green) turnovers of 4-methoxybenzonitrile. The substrate control (t_R = 17.2 mins) is shown in red and product control (t_R = 10.2 mins) in blue. For clarity the chromatograms have been offset along the x and y axes.

The oxidation of 4-bromoanisole by $WT_{CYP199A4}$ was tightly coupled (80%) and

proceeded relatively quickly at 82 min^{-1}. The same substrate was oxidised to 4-bromophenol even more rapidly by S244D at a rate of 690 min^{-1} (Table 9 and Appendix D2). 4-Methoxyanisole was oxidised very slowly to 4-methoxyphenol by $WT_{CYP199A4}$ (0.2 min^{-1}). A small improvement in the rate of 4-methoxyanisole oxidation (9 min^{-1}) was observed for S244D. Interestingly, hydroquinone was the sole product detected in the S244D reaction, suggesting further oxidation of the 4-methoxyphenol product (Figure 67). This can be explained as 4-methoxyphenol is a more favourable substrate for S244D based on its rapid oxidation to hydroquinone by this enzyme (600 min^{-1}, Table 8).

Table 9: *In vitro* turnover data for WT and S244D CYP199A4 with carboxy-modified substrates. The data are given as mean ± S.D. with $n \geq 3$. Rates are given as nmol.nmol-$P450^{-1}$.min^{-1} (min^{-1}). The average leak rate was 9.0 min^{-1} and 3.0 min^{-1} for WT and S244D CYP199A4, respectively.

Substrate	NADH (min^{-1})	PFR (min^{-1})	Coupling (%)
4-methoxybenzoic acid methyl ester	15 ± 1	2.9 ± 0.2	19 ± 1
4-methoxybenzoic acid methyl $ester_{S244D}$	18 ± 1	12 ± 2	67 ± 6
4-methoxyphenylacetic acid methyl ester	16 ± 0.4	1.4 ± 0.1	7 ± 0.4
4-methoxyphenylacetic acid methyl $ester_{S244D}$	15 ± 1	3.1 ± 0.3	21 ± 2
4-methoxybenzonitrile	20 ± 1	3.8 ± 0.2	19 ± 1
4-methoxybenzonitrile$_{S244D}$	89 ± 1	33 ± 2	37 ± 2
4-methoxyanisole	10 ± 0.4	0.16 ± 0.03	2 ± 0.3
4-methoxyanisole$_{S244D}$	55 ± 3	9 ± 1	16 ± 1
4-bromoanisole	102 ± 2	82 ± 7	80 ± 8
4-bromoanisole$_{S244D}$	773 ± 27	690 ± 34	90 ± 8
4-(trifluoromethoxy)anisole	16 ± 1	1.7 ± 0.2	11 ± 1
4-(trifluoromethoxy)anisole$_{S244D}$	50.9 ± 3.4	16.5 ± 0.8	33 ± 1
3,4-dimethoxybenzaldehyde	9 ± 0.3	1 ± 0.1	0.1 ± 0.01
3,4-dimethoxybenzaldehyde$_{S244D}$	10 ± 1	8.4 ± 0.7	83 ± 6

Virtually no change was observed in the NADH oxidation activity of S244D relative to $WT_{CYP199A4}$ with the methyl esters of 4-methoxybenzoic acid and 4-methoxyphenylacetic acid (Appendix D2). However, the product formation rates were faster due to the increased coupling efficiencies of the S244D reactions (Table 9). The acetic acid ester derivative, 4-methoxybenzyl acetate, was also tested with the enzymes, but the substrate was found to undergo ester hydrolysis under the reaction conditions, as previously observed for 4-acetoxybenzoic acid. The turnover of 4-(trifluoromethoxy)anisole by $WT_{CYP199A4}$ gave rise to 4-(trifluoromethoxy)phenol at a mere 1.7 min^{-1}. The product formation activity was higher with S244D (17 min^{-1}) due to faster NADH oxidation (51 min^{-1} vs. 16 min^{-1}) and the reaction being more

tightly coupled (33% vs. 11%). The nitrogen-containing substrates 4-aminoanisole, *N*-(4-methoxyphenyl)acetamide and 4-methoxy-*N,N*-dimethylaniline did not yield any product (Appendix D2).

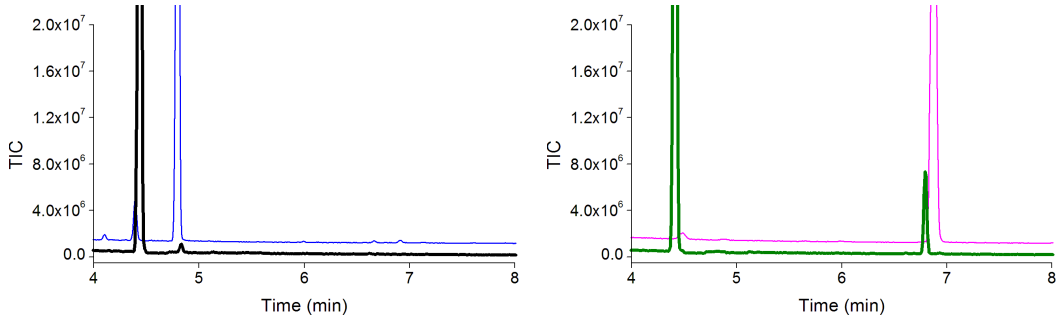

Figure 67: GC-MS analysis of the derivatised turnovers of 4-methoxyanisole (t_R = 4.4 mins) by (a) $WT_{CYP199A4}$ (black) with the 4-methoxphenol (t_R = 4.9 mins) product control shown in blue and (b) S244D (green) with the hydroquinone (t_R = 6.9 mins) product control in pink. All of the 4-methoxyphenol has been converted into hydroquinone in (b). For clarity the chromatograms have been offset along the y axis.

The addition of 3,4-dimethoxybenzaldehyde (veratraldehyde) to $WT_{CYP199A4}$ and the aspartate mutant did not result in any appreciable increase in the rates of NADH oxidation above the leak rates of the enzymes. Combined with the lack of coupling of redox equivalents to product formation ($\approx$ 1%), only trace amounts of 3-methoxy-4-hydroxybenzaldehyde (vanillin) were detected in the WT turnover. The S244D reaction was much more tightly coupled (83%), producing vanillin at a rate of 8 min^{-1} (Appendix D2). The oxidation of veratraldehyde to vanillin further demonstrates the selectivity of CYP199A4 for demethylation solely at the *para*-position. This is similar to previous studies on the WT enzyme with 3,4-dimethoxybenzoic acid (veratric acid), which was exclusively oxidised to 3-methoxy-4-hydroxybenzoic acid (vanillic acid).[3]

Given the high oxidation activity of S244D, we investigated the substrate binding affinity of this enzyme relative to $WT_{CYP199A4}$ for the methoxy-modified compounds (Table 10). In the WT enzyme, there is generally a clear relationship between the binding affinity and activity of the enzyme with a particular substrate, where tight substrate binding usually leads to fast substrate oxidation. For example, $WT_{CYP199A4}$ has high affinity for a range of *para*-substituted benzoic acids, with which it is highly active.[78,79] On the other hand, activity is low for substrates including 4-methoxyphenylacetic acid methyl ester, 4-methoxybenzonitrile and 4-methoxyphenylboronic acid, in line with the enzyme's low affinity for these substrates (Table 10 and Appendix D6).

Such a relationship between affinity and activity is less apparent in S244D. As an example, in spite of the high NADH oxidation and product formation activities of S244D

with 4-methoxybenzamide, the substrate induced a smaller spin-state shift (20%) and bound 4-fold more weakly to S244D (K_d = 3000 µM) than to the WT enzyme (Table 10).[87] While the S244D turnover of 4-methoxyphenylboronic acid was 20-fold slower when compared to 4-methoxybenzamide, the enzyme exhibited a similar binding affinity for the boronic acid derivative (K_d = 1500 µM, 20% shift).

Table 10: Substrate binding data on WT and S244D CYP199A4 with carboxy-modified substrates. The data are given as mean ± S.D. with $n \geq 3$.

	WT	WT	S244D	S244D
Substrate	% HS	K_d (µM)	% HS	K_d (µM)
4-methoxybenzoic acid	>95	0.28 ± 0.01[78]	70	880 ± 30
4-methoxybenzaldehyde	80	197 ± 7[79]	80	210 ± 4
4-methoxybenzyl alcohol	0	-[a]	40	1300 ± 79
4-methoxybenzoic acid methyl ester	10	-[a]	10	-[a]
4-methoxyphenylacetic acid methyl ester	50	3900 ± 270	<5	-[a]
4-methoxybenzyl acetate	0	-[a]	10	310 ± 35
4-methoxyacetophenone	<5	4.8 ± 0.9	10	1200 ± 120
4-methoxybenzamide	>95	660 ± 36	15	3000 ± 80
4-methoxyphenylboronic acid	0	5900 ± 230	20	1500 ± 40
4-methoxybenzonitrile	75	6000 ± 180	5	1400 ± 80
4-methoxyphenol	5	-[a]	60	110 ± 3
4-methoxyanisole	0	-[a]	5	-[a]
4-bromoanisole	55	-[a]	30	170 ± 8
4-aminoanisole	type II	-[a]	type II	310 ± 10
4-nitroanisole	0	-[a]	<5	-[a]
4-(trifluoromethoxy)anisole	0	-[a]	5	110 ± 24
3,4-dimethoxybenzaldehyde	0	-[a]	0	-[a]
N-(4-methoxyphenyl)acetamide	0	-[a]	<5	-[a]
4-methoxy-*N*,*N*-dimethylaniline	0	-[a]	<5	-[a]

[a]Not determined due to minimal spin-state shifts.

On the other hand, the addition of 4-methoxybenzaldehyde to S244D – with which the enzyme was also highly active – resulted in virtually the same spin-state shift (80%) and binding affinity (K_d = 210 µM) previously observed with $WT_{CYP199A4}$ (Figure 68a and 68b).[79] The most notable improvement in substrate binding to S244D was observed with 4-methoxyphenol. While this substrate induced negligible changes in the spin-state of $WT_{CYP199A4}$, a 60% shift was observed for S244D with 4-methoxyphenol, which bound the most tightly of the carboxy-modified substrates (K_d = 110 µM, Figure 68c and 68d).

The addition of 4-aminoanisole to S244D resulted in a type II shift, red-shifting the low-spin Soret band at 418 nm by ≈ 1 nm (Figure 68e). The substrate bound with moderate affinity to the enzyme, with a dissociation constant of 310 µM (Figure 68f). The type II binding observed suggests direct coordination of the nitrogen atom of 4-aminoanisole to the heme iron. This could inhibit commencement of the P450 catalytic cycle, resulting in the lack of product formation observed. Overall, these results indicate that a low substrate binding affinity does not imply low oxidation activity in S244D, but do provide further evidence of the role of Ser244 in substrate recognition and binding in CYP199A4.[20]

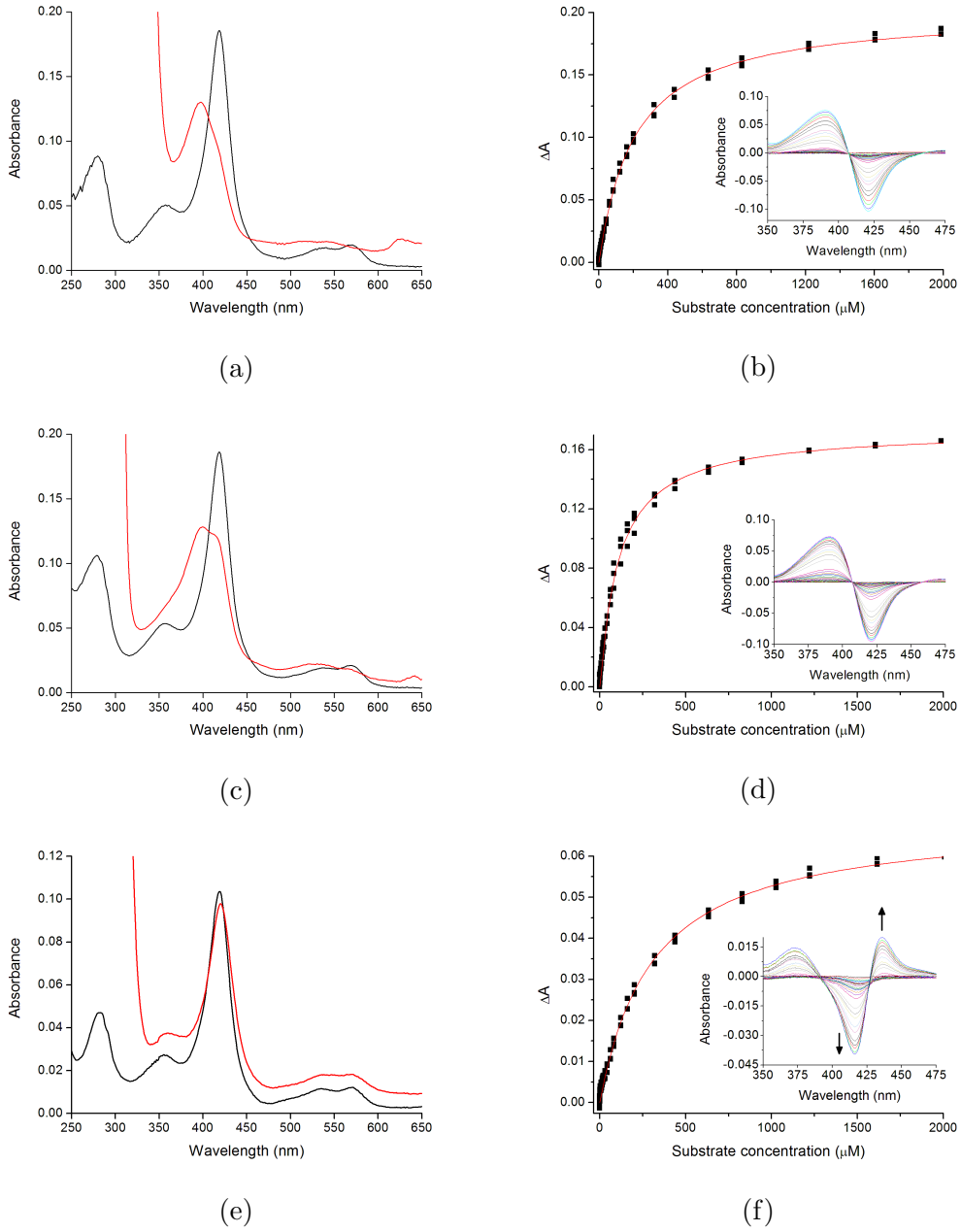

Figure 68: The respective spin-state shifts and dissociation constant analyses of S244D with 4-methoxybenzaldehyde (a) and (b), 4-methoxyphenol (c) and (d), and 4-aminoanisole (e) and (f).

6.3 Discussion

Significant improvements were observed in the activity of S244D relative to $WT_{CYP199A4}$ for non-benzoic acid substrates. The rates of NADH oxidation and product formation by this mutant with 4-methoxybenzamide, 4-methoxybenzaldehyde and 4-methoxyphenol were comparable to those reported for the demethylation of *para*-methoxy benzoic acids by $WT_{CYP199A4}$.[78] However, none exceeded that of the WT enzyme with 4-methoxybenzoic acid.[78] In contrast, the S244N mutant exhibited low oxidation activity with 4-methoxybenzoic acid and the carboxy-modified substrates, demonstrating little to no improvement when compared to $WT_{CYP199A4}$.

The substrates which yielded oxidation products were all exclusively demethylated at the *para*-methoxy position, consistent with previous results obtained for CYP199A4.[3,20,78,79] This suggests that the positioning of the substrate in the active site of S244D and S244N is likely reminiscent of the binding of 4-methoxybenzoic acid to the WT enzyme, with the methoxy group held closest to the heme iron for selective oxidation (Figure 56). It is likely that the majority of the interactions of the substrate benzene ring and methoxy group observed in the crystal structure of 4-methoxybenzoic acid-bound $WT_{CYP199A4}$ (PDB: 4DO1) remain intact in the Ser244 mutants. In addition, the carboxy-modified terminus could potentially interact with Arg92, Ser95, and Arg243 (Figure 56) as well as the acidic and neutral side chains of Asp244 and Asn244, respectively.

The binding studies on S244D revealed that unlike for the $WT_{CYP199A4}$ enzyme, there did not appear to be a clear relationship between binding affinity and oxidation activity. Additionally, the Ser $\rightarrow$ Asp mutation appeared to reduce the overall substrate binding affinity of CYP199A4. For example, while 4-methoxyphenol bound the most tightly to S244D, binding was almost 400-fold lower when compared to $WT_{CYP199A4}$ with 4-methoxybenzoic acid.[78] This implies a reduction in the substrate specificity of the CYP199A4 enzyme, which would be consistent with the replacement of a key active site residue. The reduced substrate binding affinity of S244D could potentially also be a consequence of structural changes in the active site away from Asp244 induced by this mutation.

Overall, the results show that while $WT_{CYP199A4}$ exhibits low oxidation activity for substrates in which the carboxy-terminus of the benzoic acid moiety has been modified, mutation of Ser244 to an aspartate residue significantly improves the activity of the enzyme in spite of generally weaker substrate binding. The current work demonstrates the potential of S244D as a biocatalyst for the regioselective oxidative demethylation

of benzene substrates at the *para*-position under mild conditions in the presence of reactive functional groups including aldehydes and nitrile groups. We note here that selectivity is also maintained when additional methoxy groups are present, as was observed for 3,4-dimethoxybenzaldehyde (veratraldehyde); the substrate was exclusively oxidised to 3-methoxy-4-hydroxybenzaldehyde (vanillin). The production of vanillin from veratraldehyde by CYP199A4 demonstrates the potential of the CYP199A4 system to provide alternative routes for synthesising commercially important flavour and fragrance compounds.

Future work will involve investigating the oxidative potential of S244D for additional P450 reactions including hydroxylation, *N*-demethylation and *S*-oxidation and the regioselectivity of oxidation in these reactions in order to expand the synthetic capabilities of CYP199A4. Studies on additional Ser244 and other active site mutants of CYP199A4 would also provide more information on the substrate specificity of this enzyme for *para*-substituted benzene derivatives. A directed evolution approach could be used to produce a library of CYP199A4 mutants, which could be rapidly screened for oxidation activity using colourimetric assays on substrates related to 4-nitroanisole. Together, these studies could lead to the optimisation of CYP199A4-catalysed oxidations of substituted benzenes and related compounds.

7 The Oxidation of Methyl- and Ethyl-modified Substrates by Wild-type and S244D CYP199A4

7.1 Introduction

The S244D CYP199A4 mutant has been shown to be highly active with *para*-methoxy substituted benzene derivatives for which the WT enzyme has very little activity (Chapter 6). Improvements of up to 900-fold in the rate of substrate oxidation by $WT_{CYP199A4}$ were observed for S244D with 4-methoxyphenol. Considering the favourable results obtained for this mutant, the methyl derivatives of a selection of the carboxy-modified substrates were investigated to determine if regioselective hydroxylation at the *para*-methyl position also occurs in the presence of additional functional groups (Figure 69).

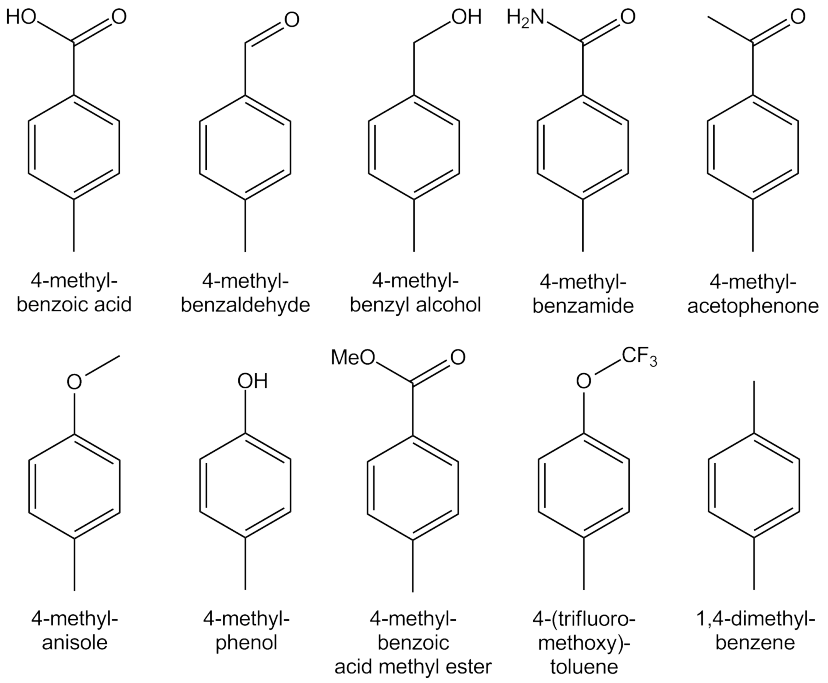

Figure 69: Methyl-modified substrates of WT and S244D CYP199A4.

Longer alkyl chain substrates are known to undergo competing hydroxylation and desaturation reactions with certain P450s. For example, 4-ethylbenzoic acid is oxidised by CYP199A4 to 4-(1-hydroxyethyl)benzoic acid ($> 50\%$) and 4-vinylbenzoic acid ($\approx 40\%$) with other minor products, and the isopropyl derivative to 4-(1-methyl-1-hydroxyethyl)benzoic acid (30%) and 4-(prop-1-en-2-yl)benzoic acid (54%, Figure 70).[79]

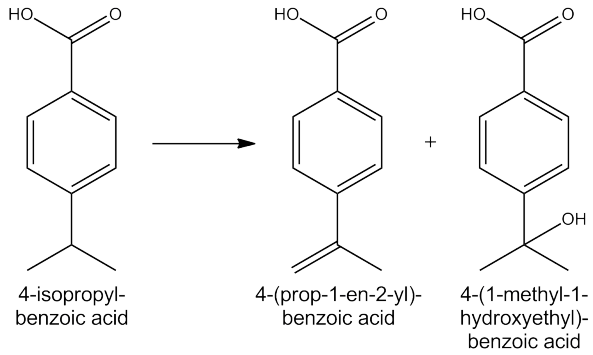

Figure 70: The major products of the CYP199A4 turnover of 4-isopropylbenzoic acid.

The mechanism of desaturation by P450s is unclear, and could be initiated by hydrogen atom abstraction from either of the α- (C_α) or β-carbons (C_β).[4,79] The alkene product could arise from two sequential hydrogen abstractions, the first from the C_α and the second from the C_β of the resulting radical intermediate. Alternatively, the radical could undergo a one-electron reduction to give a carbocation which loses a proton to yield the desaturated product (Chapter 1.2.4). If initial hydrogen abstraction occurred at the less-reactive C_β, this could be followed by a single electron transfer to Cpd II to produce a β-cation. For substrates such as 4-ethylbenzoic acid, this intermediate could rearrange to the more stable α- (benzylic) carbocation, and subsequent hydrogen abstraction from the C_β generates the desaturated product (Figure 71).[79]

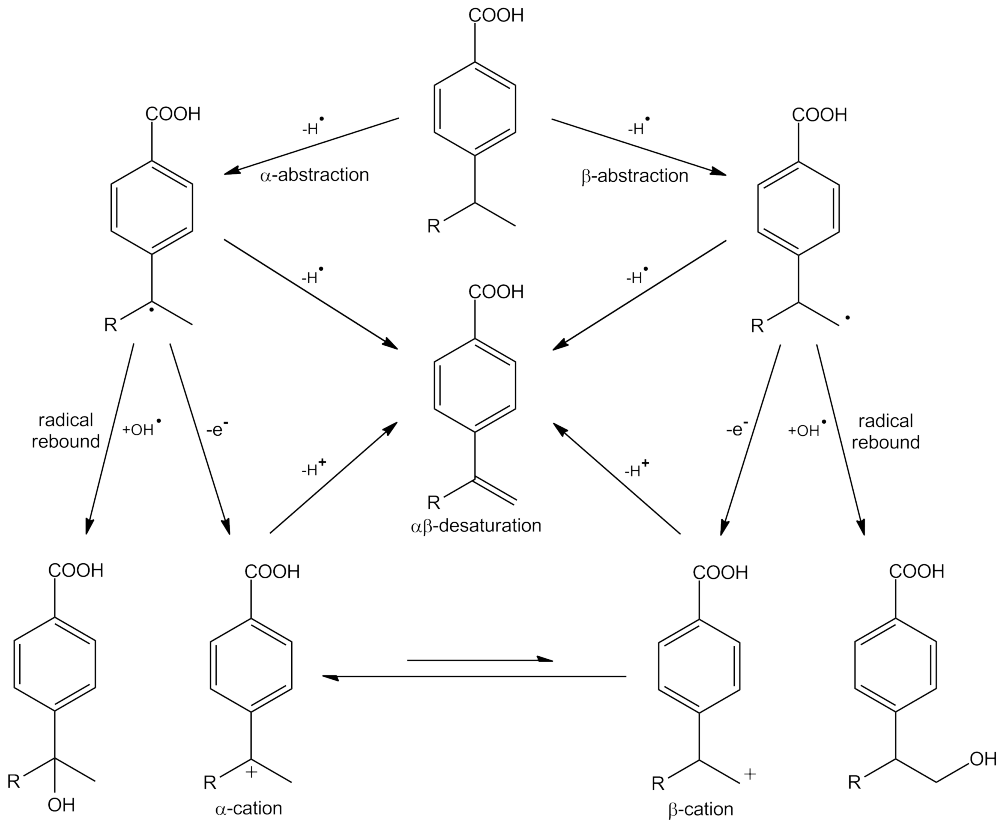

Figure 71: The mechanisms of hydroxylation and desaturation for *para*-substituted benzoic acids.

Slower radical rebound to form the α-hydroxylation product and the close proximity of both the C_α and C_β centres of 4-ethylbenzoic acid to the heme iron are believed to play significant roles in the formation of a desaturation product.[79] However, the electronic properties of a substrate and the enzyme active site among other factors, are also expected to affect the partition between the hydroxylation/desaturation pathways and their respective intermediates.[66,79]

In order to assess the electronic effects of the substituent replacing the benzoic acid carboxy terminus on the resulting product profile, ethyl derivatives of selected carboxy-modified substrates will also be studied with S244D (Figure 72).

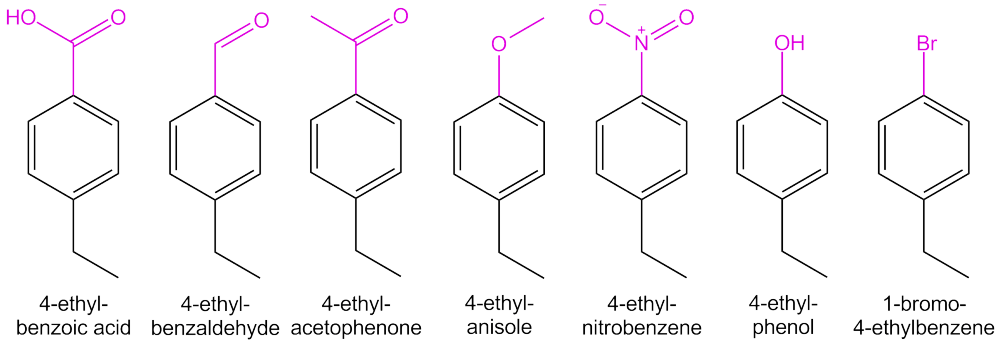

Figure 72: Ethyl-modified substrates of WT and S244D CYP199A4 including electron donating (e.g. phenol) and electron withdrawing (e.g. nitro) compounds.

7.2 Results

7.2.1 Binding Studies and Activity Assays with Methyl-modified Substrates

The substrate binding affinity and oxidation activity of $WT_{CYP199A4}$ and S244D were measured for a range of methyl-modified substrates (Table 11). The products were identified by HPLC or GC-MS coelution of the turnovers with authentic samples of the products, and calibrated against authentic standards. The substrates were exclusively hydroxylated at the *para*-methyl group in all cases.

Table 11: Substrate binding and *in vitro* turnover data for WT and S244D CYP199A4 with methyl-modified substrates. The data are given as mean ± S.D. with $n \geq 3$. Rates are given as nmol.nmol-P450^{-1}.min^{-1} (min^{-1}). The average leak rate was 9.0 min^{-1} and 3.0 min^{-1} for WT and S244D CYP199A4, respectively.

Substrate/Enzyme	% HS	K_d (µM)	NADH (min^{-1})	PFR (min^{-1})	Coupling (%)
4-methylbenzoic acid[79]	70	0.66 ± 0.01	444 ± 8	397 ± 22	89 ± 4
4-methylbenzaldehyde	55	100 ± 5	170 ± 9	-[b]	-[b]
methylbenzaldehyde$_{S244D}$	25	800 ± 26	492 ± 13	360 ± 4	73 ± 2
4-methylbenzyl alcohol	0	8.0 ± 1.7	13 ± 0.4	5.1 ± 0.9	39 ± 7
4-methylbenzyl alcohol$_{S244D}$	<5	250 ± 64	16 ± 0.4	11 ± 3	70 ± 17
4-methylacetophenone	0	7.6 ± 1.6	10 ± 0.4	-[b]	-[b]
4-methylacetophenone$_{S244D}$	0	2200 ± 150	61 ± 2	60 ± 4	96 ± 4
4-methylbenzamide	20	3000 ± 150	11 ± 0.9	0.7 ± 0.1	6.1 ± 0.6
4-methylbenzamide$_{S244D}$	0	-[a]	36 ± 1	16 ± 2	44 ± 5
4-methylphenol	0	-[a]	19 ± 1	4.0 ± 0.6	21 ± 2
4-methylphenol$_{S244D}$	55	218 ± 4	295 ± 2	260 ± 25	90 ± 2
4-methylanisole	0	-[a]	16 ± 0.3	2.1 ± 0.2	12 ± 1
4-methylanisole$_{S244D}$	15	440 ± 26	99 ± 3	42 ± 1	43 ± 2
1,4-dimethylbenzene	<5	-[a]	19 ± 1	0.7 ± 0.2	3.8 ± 0.7
1,4-dimethylbenzene$_{S244D}$	5	890 ± 83	49 ± 3	21 ± 3	43 ± 3
4-mBA methyl ester	10	2200 ± 89	16 ± 0.4	1.4 ± 0.1	8.6 ± 0.4
4-mBA methyl ester$_{S244D}$	<5	450 ± 50	15 ± 1	3.1 ± 0.3	21 ± 2
4-(trifluoromethoxy)toluene	5	-[a]	7 ± 0.8	-[b]	-[b]
4-(trifluoromethoxy)toluene$_{S244D}$	5	-[a]	27 ± 2	21 ± 2	75 ± 4

[a]Not determined due to minimal spin-state shifts. [b]No product formation.

4-Methylbenzamide induced a 20% spin-state shift in $WT_{CYP199A4}$ and bound weakly to the enzyme (K_d = 3000 µM). The addition of the same substrate to S244D did not induce any significant shift to the high-spin form. 4-Methylbenzamide did not result in any appreciable increase in NADH oxidation above the leak rate of $WT_{CYP199A4}$. This, combined with the weak coupling of redox equivalents to product formation, generated trace amounts of 4-(hydroxymethyl)benzamide at 0.7 min^{-1} (Table 11). Only small improvements in activity were observed with S244D, where faster NADH oxidation (36 min^{-1}) and tighter coupling (44%) resulted in a higher product formation rate for 4-(hydroxymethyl)benzamide (16 min^{-1}, Appendix E7).

Upon addition to $WT_{CYP199A4}$ and S244D, 4-methylbenzaldehyde induced spin-state shifts of 55% and 15%, respectively. The substrate bound more tightly to the WT enzyme (K_d = 100 µM vs. 800 µM), in line with its larger spin-state shift (Figure 73a and 73b). Despite the elevated rate of NADH oxidation (170 min^{-1}), the WT turnover of 4-methylbenzaldehyde did not give rise to any oxidation product (Figure 73c). The activity of S244D with 4-methylbenzaldehyde was high with NADH oxidation and product formation rates of 492 min^{-1} and 360 min^{-1}, respectively.

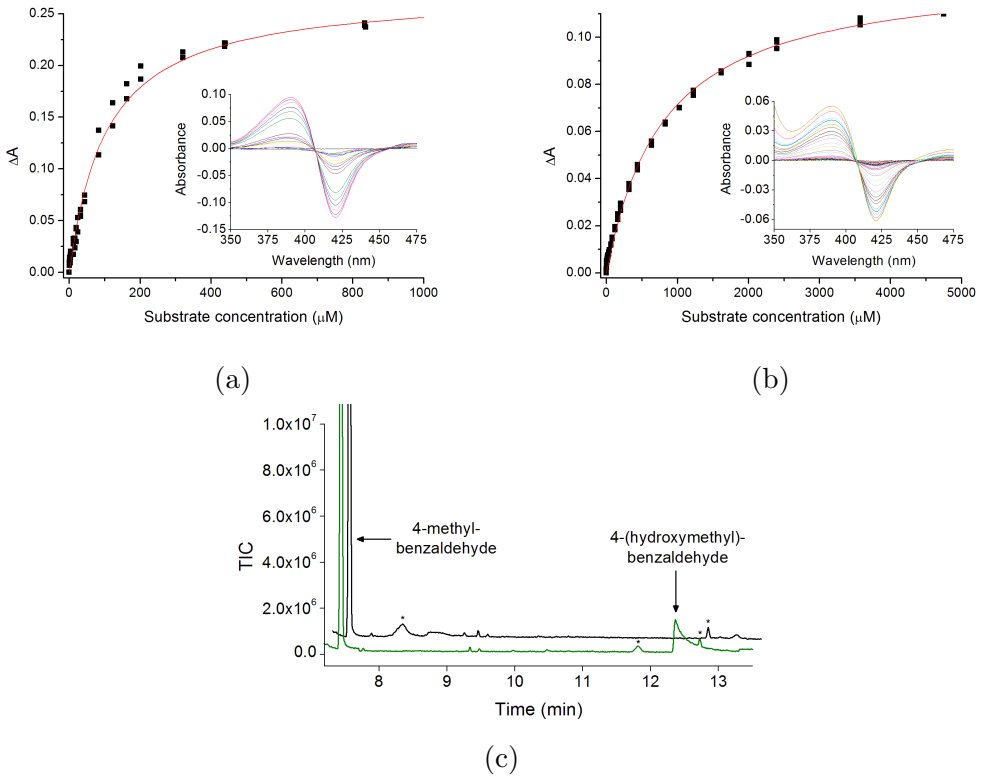

Figure 73: The binding and oxidation of 4-methylbenzaldehyde. Dissociation constant analyses with (a) WT and (b) S244D CYP199A4. (c) GC-MS analysis of the WT (black) and S244D (green) turnovers of 4-methylbenzaldehyde (t_R = 7.5 mins) to 4-(hydroxymethyl)benzaldehyde (t_R = 12.5 mins). For clarity the chromatograms have been offset along the x and y axes. Impurities are marked (*).

4-Methylacetophenone induced a negligible change in the spin-state of $WT_{CYP199A4}$ but bound relatively tightly with a dissociation constant of 7.6 µM. In comparison, the substrate bound very weakly to S244D (K_d = 2200 µM). No appreciable increase in the rate of NADH oxidation above the leak rate was observed for $WT_{CYP199A4}$ with 4-methylacetophenone, and the turnover did not give rise to any product. The same substrate was oxidised with high efficiency (96%) to 4-(hydroxymethyl)acetophenone at a moderate rate of 60 min^{-1} by S244D (Appendix E7).

No discernible change in the spin-state of $WT_{CYP199A4}$ was observed upon the addition of 4-methylphenol. However, the phenol derivative induced a 55% shift and bound with moderate affinity to S244D (K_d = 220 µM, Figure 74a and 74b). The oxidation activity of $WT_{CYP199A4}$ with 4-methylphenol was very low (Table 11). In comparison, the rates of NADH oxidation and 4-(hydroxymethyl)phenol formation were 15- and 70-fold faster with S244D at 295 min^{-1} and 260 min^{-1}, respectively (Figure 74c). The S244D turnover was also much more tightly coupled (90%), and comparable to the efficiency of 4-methylbenzoic acid hydroxylation by $WT_{CYP199A4}$.[79]

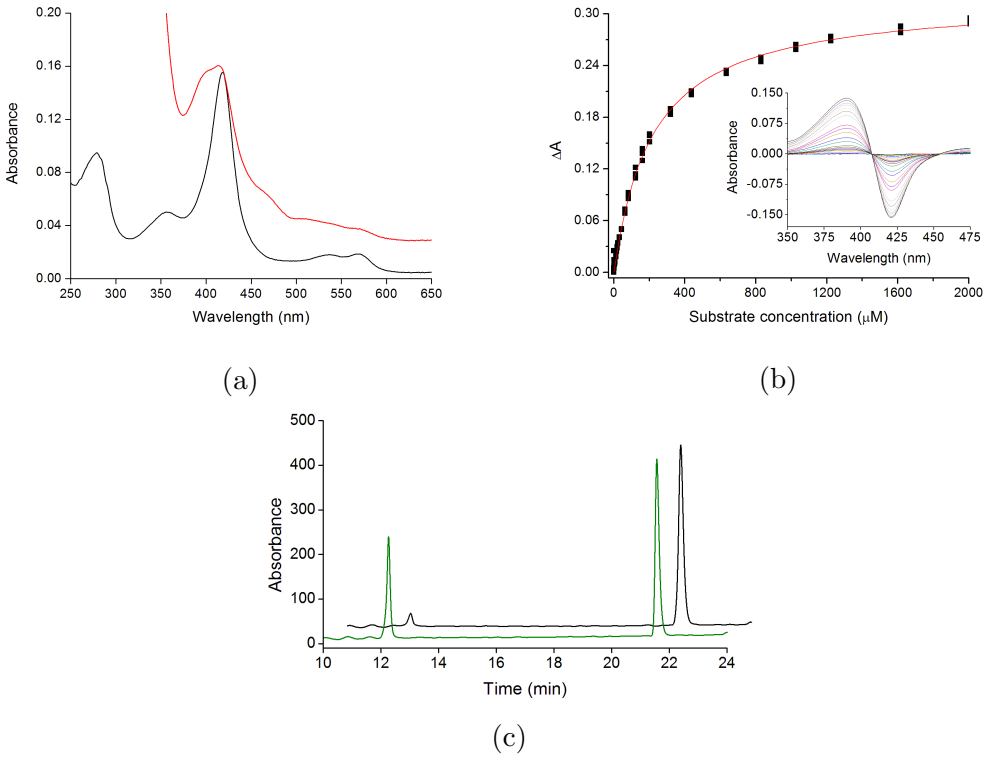

Figure 74: The binding and oxidation of 4-methylphenol. (a) Spin-state shift and (b) dissociation constant analysis with S244D. (c) HPLC analysis of the WT (black) and S244D CYP199A4 (green) turnovers of 4-methylphenol (t_R = 21.6 mins) to 4-(hydroxymethyl)phenol (t_R = 12.3 mins). For clarity the chromatograms have been offset along the x and y axes.

Minor changes were observed in the spin-states of both $WT_{CYP199A4}$ and the S244D mutant with 4-methylbenzyl alcohol. Despite this, the substrate bound tightly to

the WT enzyme (K_d = 8.0 µM), but more weakly to S244D (K_d = 250 µM). 4-Methylbenzyl alcohol did not result in any significant NADH oxidation above that of the leak rate of either enzyme (Table 11). However, as the coupling efficiency of the mutant was increased relative to $WT_{CYP199A4}$ (70% vs. 39%), a 2-fold increase in the product formation rate of 4-(hydroxymethyl)benzyl alcohol was observed (11 min^{-1} vs. 5.1 min^{-1}).

Small spin-state shifts of $\leq$ 15% were induced in $WT_{CYP199A4}$ and S244D by the remaining substrates (Appendix E2). A dissociation constant of 440 µM was measured for S244D upon the addition of 4-methylanisole, which was oxidised 20 times faster by the mutant. The oxidation of 4-methylanisole gave rise to two products, which were identified as 4-methoxybenzyl alcohol and 4-hydroxybenzyl alcohol after GC-MS analysis of the TMS-derivatised turnovers (Figure 75). 4-Hydroxybenzyl alcohol was the major product, forming 89% and 78% of the total product distribution for $WT_{CYP199A4}$ and S244D, respectively. As the enzymes can oxidise 4-methoxybenzyl alcohol faster than 4-methylanisole (Table 8 and 11), the 4-methoxybenzyl alcohol product initially formed could be further oxidised to the dihydroxy compound (Figure 75). The oxidation products indicate that 4-methylanisole is held with the methyl group positioned closest to the heme, resulting in exclusive oxidation at the methyl group. This would be consistent with the lack of any 4-methylphenol product – which would arise instead from oxidation at the methoxy group – being formed. However, we cannot rule out 4-methylphenol formation followed by rapid oxidation to 4-hydroxybenzyl alcohol as a route to the further oxidation product.

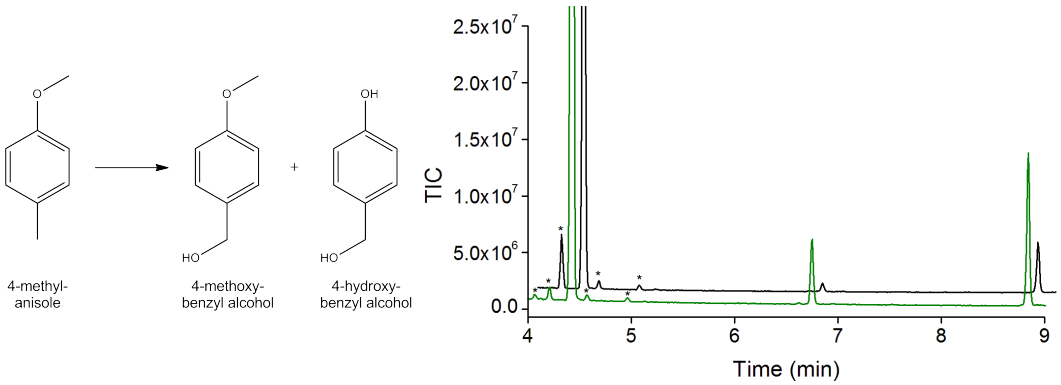

Figure 75: GC-MS analysis of the WT (black) and S244D CYP199A4 (green) turnovers of 4-methylanisole (t_R = 4.4 mins) to 4-methoxybenzyl alcohol (t_R = 6.7 mins) and 4-hydroxybenzyl alcohol (t_R = 8.8 mins). No 4-methylphenol (t_R = 8.6 mins) oxidation product is observed. For clarity the chromatograms have been offset along the x and y axes. Impurities are marked (*).

4-Methylbenzoic acid methyl ester and 1,4-dimethylbenzene bound relatively weakly to S244D, with dissociation constants of 450 µM and 890 µM, respectively (Appendix E3). The rates of NADH oxidation and product formation as well as the

coupling efficiencies were higher with the mutant than $WT_{CYP199A4}$, albeit not by a large margin (Table 11). While no oxidation product could be detected in the WT turnover of 4-(trifluoromethoxy)toluene, the same substrate gave rise to low levels of 4-(trifluoromethoxy)benzyl alcohol at a moderate rate of 21 min^{-1} with S244D (Appendix E7).

Overall, there is no apparent trend in the binding affinities of $WT_{CYP199A4}$ and S244D for the methyl-modified substrates, nor in the binding affinities of the enzymes for the substrates of a methoxy/methyl pair (Table 10 and 11). We note that of the methyl derivatives, the affinity of S244D was highest for 4-methylphenol, which is similar to the high affinity of the enzyme for 4-methoxyphenol observed previously (Chapter 6). This suggests that *para*-substituted phenols are a suitable fit for the active site of S244D.

Improvements were observed in the oxidation activity of S244D with the methyl-modified substrates in almost all cases when compared to $WT_{CYP199A4}$. However, the changes in activity were less dramatic than those for the methoxy-modified derivatives in Chapter 6. Of the methyl substrates, the activity of S244D was highest with the benzaldehyde and phenol derivatives (Figure 76). This is similar to the high oxidation activity previously observed for S244D with their methoxy counterparts, 4-methoxybenzaldehyde and 4-methoxyphenol (Figure 63). These results suggest that *para*-substituted benzaldehydes and phenols are appropriate substrates for S244D.

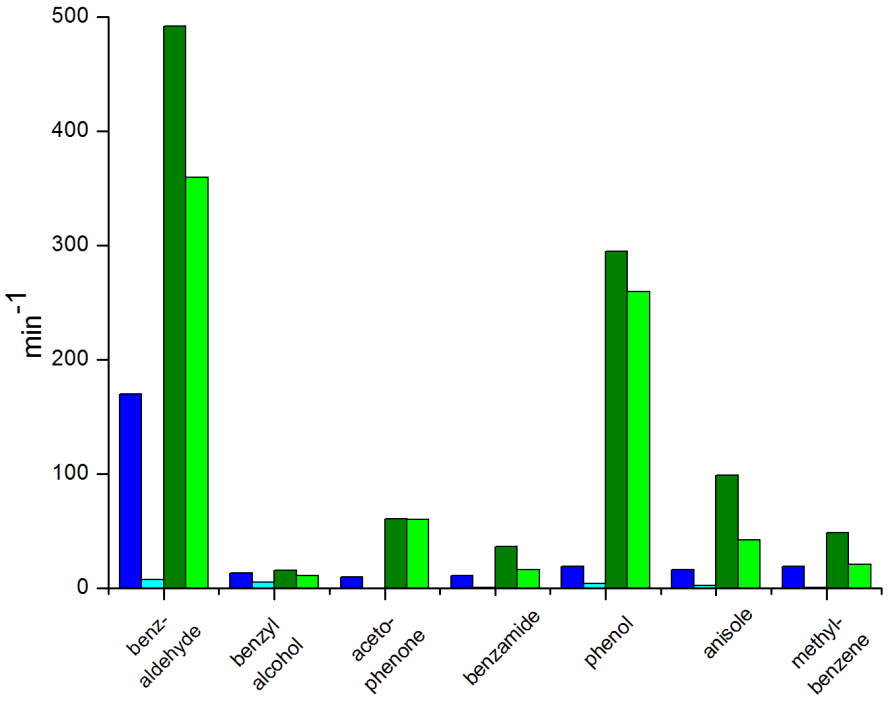

Figure 76: The respective NADH oxidation and product formation rates of WT (blue and cyan) and S244D CYP199A4 (green and lime) with selected methyl-modified substrates.

As shown in Figure 76, much smaller changes were observed between the activities of S244D and $WT_{CYP199A4}$ with the other methyl-modified substrates. We note in particular here the low oxidation activity of S244D with 4-methylbenzamide. This is in stark contrast to the activity of this mutant enzyme with 4-methoxybenzamide, for which the oxidation activity and coupling efficiency were the highest (Chapter 6).

7.2.2 Substrate Binding Studies on Ethyl-modified Substrates

4-Ethylbenzoic acid induces a similar spin-state shift and binds nearly as tightly as 4-methoxybenzoic acid to $WT_{CYP199A4}$ (> 95% shift, K_d = 0.34 µM).[79] When the same substrate was tested with S244D, a comparable change in the spin-state was observed (90%), but binding was over 4 orders of magnitude weaker (K_d = 2800 µM, Figure 77a and 77b). Comparable shifts of 40% and 30% were also observed for $WT_{CYP199A4}$ and S244D with 4-ethylbenzaldehyde, respectively. The substrate bound marginally more tightly to the WT enzyme with a dissociation constant of 200 µM vs. 280 µM, in line with its larger spin-state shift (Table 12 and Appendix E6).

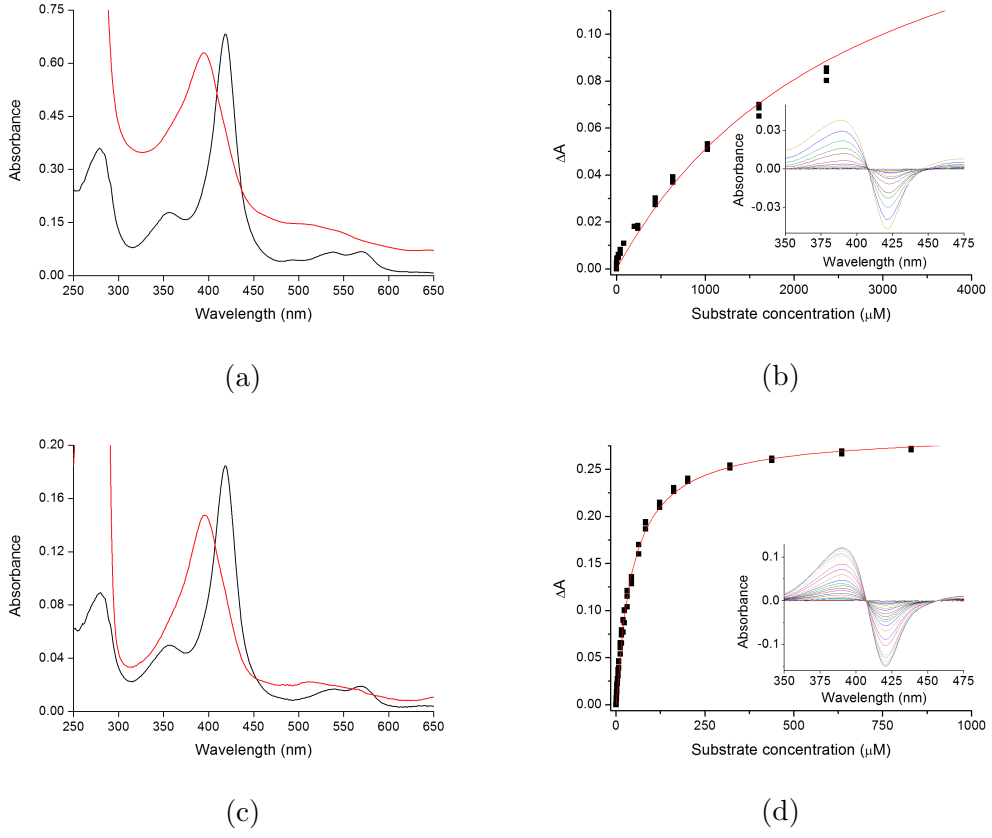

Figure 77: The respective spin-state shifts and dissociation constant analyses of S244D with 4-ethylbenzoic acid (a) and (b) and 4-ethyphenol (c) and (d).

4-Ethylphenol induced a 40% shift in the spin-state of $WT_{CYP199A4}$ but bound weakly

to the enzyme (K_d = 1200 µM). In comparison, a 90% shift was observed for S244D with 4-ethylphenol (Figure 77c), which bound the most tightly of all of the substrates tested with this mutant (K_d = 47 µM, Figure 77d).

The addition of 4-ethylanisole and 1-bromo-4-ethylbenzene resulted in minimal changes in the spin-state of $WT_{CYP199A4}$, suggesting that the substrates bound very weakly. 4-Ethylanisole induced a 20% shift in S244D and bound relatively tightly (K_d = 96 µM). A 25% shift was observed for S244D with 1-bromo-4-ethylbenzene, which bound with a dissociation constant of 140 µM (Appendix E6). No discernible shifts were observed for either enzyme with 4-ethylacetophenone. Accurate spin-state shifts and dissociation constants were unable to be determined for 4-ethylnitrobenzene as the substrate absorbs strongly at 265 nm, and a shoulder of this band interfered with the increase in absorbance at ≈ 390 nm.

Table 12: Substrate binding and *in vitro* turnover data for WT and S244D CYP199A4 with ethyl-modified substrates. The data are given as mean ± S.D. with $n \geq 3$. Rates are given as nmol.nmol-P450^{-1}.min^{-1} (min^{-1}). The average leak rate was 9.0 min^{-1} and 3.0 min^{-1} for WT and S244D CYP199A4, respectively.

Substrate/Enzyme	% HS	K_d (µM)	NADH (min^{-1})	PFR (min^{-1})	Coupling (%)
4-ethylbenzoic acid[79]	> 95	0.34 ± 0.02	1180 ± 34	1030 ± 52	88 ± 2
4-ethylbenzoic acid$_{S244D}$	90	2800 ± 250	77 ± 2	58 ± 8	74 ± 8
4-ethylbenzaldehyde	40	200 ± 8	51 ± 4	0.7 ± 0.01	1.4 ± 0.1
4-ethylbenzaldehyde$_{S244D}$	30	280 ± 8	564 ± 10	320 ± 13	57 ± 2
4-ethylacetophenone	0	-[a]	10 ± 1	1.2 ± 0.3	13 ± 3
4-ethylacetophenone$_{S244D}$	< 5	-[a]	92 ± 4	30 ± 1	33 ± 1
4-ethylphenol	40	1200 ± 80	27 ± 1	17 ± 2	62 ± 8
4-ethylphenol$_{S244D}$	90	47 ± 1	569 ± 42	500 ± 45	88 ± 3
4-ethylanisole	< 5	-[a]	12 ± 1	1.4 ± 0.3	12 ± 2
4-ethylanisole$_{S244D}$	20	96 ± 10	61 ± 4	15 ± 1	25 ± 3
4-ethylnitrobenzene	10	-[a]	16 ± 1	1.4 ± 0.1	9.1 ± 0.8
4-ethylnitrobenzene$_{S244D}$	15	-[a]	270 ± 13	220 ± 19	81 ± 5
1-bromo-4-ethylbenzene	5	-[a]	23 ± 1	-[b]	-[b]
1-bromo-4-ethylbenzene$_{S244D}$	25	140 ± 9	133 ± 6	-[b]	-[b]

[a]Not determined due to minimal spin-state shifts or interfering absorbances. [b] No product formation.

A comparison of the binding affinities of $WT_{CYP199A4}$ for the ethyl-modified substrates with their carboxy- and methyl-modified counterparts reveals that the enzyme appears to have comparable binding affinities for the methoxy and ethyl derivatives of a partic-

ular substrate. Larger differences are generally observed in the affinity of $WT_{CYP199A4}$ for a methyl derivative. Similar observations can tentatively be made for S244D. We note that the high affinity of S244D for 4-ethylphenol again demonstrates that replacement of the benzoic acid carboxy terminus with an alcohol group is favourable for binding to S244D.

7.2.3 Activity and Product Formation Assays with Ethyl Substrates

The NADH oxidation and product formation rates were measured for $WT_{CYP199A4}$ and S244D with each of the ethyl-modified substrates. (Table 12).[79] 4-Ethylbenzoic acid is oxidised at approximately half the rate of 4-methoxybenzoic acid by $WT_{CYP199A4}$ and yields two major products, 4-vinylbenzoic acid (38%) and 4-(1-hydroxyethyl)benzoic acid (51%).[3] Small amounts of 4-epoxyethylbenzoic acid (4%) and 4-acetylbenzoic acid (4%), which presumably arise from further oxidation of the major products, were also detected, together with low levels of the β-hydroxylation product 4-(2-hydroxyethyl)benzoic acid (3%, Figure 78). The minor products were identified based on their mass spectra and fragmentation patterns.[3]

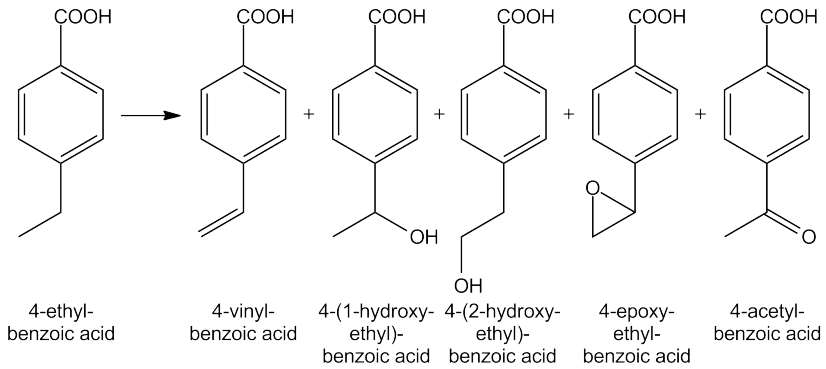

Figure 78: The oxidation of 4-ethylbenzoic acid by $WT_{CYP199A4}$.

The rates of NADH oxidation and product formation of S244D with 4-ethylbenzoic acid were 77 min^{-1} and 58 min^{-1}, respectively. This is much lower than the activity of $WT_{CYP199A4}$ with the same substrate. However, the S244D reaction remained tightly coupled (74%), with altered product ratios containing 4-(1-hydroxyethyl)benzoic acid (36%), 4-(2-hydroxyethyl)benzoic acid (< 10%), and 4-vinylbenzoic acid as the dominant product (45%, Figure 79a). Two minor products which formed 9% of the product distribution in a ratio of 7:2 were also observed, and are presumably the epoxide and ketone further oxidation products (Figure 79b).

4-Ethylbenzaldehyde was oxidised by $WT_{CYP199A4}$ to 4-(1-hydroxyethyl)benzaldehyde (94%) and 4-vinylbenzaldehyde (6%) very slowly due to poor coupling of redox equiva-

lents to product formation (Table 12). The rate of product formation improved 450-fold with S244D (320 min^{-1}), and the coupling efficiency was also higher (57%). The same α-hydroxylation and desaturation products were generated by S244D, albeit in different proportions (79% and 21%, respectively, Appendix E8).

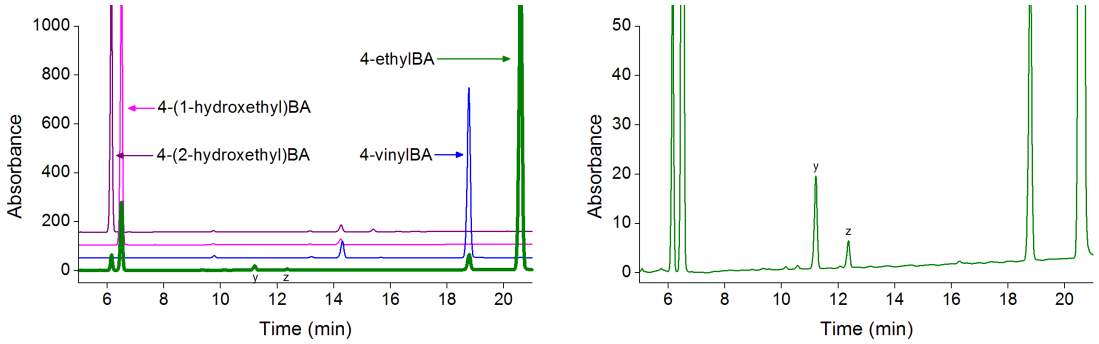

Figure 79: (a) HPLC analysis of the S244D turnover (green) of 4-ethylbenzoic acid. The 4-vinylbenzoic acid (t_R = 18.9 mins) product control is shown in blue, 4-(1-hydroxyethyl)benzoic acid (t_R = 6.5 mins) in pink and 4-(2-hydroxyethyl)benzoic acid (t_R = 6.1 mins) in purple. (b) A zoomed in version highlighting the two further oxidation products y and z at t_R = 11.2 mins and t_R = 12.4 mins. For clarity the chromatograms in (a) have been offset along the y axis.

While the WT turnover of 4-ethylnitrobenzene produced trace amounts of product, a significant improvement was observed with S244D. The NADH oxidation rate was increased by nearly 20-fold (270 min^{-1}), and the product formation rate by 150-fold (220 min^{-1}). The coupling efficiency of the S244D turnover was also high (81%). Only 4-(1-hydroxyethyl)nitrobenzene was present in the turnover of 4-ethylnitrobenzene by $WT_{CYP199A4}$. However, trace amounts ($\approx$ 1%) of an additional desaturation product 4-vinylnitrobenzene were detected in the S244D turnover (Figure 80).

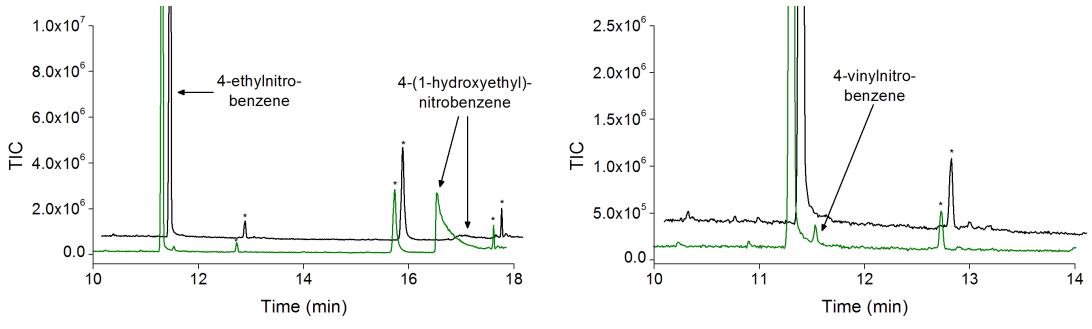

Figure 80: (a) GCMS analysis of the WT (black) and S244D CYP199A4 (green) turnovers of 4-ethylnitrobenzene to 4-vinylnitrobenzene (t_R = 11.6 mins) and 4-(1-hydroxyethyl)nitrobenzene (t_R = 16.9 mins). (b) A zoomed in version highlighting the formation of the 4-vinylnitrobenzene product. For clarity the chromatograms have been offset along the x and y axes. Impurities are marked (*).

The addition of 4-ethylacetophenone to $WT_{CYP199A4}$ did not result in NADH oxida-

tion above that of the leak rate. Together with the diminished coupling efficiency of the reaction, 4-(1-hydroxyethyl)acetophenone (98%) and a very small amount of the desaturation product 4-vinylacetophenone (2%) were generated at a meagre rate of 1 min^{-1}. A 10-fold increase in the rate of NADH oxidation was observed with S244D (92 min^{-1}), along with a moderate improvement in the coupling efficiency (33% vs. 13%). The mutant yielded the same two products as the WT enzyme, an α-hydroxylation (97%) and a desaturation (3%) product, albeit more quickly at 30 min^{-1} (Appendix E8).

The NADH oxidation rate of the WT enzyme with 4-ethylphenol was relatively slow (27 min^{-1}). However, moderate coupling of redox equivalents to product formation (62%) generated 4-vinylphenol and 4-(1-hydroxyethyl)phenol at 17 min^{-1} (Figure 81). The rate of NADH oxidation by S244D was significantly faster at 569 min^{-1}, which, together with the higher coupling efficiency (88%), resulted in a 30-fold increase in the rate of product formation (500 min^{-1}). The overall product distribution for both $WT_{CYP199A4}$ and S244D with 4-ethylphenol consisted of 22% of the desaturation product, 4-vinylphenol, with the remaining 78% assigned to 4-(1-hydroxyethyl)phenol.

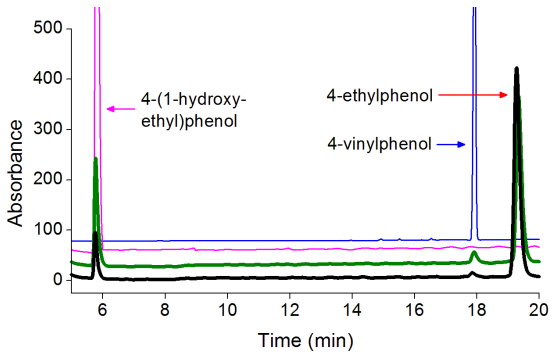

Figure 81: HPLC analysis of the WT (black) and S244D CYP199A4 (green) turnovers of 4-ethylphenol. The 4-vinylphenol (t_R = 18.1 mins) product control is shown in blue and 4-(1-hydroxyethyl)phenol (t_R = 6.0 mins) in pink. For clarity the chromatograms have been offset along the y axis.

A minimal increase in NADH oxidation above the leak rate was observed upon the addition of 1-bromo-4-ethylbenzene to $WT_{CYP199A4}$ (Table 12). While the rate of NADH oxidation was much faster with S244D, no oxidation product could be detected for 1-bromo-4-ethylbenzene in either turnover.

The WT turnover of 4-ethylanisole was very slow, and only a moderate improvement was observed with S244D. Interestingly, five oxidation products were detected in the turnover by S244D; 1-(4-methoxyphenyl)ethanol (70%), 4-ethylphenol (11%), 4-(1-hydroxyethyl)phenol (9%), 4-vinylphenol ($\approx$ 6%) and 4-vinylanisole ($\approx$ 4%, Figure 82). The three minority products presumably arise from further oxidation of the major products 1-(4-methoxyphenyl)ethanol and 4-ethylphenol. 1-(4-Methoxyphenyl)ethanol

(≈ 49%), 4-ethylphenol (≈ 45%) and 4-vinylanisole (≈ 4%) accounted for ≈ 98% of the total product distribution of the WT enzyme (Figure 82).

The product distribution arising from the WT and S244D turnovers of 4-ethylanisole is interesting as it suggests that the substrate can bind with either terminus positioned closest to the heme iron for oxidation. This indicates that the ethyl or methoxy group can be accommodated in the benzoic acid carboxylate binding pocket of the enzyme.

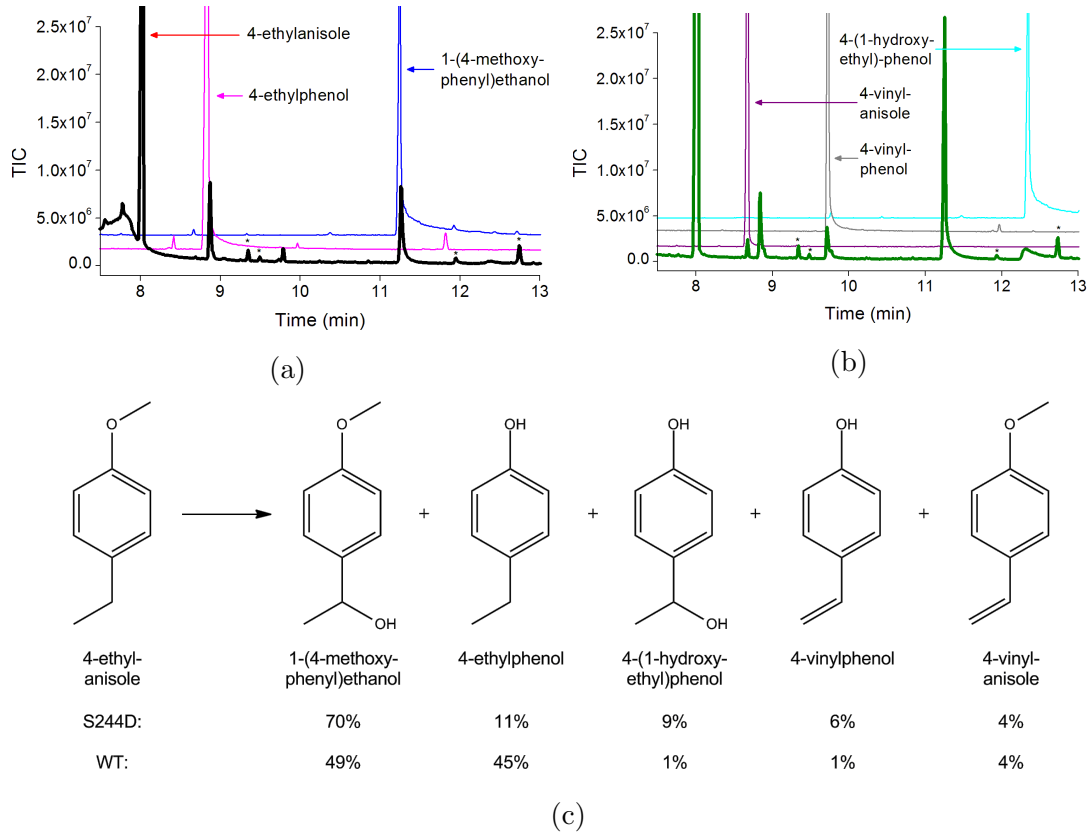

Figure 82: GC-MS analysis of the (a) WT (black) and (b) S244D CYP199A4 (green) turnovers of 4-ethylanisole. For clarity, the product controls have been shown across (a) and (b), and the chromatograms have been offset along the y axis. In (a), 4-ethylphenol (t_R = 8.8 mins) is shown in pink and 1-(4-methoxyphenyl)ethanol (t_R = 11.3 mins) in blue. In (b), 4-vinylanisole (t_R = 8.7 mins) is shown in purple, 4-vinylphenol (t_R = 9.7 mins) in grey and 4-(1-hydroxyethyl)phenol (t_R = 12.3 mins) in cyan. Impurities are marked (*). (c) The product distribution of 4-ethylanisole oxidation by S244D and WT CYP199A4.

As expected, improvements were observed in the activity of S244D with the ethyl-modified derivatives when compared to $WT_{CYP199A4}$ (Figure 83). The oxidation activity of S244D was again highest with the benzaldehyde and phenol derivatives, which is consistent with our previous findings and provides further evidence to suggest that *para*-substituted benzaldehydes and phenols are good substrates for S244D. Overall, it appears that the oxidation activity of S244D is greater with the ethyl derivative of a methyl/ethyl pair, and more comparable to its activity with the corresponding

methoxy-modified derivatives (Figure 83).

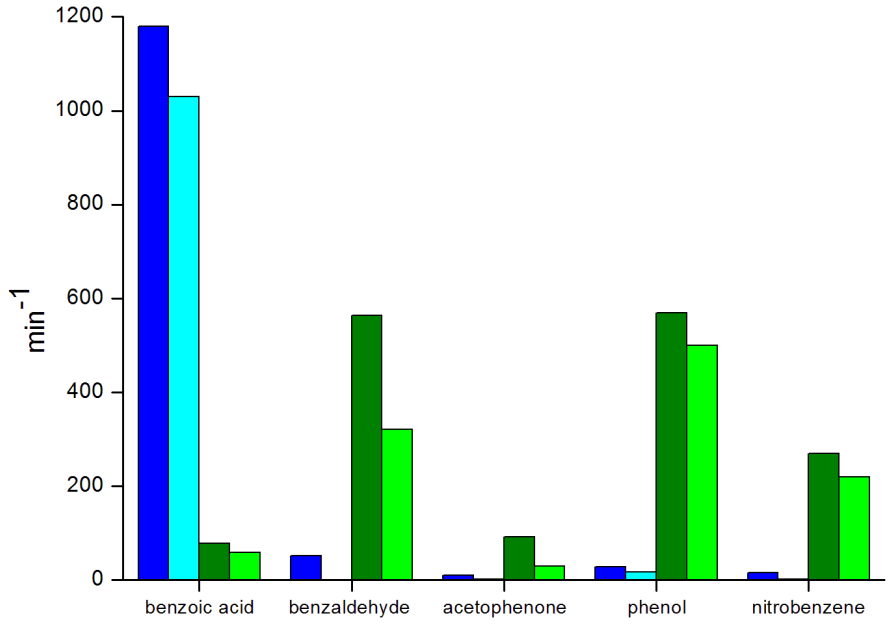

(a)

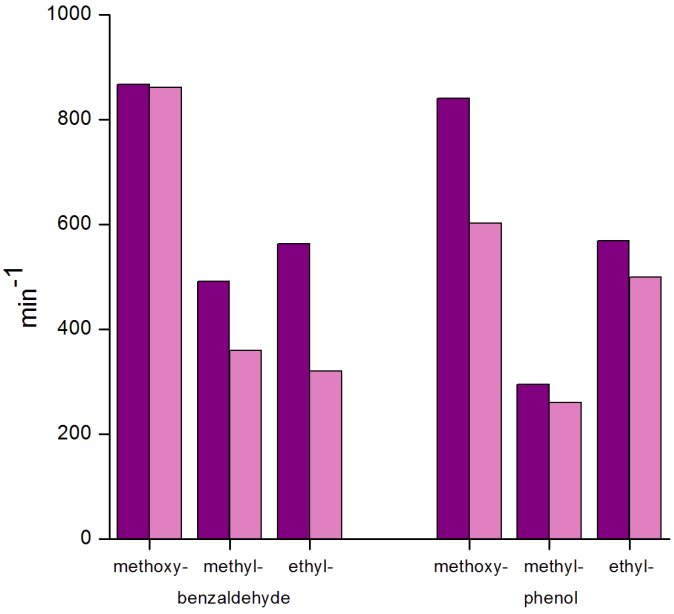

(b)

Figure 83: (a) The respective NADH oxidation and product formation rates of WT (blue and cyan) and S244D CYP199A4 (green and lime) with selected ethyl-modified substrates. (b) The respective NADH oxidation and product formation rates of S244D (purple and pink) with benzaldehyde and phenol derivatives.

Determination of the enantioselectivity of the α-hydroxylation products

Oxidation of the ethyl-modified substrates to α-hydroxylation products generates a stereocentre at the α-carbon, such that the products could be a single or mixture of enantiomers. In order to determine the enantioselectivity of S244D (or lack thereof),

the ethyl turnovers were coeluted with authentic samples of their α-hydroxylation products, where available. When an authentic product standard was unavailable, a racemic mixture of the product synthesised using $NaBH_4$ and the appropriate aldehyde or ketone precursor was used for coelution (Chapter 2.7).

GC analysis revealed the presence of a single enantiomer of 4-(1-hydroxyethyl)benzaldehyde arising from the turnover of 4-ethylbenzaldehyde (Figure 84a). When the turnover of 4-ethylacetophenone was coeluted with a racemic mixture of 4-(1-hydroxyethyl)acetophenone, a single enantiomer of this α-hydroxylation product was also observed (Figure 84b). GC analysis of the turnover of 4-ethylnitrobenzene also showed the presence of a single peak which could be one enantiomer of 4-(1-hydroxyethyl)nitrobenzene (Figure 84c).

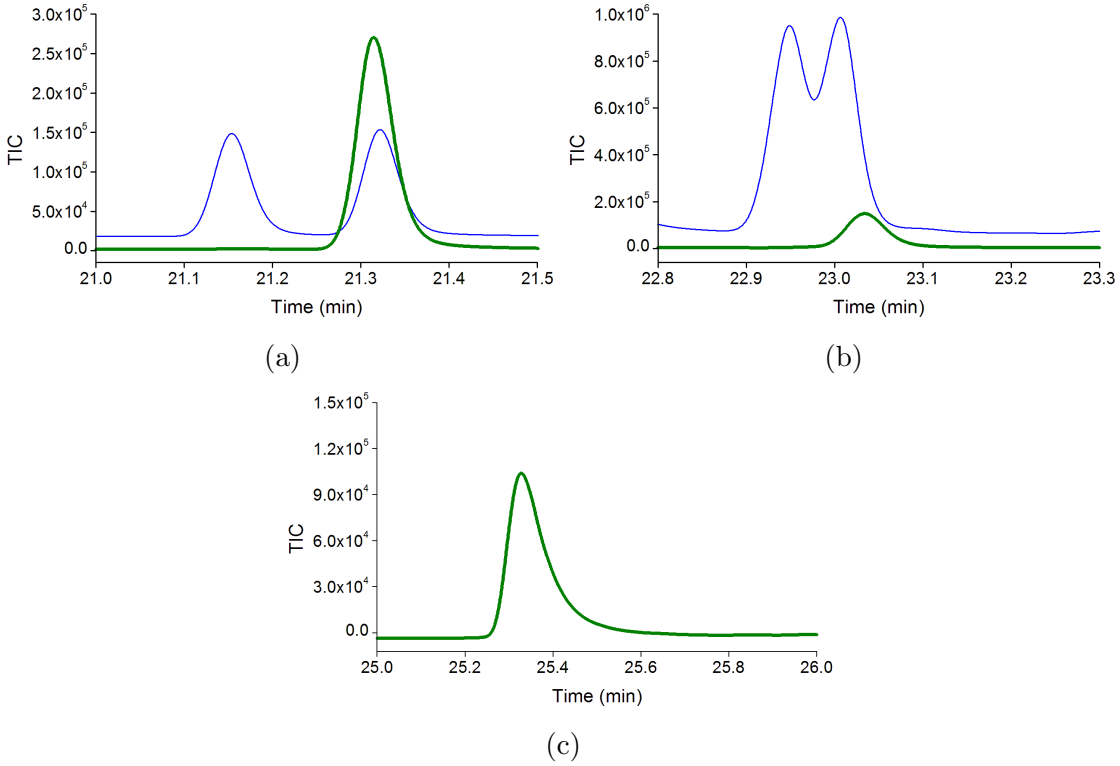

Figure 84: Chiral GC analysis of the S244D turnovers (green) of (a) 4-ethylbenzaldehyde (b) 4-ethylacetophenone and (c) 4-ethylnitrobenzene†. The respective α-hydroxylation products are shown in blue. †No authentic product standard or aldehyde or ketone precursors were available. For clarity the chromatograms have been offset along the y axis.

The turnovers of 4-ethylbenzoic acid and 4-ethylphenol were coeluted with authentic samples of their α-hydroxylation products and analysed via HPLC. The α-hydroxylation products were predominantly observed as a single enantiomer (Figure 85a and 85b).

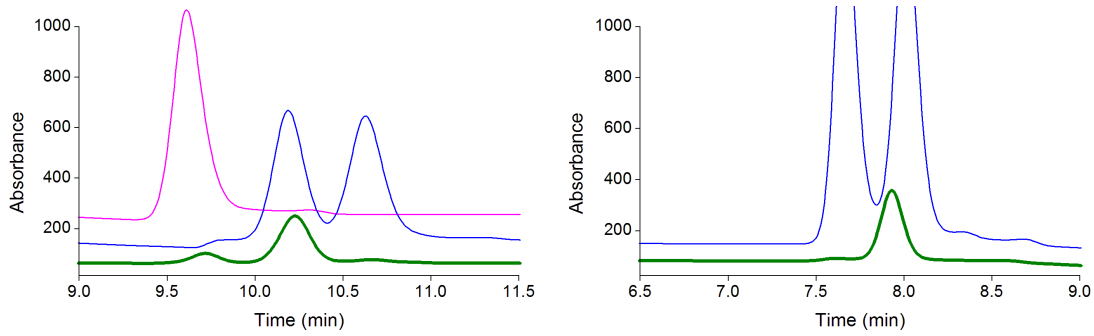

(a) (b)

Figure 85: Chiral HPLC analysis of the S244D turnovers (green) of (a) 4-ethylbenzoic acid† and (b) 4-ethylphenol. The respective α-hydroxylation products are shown in blue. †4-(2-Hydroxyethyl)benzoic acid is shown in pink. For clarity the chromatograms have been offset along the y axis.

7.3 Discussion

The spin-state shifts, binding affinities and turnover activities of both WT and S244D CYP199A4 were generally lower for the methyl counterpart of a methoxy/methyl pair of substrates. This is consistent with previous studies on $WT_{CYP199A4}$ with 4-methylbenzoic acid.[79] Based on the crystal structures of 4-methoxy- and 4-ethyl-benzoic acid-bound CYP199A4 (PDB: 4DO1 and 4EGM), it has been proposed that the smaller methyl substituent of 4-methylbenzoic acid is too far away from the heme iron centre to induce complete dissociation of the water ligand.[79] This is believed to account for its lower spin-state shift and weaker binding relative to 4-methoxybenzoic acid.[79] The results obtained here with the methyl substrates, when compared to the methoxy and ethyl derivatives, are consistent with these observations.

The methyl-modified substrates were exclusively hydroxylated at the *para*-methyl position in all cases. This suggests that the enzyme-substrate interactions for every methyl derivative bear some resemblance to those of 4-methylbenzoic acid-bound CYP199A4, and help position the substrates with their methyl substituents closest to the heme iron centre.

$WT_{CYP199A4}$ displays comparable affinities for the substrates of a methoxy/ethyl pair, and a similar observation can tentatively be made for S244D. The crystal structures of CYP199A4 in complex with 4-methoxy- and 4-ethyl-benzoic acid reveal that the enzyme-substrate contacts are very similar for the two substrates.[79] Therefore, it seems likely that the interactions of $WT_{CYP199A4}$ and S244D with the ethyl substrates would be reminiscent of those with the corresponding methoxy derivatives, resulting in comparable substrate binding affinities.

The product levels detected in the WT turnovers of the ethyl substrates were lower than S244D as a consequence of reduced NADH oxidation activity and coupling efficiency. The substrates which were oxidised gave rise to an α-hydroxylation and a C_α–C_β desaturation product in all cases. The alcohol was the major product and present (predominantly) as a single enantiomer (Table 13).

The electronic properties of the substituents *para* to the ethyl group are predicted to influence the partition between the hydroxylation and desaturation pathways. If desaturation proceeds via a cationic intermediate, electron donating groups should help stabilise this species and be favourable for the formation of a desaturation product. However, strongly electron withdrawing substituents, such as the nitro group of 4-ethylnitrobenzene, would be predicted to destabilise a cationic intermediate. As a consequence, only trace amounts of the desaturation product would be formed, as

was observed in the turnover of 4-ethylnitrobenzene (Table 13). In order for accurate comparisons to be made, only the product profiles of the substrates which gave moderate to high levels of product with S244D will be discussed here. Like the nitro group, the ketone substituent of 4-ethylacetophenone is electron withdrawing, and low levels of 4-vinylacetophenone were observed. As the aldehyde functionality of 4-ethylbenzaldehyde is only weakly electron withdrawing, it could favour desaturation compared to the nitro group. A larger proportion of the desaturation product was observed for 4-ethylbenzaldehyde, in agreement with this notion, though we note that comparatively lower levels of 4-vinylbenzaldehyde were formed in the WT turnover (Table 13).

Table 13: The distribution of α-hydroxylation and C_α–C_β desaturation products for selected ethyl-modified substrates with S244D and WT CYP199A4 (in brackets).

Substrate	α-hydroxylation (%)	C_α–C_β desaturation (%)
4-ethylnitrobenzene	99 ($\approx$ 100)	1 (-)
4-ethylacetophenone	97 (98)	3 (2)
4-ethylbenzaldehyde	79 (94)	21 (6)
4-ethylphenol	78 (78)	22 (22)
4-ethylbenzoic acid	36[a] (51)	45 (38)

[a]The β-hydroxylation product formed $\approx$ 10% of the total product distribution.

In contrast to the nitro, ketone and aldehyde derivatives, the hydroxyl group of 4-ethylphenol is electron donating, and would therefore help stabilise a positive charge. Thus, the ratio of desaturation/hydroxylation product formed for 4-ethylphenol > 4-ethylbenzaldehyde > 4-ethylacetophenone > 4-ethylnitrobenzene, which is consistent with their relative electron donating abilities or lack thereof (Table 13). The ratio of desaturation/hydroxylation products was the highest for 4-ethylphenol. This provides evidence in support of a cationic species on the desaturation pathway.

It is important to note that the electron withdrawing power of the carboxylic acid of 4-ethylbenzoic acid should be quite comparable with the ketone group and disfavour the desaturation pathway. However, a much higher percentage of the desaturation product, the highest of the substrates tested here, was observed. At physiological pH (7.4), 4-ethylbenzoic acid exists in its anionic benzoate form.[20,146] It appears that the overall negative charge of this anionic form of 4-ethylbenzoic acid is best equipped to stabilise a positive charge on the α-carbon, leading to increased desaturation product formation (Table 13).

It has been proposed that the accessibility of more than one carbon centre of 4-

ethylbenzoic acid to the heme iron of CYP199A4 is significant in the formation of the alkene desaturation product.[79] Without a crystal structure, it is difficult to predict the locations of ethyl groups in S244D relative to the WT enzyme. However, it is possible that the enzyme-substrate interactions, especially those opposite the ethyl group, are somewhat unique for each compound, such that the distance of the C_α–C_β bond to the heme iron varies slightly. The more favourable substrate orientations would then lead to a higher percentage of desaturation. Our results show that the partition between desaturation/hydroxylation is likely to be influenced by the electronic properties of the substrate, and supports the involvement of a cationic intermediate in desaturation. Structural studies and further investigation using substituted-ethyl analogues, particularly those with electron donating groups, could shed additional light on the features governing desaturation/hydroxylation and the intermediates likely involved. With the appropriate functional groups present, the partition between the desaturation/hydroxylation pathways could be modulated to give the desired ratio of products, which would be a unique synthetic application for this enzyme. Replacement of the ethyl moiety with other alkyl chains such as an isopropyl or butyl group could also provide some interesting insight into these competing activities. Additionally, whether the initial hydrogen abstraction occurs at the α- or β-carbon could be investigated using substrates with deuterated alkyl substituents.

Our findings with the methyl and ethyl substrates tested in this work suggest potential applications for CYP199A4 in selective synthesis. The enzyme is highly regioselective for oxidation solely at the *para*-position even in the presence of additional functional groups. Future work will involve investigating the activity of CYP199A4 with *ortho*- and *meta*-methyl substituted substrates, as well as dimethyl-substituted compounds to determine whether the regioselectivity of the enzyme is retained. The current work with the ethyl substrates also demonstrates the high enantioselectivity of CYP199A4, and the stereochemistry of the α-hydroxylated products will be determined in the near future. This could lead to the synthetic application of this enzyme in stereoselective hydroxylation reactions.

8 Conclusions and Future Directions

Different groups of *para*-substituted benzene substrates were tested with CYP199A4 to explore various properties of this enzyme and the mechanism of P450 reactions. The binding affinity and oxidative activity of CYP199A4 with a range of *para*-substituted benzoic acids was shown to be influenced by the substituent at the 4-position. The enzyme had moderate to high affinity for these compounds, whose functional groups included an aldehyde, ketone, alkene and alkyne. The substrates which gave rise to product were exclusively oxidised at the *para*-position to a single product in almost all cases, with a possible rearrangement product also being observed for 4-vinylbenzoic acid. The oxidation of 4-formyl- and 4-ethynyl-benzoic acid to terephthalic acid and 4-carboxyphenylacetic acid were the first observations of aldehyde and alkyne oxidation by CYP199A4, respectively. However, when compared to 4-methoxybenzoic acid, the activity and coupling efficiency of CYP199A4 with the benzoic acid derivatives was lower. The low levels of peroxide formation implied a significant degree of oxidase uncoupling, which presumably was a consequence of the benzoic acids' *para*-substituents being in a non-optimal position for efficient oxidation. Overall, the results demonstrated a selection of different oxidative activities of CYP199A4, and the high regioselectivity of the enzyme for oxidation at the *para*-position. Therefore, with the appropriate substrates, the CYP199A4 system could be used to investigate the mechanisms of different P450 reactions.

With this in mind, the active oxidants involved in CYP199A4 catalysis were investigated using the active site mutants, $T252A_{CYP199A4}$ and $D251N_{CYP199A4}$. While the affinity of $T252A_{CYP199A4}$ for the benzoic acids was comparable to the WT enzyme, substrate binding was modified in all cases with $D251N_{CYP199A4}$. The latter suggested that changes in the active site of this mutant were more significant. An important observation was that in spite of the general increase in peroxide uncoupling in $T252A_{CYP199A4}$, the mutation did not induce total uncoupling via this pathway for any substrate. The concurrent reduction in oxidase uncoupling also suggested that Cpd I might not be the sole active oxidant. The accelerated turnover of 4-ethynylbenzoic acid by $T252A_{CYP199A4}$ indicated the possible involvement of Cpd 0 in alkyne oxidation. In comparison, a reduction in the activity of the threonine mutant together with increased peroxide formation for 4-methoxybenzoic acid implicated Cpd I in demethylation. In the case of 4-formylbenzoic acid, the lack of peroxide uncoupling in $T252A_{CYP199A4}$, along with the increased product formation and coupling efficiency of $D251N_{CYP199A4}$, suggested the involvement of the peroxo-anion in aldehyde oxidation. Further investigation into the activity of WT, T252A and D251N CYP199A4 with related benzoic

acid compounds is required in order to verify the current findings. These compounds can also be used to probe for additional oxidative activities of CYP199A4 including lyase and deformylation activity. Crystallographic studies, which are currently underway, cryoradiolytic reduction experiments and studies with additional Asp251 and Thr252 mutants will enable further characterisation of the active oxidants and their role in substrate oxidation.

In spite of their larger size when compared to benzoic acids, substituted cinnamic acids and closely related acidic derivatives were able to be accommodated within the active site of CYP199A4. As the overall binding affinity and oxidative activity of CYP199A4 with 4-methoxybenzoic acid > 4-methoxycinnamic acid > 3-(4-methoxyphenyl)propionic acid > 4-methoxyphenylacetic acid, this highlights the selectivity of the enzyme for a planar, benzoic acid- or cinnamic acid-like framework. The binding of the cinnamic acid derivatives provided further evidence for the requirement of a *para*-substituent for tight-binding. Relative to 4-methoxycinnamic acid, additional substituents at the *ortho*- and *meta*-positions were found to reduce the affinity of the enzyme. The cinnamic, phenylacetic and propionic acids were all exclusively oxidised at the *para*-position, again demonstrating the high regioselectivity of CYP199A4. 4-Isopropylcinnamic acid gave rise to four oxidation products; two hydroxylation, one desaturation and one further oxidation (epoxide) product. Further investigation is needed to determine the factors controlling the partition between desaturation and hydroxylation catalysed by CYP199A4. Structural studies on cinnamic acid derivatives with CYP199A4 would provide further information on the enzyme-substrate interactions which control the substrate specificity and selectivity of this enzyme. As cinnamic acids are important biosynthetic precursors and possess numerous medicinal properties, CYP199A4 could be utilised for the biocatalytic production of cinnamic acids and related derivatives for pharmaceutical purposes.

While the oxidation activity of $WT_{CYP199A4}$ with *para*-methoxy substituted benzene derivatives was low, significant improvements were observed with the S244D mutant of CYP199A4. The activity of S244D with 4-methoxybenzamide, 4-methoxybenzaldehyde and 4-methoxyphenol was comparable to $WT_{CYP199A4}$ with 4-methoxybenzoic acid. The exclusive demethylation of these compounds suggested that the enzyme-substrate interactions which hold the methoxy group of 4-methoxybenzoic acid above the heme iron for selective oxidation remain intact in S244D when *para*-methoxy substituted benzenes are bound. An interesting observation was the lack of any apparent correlation between the binding affinity and activity of this mutant, and additional studies are necessary to shed light on the features which govern this. The results with the methoxy-substituted benzene derivatives demonstrate the biocatalytic potential of

CYP199A4 for regioselective demethylation in the presence of additional and more reactive functional groups. As an example, CYP199A4 could provide an alternative route for synthesising the important flavour compound vanillin via exclusive demethylation of veratraldehyde at the *para*-methoxy position.

With encouraging results obtained for S244D with the methoxy-substituted benzenes, a selection of methyl- and ethyl-substituted analogues was also investigated. As predicted, the regioselectivity of oxidation was maintained. The methyl derivatives were hydroxylated solely at the *para*-methyl position, though the overall activity of WT and S244D CYP199A4 was lower with these substrates when compared to their methoxy counterparts. The spin-state shifts and binding affinity of the two enzymes were generally also lower with the methyl derivatives. In comparison, the binding affinity of the enzymes with the substrates of a methoxy/ethyl pair was relatively similar. Together, these results reaffirm that the tightness of substrate binding is influenced by the size of the substituent at the *para*-position.

Most of the ethyl derivatives were oxidised to an α-hydroxylation and a C_α–C_β desaturation product. The alcohol was the major product and present as a single enantiomer, demonstrating the enantioselectivity of the enzyme. The electronic properties of the ethyl substrates were found to influence the relative distribution of the two products. The negatively charged benzoate derivative gave rise to the largest proportion of desaturation product. This was followed by the electron donating phenol derivative, while the strongly electron withdrawing nitro analogue gave rise to very little. These results implicated a cationic intermediate in CYP199A4-catalysed desaturation. It was noted that like with 4-methoxyphenol, S244D exhibited high oxidation activity and affinity for 4-methyl- and 4-ethyl-phenol, demonstrating that phenols are appropriate substrates for S244D. Additional studies including the investigation of larger alkyl chain substrates are needed in order to understand the properties that influence the partition between the desaturation/hydroxylation pathways. With the appropriate substituted-benzene framework, the proportion of the desaturation/hydroxylation products could be uniquely tailored to generate the desired ratio of products for use in novel synthetic applications. Future studies could be directed toward the oxidation of larger substrates with an assortment of functionalities in different locations.

Overall, the results demonstrate the potential of CYP199A4 as both a model system to understand P450 reactions and a biocatalyst for the synthetically challenging regioselective oxyfunctionalisation of a wide range of *para*-substituted benzene derivatives. Where the activity of the WT enzyme is highest for benzoic acids, a comparable level of activity can be achieved by the S244D mutant with a diverse selection of aromatic

compounds. Future work will involve using the CYP199A4 system to investigate additional P450 reactions and their mechanisms, and exploring the regioselectivity of CYP199A4 in these various oxidation reactions.

References

[1] Nelson, D. R. The Cytochrome P450 Homepage. **2009**, *http://drnelson.uthsc.edu/CytochromeP450.html*.

[2] Nelson, D. R.; Koymans, L.; Kamataki, T.; Stegeman, J. J.; Feyereisen, R.; Waxman, D. J.; Waterman, M. R.; Gotoh, O.; Coon, M. J.; Estabrook, R. W.; Gunsalus, I. C.; Nebert, D. W. P450 superfamily: update on new sequences, gene mapping, accession numbers and nomenclature. *Pharmacogenetics* **1996**, *6*, 1–42.

[3] Bell, S. G.; Tan, A. B. H.; Johnson, E. O. D.; Wong, L.-L. Selective oxidative demethylation of veratric acid to vanillic acid by CYP199A4 from *Rhodopseudomonas palustris* HaA2. *Mol. BioSyst.* **2009**, *6*, 206–214.

[4] Ortiz de Montellano, P. R. In *Cytochrome P450: Structure, Mechanism, and Biochemistry*, 4th ed.; Ortiz de Montellano, P. R., Ed.; Springer International Publishing, 2015; Chapter 4, pp 111–176.

[5] Guengerich, F. P. Common and Uncommon Cytochrome P450 Reactions Related to Metabolism and Chemical Toxicity. *Chem. Res. Toxicol.* **2001**, *14*, 611–650.

[6] Meunier, B.; De Visser, S. P.; Shaik, S. Mechanism of Oxidation Reactions Catalyzed by Cytochrome P450 Enzymes. *Chem. Rev.* **2004**, *104*, 3947–3980.

[7] Denisov, I. G.; Sligar, S. G. In *Cytochrome P450: Structure, Mechanism, and Biochemistry*, 4th ed.; Ortiz de Montellano, P. R., Ed.; Springer International Publishing, 2015; Chapter 4, pp 69–109.

[8] Rittle, J.; Green, M. T. Cytochrome P450 Compound I: Capture, Characterization, and C-H Bond Activation Kinetics. *Science* **2010**, *330*, 933–937.

[9] Poulos, T. L.; Raag, R. Cytochrome P450cam: crystallography, oxygen activation, and electron transfer. *FASEB J.* **1992**, *6*, 674–679.

[10] Gunsalus, I. C.; Wagner, G. C. Bacterial P-450$_{\text{cam}}$ methylene monooxygenase components: Cytochrome m, putidaredoxin, and putidaredoxin reductase. *Methods Enzymol.* **1978**, *52*, 166–188.

[11] Poulos, T. L.; Finzel, B. C.; Gunsalus, I. C.; Wagner, G. C.; Kraut, J. The 2.6-A crystal structure of Pseudomonas putida cytochrome P-450. *J. Biol. Chem.* **1985**, *260*, 16122–16130.

[12] Waskell, L.; Kim, J.-J. P. In *Cytochrome P450: Structure, Mechanism, and Biochemistry*, 4th ed.; Ortiz de Montellano, P. R., Ed.; Springer International Publishing, 2015; Chapter 2, pp 33–68.

[13] Hannemann, F.; Bichet, A.; Ewen, K. M.; Bernhardt, R. Cytochrome P450 systems - biological variations of electron transport chains. *Biochim. Biophys. Acta* **2007**, *1770*, 330–344.

[14] Zanger, U.; Raimundo, S.; Eichelbaum, M. Cytochrome P450 2D6: overview and update on pharmacology, genetics, biochemistry. *Naunyn. Schmiedebergs Arch. Pharmacol.* **2004**, *369*, 23–37.

[15] Nordblom, G. D.; White, R. E.; Coon, M. J. Studies on hydroperoxide-dependent substrate hydroxylation by purified liver microsomal cytochrome P-450. *Arch. Biochem. Biophys.* **1976**, *175*, 524–533.

[16] Hawkes, D. B.; Adams, G. W.; Burlingame, A. L.; de Montellano, P. R. O.; De Voss, J. J. Cytochrome $P450_{cin}$ (CYP176A), isolation, expression, and characterization. *J. Biol. Chem.* **2002**, *277*, 27725–27732.

[17] Girhard, M.; Bakkes, P. J.; Mahmoud, O.; Urlacher, V. B. In *Cytochrome P450: Structure, Mechanism, and Biochemistry*, 4th ed.; Ortiz de Montellano, P. R., Ed.; Springer International Publishing, 2015; Chapter 8, pp 451–520.

[18] Daff, S. N.; Chapman, S. K.; L.Turner, K.; Holt, R. A.; Govindaraj, S.; T. L. Poulos, a. A. W. M. Redox Control of the Catalytic Cycle of Flavocytochrome P-450 BM3. *Biochemistry* **1997**, *36*, 13816–13823.

[19] Nagano, S.; Poulos, T. L. Crystallographic Study on the Dioxygen Complex of Wild-type and Mutant Cytochrome P450cam: IMPLICATIONS FOR THE DIOXYGEN ACTIVATION MECHANISM. *J. Biol. Chem.* **2005**, *280*, 31659–31663.

[20] Bell, S. G.; Yang, W.; Tan, A. B. H.; Zhou, R.; Johnson, E. O. D.; Zhang, A.; Zhou, W.; Rao, Z.; Wong, L.-L. The crystal structures of 4-methoxybenzoate bound CYP199A2 and CYP199A4: structural changes on substrate binding and the identification of an anion binding site. *Dalton Trans.* **2012**, *41*, 8703–8714.

[21] Modi, A. R.; Dawson, J. H. In *Monooxygenase, Peroxidase and Peroxygenase Properties and Mechanisms of Cytochrome P450*; Hrycay, E. G., Bandiera, S. M., Eds.; Springer International Publishing, 2015; Chapter 2, pp 63–81.

[22] Loida, P. J.; Sligar, S. G. Molecular recognition in cytochrome P-450: Mechanism for the control of uncoupling reactions. *Biochemistry* **1993**, *32*, 11530–11538.

[23] Denisov, I. G.; Makris, T. M.; Sligar, S. G.; Schlichting, I. Structure and Chemistry of Cytochrome P450. *Chem. Rev.* **2005**, *105*, 2253–2278.

[24] Raag, R.; Martinis, S. A.; Sligar, S. G.; Poulos, T. L. Crystal structure of the cytochrome P-450CAM active site mutant Thr252Ala. *Biochemistry* **1991**, *30*, 11420–11429.

[25] Davydov, R.; Perera, R.; Jin, S.; Yang, T.-C.; Bryson, T. A.; Sono, M.; Dawson, J. H.; Hoffman, B. M. Substrate Modulation of the Properties and Reactivity of the Oxy-Ferrous and Hydroperoxo-Ferric Intermediates of Cytochrome P450cam As Shown by Cryoreduction-EPR/ENDOR Spectroscopy. *J. Am. Chem. Soc.* **2005**, *127*, 1403–1413.

[26] Vaz, A. D. N.; McGinnity, D. F.; Coon, M. J. Epoxidation of olefins by cytochrome P450: Evidence from site-specific mutagenesis for hydroperoxo-iron as an electrophilic oxidant. *Proc. Natl. Acad. Sci. U.S.A.* **1998**, *95*, 3555–3560.

[27] Jin, S.; Makris, T. M.; Bryson, T. A.; Sligar, S. G.; Dawson, J. H. Epoxidation of Olefins by Hydroperoxo Ferric Cytochrome P450. *J. Am. Chem. Soc.* **2003**, *125*, 3406–3407.

[28] Cryle, M. J.; De Voss, J. J. Is the Ferric Hydroperoxy Species Responsible for Sulfur Oxidation in Cytochrome P450s? *Angew. Chem. Int. Ed.* **2006**, *45*, 8221–8223.

[29] Kerber, W. D.; Ramdhanie, B.; Goldberg, D. P. H_2O_2 Oxidations Catalyzed by an Iron(III) Corrolazine: Avoiding High-Valent Iron Oxido Species? *Angew. Chem. Int. Ed.* **2007**, *46*, 3718–3721.

[30] Coon, M. J.; Vaz, A. D. N.; McGinnity, D. F.; Peng, H.-M. Multiple Activated Oxygen Species in P450 Catalysis: Contributions to Specificity in Drug Metabolism. *Drug Metab. Dispos.* **1998**, *26*, 1190–1193.

[31] Vaz, A. D.; Pernecky, S. J.; Raner, G. M.; Coon, M. J. Peroxo-iron and oxenoid-iron species as alternative oxygenating agents in cytochrome P450-catalyzed reactions: switching by threonine-302 to alanine mutagenesis of cytochrome P450 2B4. *Proc. Natl. Acad. Sci. U.S.A.* **1996**, *93*, 4644–4648.

[32] Shaik, S.; Kumar, D.; de Visser, S. P.; Altun, A.; Thiel, W. Theoretical Perspective on the Structure and Mechanism of Cytochrome P450 Enzymes. *Chem. Rev.* **2005**, *105*, 2279–2328.

[33] Shaik, S.; Hirao, H.; Kumar, D. Reactivity patterns of cytochrome P450 enzymes: multifunctionality of the active species, and the two states-two oxidants conundrum. *Nat. Prod. Rep.* **2007**, *24*, 533–552.

[34] Shaik, S.; Cohen, S.; Wang, Y.; Chen, H.; Kumar, D.; Thiel, W. P450 Enzymes: Their Structure, Reactivity, and Selectivity - Modeled by QM/MM Calculations. *Chem. Rev.* **2010**, *110*, 949–1017.

[35] de Visser, S. P. In *Inorganic/Bioinorganic Reaction Mechanisms*; van Eldik, R., Ivanović-Burmazović, I., Eds.; Academic Press, 2012; pp 1–31.

[36] de Visser, S. P.; Porro, C. S.; Quesne, M. G.; Sainna, M. A.; Munro, A. W. Overview on Theoretical Studies Discriminating the Two-Oxidant Versus Two-State-Reactivity Models for Substrate Monoxygenation by Cytochrome P450 Enzymes. *Curr. Top. Med. Chem.* **2013**, *13*, 2218–2232.

[37] Groves, J. T.; McClusky, G. A. Aliphatic hydroxylation via oxygen rebound. Oxygen transfer catalyzed by iron. *J. Am. Chem. Soc.* **1976**, *98*, 859–861.

[38] Ortiz de Montellano, P. R.; Stearns, R. A. Timing of the radical recombination step in cytochrome P-450 catalysis with ring-strained probes. *J. Am. Chem. Soc.* **1987**, *109*, 3415–3420.

[39] Newcomb, M.; Le Tadic, M.-H.; Putt, D. A.; Hollenberg, P. F. An incredibly fast apparent oxygen rebound rate constant for hydrocarbon hydroxylation by cytochrome P-450 enzymes. *J. Am. Chem. Soc.* **1995**, *117*, 3312–3313.

[40] Newcomb, M.; Le Tadic-Biadatti, M.-H.; Chestney, D. L.; Roberts, E. S.; Hollenberg, P. F. A nonsynchronous concerted mechanism for cytochrome P-450 catalyzed hydroxylation. *J. Am. Chem. Soc.* **1995**, *117*, 12085–12091.

[41] Newcomb, M.; Shen, R.; Choi, S.-Y.; Toy, P. H.; Hollenberg, P. F.; Vaz, A. D. N.; Coon, M. J. Cytochrome P450-Catalyzed Hydroxylation of Mechanistic Probes that Distinguish between Radicals and Cations. Evidence for Cationic but Not for Radical Intermediates. *J. Am. Chem. Soc.* **2000**, *122*, 2677–2686.

[42] Newcomb, M.; Shen, R.; Lu, Y.; Coon, M. J.; Hollenberg, P. F.; Kopp, D. A.; Lippard, S. J. Evaluation of Norcarane as a Probe for Radicals in Cytochome P450- and Soluble Methane Monooxygenase-Catalyzed Hydroxylation Reactions. *J. Am. Chem. Soc.* **2002**, *124*, 6879–6886.

[43] Toy, P. H.; Newcomb, M.; Hollenberg, P. F. Hypersensitive Mechanistic Probe Studies of Cytochrome P450-Catalyzed Hydroxylation Reactions. Implications for the Cationic Pathway. *J. Am. Chem. Soc.* **1998**, *120*, 7719–7729.

[44] Toy, P. H.; Newcomb, M.; Coon, M. J.; Vaz, A. D. N. Two Distinct Electrophilic Oxidants Effect Hydroxylation in Cytochrome P-450-Catalyzed Reactions. *J. Am. Chem. Soc.* **1998**, *120*, 9718–9719.

[45] Newcomb, M.; Toy, P. H. Hypersensitive radical probes and the mechanisms of cytochrome P450-catalyzed hydroxylation reactions. *Acc. Chem. Res.* **2000**, *33*, 449–455.

[46] Shaik, S.; Cohen, S.; de Visser, S.; Sharma, P.; Kumar, D.; Kozuch, S.; Ogliaro, F.; Danovich, D. The Rebound Controversy: An Overview and Theoretical Modeling of the Rebound Step in C-H Hydroxylation by Cytochrome P450. *Eur. J. Inorg. Chem.* **2004**, *2004*, 207–226.

[47] Kamachi, T.; ; Yoshizawa, K. A Theoretical Study on the Mechanism of Camphor Hydroxylation by Compound I of Cytochrome P450. *J. Am. Chem. Soc.* **2003**, *125*, 4652–4661.

[48] Guallar, V.; Baik, M.-H.; Lippard, S. J.; Friesner, R. A. Peripheral heme substituents control the hydrogen-atom abstraction chemistry in cytochromes P450. *Proc. Natl. Acad. Sci. U.S.A.* **2003**, *100*, 6998–7002.

[49] Li, C.; Wu, W.; Kumar, D.; Shaik, S. Kinetic Isotope Effect is a Sensitive Probe of Spin State Reactivity in C-H Hydroxylation of *N,N*-Dimethylaniline by Cytochrome P450. *J. Am. Chem. Soc.* **2006**, *128*, 394–395.

[50] Yong Wang, a. D. K.; Yang, C.; Han, K.; Shaik, S. Theoretical Study of N-Demethylation of Substituted *N,N*-Dimethylanilines by Cytochrome P450: The Mechanistic Significance of Kinetic Isotope Effect Profiles. *J. Phys. Chem. B* **2007**, *111*, 7700–7710.

[51] Wong, L.-L.; Bell, S. G. *Encyclopedia of Inorganic Chemistry*; John Wiley & Sons, Ltd, 2006; pp 1–30.

[52] Keizers, P. H.; Schraven, L. H.; de Graaf, C.; Hidestrand, M.; Ingelman-Sundberg, M.; van Dijk, B. R.; Vermeulen, N. P.; Commandeur, J. N. Role of the conserved threonine 309 in mechanism of oxidation by cytochrome P450 2D6. *Biochem. Biophys. Res. Commun.* **2005**, *338*, 1065–1074.

[53] Ishigooka, M.; Shimizu, T.; Hiroya, K.; Hatano, M. Role of Glu318 at the putative distal site in the catalytic function of cytochrome P450d. *Biochemistry* **1992**, *31*, 1528–1531.

[54] Stok, J. E.; Yamada, S.; Farlow, A. J.; Slessor, K. E.; Voss, J. J. D. Cytochrome $P450_{cin}$ (CYP176A1) D241N: Investigating the role of the conserved acid in the active site of cytochrome P450s. *BBA-Proteins Proteom.* **2013**, *1834*, 688–696.

[55] Yeom, H.; Sligar, S. G. Oxygen Activation by Cytochrome P450BM-3: Effects of Mutating an Active Site Acidic Residue. *Arch. Biochem. Biophys.* **1997**, *337*, 209–216.

[56] Cryle, M. J.; De Voss, J. J. The Role of the Conserved Threonine in $P450_{BM3}$ Oxygen Activation: Substrate-Determined Hydroxylation Activity of the Thr268Ala Mutant. *ChemBioChem* **2008**, *9*, 261–266.

[57] Hiroya, K.; Murakami, Y.; Shimizu, T.; Hatano, M.; Demontellano, P. Differential Roles of Glu318 and Thr319 in Cytochrome P450 1A2 Catalysis Supported by NADPH-Cytochrome P450 Reductase and *tert*-Butyl Hydroperoxide. *Arch. Biochem. Biophys.* **1994**, *310*, 397–401.

[58] Ogliaro, F.; de Visser, S. P.; Cohen, S.; Sharma, P. K.; Shaik, S. Searching for the Second Oxidant in the Catalytic Cycle of Cytochrome P450: A Theoretical Investigation of the Iron(III)-Hydroperoxo Species and Its Epoxidation Pathways. *J. Am. Chem. Soc.* **2002**, *124*, 2806–2817.

[59] Kamachi, T.; Shiota, Y.; Ohta, T.; Yoshizawa, K. Does the Hydroperoxo Species of Cytochrome P450 Participate in Olefin Epoxidation with the Main Oxidant, Compound I? Criticism from Density Functional Theory Calculations. *Bull. Chem. Soc. Jpn.* **2003**, *76*, 721–732.

[60] Park, M. J.; Lee, J.; Suh, Y.; Kim, J.; Nam, W. Reactivities of Mononuclear Non-Heme Iron Intermediates Including Evidence that Iron(III)-Hydroperoxo Species Is a Sluggish Oxidant. *J. Am. Chem. Soc.* **2006**, *128*, 2630–2634.

[61] Altun, A.; Shaik, S.; Thiel, W. What is the Active Species of Cytochrome P450 during Camphor Hydroxylation? QM/MM Studies of Different Electronic States of Compound I and of Reduced and Oxidized Iron-Oxo Intermediates. *J. Am. Chem. Soc.* **2007**, *129*, 8978–8987.

[62] de Visser, S. P.; Ogliaro, F.; Shaik, S. How Does Ethene Inactivate Cytochrome P450 En Route to Its Epoxidation? A Density Functional Study. *Angew. Chem. Int. Ed.* **2001**, *40*, 2871–2874.

[63] Ortiz de Montellano, P. R.; Kunze, K. L. Shift of the acetylenic hydrogen during chemical and enzymatic oxidation of the biphenylacetylene triple bond. *Arch. Biochem. Biophys.* **1981**, *209*, 710–712.

[64] Ortiz de Montellano, P. R.; Komives, E. A. Branchpoint for heme alkylation and metabolite formation in the oxidation of arylacetylenes by cytochrome P-450. *J. Biol. Chem.* **1985**, *260*, 3330–3336.

[65] Ortiz de Montellano, P. R. Hydrocarbon Hydroxylation by Cytochrome P450 Enzymes. *Chem. Rev.* **2010**, *110*, 932–948.

[66] Ji, L.; Faponle, A. S.; Quesne, M. G.; Sainna, M. A.; Zhang, J.; Franke, A.; Kumar, D.; van Eldik, R.; Liu, W.; de Visser, S. P. Drug Metabolism by Cytochrome P450 Enzymes: What Distinguishes the Pathways Leading to Substrate Hydroxylation Over Desaturation? *Chem. Eur. J.* **2015**, *21*, 9083–9092.

[67] Kumar, D.; de Visser, S. P.; Shaik, S. Oxygen Economy of Cytochrome P450: What Is the Origin of the Mixed Functionality as a Dehydrogenase-Oxidase Enzyme Compared with Its Normal Function? *J. Am. Chem. Soc.* **2004**, *126*, 5072–5073.

[68] Lai, W.; Chen, H.; Cohen, S.; Shaik, S. Will P450cam hydroxylate or desaturate alkanes? QM and QM/MM studies. *J. Phys. Chem. Lett.* **2011**, *2*, 2229–2235.

[69] Liu, X.; Wang, Y.; Han, K. Systematic study on the mechanism of aldehyde oxidation to carboxylic acid by cytochrome P450. *J. Biol. Inorg. Chem.* **2007**, *12*, 1073–1081.

[70] O'Reilly, E.; Kohler, V.; Flitsch, S. L.; Turner, N. J. Cytochromes P450 as useful biocatalysts: addressing the limitations. *Chem. Commun.* **2011**, *47*, 2490–2501.

[71] Carmichael, A. B.; Wong, L.-L. Protein engineering of *Bacillus megaterium* CYP102. *Eur. J. Biochem.* **2001**, *268*, 3117–3125.

[72] Shinkyo, R.; Kamakura, M.; Ikushiro, S.-i.; Inouye, K.; Sakaki, T. Biodegradation of dioxins by recombinant *Escherichia coli* expressing rat CYP1A1 or its mutant. *Appl. Microbiol. Biotechnol.* **2006**, *72*, 584–590.

[73] Furuya, T.; Arai, Y.; Kino, K. Biotechnological Production of Caffeic Acid by Bacterial Cytochrome P450 CYP199A2. *Appl. Environ. Microbiol.* **2012**, *78*, 6087–6094.

[74] Auclair, K.; Polic, V. In *Monooxygenase, Peroxidase and Peroxygenase Properties and Mechanisms of Cytochrome P450*; Hrycay, E. G., Bandiera, S. M., Eds.; Springer International Publishing, 2015; Chapter 8, pp 209–228.

[75] Julsing, M. K.; Cornelissen, S.; Buhler, B.; Schmid, A. Heme-iron oxygenases: powerful industrial biocatalysts? *Curr. Opin. Chem. Biol.* **2008**, *12*, 177–186.

[76] Urlacher, V. B.; Girhard, M. Cytochrome P450 monooxygenases: an update on perspectives for synthetic application. *Trends Biotechnol.* **2012**, *30*, 26–36.

[77] Behrendorff, J. B.; Huang, W.; Gillam, E. M. Directed evolution of cytochrome P450 enzymes for biocatalysis: exploiting the catalytic versatility of enzymes with relaxed substrate specificity. *Biochem. J.* **2015**, *467*, 1–15.

[78] Coleman, T.; Chao, R. R.; Bruning, J. B.; De Voss, J. J.; Bell, S. G. CYP199A4 catalyses the efficient demethylation and demethenylation of para-substituted benzoic acid derivatives. *RSC Adv.* **2015**, *5*, 52007–52018.

[79] Bell, S. G.; Zhou, R.; Yang, W.; Tan, A. B. H.; Gentleman, A. S.; Wong, L.-L.; Zhou, W. Investigation of the Substrate Range of CYP199A4: Modification of the Partition between Hydroxylation and Desaturation Activities by Substrate and Protein Engineering. *Chem. Eur. J.* **2012**, *18*, 16677–16688.

[80] Larimer, F. W. et al. Complete genome sequence of the metabolically versatile photosynthetic bacterium *Rhodopseudomonas palustris*. *Nat. Biotechnol.* **2004**, *22*, 55–61.

[81] Harwood, C. S.; Gibson, J. Anaerobic and Aerobic Metabolism of Diverse Aromatic Compounds by the Photosynthetic Bacterium *Rhodopseudomonas palustris*. *Appl. Environ. Microbiol.* **1988**, *54*, 712–717.

[82] Huang, J. J.; Heiniger, E. K.; McKinlay, J. B.; Harwood, C. S. Production of Hydrogen Gas from Light and the Inorganic Electron Donor Thiosulfate by *Rhodopseudomonas palustris*. *Appl. Environ. Microbiol.* **2010**, *76*, 7717–7722.

[83] Pang, X.; Xu, F.; Bell, S. G.; Guo, D.; Wong, L.-L.; Rao, Z. Purification, crystallization and preliminary crystallographic analysis of cytochrome P450 203A1 from *Rhodopseudomonas palustris*. *Acta Crystallogr. Sect. F* **2007**, *63*, 342–345.

[84] Peng, Y.; Xu, F.; Bell, S. G.; Wong, L.-L.; Rao, Z. Crystallization and preliminary X-ray diffraction studies of a ferredoxin reductase from *Rhodopseudomonas palustris* CGA009. *Acta Crystallogr. Sect. F* **2007**, *63*, 422–425.

[85] Oda, Y.; Wanders, W.; Huisman, L. A.; Meijer, W. G.; Gottschal, J. C.; Forney, L. J. Genotypic and Phenotypic Diversity within Species of Purple Nonsulfur Bacteria Isolated from Aquatic Sediments. *Appl. Environ. Microbiol.* **2002**, *68*, 3467–3477.

[86] Bell, S. G.; Hoskins, N.; Xu, F.; Caprotti, D.; Rao, Z.; Wong, L.-L. Cytochrome P450 enzymes from the metabolically diverse bacterium *Rhodopseudomonas palustris*. *Biochem. Biophys. Res. Commun.* **2006**, *342*, 191–196.

[87] Coleman, T. *Investigation of the substrate range and mechanism of CYP199A4 catalysed oxidations*; The University of Adelaide, 2013.

[88] Bell, S.; Yang, W.; Dale, A.; Zhou, W.; Wong, L.-L. Improving the affinity and activity of CYP101D2 for hydrophobic substrates. *Appl. Microbiol. Biotechnol.* **2013**, *97*, 3979–3990.

[89] Imai, M.; Shimada, H.; Watanabe, Y.; Matsushima-Hibiya, Y.; Makino, R.; Koga, H.; Horiuchi, T.; Ishimura, Y. Uncoupling of the cytochrome P-450cam monooxygenase reaction by a single mutation, threonine-252 to alanine or valine: possible role of the hydroxy amino acid in oxygen activation. *Proc. Natl. Acad. Sci. U.S.A.* **1989**, *86*, 7823–7827.

[90] Martinis, S. A.; Atkins, W. M.; Stayton, P. S.; Sligar, S. G. A conserved residue of cytochrome P-450 is involved in heme-oxygen stability and activation. *J. Am. Chem. Soc.* **1989**, *111*, 9252–9253.

[91] Gerber, N. C.; Sligar, S. G. Catalytic mechanism of cytochrome P-450: evidence for a distal charge relay. *J. Am. Chem. Soc.* **1992**, *114*, 8742–8743.

[92] Gerber, N. C.; Sligar, S. G. A role for Asp-251 in cytochrome P-450cam oxygen activation. *J. Biol. Chem.* **1994**, *269*, 4260–4266.

[93] Vidakovic, M.; Sligar, S. G.; Li, H.; Poulos, T. L. Understanding the Role of the Essential Asp251 in Cytochrome P450cam Using Site-Directed Mutagenesis, Crystallography, and Kinetic Solvent Isotope Effect. *Biochemistry* **1998**, *37*, 9211–9219.

[94] Furuya, T.; Kino, K. Discovery of 2-Naphthoic Acid Monooxygenases by Genome Mining and their Use as Biocatalysts. *ChemSusChem* **2009**, *2*, 645–649.

[95] Furuya, T.; Kino, K. Regioselective oxidation of indole- and quinolinecarboxylic acids by cytochrome P450 CYP199A2. *Appl. Microbiol. Biotechnol.* **2010**, *85*, 1861–1868.

[96] Rodrigues, J.; Araujo, R.; Prather, K.; Kluskens, L.; Rodrigues, L. Heterologous production of caffeic acid from tyrosine in *Escherichia coli*. *Enzyme Microb. Technol.* **2015**, *71*, 36–44.

[97] Xu, F.; Bell, S. G.; Rao, Z.; Wong, L.-L. Structure-activity correlations in pentachlorobenzene oxidation by engineered cytochrome P450cam. *Protein Eng. Des. Sel.* **2007**, *20*, 473–480.

[98] Dawson, J. H.; Andersson, L. A.; Sono, M. Spectroscopic investigations of ferric cytochrome P-450-CAM ligand complexes. Identification of the ligand trans to cysteinate in the native enzyme. *J. Biol. Chem.* **1982**, *257*, 3606–3617.

[99] Luthra, A.; Denisov, I. G.; Sligar, S. G. Spectroscopic features of cytochrome P450 reaction intermediates. *Arch. Biochem. Biophys.* **2011**, *507*, 26–35.

[100] Parker, J. E.; Warrilow, A. G. S.; Price, C. L.; Mullins, J. L.; Kelly, D. E.; Kelly, S. L. Resistance to antifungals that target CYP51. *J. Chem. Biol.* **2014**, *7*, 143–161.

[101] Correia, M. A.; Hollenberg, P. F. In *Cytochrome P450: Structure, Mechanism, and Biochemistry*, 4th ed.; Ortiz de Montellano, P. R., Ed.; Springer International Publishing, 2015; Chapter 5, pp 177–259.

[102] Jefcoate, C. R.; Simpson, E. R.; Boyd, G. S. Spectral Properties of Rat Adrenal-Mitochondrial Cytochrome P-450. *Eur. J. Biochem.* **1974**, *42*, 539–551.

[103] Kumaki, K.; Sato, M.; Kon, H.; Nebert, D. W. Correlation of type I, type II, and reverse type I difference spectra with absolute changes in spin state of hepatic microsomal cytochrome P-450 iron from five mammalian species. *J. Biol. Chem.* **1978**, *253*, 1048–1058.

[104] Lane, B. S.; ; Burgess, K. A Cheap, Catalytic, Scalable, and Environmentally Benign Method for Alkene Epoxidations. *J. Am. Chem. Soc.* **2001**, *123*, 2933–2934.

[105] Park, J.-W.; Lee, J.-K.; Kwon, T.-J.; Yi, D.-H.; Kim, Y.-J.; Moon, S.-H.; Suh, H.-H.; Kang, S.-M.; Park, Y.-I. Bioconversion of compactin into pravastatin by *Streptomyces* sp. *Biotechnol. Lett.* **2003**, *25*, 1827–1831.

[106] Ryerson, C. C.; Ballou, D. P.; Walsh, C. Mechanistic studies on cyclohexanone oxygenase. *Biochemistry* **1982**, *21*, 2644–2655.

[107] Taschner, M. J.; Aminbhavi, A. S. α-Oxygenation of a trans-3,4-disubstituted γ-lactone. A comparative study. *Tetrahedron Lett.* **1989**, *30*, 1029–1032.

[108] Evans, D. A.; Gage, J. R.; Leighton, J. L. Total synthesis of (+)-calyculin A. *J. Am. Chem. Soc.* **1992**, *114*, 9434–9453.

[109] Kim, T. W.; Hwang, J. Y.; Kim, Y. S.; Joo, S. H.; Chang, S. C.; Lee, J. S.; Takatsuto, S.; Kim, S. K. Arabidopsis CYP85A2, a Cytochrome P450, Mediates the Baeyer-Villiger Oxidation of Castasterone to Brassinolide in Brassinosteroid Biosynthesis. *Plant Cell* **2005**, *17*, 2397–2412.

[110] Tuck, S. F.; Patel, H.; Safi, E.; Robinson, C. H. Lanosterol 14α-demethylase ($P450_{14DM}$): effects of $P450_{14DM}$ inhibitors on sterol biosynthesis downstream of lanosterol. *J. Lipid Res.* **1991**, *32*, 893–902.

[111] Shyadehi, A. Z.; Lamb, D. C.; Kelly, S. L.; Kelly, D. E.; Schunck, W.-H.; Wright, J. N.; Corina, D.; Akhtar, M. The Mechanism of the Acyl-Carbon Bond Cleavage Reaction Catalyzed by Recombinant Sterol 14α-Demethylase of *Candida albicans* (Other Names Are: Lanosterol 14α-Demethylase, P-450_{14DM}, and CYP51). *J. Biol. Chem.* **1996**, *271*, 12445–12450.

[112] Chen, S.; Hossain, M. S.; Frank W. Foss, J. Organocatalytic Dakin Oxidation by Nucleophilic Flavin Catalysts. *Org. Lett.* **2012**, *14*, 2806–2809, PMID: 22587606.

[113] Roy, A.; Reddy, K. R.; Mohanta, P. K.; Ila, H.; Junjappat, H. Hydrogen Peroxide/Boric Acid: An Efficient System for Oxidation of Aromatic Aldehydes and Ketones to Phenols. *Synth. Commun.* **1999**, *29*, 3781–3791.

[114] Matsumoto, M.; Kobayashi, K.; Hotta, Y. Acid-catalyzed oxidation of benzaldehydes to phenols by hydrogen peroxide. *J. Org. Chem.* **1984**, *49*, 4740–4741.

[115] Ost, T. W. B.; Clark, J.; Mowat, C. G.; Miles, C. S.; Walkinshaw, M. D.; Reid, G. A.; Chapman, S. K.; Daff, S. Oxygen Activation and Electron Transfer in Flavocytochrome P450 BM3. *J. Am. Chem. Soc.* **2003**, *125*, 15010–15020.

[116] Clark, J. P.; Miles, C. S.; Mowat, C. G.; Walkinshaw, M. D.; Reid, G. A.; Daff, S. N.; Chapman, S. K. The role of Thr268 and Phe393 in cytochrome P450 BM3. *J. Inorg. Biochem.* **2006**, *100*, 1075–1090.

[117] Denisov, I. G.; Grinkova, Y. V.; Baas, B. J.; Sligar, S. G. The Ferrous-Dioxygen Intermediate in Human Cytochrome P450 3A4: SUBSTRATE DEPENDENCE OF FORMATION AND DECAY KINETICS. *J. Biol. Chem.* **2006**, *281*, 23313–23318.

[118] Sligar, S. G. Coupling of spin, substrate, and redox equilibriums in cytochrome P450. *Biochemistry* **1976**, *15*, 5399–5406.

[119] Kimata, Y.; Shimada, H.; Hirose, T.; Ishimura, Y. Role of THR-252 in Cytochrome $P450_{CAM}$: A Study with Unnatural Amino Acid Mutagenesis. *Biochem. Biophys. Res. Commun.* **1995**, *208*, 96–102.

[120] Nagano, S. In *Fifty Years of Cytochrome P450 Research*; Yamazaki, H., Ed.; Springer Japan, 2014; Chapter 5, pp 95–106.

[121] Yeom, H.; Sligar, S. G.; Li, H.; Poulos, T. L.; Fulco, A. J. The role of Thr268 in oxygen activation of cytochrome P450BM-3. *Biochemistry* **1995**, *34*, 14733–14740.

[122] Truan, G.; Peterson, J. A. Thr268 in Substrate Binding and Catalysis in P450BM-3. *Arch. Biochem. Biophys.* **1998**, *349*, 53 – 64.

[123] Lee-Robichaud, P.; Akhtar, M. E.; Akhtar, M. An analysis of the role of active site protic residues of cytochrome P-450s: mechanistic and mutational studies on 17α-hydroxylase-17,20-lyase (P-45017α also CYP17). *Biochem. J.* **1998**, *330*, 967–974.

[124] Hiroya, K.; Ishigooka, M.; Shimizu, T.; Hatano, M. Role of Glu318 and Thr319 in the catalytic function of cytochrome P450d (P4501A2): effects of mutations on the methanol hydroxylation. *FASEB J.* **1992**, *6*, 749–51.

[125] Parikh, A.; Josephy, P. D.; Guengerich, F. P. Selection and Characterization of Human Cytochrome P450 1A2 Mutants with Altered Catalytic Properties. *Biochemistry* **1999**, *38*, 5283–5289.

[126] Zhou, D.; Korzekwa, K.; Poulos, T.; Chen, S. A site-directed mutagenesis study of human placental aromatase. *J. Biol. Chem.* **1992**, *267*, 762–768.

[127] Hanioka, N.; Gonzalez, F.; Lindberg, N.; Liu, G.; Gelboin, H.; Korzekwa, K. Site-directed mutagenesis of cytochrome P450s CYP2A1 and CYP2A2: influence of the distal helix on the kinetics of testosterone hydroxylation. *Biochemistry* **1992**, *31*, 3364–3370.

[128] Batabyal, D.; Poulos, T. L. Crystal Structures and Functional Characterization of Wild-Type CYP101D1 and Its Active Site Mutants. *Biochemistry* **2013**, *52*, 8898–8906.

[129] Tuck, S. F.; Hiroya, K.; Shimizu, T.; Hatano, M.; de Montellano, P. R. O. The cytochrome P450 1A2 active site: Topology and perturbations caused by glutamic acid-318 and threonine-319 mutations. *Biochemistry* **1993**, *32*, 2548–2553.

[130] Wang, B.; Li, C.; Dubey, K. D.; Shaik, S. Quantum Mechanical/Molecular Mechanical Calculated Reactivity Networks Reveal How Cytochrome P450cam and Its T252A Mutant Select Their Oxidation Pathways. *J. Am. Chem. Soc.* **2015**, *137*, 7379–7390.

[131] Wang, B.; Li, C.; Cho, K.-B.; Nam, W.; Shaik, S. The $Fe^{III}(H_2O_2)$ Complex as a Highly Efficient Oxidant in Sulfoxidation Reactions: Revival of an Underrated

Oxidant in Cytochrome P450. *J. Chem. Theory Comput.* **2013**, *9*, 2519–2525, PMID: 26583848.

[132] Taschner, M. J.; Black, D. J. The enzymatic Baeyer-Villiger oxidation: enantioselective synthesis of lactones from mesomeric cyclohexanones. *J. Am. Chem. Soc.* **1988**, *110*, 6892–6893.

[133] Cupp-Vickery, J. R.; Poulos, T. L. Structure of cytochrome P450eryF involved in erythromycin biosynthesis. *Nat. Struct. Mol. Biol.* **1995**, *2*, 144–153.

[134] Zhao, B.; Guengerich, F. P.; Voehler, M.; Waterman, M. R. Role of Active Site Water Molecules and Substrate Hydroxyl Groups in Oxygen Activation by Cytochrome P450 158A2 A NEW MECHANISM OF PROTON TRANSFER. *J. Biol. Chem.* **2005**, *280*, 42188–42197.

[135] Fischer, R. T.; Trzaskos, J. M.; Magolda, R. L.; Ko, S. S.; Brosz, C. S.; Larsen, B. Lanosterol 14 alpha-methyl demethylase. Isolation and characterization of the third metabolically generated oxidative demethylation intermediate. *J. Biol. Chem.* **1991**, *266*, 6124–6132.

[136] Corina, D. L.; Miller, S. L.; Wright, J. N.; Akhtar, M. The mechanism of cytochrome P-450 dependent C-C bond cleavage: studies on 17α-hydroxylase-17,20-lyase. *J. Chem. Soc. Chem. Commun.* **1991**, 782–783.

[137] Akhtar, M.; Corina, D.; Miller, S.; Shyadehi, A. Z.; Wright, J. N. Mechanism of the Acyl-Carbon Cleavage and Related Reactions Catalyzed by Multifunctional P-450s: Studies on Cytochrome P-450$_{17\alpha}$. *Biochemistry* **1994**, *33*, 4410–4418.

[138] Davydov, R.; Macdonald, I. D. G.; Makris, T. M.; Sligar, S. G.; Hoffman, B. M. EPR and ENDOR of Catalytic Intermediates in Cryoreduced Native and Mutant Oxy-Cytochromes P450cam: Mutation-Induced Changes in the Proton Delivery System. *J. Am. Chem. Soc.* **1999**, *121*, 10654–10655.

[139] Davydov, R.; Hoffman, B. M. Active intermediates in heme monooxygenase reactions as revealed by cryoreduction/annealing, EPR/ENDOR studies. *Arch. Biochem. Biophys.* **2011**, *507*, 36–43.

[140] Kim, D.; Heo, Y.-S.; de Montellano, P. R. O. Efficient catalytic turnover of cytochrome P450$_{\mathrm{cam}}$ is supported by a T252N mutation. *Arch. Biochem. Biophys.* **2008**, *474*, 150–156.

[141] Guzman, J. D. Natural Cinnamic Acids, Synthetic Derivatives and Hybrids with Antimicrobial Activity. *Molecules* **2014**, *19*, 19292–19349.

[142] Clifford, M. N. Chlorogenic acids and other cinnamates - nature, occurrence and dietary burden. *J. Sci. Food Agric.* **1999**, *79*, 362–372.

[143] Xing, Y.; Peng, H.; Zhang, M.; Li, X.; Zeng, W.; Yang, X. Caffeic acid product from the highly copper-tolerant plant *Elsholtzia splendens* post-phytoremediation: its extraction, purification, and identification. *J. Zhejiang Univ. Sci. B* **2012**, *13*, 487–493.

[144] Turner, L. B.; Mueller-Harvey, I.; McAllan, A. B. Light-induced isomerization and dimerization of cinnamic acid derivatives in cell walls. *Phytochemistry* **1993**, *33*, 791–796.

[145] Clampitt, B. H.; Callis, J. W. Photochemical Isomerization of Cinnamic Acid in Aqueous Solutions. *J. Phys. Chem.* **1962**, *66*, 201–204.

[146] Bell, S. G.; Xu, F.; Forward, I.; Bartlam, M.; Rao, Z.; Wong, L.-L. Crystal Structure of CYP199A2, a *Para*-Substituted Benzoic Acid Oxidizing Cytochrome P450 from *Rhodopseudomonas palustris*. *J. Mol. Biol.* **2008**, *383*, 561–574.

[147] Lin, Y.; Yan, Y. Biosynthesis of caffeic acid in *Escherichia coli* using its endogenous hydroxylase complex. *Microb. Cell Fact.* **2012**, *11*, 1–9.

[148] Prieto, M. A.; Perez-Aranda, A.; Garcia, J. L. Characterization of an *Escherichia coli* aromatic hydroxylase with a broad substrate range. *J. Bacteriol.* **1993**, *175*, 2162–2167.

[149] Louie, T. M.; Xie, X. S.; Xun, L. Coordinated Production and Utilization of $FADH_2$ by NAD(P)H-Flavin Oxidoreductase and 4-Hydroxyphenylacetate 3-Monooxygenase. *Biochemistry* **2003**, *42*, 7509–7517.

Appendix A Data for Chapter 3

HPLC analysis

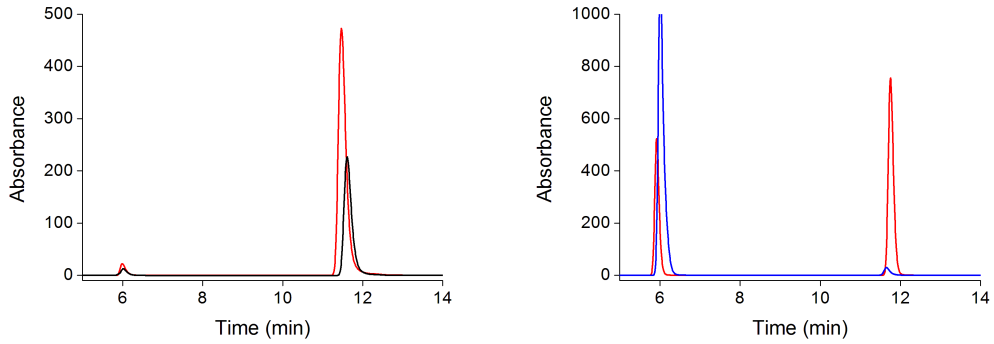

(a) (b)

Figure A1: (a) HPLC analysis of the $WT_{CYP199A4}$ turnover (black) of 4-acetoxybenzoic acid. The substrate control (t_R = 11.8 mins) is shown in red. (b) HPLC analysis of the substrate control after ≈ 4 hours (red) and ≈ 24 hours (blue) showing its hydrolysis to 4-hydroxybenzoic acid (t_R = 6.0 mins) in Tris buffer (50 mM, pH 7.4).

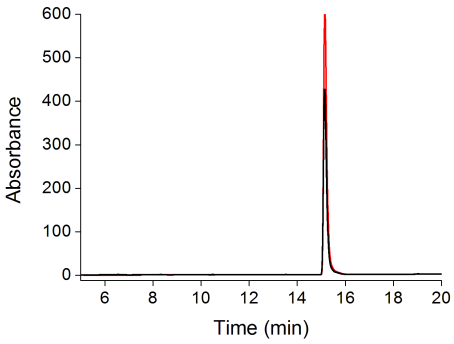

(a)

Figure A2: HPLC analysis of the $WT_{CYP199A4}$ turnover (black) of 4-acetamidobenzoic acid. The substrate control (t_R = 15.2 mins) is shown in red.

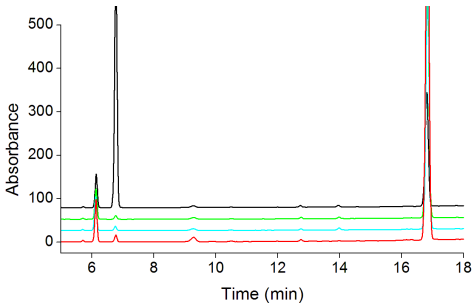

(a)

Figure A3: HPLC analysis of the *in vitro* turnover controls for 4-ethynylbenzoic acid. The 4-ethynylbenzoic acid substrate control (t_R = 16.8 mins) is shown in red, the "turnover" of 4-ethynylbenzoic acid in the absence of the CYP199A4 P450 enzyme in cyan and the 'turnover' of 4-ethynylbenzoic acid in the absence of NADH in lime. The $WT_{CYP199A4}$ turnover of 4-ethynylbenzoic acid has also been shown in black to demonstrate the lack of 4-carboxyphenylacetic acid (t_R = 6.8 mins) formation in the absence of P450.

Mass spectra analysis

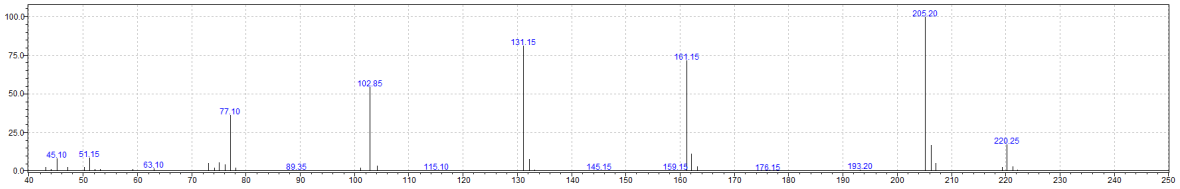

(a)

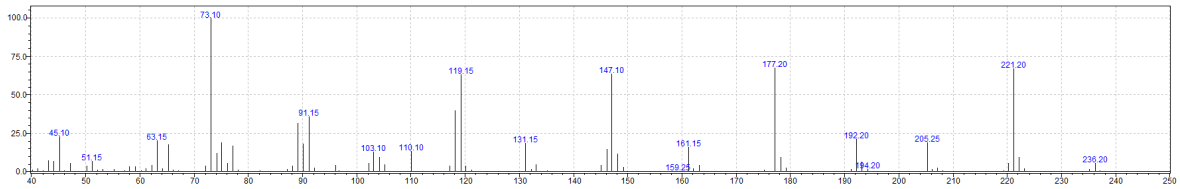

(b)

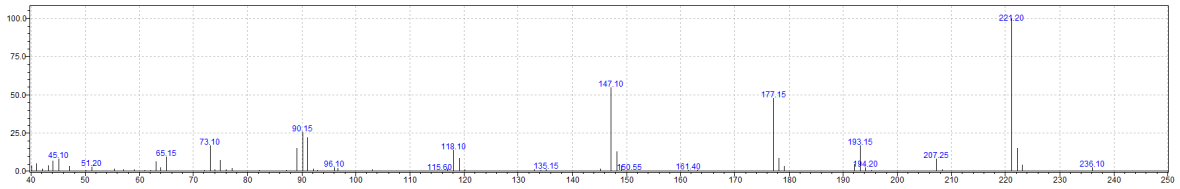

(c)

Figure A4: Mass spectra of (a) 4-vinylbenzoic acid (b) 4-(oxiran-2-yl)benzoic acid and (c) the possible aldehyde rearrangement product of 4-vinylbenzoic acid.

NMR analysis

4-(oxiran-2-yl)benzoic acid

^{1}H NMR (500 MHz, DMSO) δ 12.92 (s, 1H, H1), 7.89 (d, J = 8.3 Hz, 2H, H4), 7.45 (d, J = 8.3 Hz, 2H, H5), 4.02 (dd, J = 4.1, 2.6 Hz, 1H, H7), 3.17 (dd, J = 5.4, 4.1 Hz, 1H, H8), 2.86 (dd, J = 5.4, 2.6 Hz, 1H, H8).

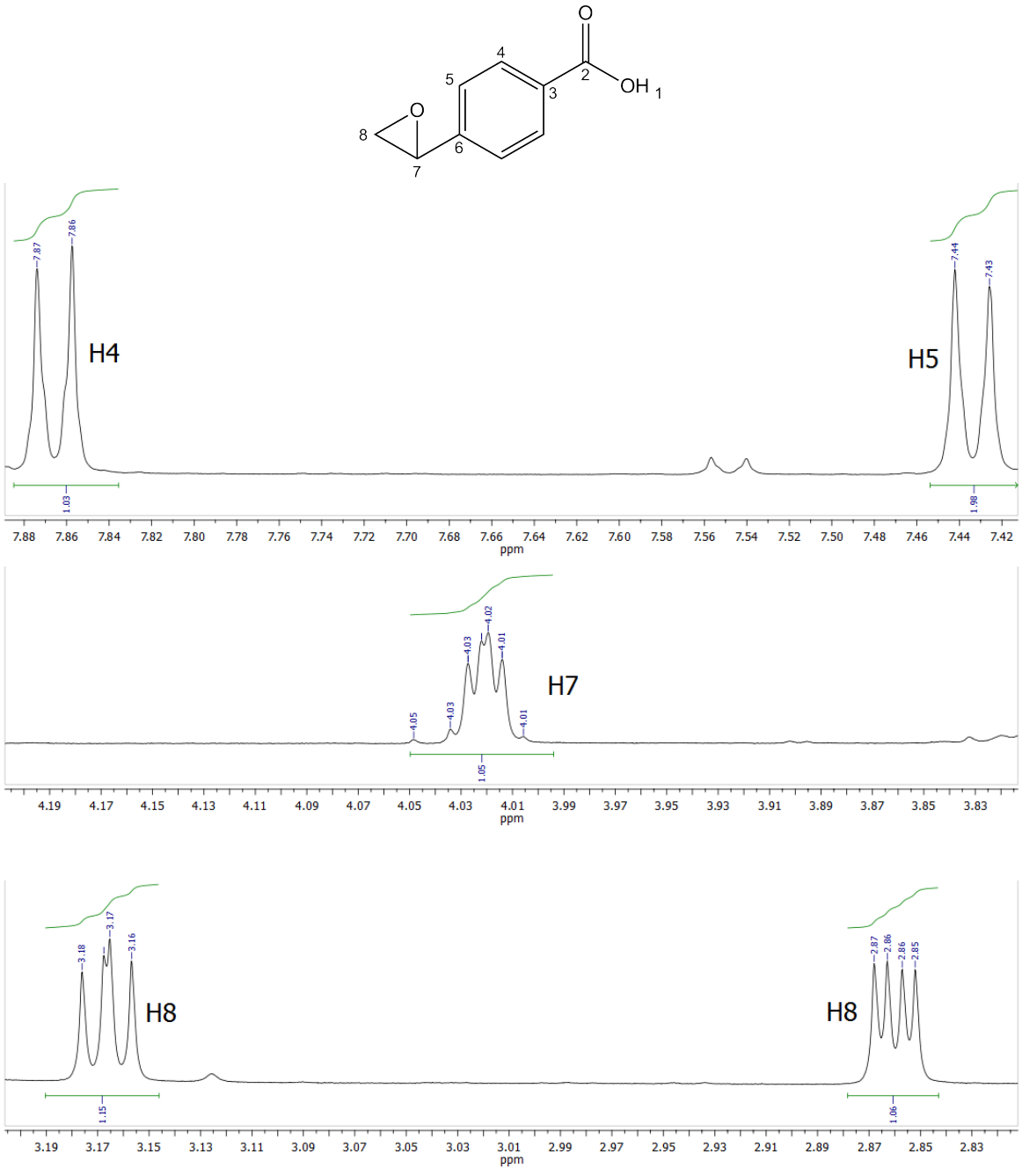

Figure A5: ^{1}H NMR for 4-(oxiran-2-yl)benzoic acid.

4-(hydroxyacetyl)benzoic acid

^{1}H NMR (500 MHz, DMSO) δ 8.05 (d, J = 8.2 Hz, 2H, H4), 8.01 (d, J = 8.2 Hz, 2H, H5), 5.18 (bs, 1H, H9), 4.82 (s, 2H, H8).

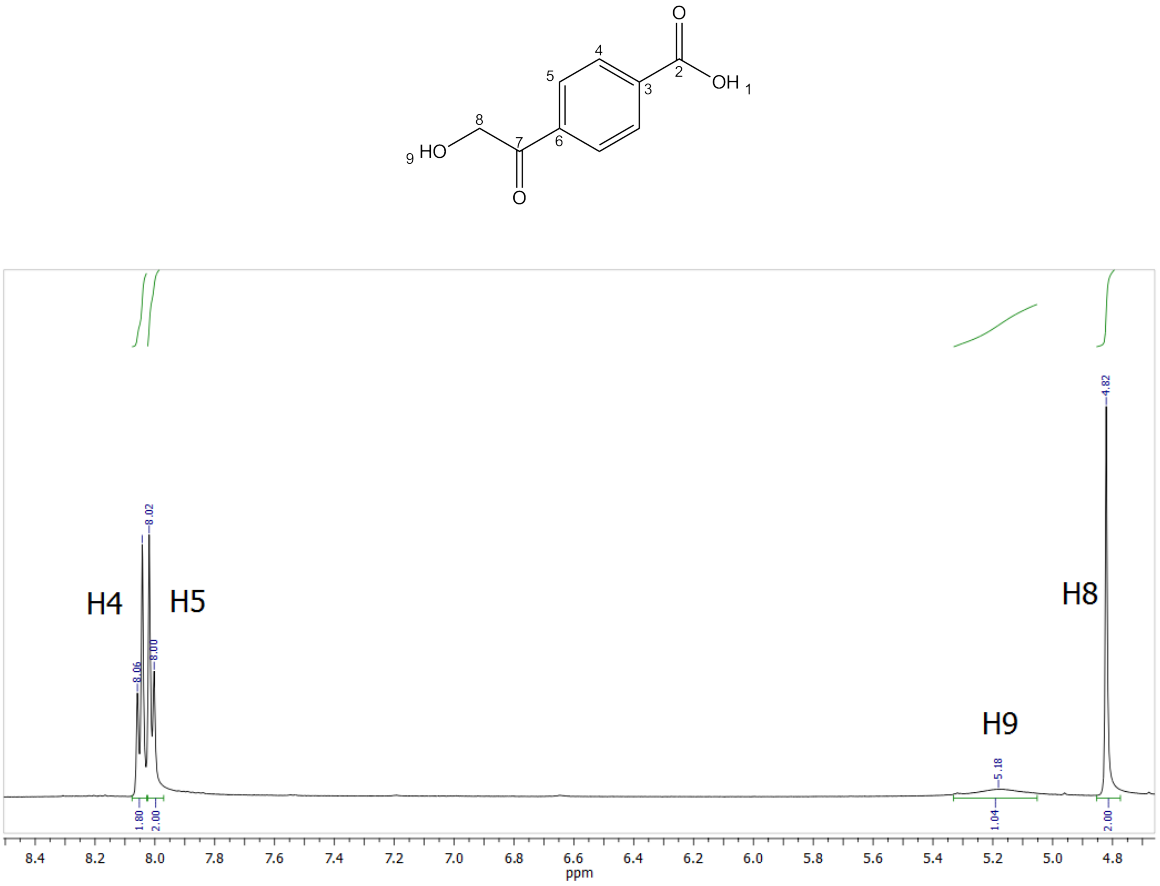

Figure A6: ^{1}H NMR for 4-(hydroxyacetyl)benzoic acid.

Appendix B Data for Chapter 4

Spin-state shifts

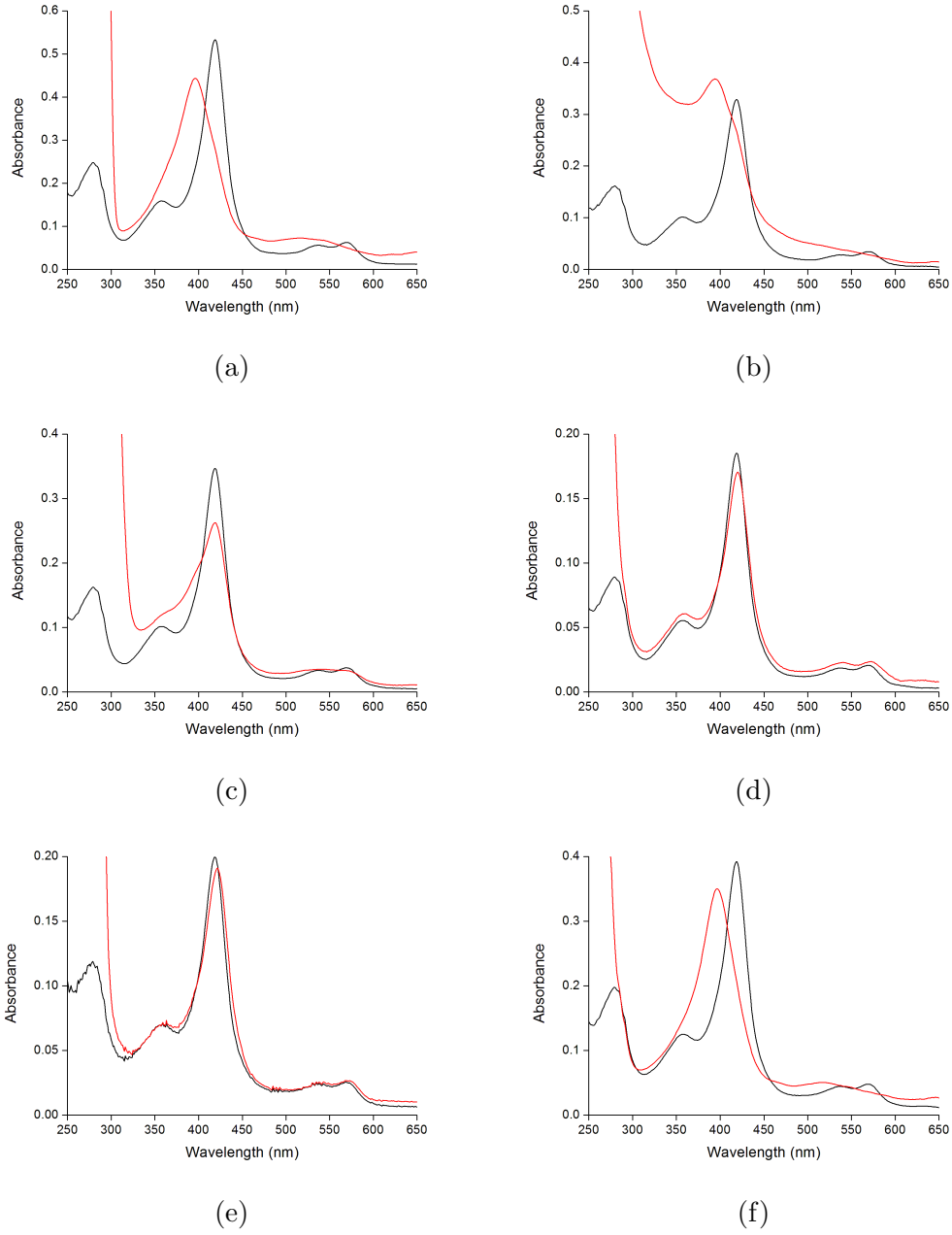

Figure B1: Spin-state shifts of T252A$_{CYP199A4}$ with (a) 4-vinylbenzoic acid (b) 4-ethynylbenzoic acid (c) 4-formylbenzoic acid (d) 4-acetylbenzoic acid (e) 4-acetamidobenzoic acid and (f) 4-acetoxybenzoic acid.

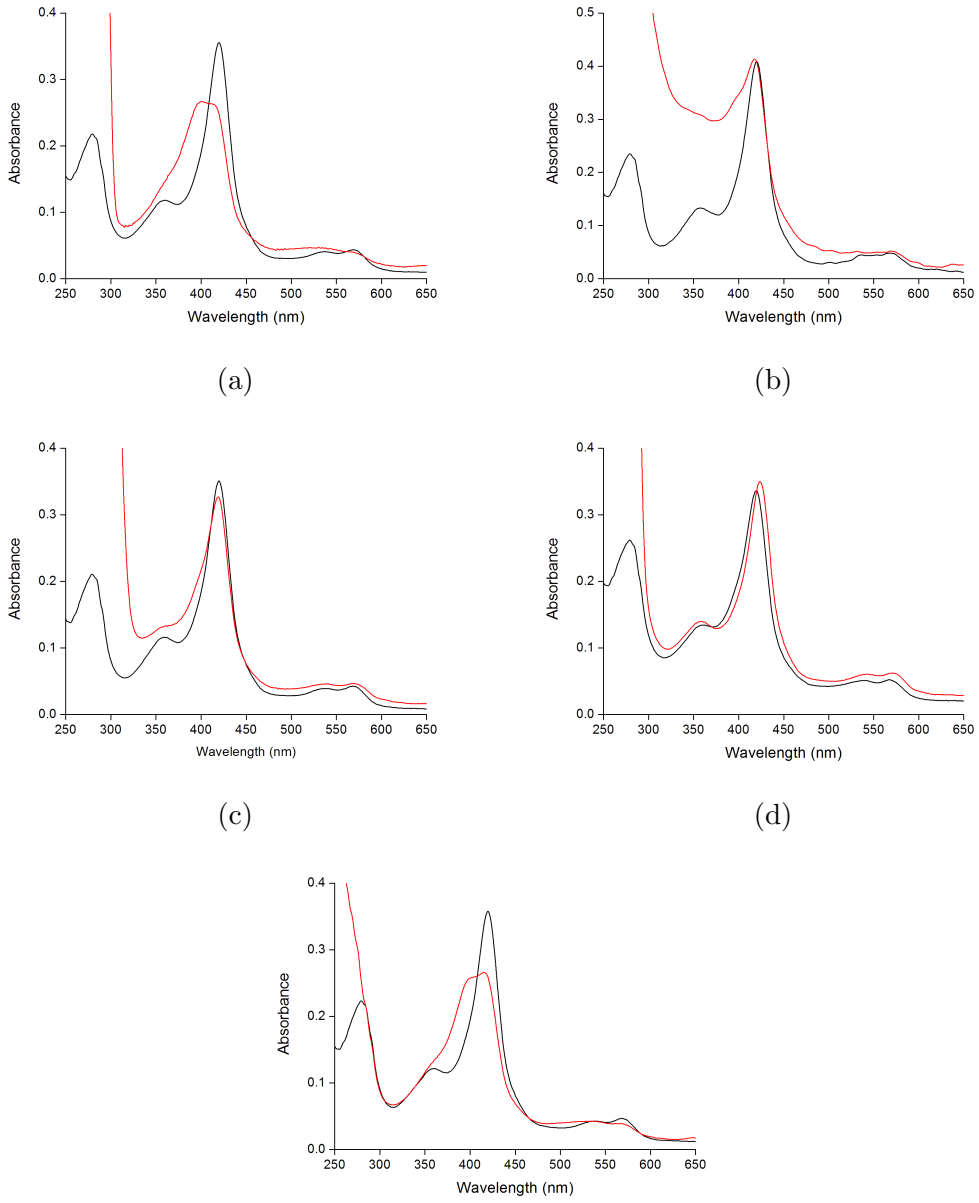

Figure B2: Spin-state shifts of D251N$_{CYP199A4}$ with (a) 4-vinylbenzoic acid (b) 4-ethynylbenzoic acid (c) 4-formylbenzoic acid (d) 4-acetamidobenzoic acid and (e) 4-acetoxybenzoic acid.

Dissociation constant analysis

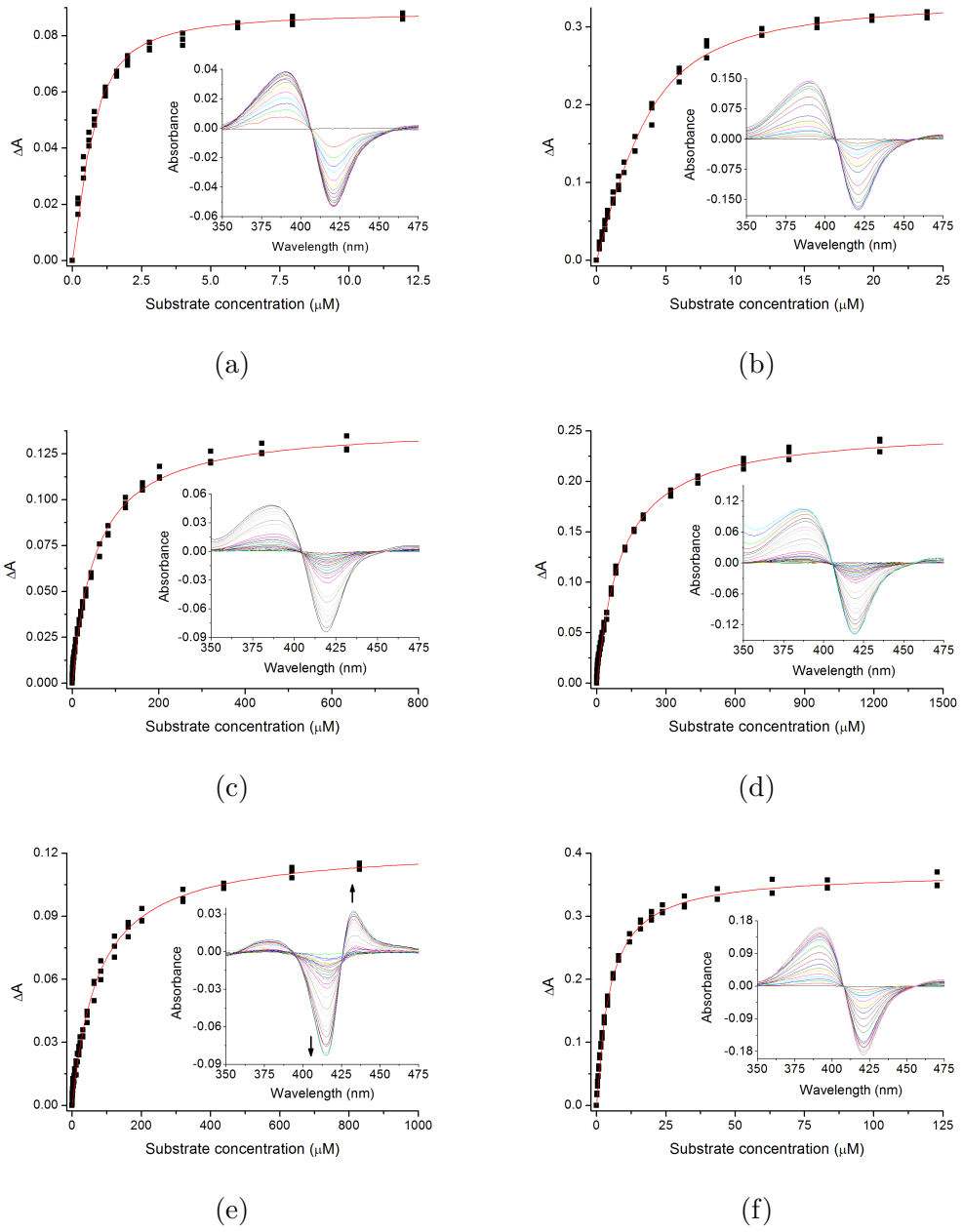

Figure B3: Dissociation constant analyses of $T252A_{CYP199A4}$ with (a) 4-vinylbenzoic acid (b) 4-ethynylbenzoic acid (c) 4-formylbenzoic acid (d) 4-acetylbenzoic acid (e) 4-acetamidobenzoic acid and (f) 4-acetoxybenzoic acid.

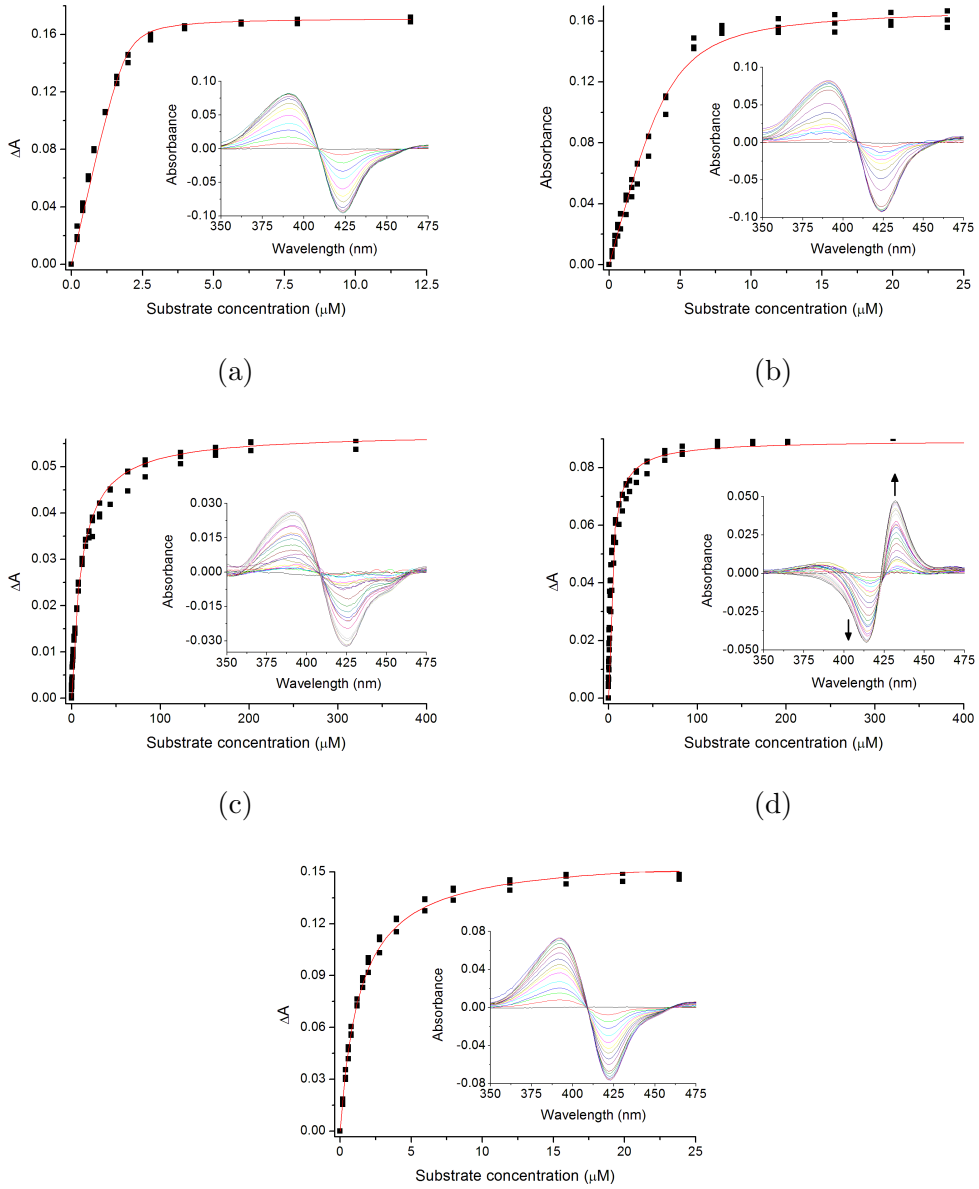

Figure B4: Dissociation constant analyses of D251N$_{CYP199A4}$ with (a) 4-vinylbenzoic acid (b) 4-ethynylbenzoic acid (c) 4-formylbenzoic acid (d) 4-acetamidobenzoic acid and (e) 4-acetoxybenzoic acid.

Appendix C Data for Chapter 5

Spin-state shifts

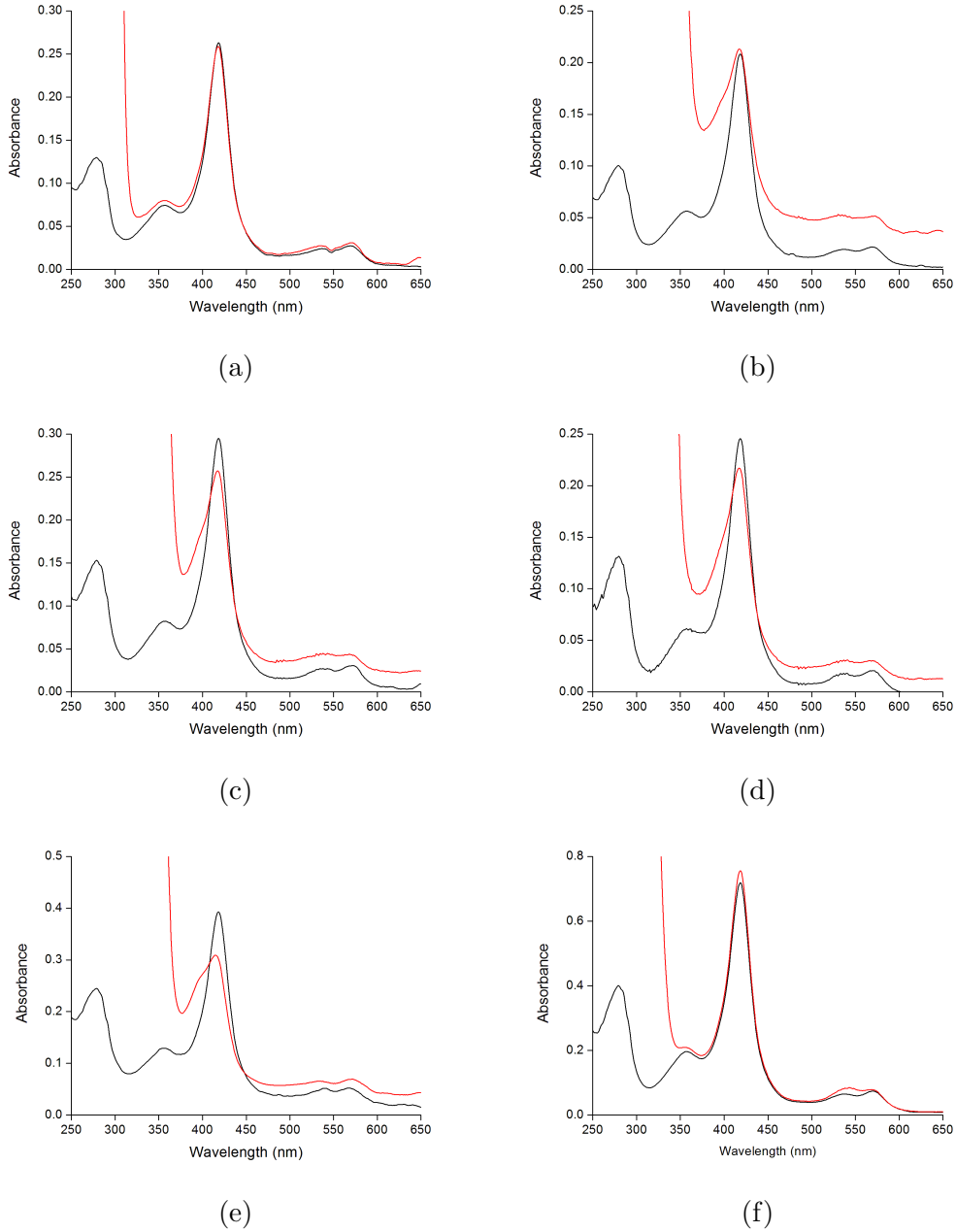

Figure C1: Spin-state shifts of CYP199A4 with (a) cinnamic acid (b) 3,4-dimethoxycinnamic acid (c) 2,4-dimethoxycinnamic acid (d) 3-hydroxy-4-methoxycinnamic acid (e) 3-(4-methylenedioxy)cinnamic acid and (f) 3,4,5-trimethoxycinnamic acid.

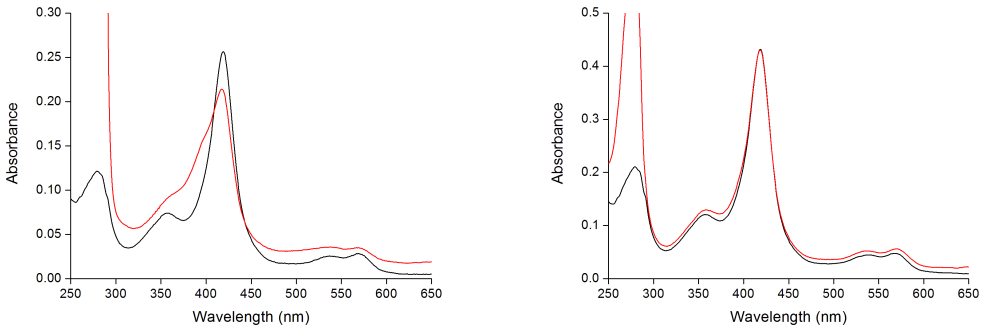

(a) (b)

Figure C2: Spin-state shifts of CYP199A4 with (a) 3-(4-methoxyphenyl)propionic acid and (b) 4-methoxyphenylacetic acid.

Dissociation constant analysis

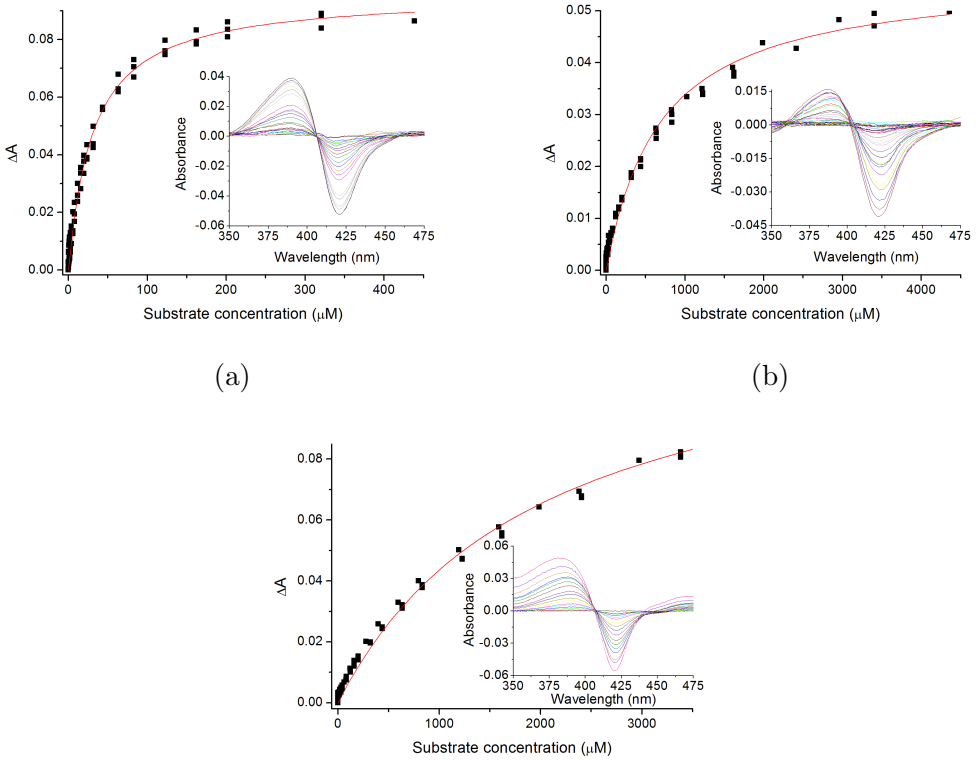

(a) (b)

(c)

Figure C3: Dissociation constants analyses of CYP199A4 with (a) 3-(4-methoxyphenyl)propionic acid (b) 4-methoxyphenylacetic acid and (c) 4-methylphenylacetic acid.

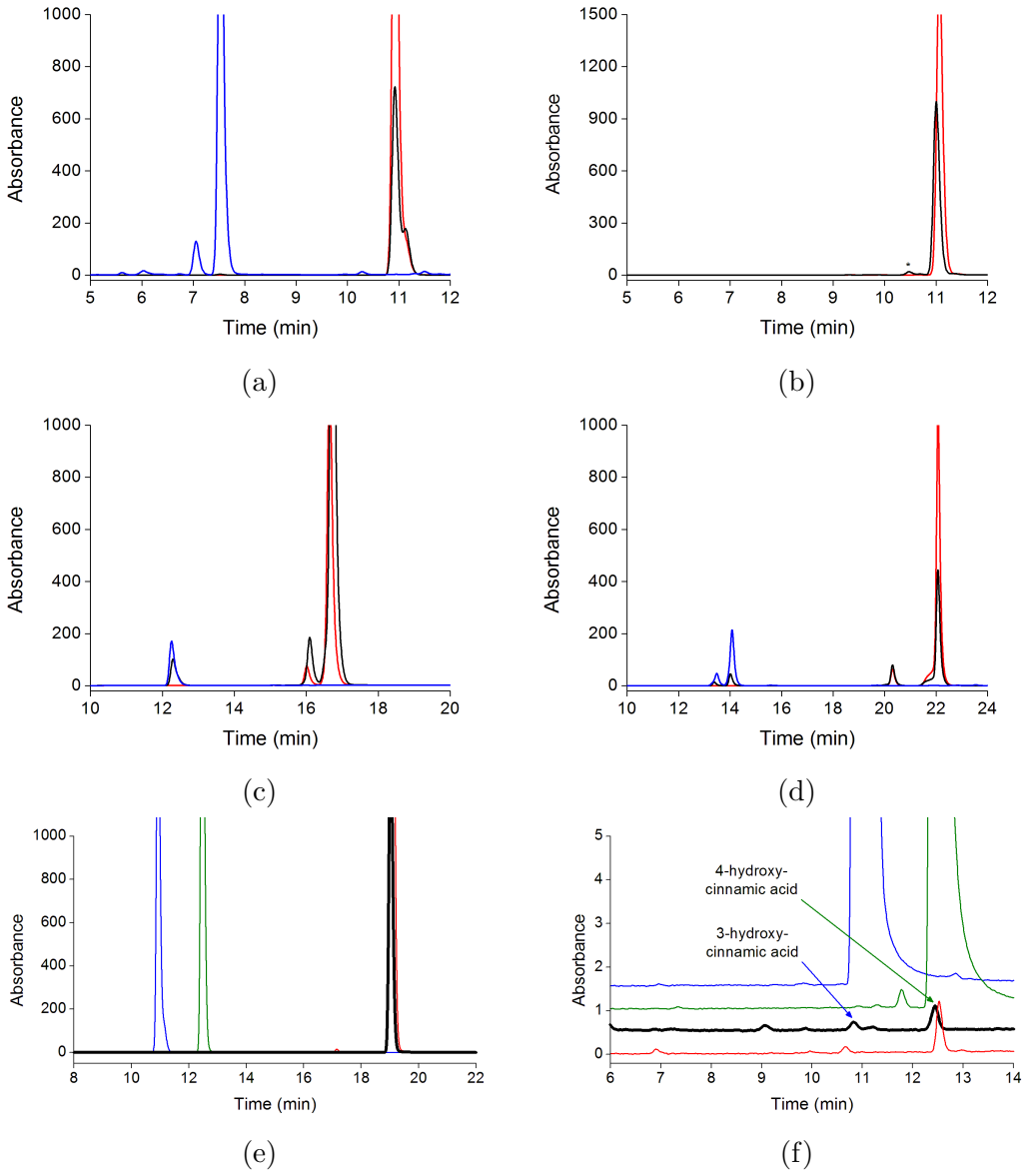

Figure C4: HPLC analysis of the *in vitro* CYP199A4 turnovers (black) of (a) 4-hydroxycinnamic acid; the substrate control (t_R = 11.0 mins) is in red and 3,4-dihydroxycinnamic acid product control (t_R = 7.1 mins, *cis*, t_R = 7.5 mins, *trans*) in blue (b) 3,5-dimethoxy-4-hydroxycinnamic acid; the substrate control (t_R = 11.1 mins) is in red (c) 3,4-dimethoxycinnamic acid; the substrate control (t_R = 16.0 mins, *cis*, t_R = 16.7 mins, *trans*) is in red and 3-methoxy-4-hydroxycinnamic acid product control (t_R = 12.3 mins) in blue and (d) 2,4-dimethoxycinnamic acid; the substrate control (t_R = 20.3 mins, *cis*, t_R = 22.1 mins, *trans*) is in red and 2-methoxy-4-hydroxycinnamic acid product control after purification by semi-prep HPLC (t_R = 13.4 mins, *cis*, t_R = 14.0 mins, *trans*) in blue and (e) cinnamic acid with (f) the likely product region highlighted; the substrate control (t_R = 19.1 mins) is in red, 3-hydroxycinnamic acid product control (t_R = 12.5 mins) in green and 4-hydroxycinnamic acid product control in blue. For clarity the chromatograms in (f) have been offset along the y axis.

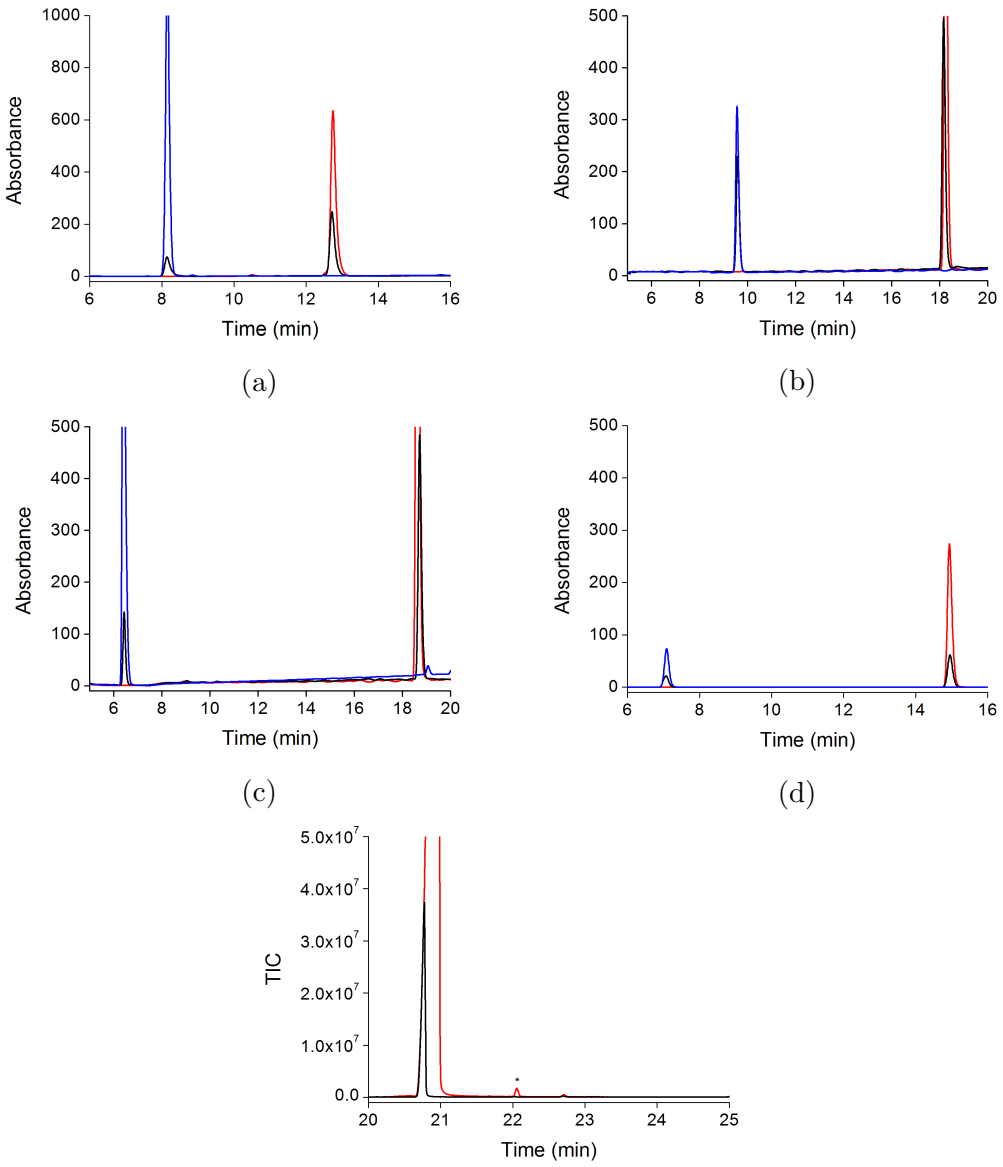

Figure C5: HPLC analysis of the *in vitro* CYP199A4 turnovers (black) of (a) 3-hydroxy-4-methoxycinnamic acid; the substrate control (t_R = 12.8 mins) is in red and 3,4-dihydroxycinnamic acid product control (t_R = 7.5 mins) in blue (b) 3-(4-methoxyphenyl)propionic acid; the substrate control (t_R = 18.1 mins) is in red and 3,4-dihydroxycinnamic acid product control (t_R = 19.6 mins) in blue (c) 4-methylphenylacetic acid; the substrate control (t_R = 18.7 mins) is in red and 4-(hydroxymethyl)phenylacetic acid product control (t_R = 6.5 mins) in blue and (d) 4-methoxyphenylacetic acid; the substrate control (t_R = 15.0 mins) is in red and 4-hydroxyphenylacetic acid product control (t_R = 7.0 mins) in blue. (e) GC-MS analysis of the derivatised CYP199A4 turnover (black) of 3,4,5-dimethoxycinnamic acid; the substrate control (t_R = 20.8 mins) is in red. Impurities are marked (*).

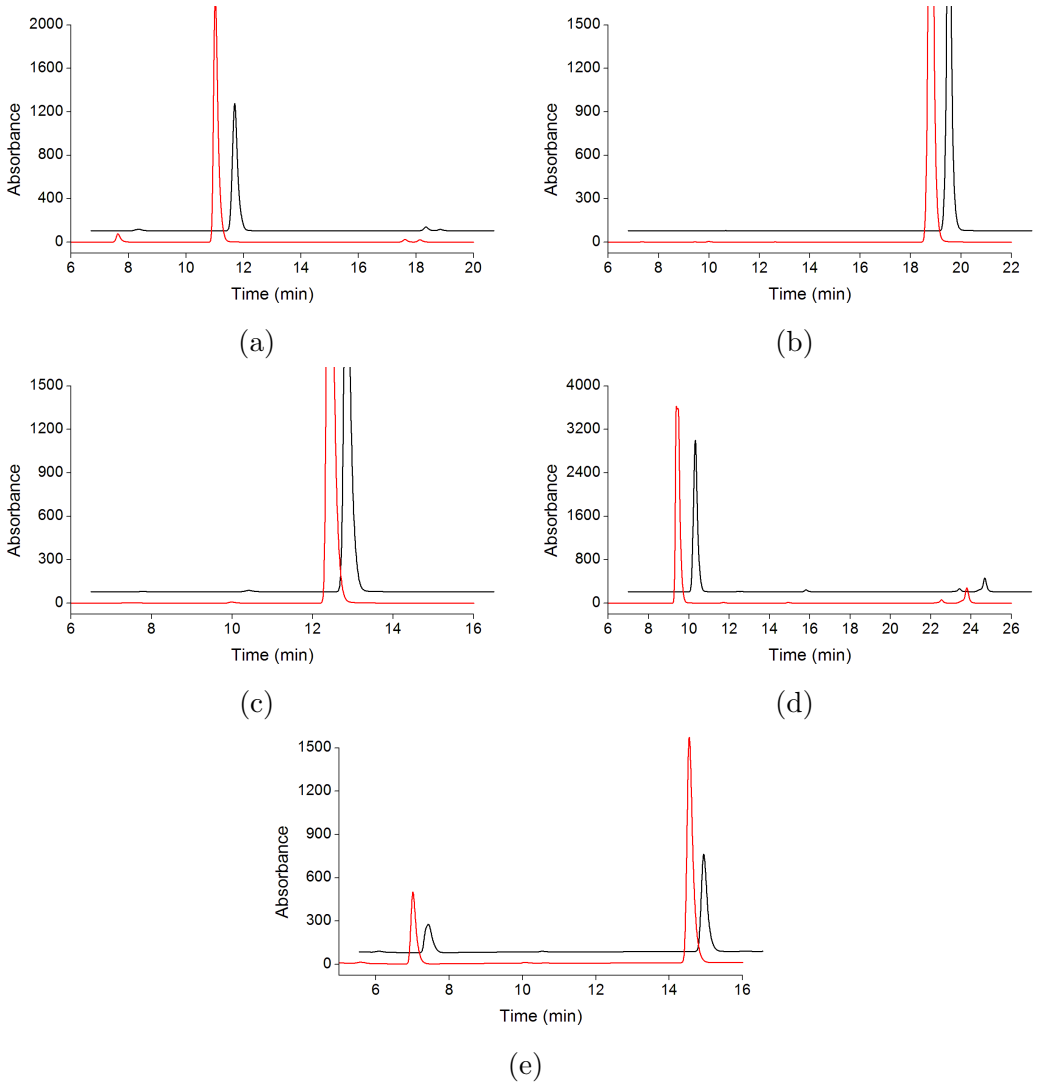

Figure C6: HPLC analysis of the *in vivo* CYP199A4 turnovers after 4 hours (black) and 24 hours (red) of (a) 4-methoxycinnamic acid ($t_R = 17.6$ mins, *cis* and $t_R = 18.2$ mins, *trans*) to 4-hydroxycinnamic acid ($t_R = 11.1$ mins) (b) cinnamic acid ($t_R = 18.1$ mins) (c) 3-hydroxycinnamic acid ($t_R = 12.5$ mins) (d) 4-methylcinnamic acid ($t_R = 22.5$ mins) to 4-(hydroxymethyl)cinnamic acid ($t_R = 9.4$ mins) and (e) 4-methoxyphenylacetic acid ($t_R = 14.5$ mins) to 4-hydroxyphenylacetic acid ($t_R = 7.0$ mins). The internal standard ($t_R = 23.8$ mins) is also shown in (d). For clarity the chromatograms have been offset along the x and y axes.

NMR analysis

4-methoxycinnamic acid

^{1}H NMR (500 MHz, DMSO) δ 12.21 (bs, 1H, H1), 7.63 (d, J = 8.6 Hz, 2H, H6), 7.54 (d, J = 16.0 Hz, 1H, H4), 6.97 (d, J = 8.6 Hz, 2H, H7), 6.37 (d, J = 16.0 Hz, 1H, H3), 3.79 (s, 3H, H9).

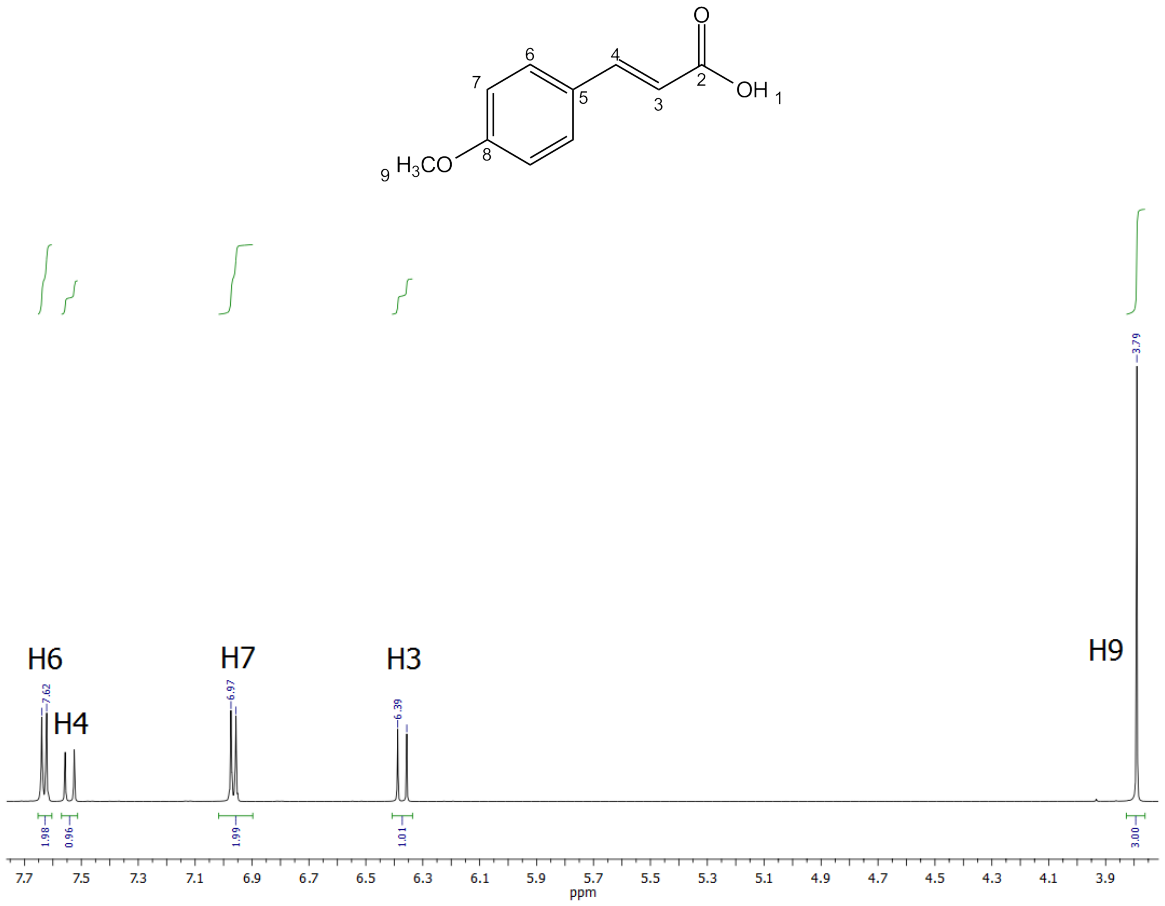

Figure C7: ^{1}H NMR for 4-methoxycinnamic acid.

2,4-dimethoxycinnamic acid

^{1}H NMR (500 MHz, DMSO) δ 12.09 (bs, 1H, H1), 7.75 (d, J = 16.1 Hz, 1H, H4), 7.61 (d, J = 8.6 Hz, 1H, H6), 6.61 (d, J = 2.3 Hz, 1H, H9), 6.57 (dd, J = 8.6, 2.3 Hz, 1H, H8), 6.37 (d, J = 16.1 Hz, 1H, H3), 3.86 (s, 3H, H11), 3.81 (s, 3H, H12).

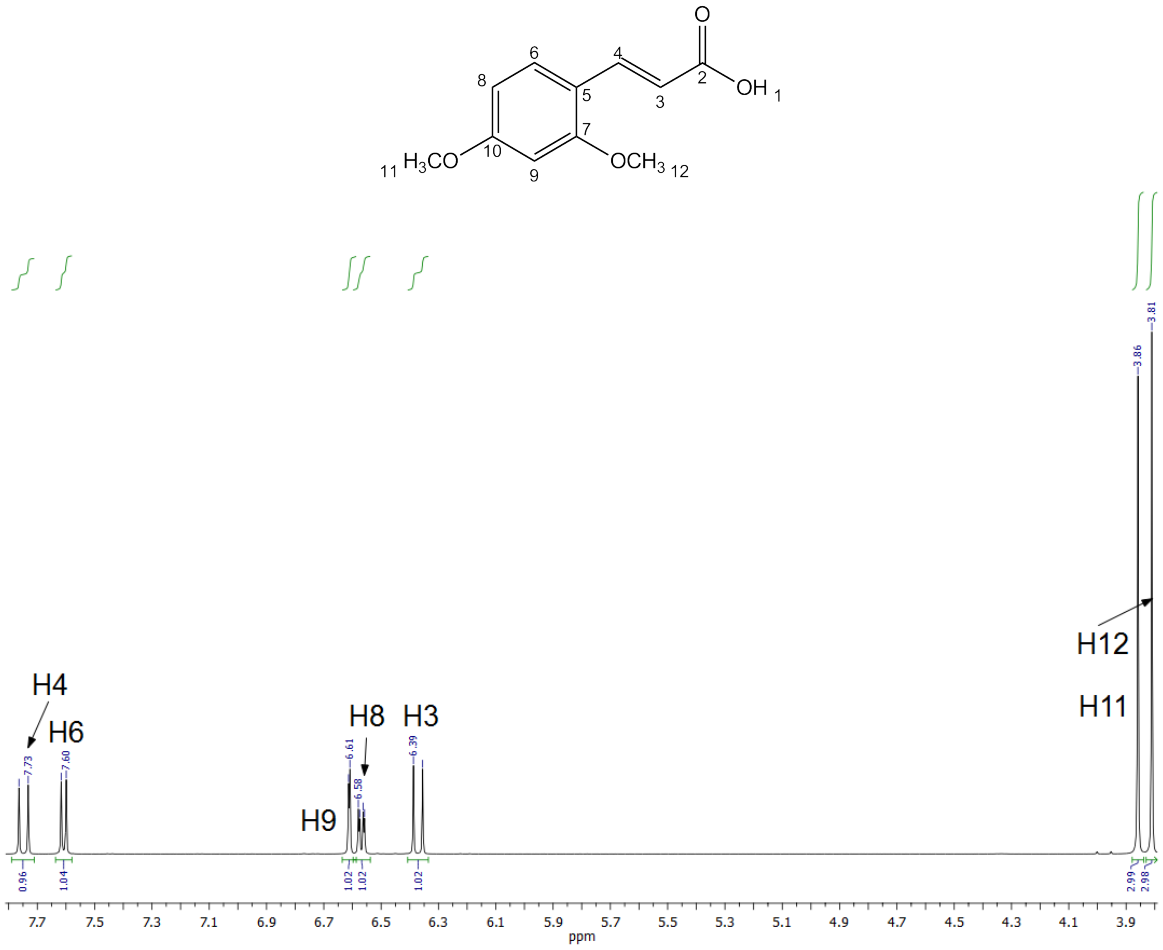

Figure C8: ^{1}H NMR for 2,4-dimethoxycinnamic acid.

2-methoxy-4-hydroxycinnamic acid

^{1}H NMR (500 MHz, DMSO) δ 10.05 (bs, 1H, H1), 7.73 (d, J = 16.1 Hz, 1H, H4), 7.48 (d, J = 8.5 Hz, 1H, H6), 6.44 (d, J = 2.2 Hz, 1H, H9), 6.40 (dd, J = 8.4, 2.2 Hz, 1H, H8), 6.29 (d, J = 16.0 Hz, 1H, H3), 3.81 (s, 3H, H12); ^{13}C NMR (125 MHz, DMSO) δ 168.32 (C2), 161.21 (C10), 159.50 (C7), 139.13 (C4), 130.03 (C6), 115.07 (C5), 113.81 (C3), 108.09 (C8), 99.04 (C9), 55.44 (C12).

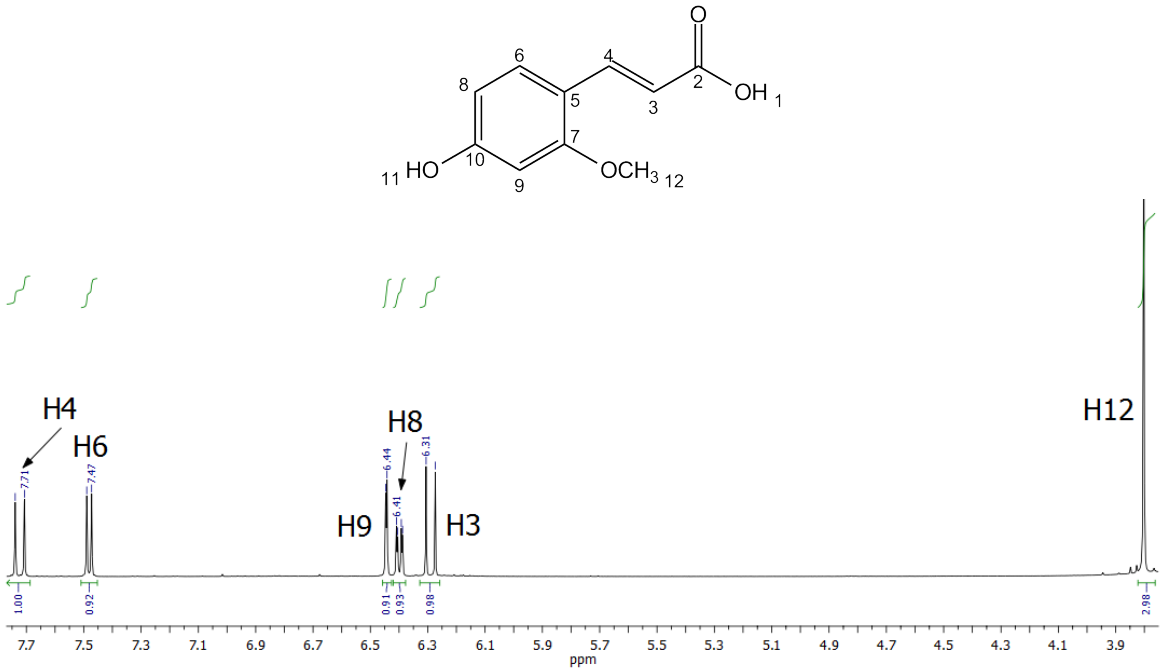

(a)

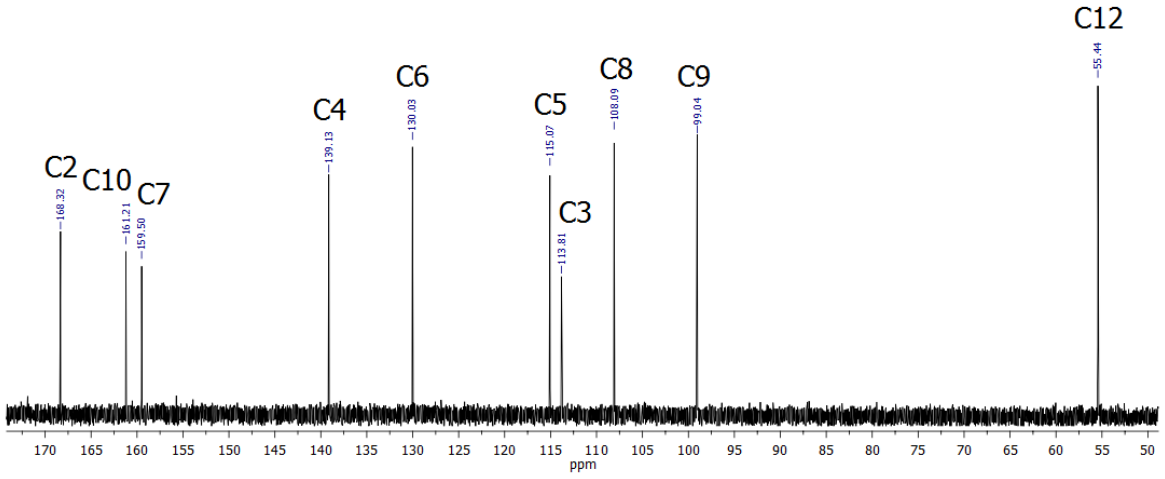

(b)

Figure C9: (a) ^{1}H NMR and (b) ^{13}C NMR for 2-methoxy-4-hydroxycinnamic acid.

4-(hydroxymethyl)cinnamic acid

^{1}H NMR (500 MHz, DMSO) δ 7.63 (d, J = 7.9 Hz, 2H, H6), 7.57 (d, J = 16.0 Hz, 1H, H4), 7.35 (d, J = 7.9 Hz, 2H, H7), 6.49 (d, J = 16.0 Hz, 1H, H3), 5.25 (bs, 1H, H10), 4.52 (s, 2H, H9); ^{13}C NMR (125 MHz, DMSO) δ 167.64 (C2), 144.98 (C4), 143.82 (C8), 132.64 (C5), 128.02, (C7) 126.74 (C6), 118.55 (C3), 62.53 (C9).

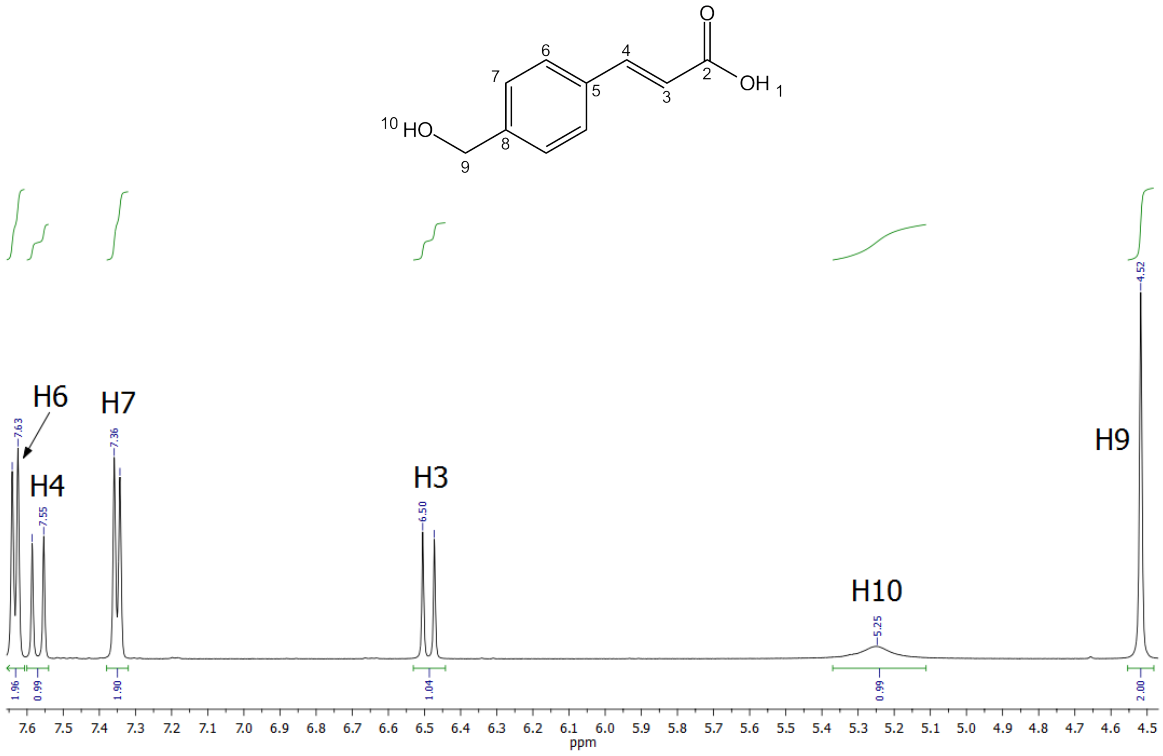

(a)

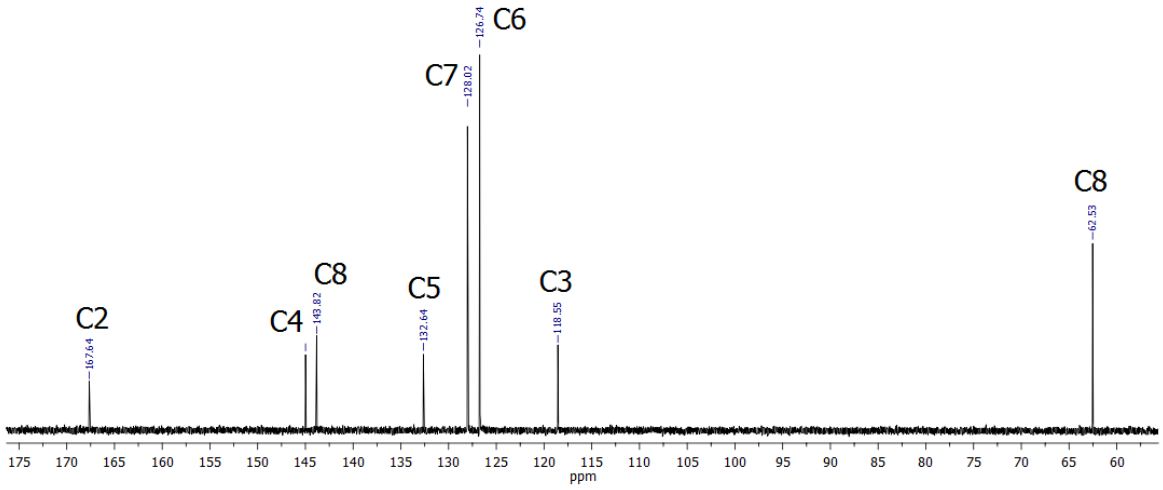

(b)

Figure C10: (a) ^{1}H NMR and (b) ^{13}C NMR for 4-(hydroxymethyl)cinnamic acid.

4-(2-hydroxyisopropyl)cinnamic acid

^{1}H NMR (500 MHz, DMSO) δ 7.59 (d, J = 8.2 Hz, 2H, H6), 7.54 (d, J = 16.0 Hz, 1H, H4), 7.26 (d, J = 8.2 Hz, 2H, H5), 6.46 (d, J = 16.0 Hz, 1H, H3), 3.50 (dd, J = 10.4, 6.5 Hz, 1H, H11), 3.44 (dd, J = 10.4, 6.5 Hz, 1H, H11), 2.87 – 2.77 (m, 1H, H9), 1.19 (d, J = 7.0 Hz, 3H, H10); ^{13}C NMR (125 MHz, DMSO) δ 167.64 (C2), 147.56 (C4), 143.92 (C8), 132.37 (C5), 128.07 (C6), 127.92 (C7), 118.21 (C3), 66.72 (C11), 41.91 (C9), 17.78 (C10).

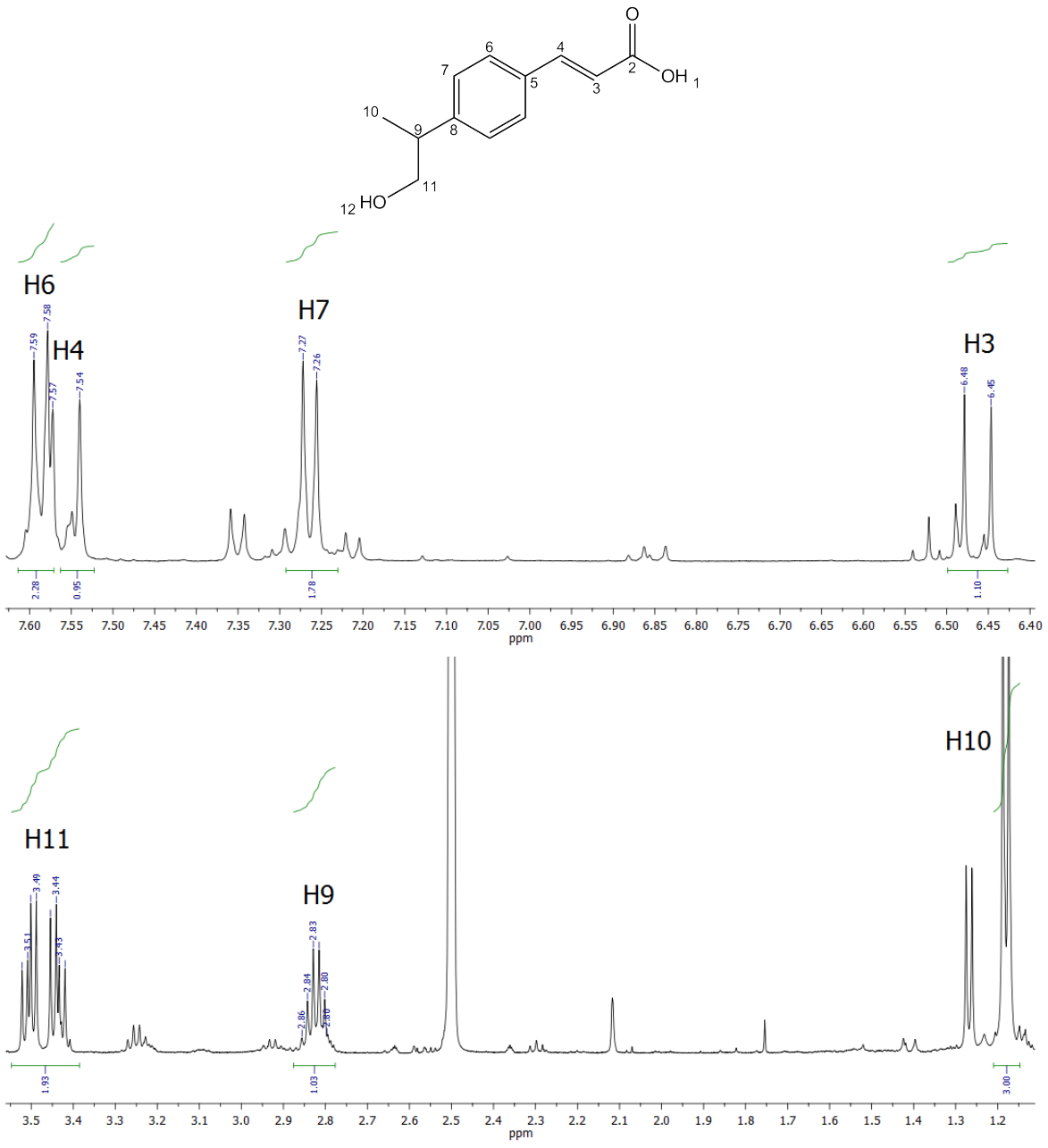

Figure C11: ^{1}H NMR for 4-(2-hydroxyisopropyl)cinnamic acid.

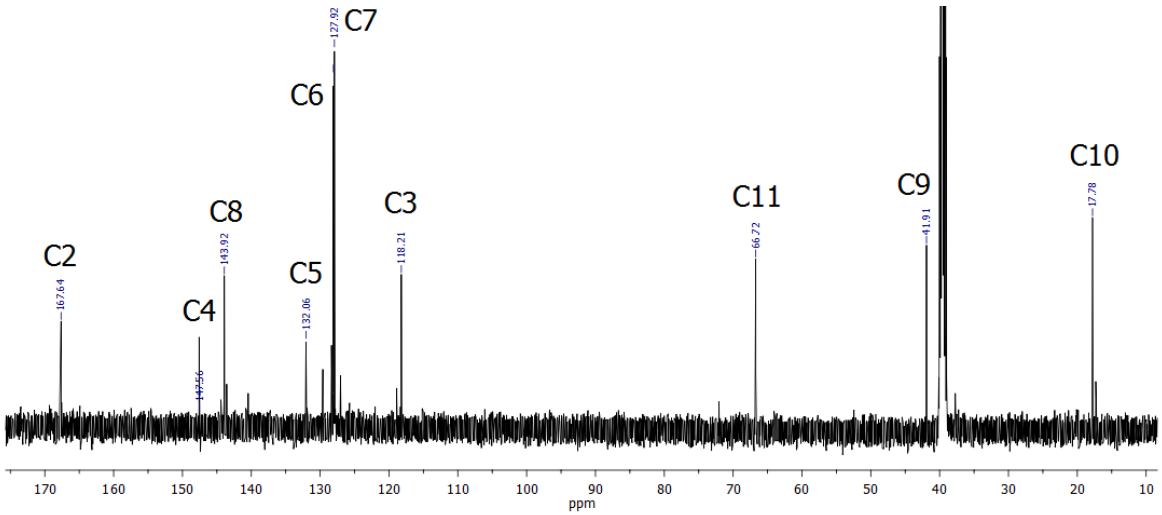

Figure C12: ^{13}C NMR for 4-(2-hydroxyisopropyl)cinnamic acid.

4-(1,2-epoxyisopropyl)cinnamic acid

^{1}H NMR (500 MHz, DMSO) δ 7.60 (d, J = 8.4 Hz, 2H, H6), 7.56 (d, J = 16.0 Hz, 1H, H4), 7.48 (d, J = 8.4 Hz, 2H, H7), 6.48 (d, J = 16.0 Hz, 1H, H3), 3.42 (d, J = 10.8 Hz, 1H, H11), 3.39 (d, J = 10.8 Hz, 1H, H11), 1.38 (s, 3H, H10); ^{13}C NMR (125 MHz, DMSO) δ 167.64 (C2), 149.94 (C4), 143.91 (C8), 132.09 (C5), 127.51 (C6), 126.08 (C7), 118.36 (C3), 73.71 (C9), 70.27 (C11), 25.96 (C10).

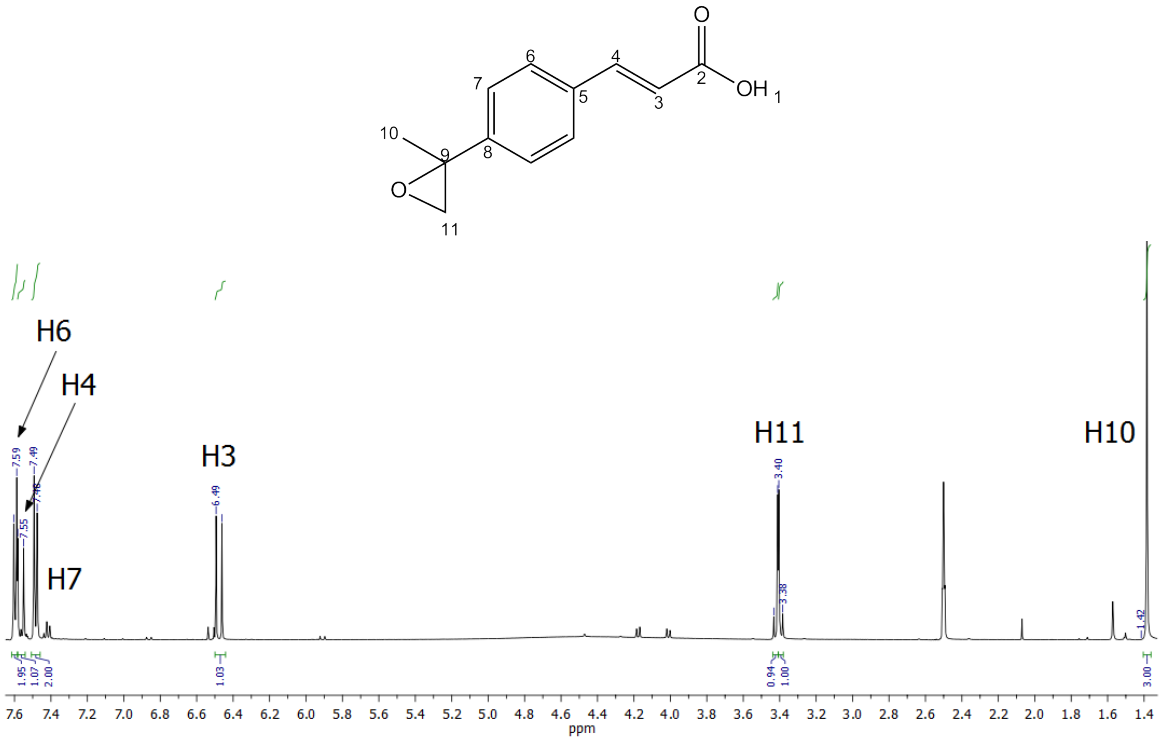

Figure C13: ^{1}H NMR for 4-(1,2-epoxyisopropyl)cinnamic acid.

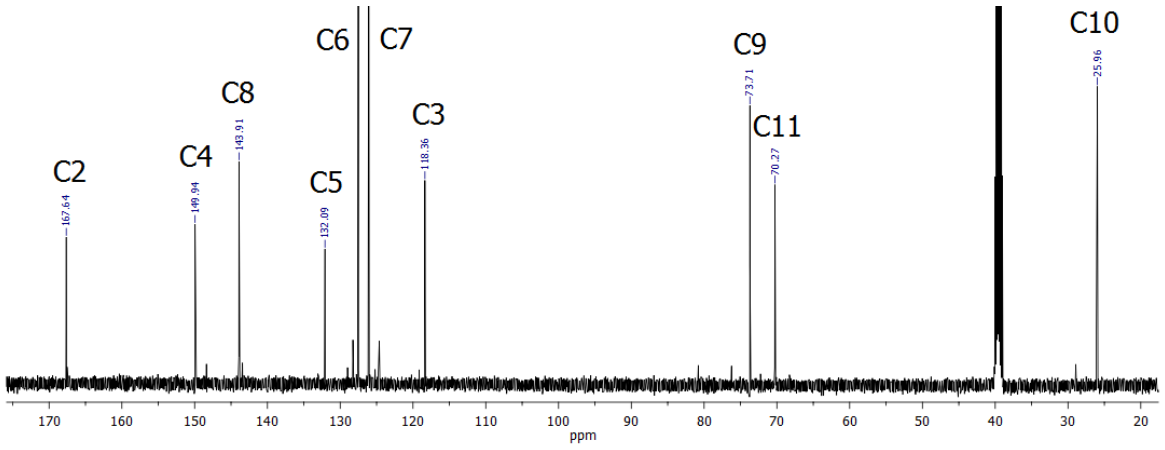

(a)

Figure C14: ^{13}C NMR for 4-(1,2-epoxyisopropyl)cinnamic acid.

4-(1-hydroxyisopropyl)cinnamic acid†

^{1}H NMR (500 MHz, DMSO) δ 7.66 (d, J = 8.4 Hz, 2H, H6), 7.60 (d, J = 16.0 Hz, 1H, H4), 7.49 (d, J = 8.4 Hz, 2H, H7), 6.67 (d, J = 16.0 Hz, 1H, H3), 1.42 (s, 3H, H10).

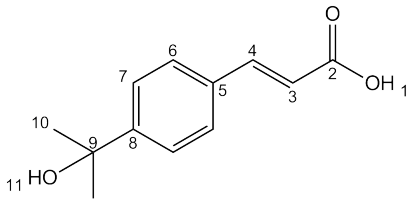

†After semi-prep HPLC purification, NMR analysis showed significant levels of 4-(prop-1-en-2yl)cinnamic acid, suggesting that 4-(1-hydroxyisopropyl)cinnamic acid is unstable and can undergo a desaturation reaction to form the alkene.

4-(prop-1-en-2yl)cinnamic acid

^{1}H NMR (500 MHz, DMSO) δ 7.62 (d, J = 8.3 Hz, 2H, H6), 7.57 (d, J = 16.0 Hz, 1H, H4), 7.34 (d, J = 8.3 Hz, 2H, H7), 6.52 (d, J = 16.0 Hz, 1H, H3), 5.52 (d, J = 1.4 Hz, 1H, H11), 5.16 (d, J = 1.4 Hz, 1H, H11), 2.12 (s, 3H, H10).

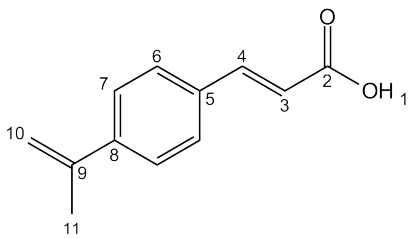

Mass spectra analysis

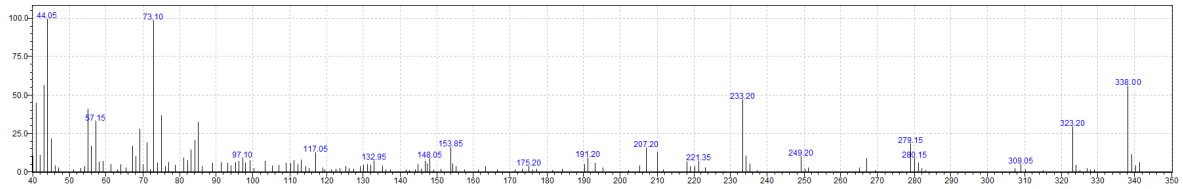

(a)

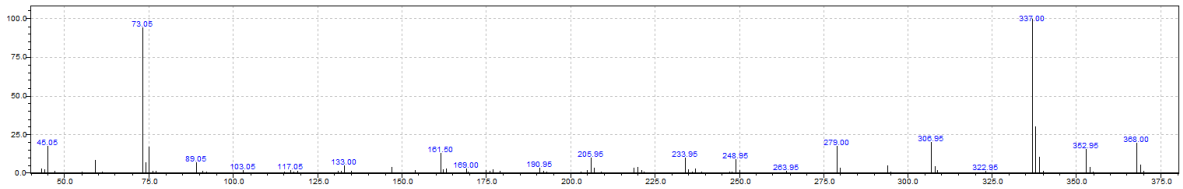

(b)

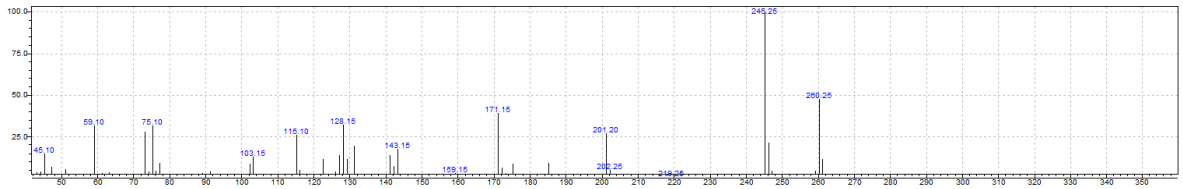

(c)

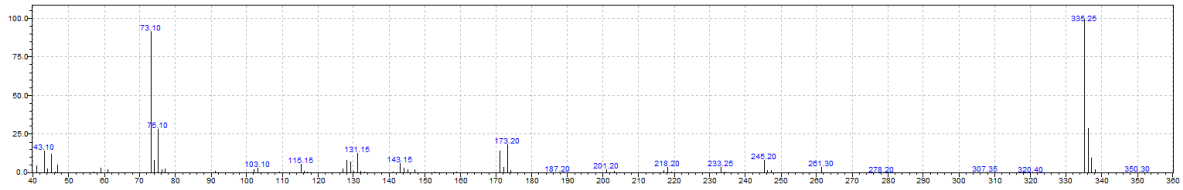

(d)

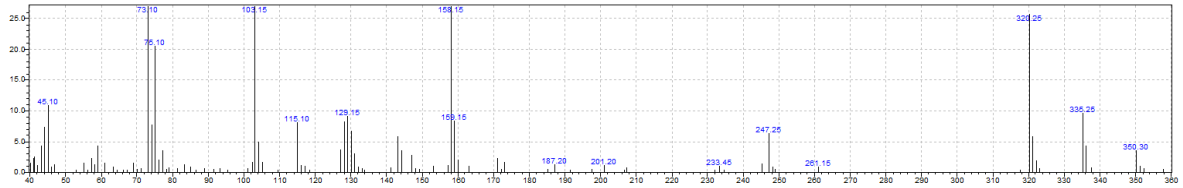

(e)

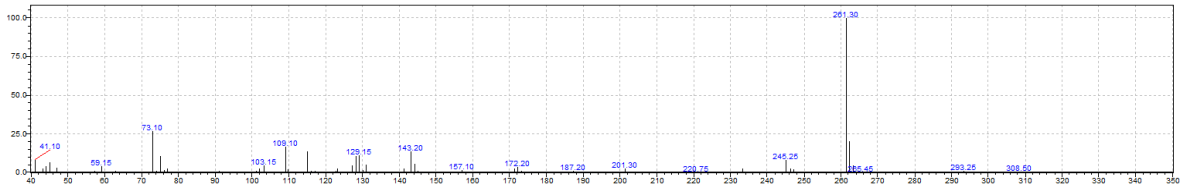

(f)

Figure C15: Mass spectra of (a) 2-methoxy-4-hydroxycinnamic acid (b) 2,3-dimethoxy-4-hydroxycinnamic acid (c) 4-(prop-1-en-2yl)cinnamic acid (d) 4-(1-hydroxyisopropyl)cinnamic acid (e) 4-(2-hydroxyisopropyl)cinnamic acid and (f) 4-(1,2-epoxyisopropyl)cinnamic acid.

Appendix D Data for Chapter 6

HPLC and GC-MS analysis

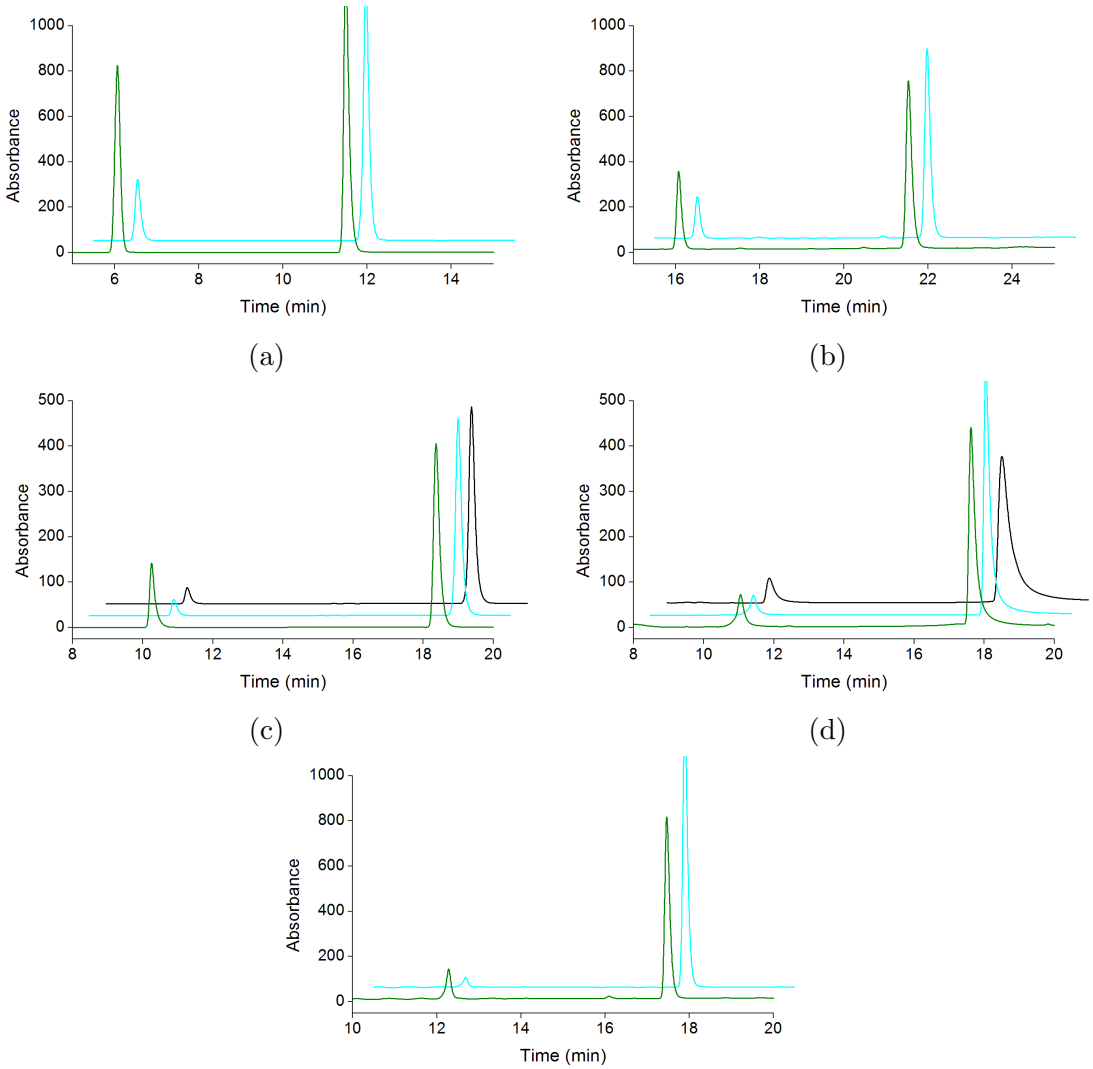

Figure D1: HPLC analysis of the *in vitro* WT (black), S244N (cyan) and S244D CYP199A4 (green) turnovers of (a) 4-methoxybenzoic acid (t_R = 11.6 mins) to 4-hydroxybenzoic acid (t_R = 6.1 mins) (b) 4-methoxybenzaldehyde (t_R = 21.9 mins) to 4-hydroxybenzaldehyde (t_R = 16.2 mins) (c) 4-methoxyacetophenone (t_R = 18.5 mins) to 4-hydroxyacetophenone (t_R = 10.4 mins) (d) 4-methoxyphenylboronic acid (t_R = 17.6 mins) to 4-hydroxyphenylboronic acid (t_R = 11.0 mins) and (e) 4-methoxybenzyl alcohol (t_R = 17.5 mins) to 4-hydroxybenzyl alcohol (t_R = 12.3 mins).

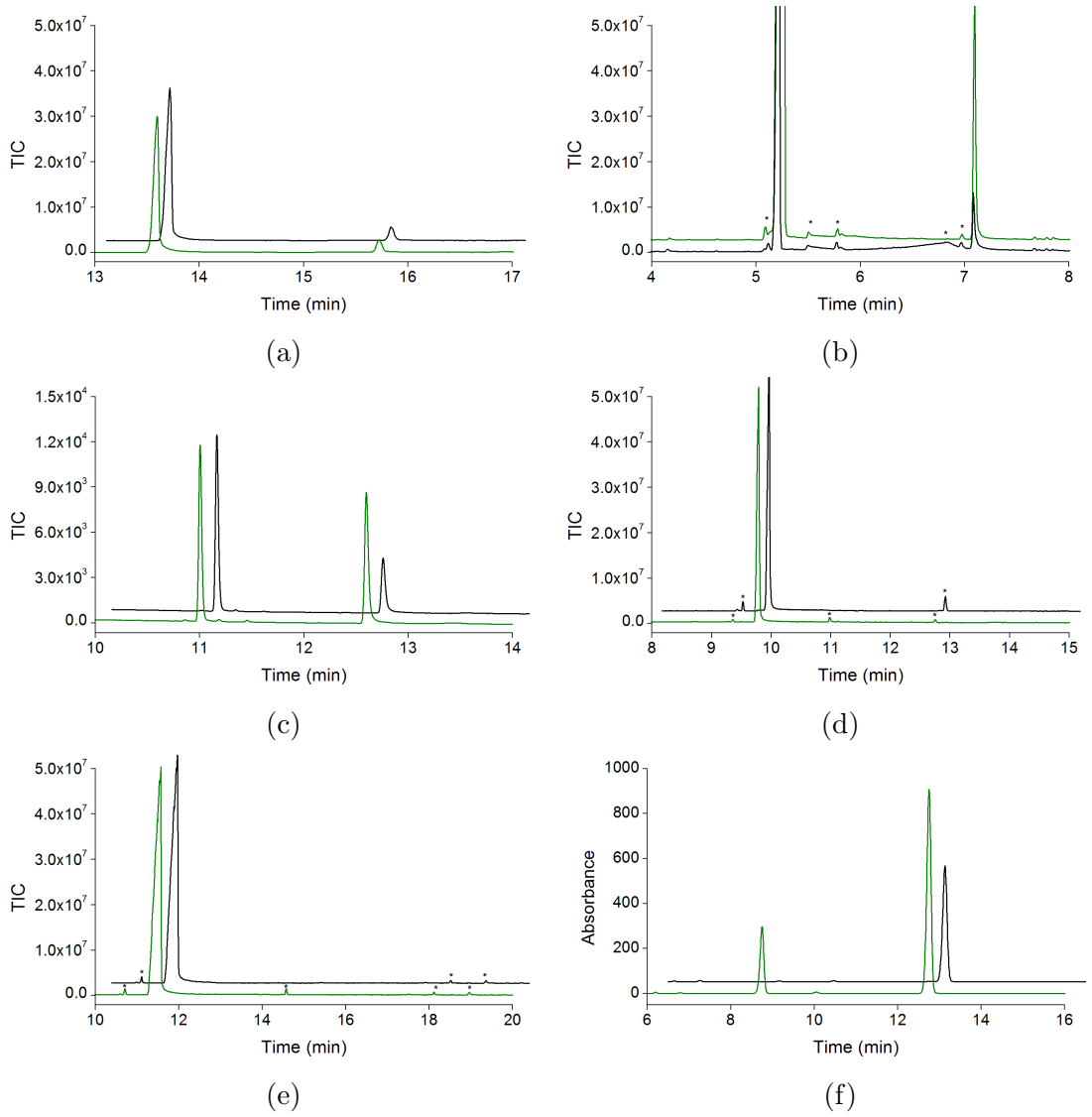

Figure D2: GC-MS analysis of the *in vitro* WT (black) and S244D CYP199A4 (green) turnovers of (a) 4-methoxyphenylacetic acid methyl ester (t_R = 15.7 mins) to 4-hydroxyphenylacetic acid methyl ester (t_R = 13.6 mins) (b) 4-(trifluoromethoxy)anisole (t_R = 5.2 mins) to 4-(trifluoromethoxy)phenol (t_R = 7.1 mins) (c) 4-bromoanisole (t_R = 11.0 mins) to 4-bromophenol (t_R = 12.6 mins) (d) 4-aminoanisole (t_R = 9.8 mins, no product) and (e) *N*-(4-methoxyphenyl)acetamide (t_R = 11.4 mins, no product). (f) HPLC analysis of the turnovers of veratraldehyde (t_R = 12.8 mins) to vanillin (t_R = 8.7 mins). Impurities are marked (*).

Spin-state shifts

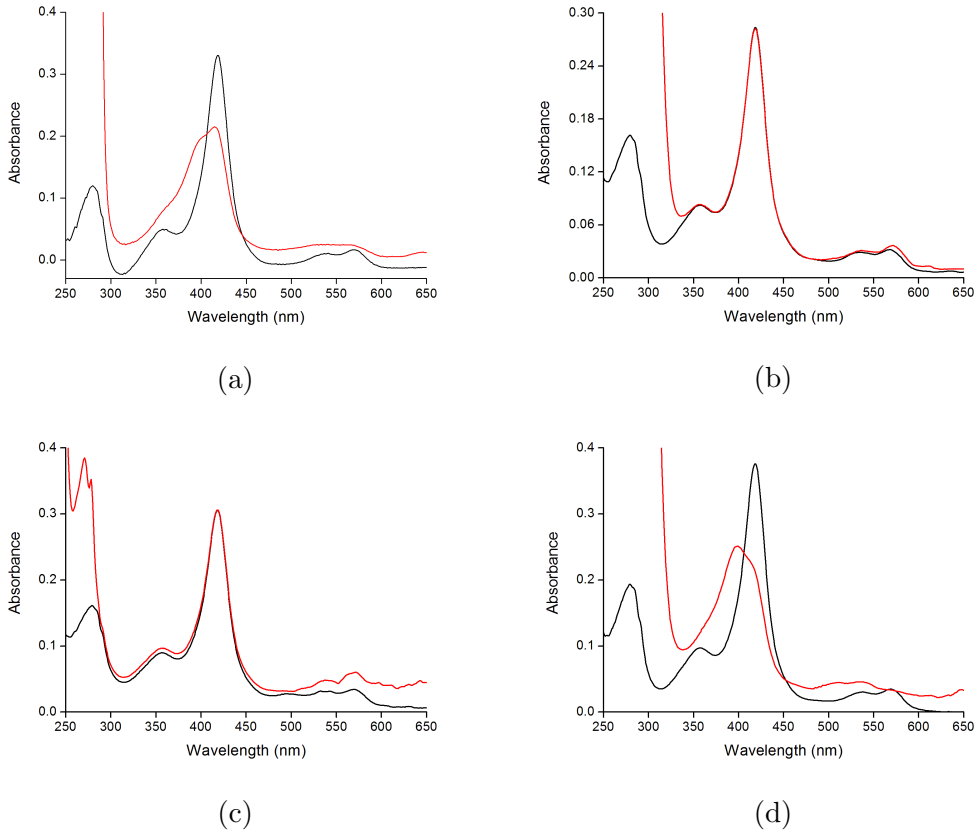

Figure D3: Selected spin-state shifts of $WT_{CYP199A4}$ with (a) 4-methoxyphenylacetic acid methyl ester (b) 4-methoxyacetophenone (c) 4-methoxyphenylboronic acid and (d) 4-methoxybenzonitrile.

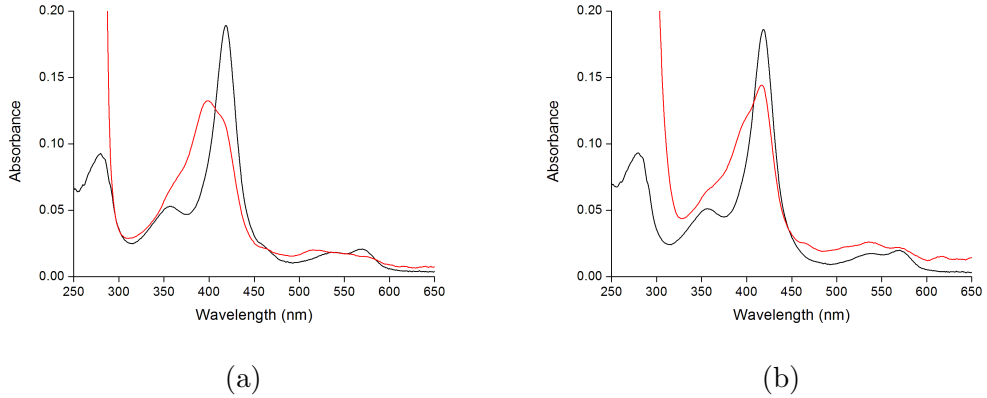

Figure D4: Spin-state shifts of S244D with (a) 4-methoxybenzoic acid and (b) 4-methoxybenzyl alcohol.

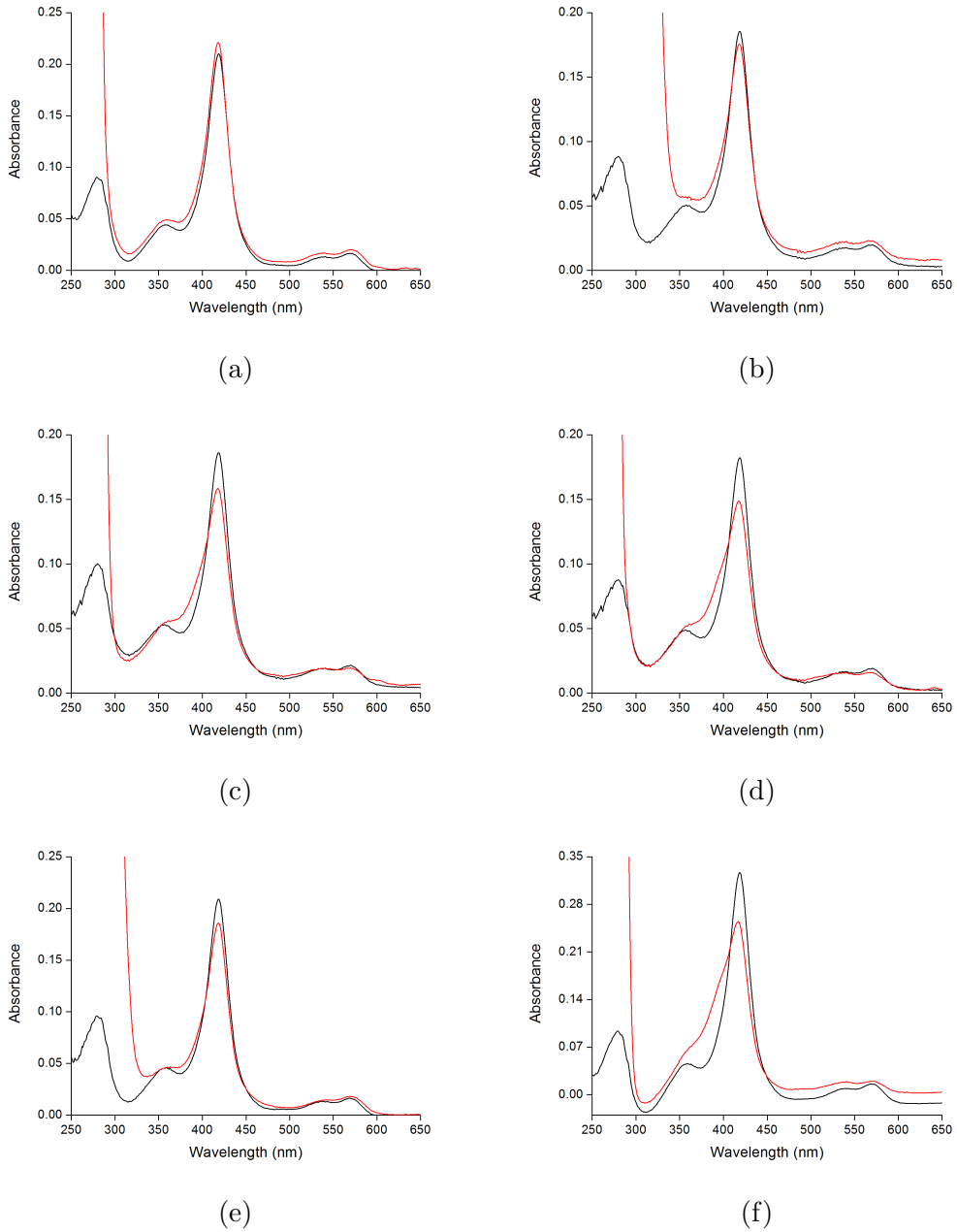

Figure D5: Spin-state shifts of S244D with (a) 4-methoxybenzyl acetate (b) 4-methoxyacetophenone (c) 4-methoxybenzamide (d) 4-methoxyphenylboronic acid (e) 4-methoxybenzonitrile and (f) 4-bromoanisole.

Dissociation constant analysis

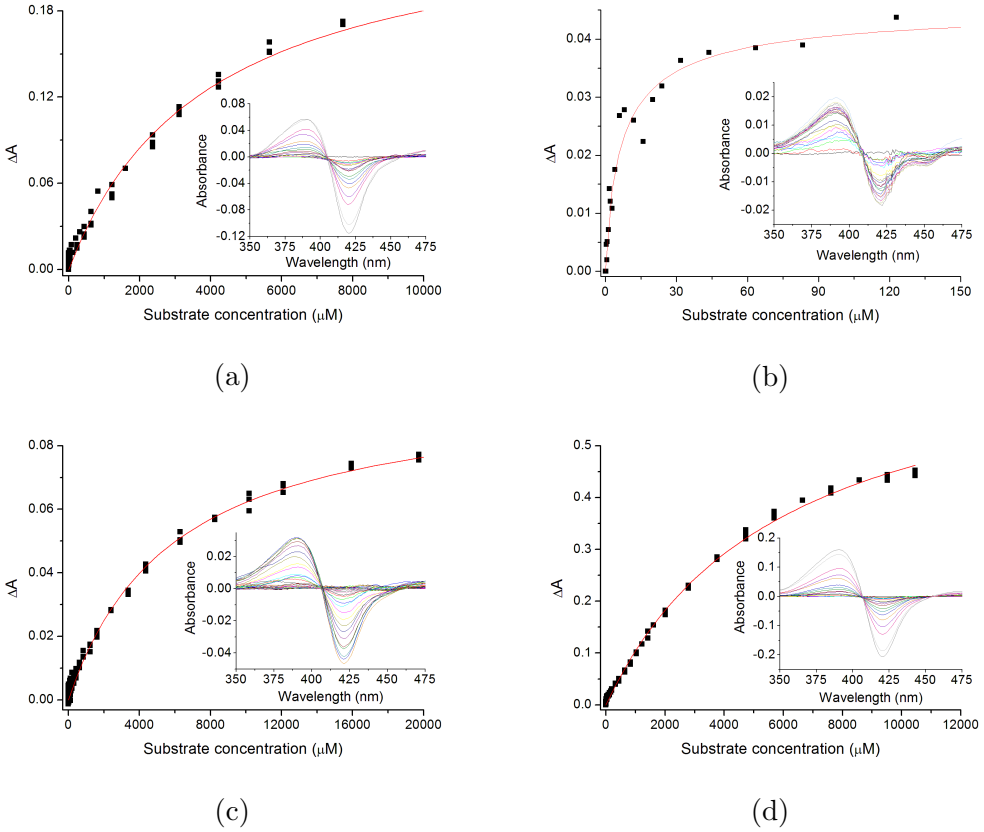

Figure D6: Dissociation constant analyses of $WT_{CYP199A4}$ with (a) 4-methoxyphenylacetic acid methyl ester (b) 4-methoxyacetophenone (c) 4-methoxyphenylboronic acid and (d) 4-methoxybenzonitrile.

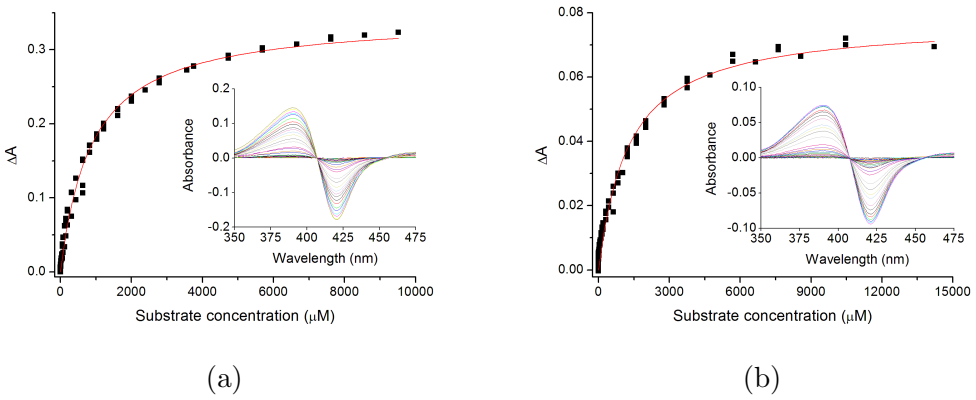

Figure D7: Dissociation constant analyses of S244D with (a) 4-methoxybenzoic acid and (b) 4-methoxybenzyl alcohol.

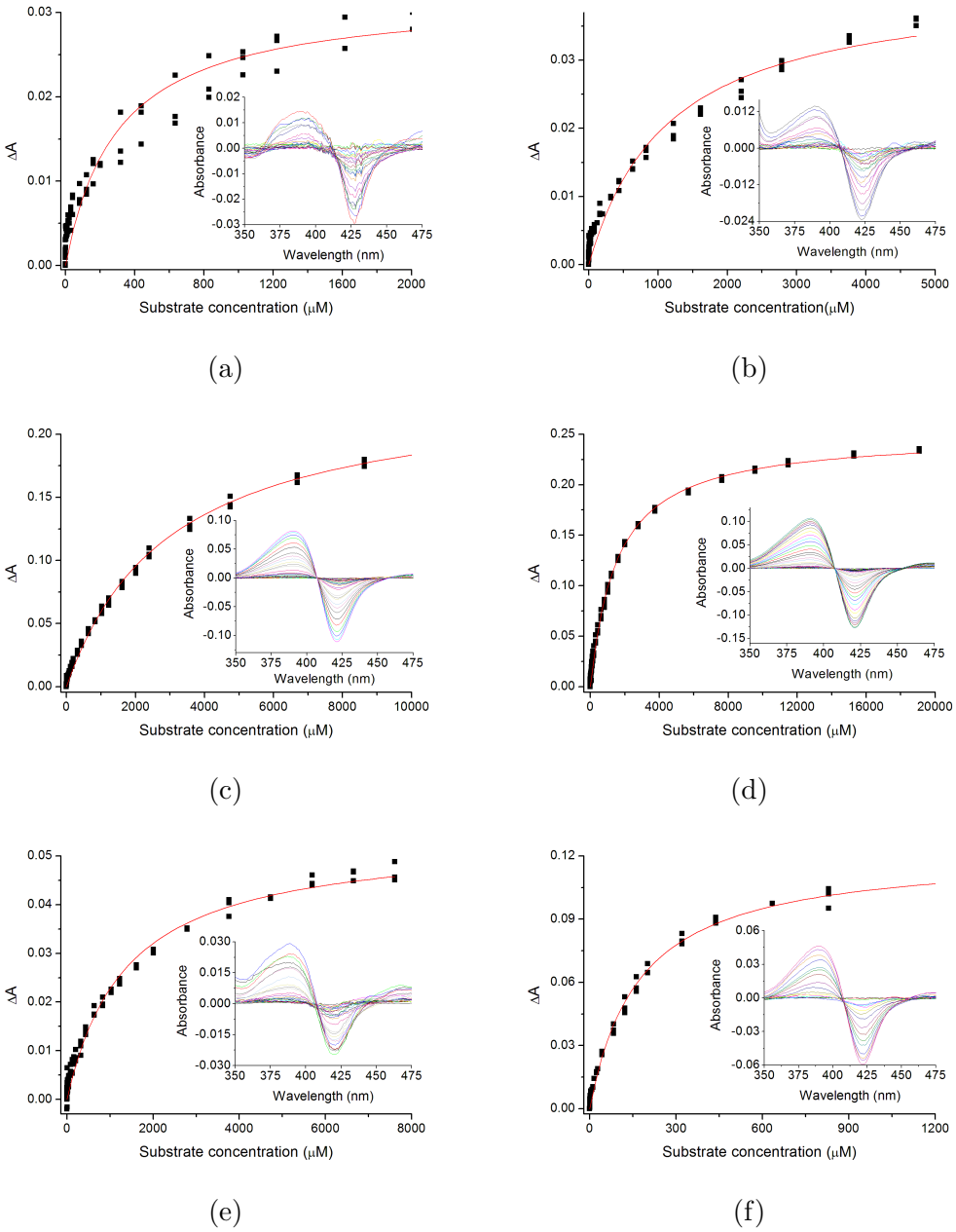

Figure D8: Dissociation constant analyses of S244D with (a) 4-methoxybenzyl acetate (b) 4-methoxyacetophenone (c) 4-methoxybenzamide and (d) 4-methoxyphenylboronic acid (e) 4-methoxybenzonitrile and (f) 4-bromoanisole.

Appendix E Data for Chapter 7

Spin-state shifts

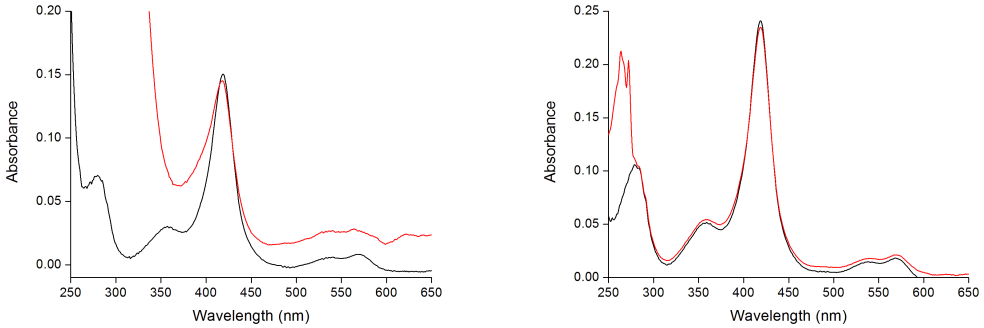

(a)

(b)

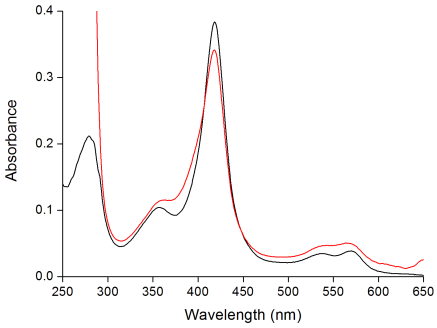

(c)

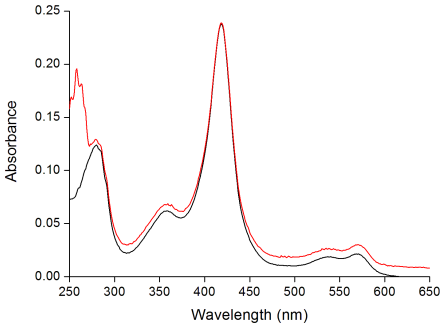

(d)

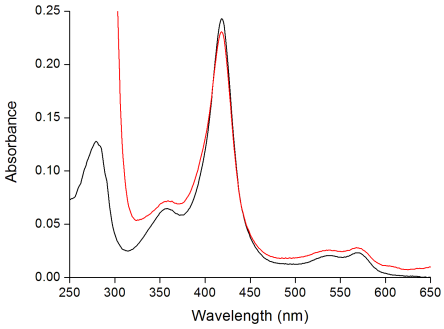

(e)

Figure E1: Selected spin-state shifts of S244D with (a) 4-methylbenzaldehyde (b) 4-methylbenzyl alcohol (c) 4-methylbenzoic acid methyl ester (d) 1,4-dimethylbenzene and (e) 4-(trifluoromethoxy)toluene.

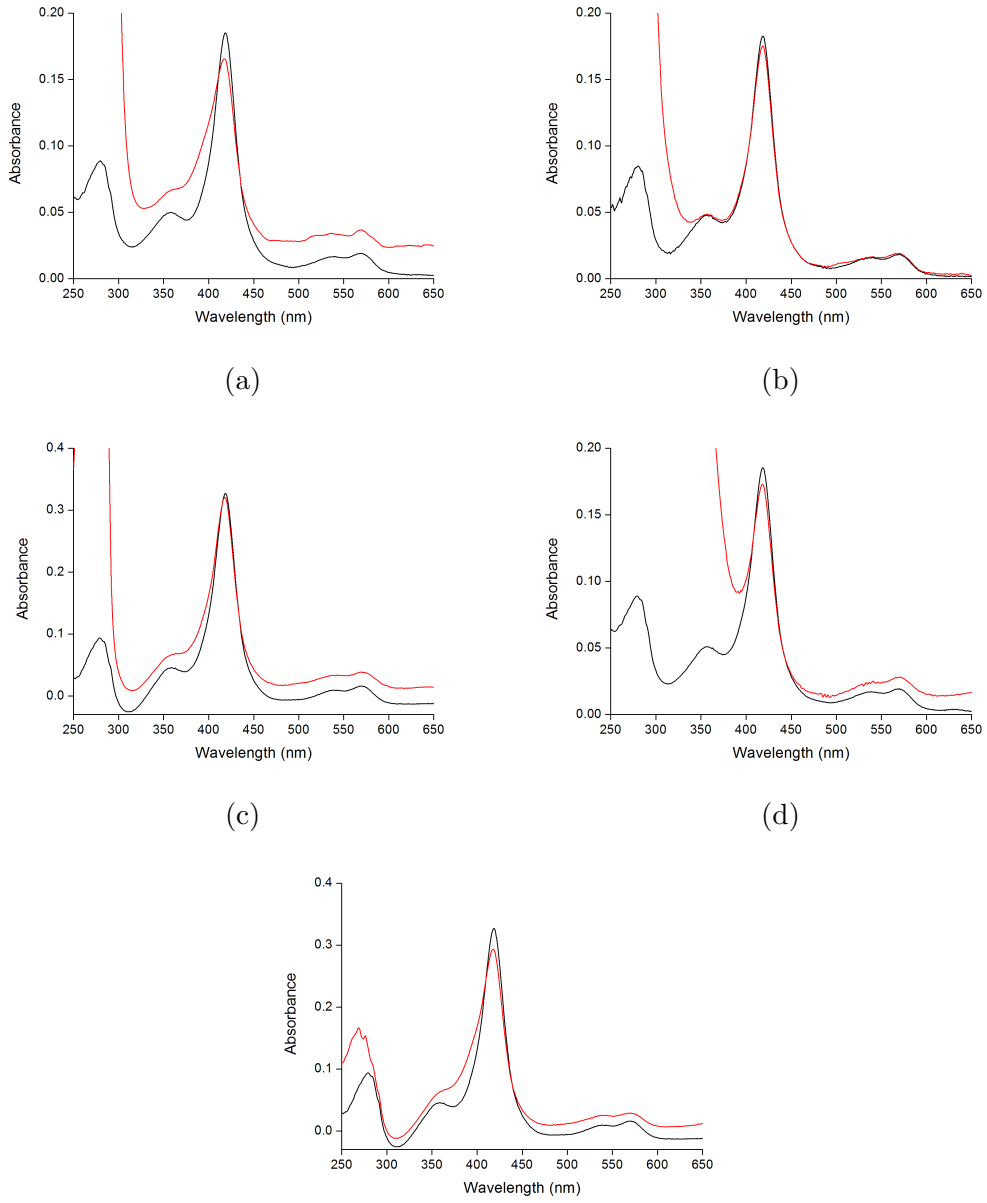

Figure E2: Selected spin-state shifts of S244D with (a) 4-ethylbenzaldehyde (b) 4-ethylacetophenone (c) 4-ethylanisole (d) 4-ethylnitrobenzene and (e) 1-bromo-4-ethylbenzene.

Dissociation constant analysis

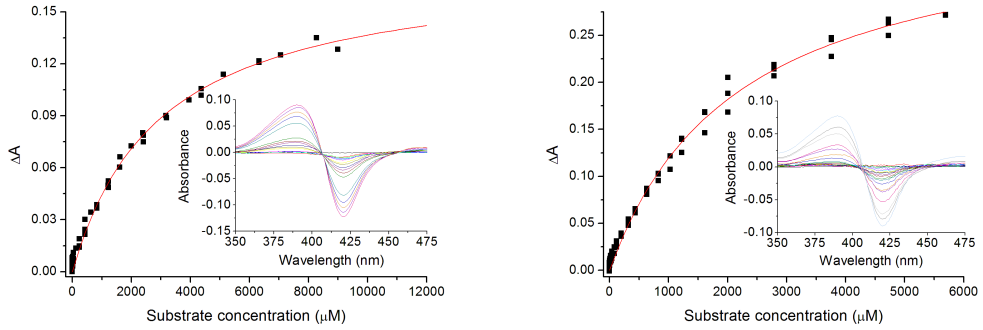

(a) (b)

Figure E3: Selected dissociation constant analyses of $WT_{CYP199A4}$ with (a) 4-methylbenzamide and (b) 4-methylbenzoic acid methyl ester.

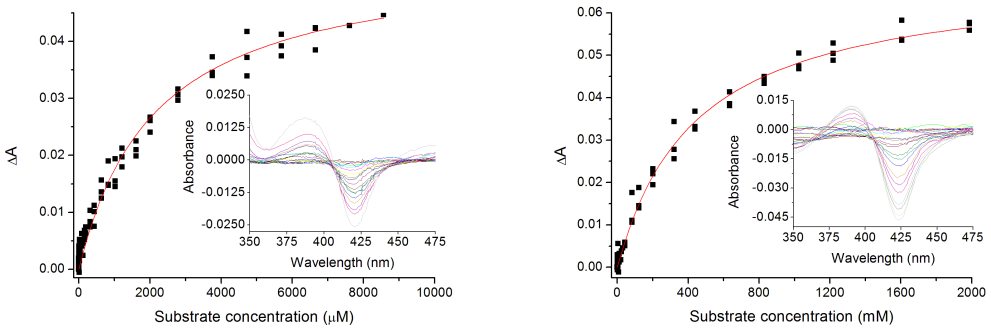

(a) (b)

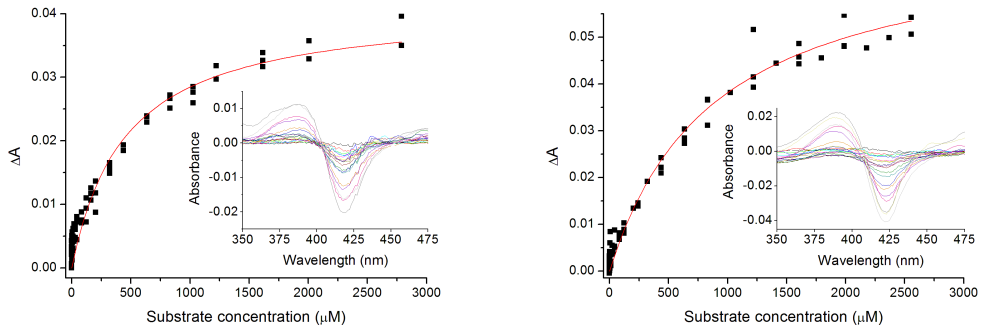

(c) (d)

Figure E4: Selected dissociation constant analyses of S244D with (a) 4-methylacetophenone (b) 4-methylanisole (c) 4-methylbenzoic acid methyl ester and (d) 1,4-dimethylbenzene (*p*-xylene).

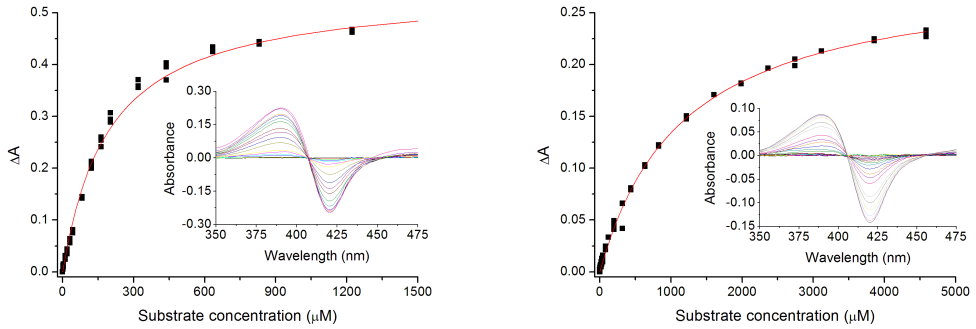

(a) (b)

Figure E5: Selected dissociation constant analyses of $WT_{CYP199A4}$ with (a) 4-ethylbenzaldehyde and (b) 4-ethylphenol.

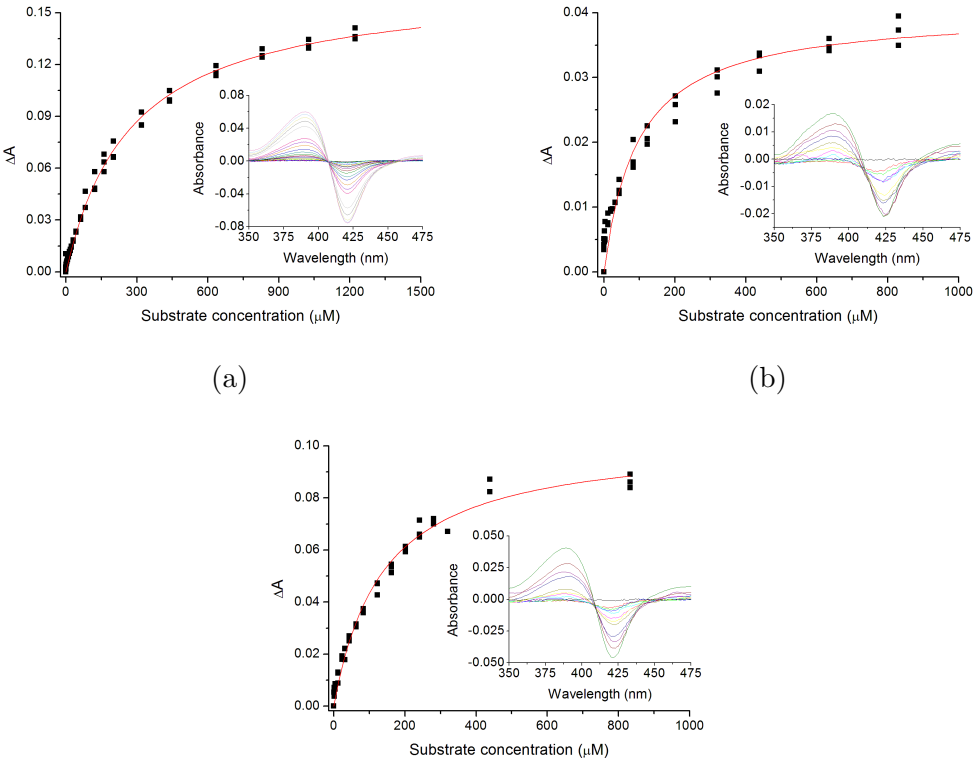

(a) (b)

(c)

Figure E6: Selected dissociation constant analyses of S244D with (a) 4-ethylbenzaldehyde (b) 4-ethylanisole and (c) 1-bromo-4-ethylbenzene.

HPLC and GC-MS analysis

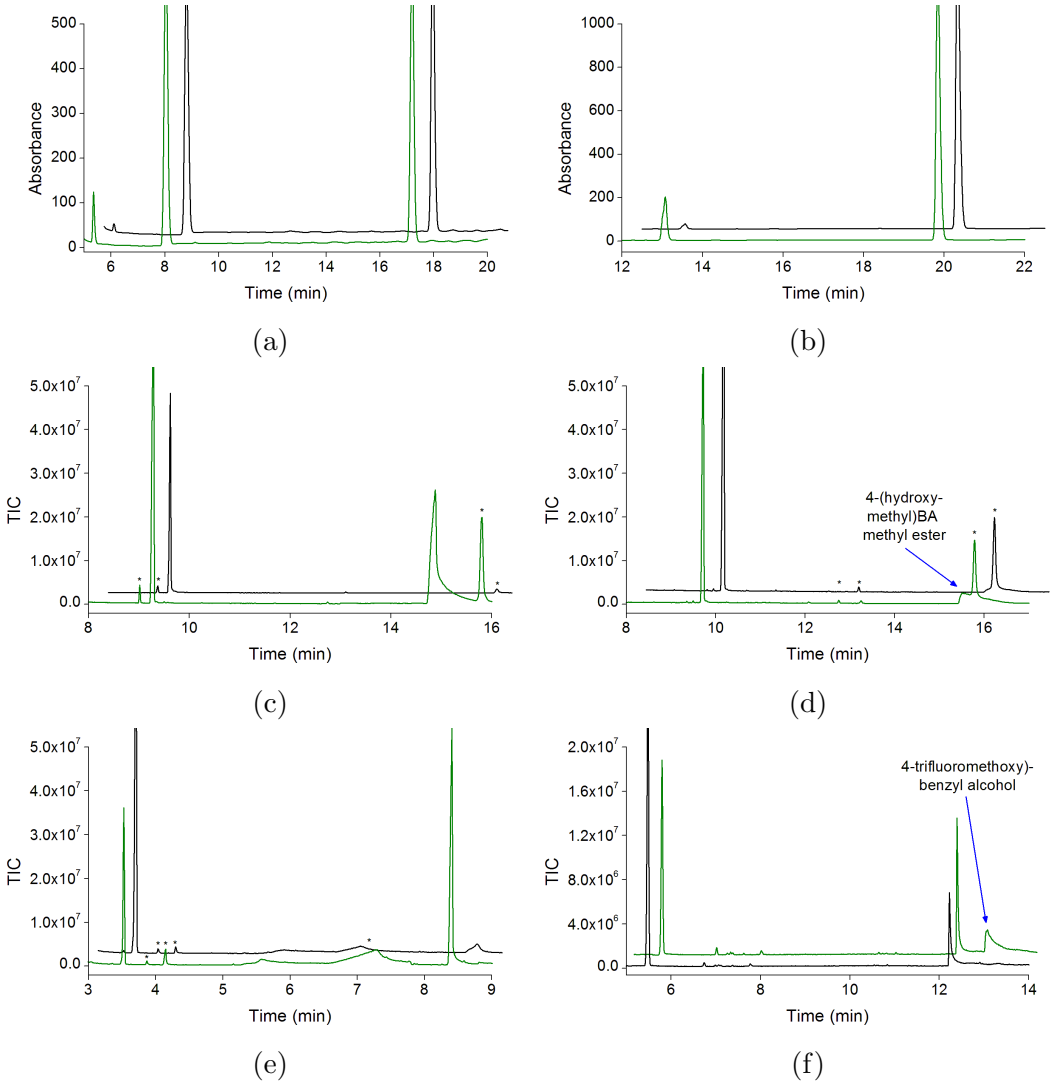

Figure E7: HPLC analysis of the WT (black) and S244D CYP199A4 (green) turnovers of (a) 4-methylbenzyl alcohol (t_R = 17.2 mins) to 4-(hydroxymethyl)benzyl alcohol (t_R = 5.4 mins) and (b) 4-methylbenzamide (t_R = 19.9 mins) to 4-(hydroxymethyl)benzamide (t_R = 13.0 mins). GC-MS analysis of the WT (black) and S244D CYP199A4 (green) turnovers of (c) 4-methylacetophenone (t_R = 9.3 mins) to 4-(hydroxymethyl)acetophenone (t_R = 14.9 mins) (d) 4-methylbenzoic acid methyl ester (t_R = 9.7 mins) to 4-(hydroxymethyl)benzoic acid methyl ester (t_R = 15.6 mins) (e) 1,4-dimethylbenzene (t_R = 3.5 mins) to 4-methylbenzyl alcohol (t_R = 8.4 mins) and (f) 4-(trifluoromethoxy)toluene (t_R = 5.6 mins) to 4-(trifluoromethoxy)benzyl alcohol (t_R = 13.0 mins). The internal standard has also been shown in (a) and (f) at t_R = 8.0 mins and t_R = 12.3 mins, respectively. For clarity the chromatograms have been offset along the x and y axes. Impurities are marked (*).

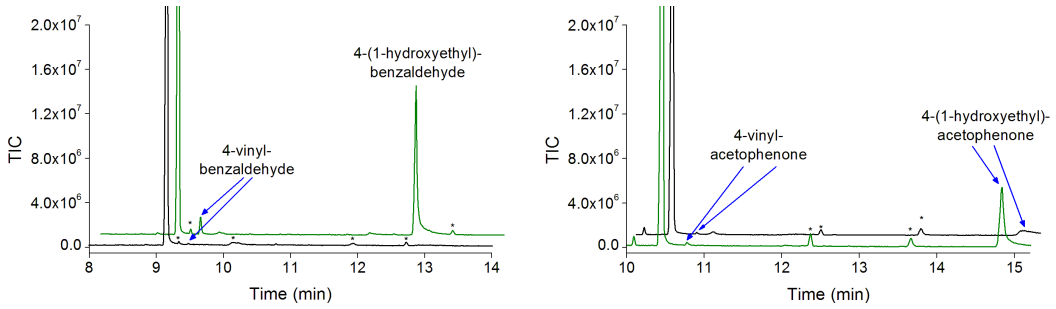

(a) (b)

Figure E8: GC-MS analysis of the WT (black) and S244D CYP199A4 (green) turnovers of (a) 4-ethylbenzaldehyde (t_R = 9.2 mins) to 4-vinylbenzaldehyde (t_R = 9.5 mins) and 4-(1-hydroxyethyl)benzaldehyde (t_R = 12.7 mins) and (b) 4-ethylacetophenone (t_R = 10.5 mins) to 4-vinyl-acetophenone (t_R = 10.8 mins) and 4-(1-hydroxyethyl)acetophenone (t_R = 15.0 mins). For clarity the chromatograms have been offset along the x and y axes. Impurities are marked (*).

Mass spectra analysis

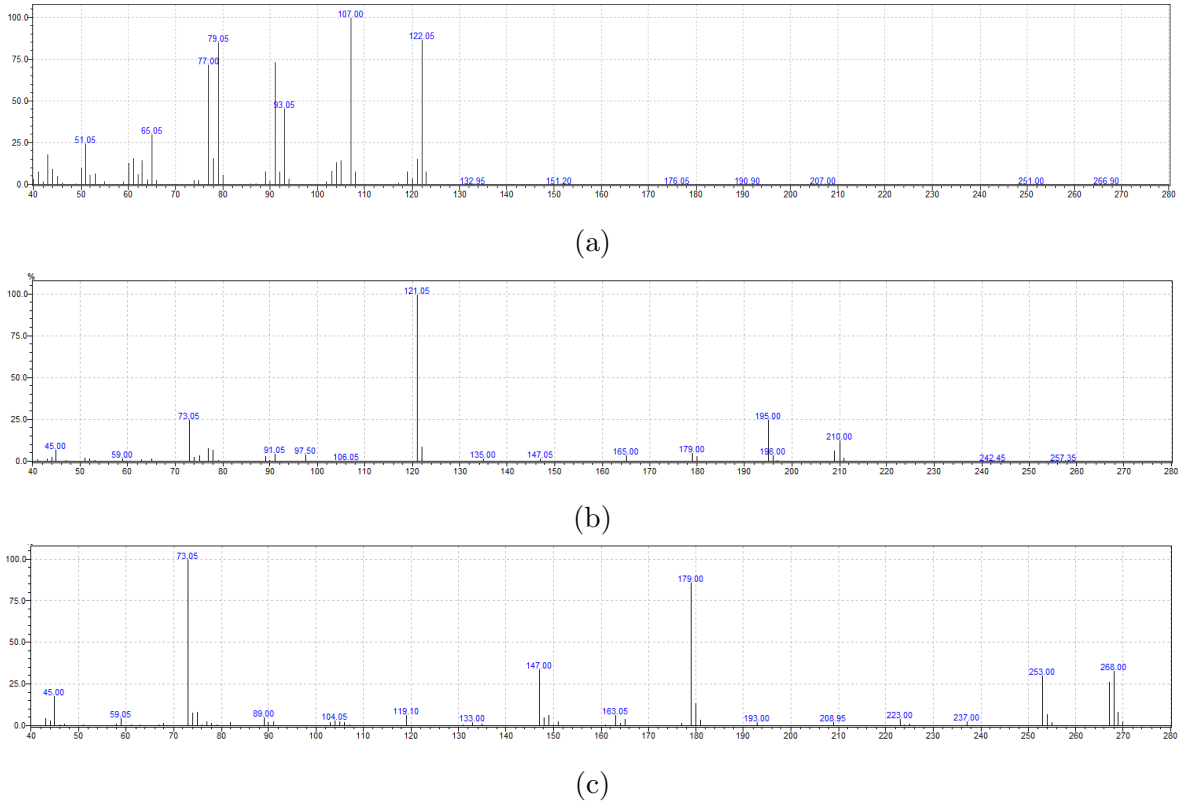

(a)

(b)

(c)

Figure E9: Mass spectra of derivatised (a) 4-methylanisole and its oxidation products (b) 4-methoxybenzyl alcohol and (c) 4-hydroxybenzyl alcohol

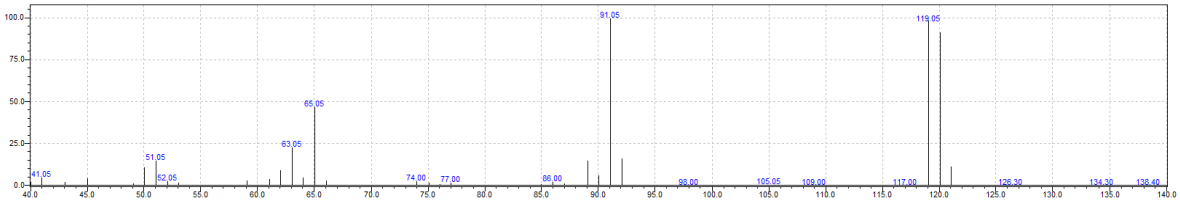

(a)

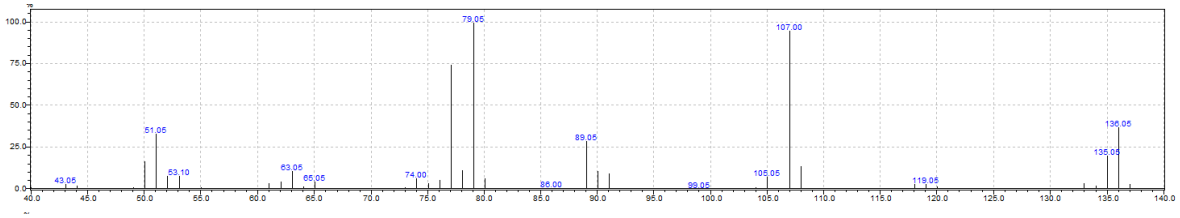

(b)

Figure E10: Mass spectra of (a) 4-methylbenzaldehyde and (b) 4-(hydroxymethyl)benzaldehyde.

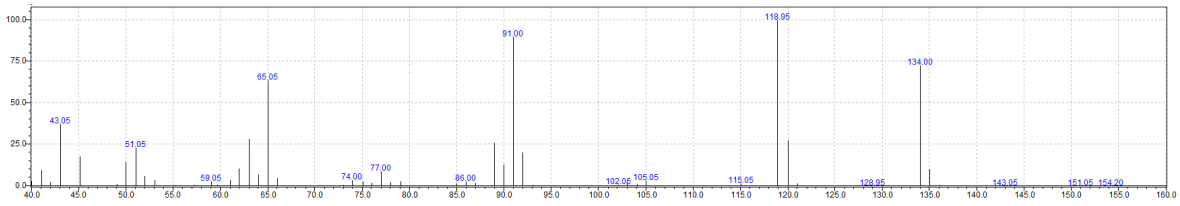

(a)

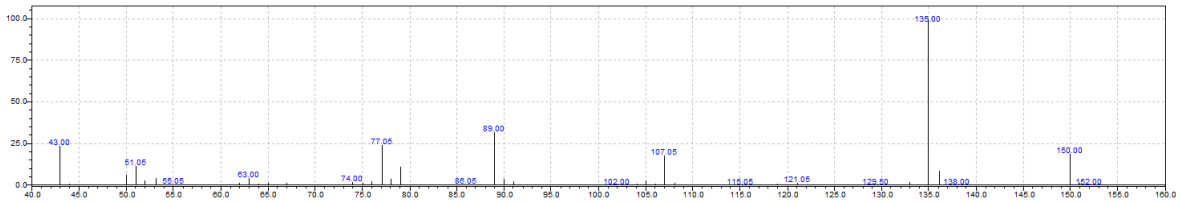

(b)

Figure E11: Mass spectra of (a) 4-methylacetophenone and (b) 4-(hydroxymethyl)acetophenone.

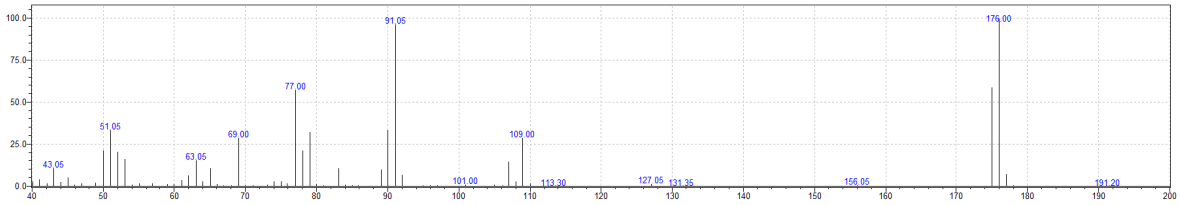

(a)

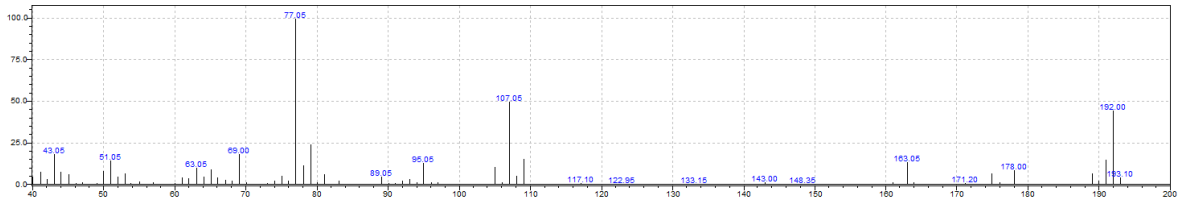

(b)

Figure E12: Mass spectra of (a) 4-(trifluoromethoxy)toluene and (b) 4-(trifluoromethoxy)benzyl alcohol.

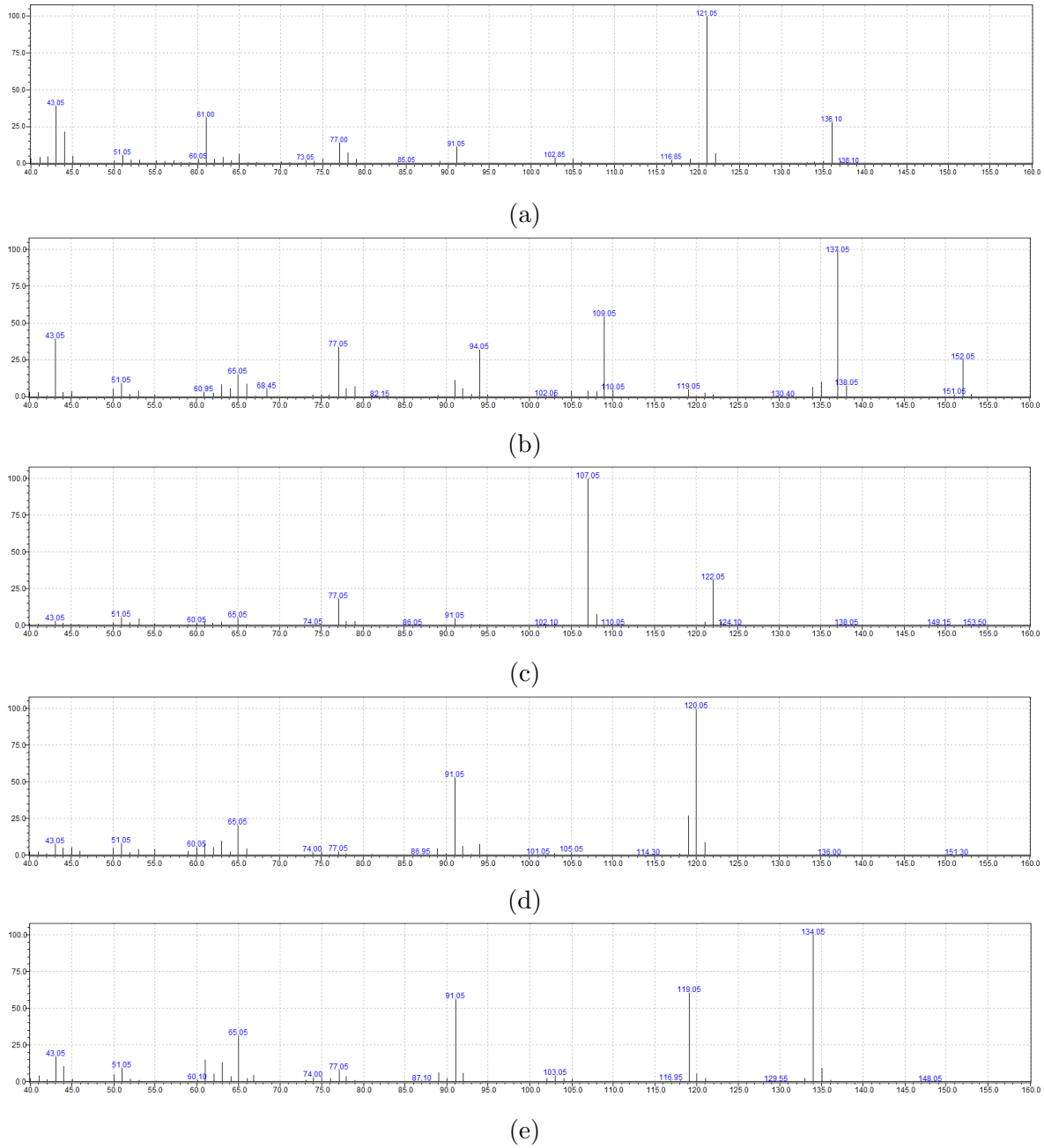

Figure E13: Mass spectra of (a) 4-ethylanisole and its oxidation products (b) 1-(4-methoxyphenyl)ethanol (c) 4-ethylphenol (d) 4-vinylphenol and (e) 4-vinylanisole.

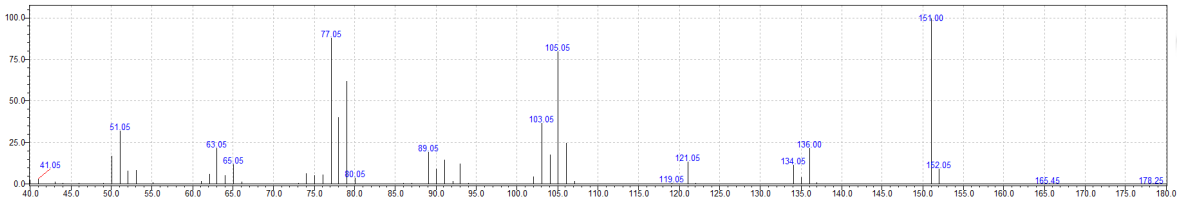

(a)

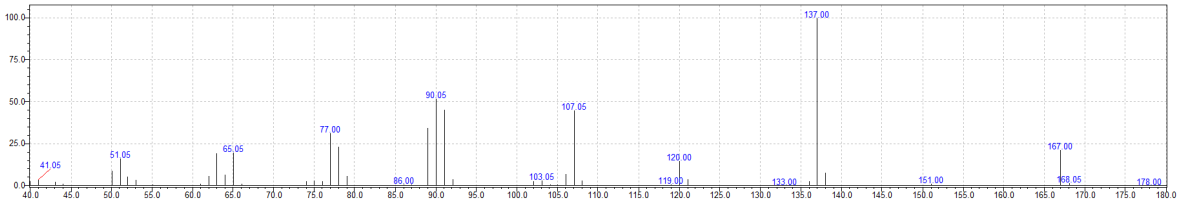

(b)

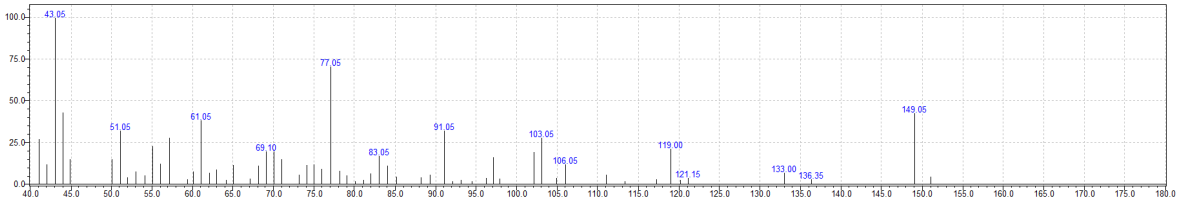

(c)

Figure E14: Mass spectra of (a) 4-ethylnitrobenzene and its oxidation products (b) 4-(1-hydroxyethyl)nitrobenzene and (c) 4-vinylnitrobenzene.

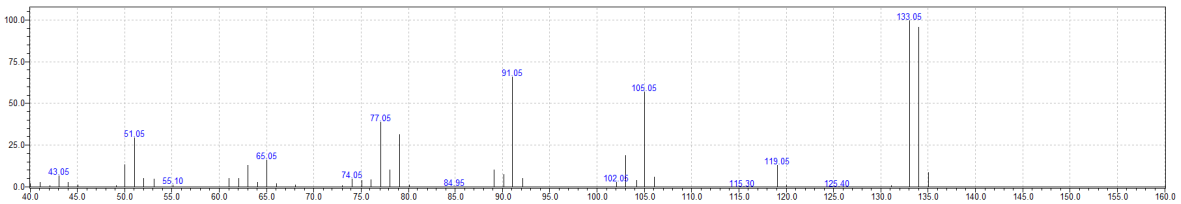

(a)

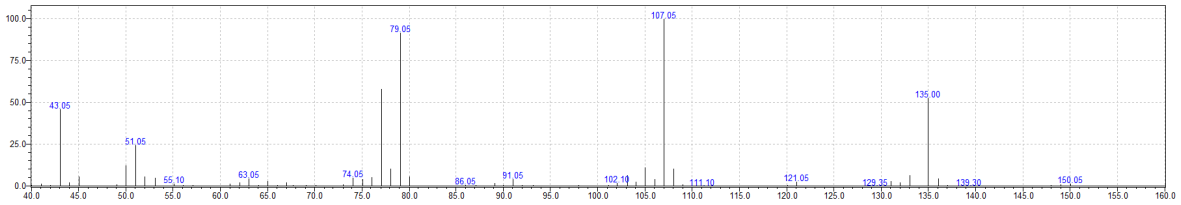

(b)

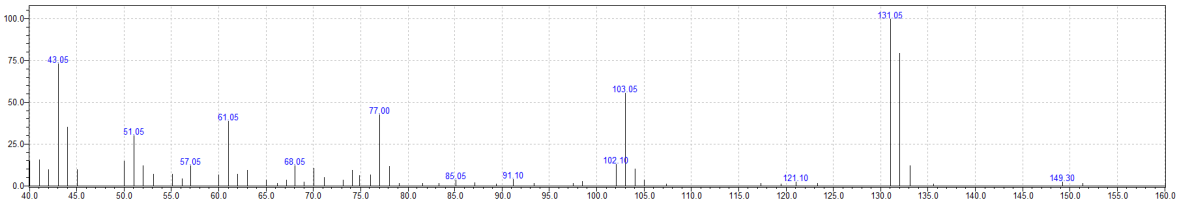

(c)

Figure E15: Mass spectra of (a) 4-ethylbenzaldehyde and its oxidation products (b) 4-(1-hydroxyethyl)benzaldehyde and (c) 4-vinylbenzaldehyde.

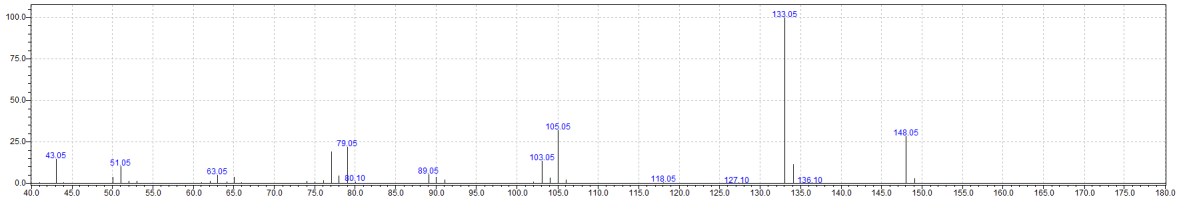

(a)

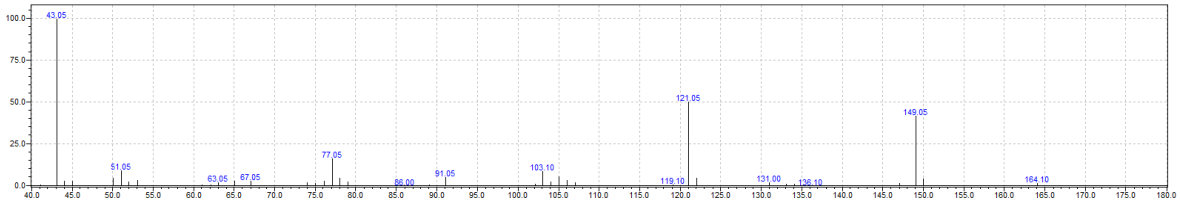

(b)

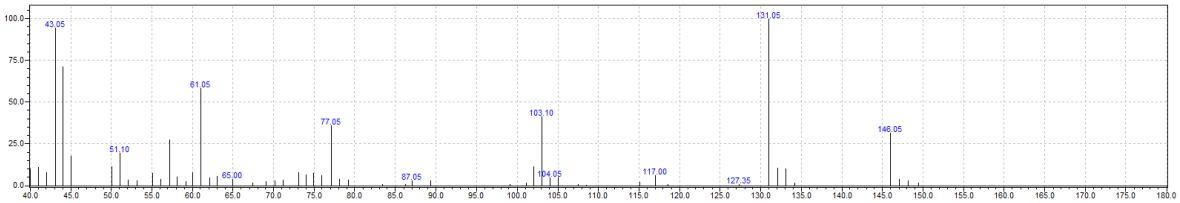

(c)

Figure E16: Mass spectra of (a) 4-ethylacetophenone and its oxidation products (b) 4-(1-hydroxyethyl)acetophenone and (c) 4-vinylacetophenone.